UNIVERSITÀ DEGLI STUDI DI MILANO
Dottorato di Ricerca in Scienze della Terra
Ciclo XXVI

Calcareous nannofossil revised biostratigraphy of the latest Albian-earliest Campanian time interval (Late Cretaceous)

Ph.D. Thesis

Fabio Russo

Matricola R08989

Tutore	**Anno Accademico**	*Coordinatore*
Prof.ssa Elisabetta Erba	**2012-2013**	**Prof.ssa Elisabetta Erba**

Contents

Abstract

Calcareous nannoplankton appeared in the Late Triassic and rapidly evolved during the Jurassic and Cretaceous, reaching a diversity maximum in the Late Cretaceous. The widespread distribution, the high abundance and assemblage diversity of Late Cretaceous nannofloras make calcareous nannofossils a very effective biostratigraphic tool for high-resolution dating and correlations.

This study is focused on the revision of nannofossil biostratigraphic events in the Upper Cretaceous. The major objective is to refine the biostratigraphic schemes available for the latest Albian-earliest Campanian time interval by the investigation of eight selected sections. These are located in different sedimentary basins in order to assess nannofossil bioevents in different paleoceanographic regimes and/or latitudes and evaluate the applicability of the three major nannofossil zonations.

Sites and sections studied are: DSDP Site 463 (Mid-Pacific Mountains – Pacific Ocean), ODP Site 763 (Exmouth Plateau – Indian Ocean), ODP Site 1138 (Kerguelen Plateau – Indian Ocean), ODP Site 1261 (Demerara Rise – Atlantic Ocean), Monte Petrano (Umbria-Marche Basin – Italy), Clote de Chevalier (Vocontian Basin – France), Rock Canyon, Pueblo (Western Interior Basin – Colorado), Tarfaya Core (Tarfaya Basin – Morocco).

Biostratigraphic investigation was performed on a total of 564 smear slides analyzed using standard light microscope techniques under cross polarizers and transmitted light, at 1250X magnification. I produced semi-quantitative range charts of all taxa providing information on their preservation, total and single taxon abundance.

Taxonomic revision was applied to cases of potential misidentification and discrepant attribution. Taxonomic notes and remarks based on personal observation are provided. Also, photographic plates illustrate all zonal/subzonal markers and some other common species.

The results were compared to those from other sections published in literature to test reliability of biozonations and discriminate global, regional or local events. Nannofossil biohorizons were also examined in the context of stage boundary definition. More specifically, for each stage

boundary the data documented for GSSP sections and/or presented for GSSP proposals were analyzed and the result of my investigation were used to provide information about the applicability of nannofossil events.

Adopting the three zonations, a total of 17 zonal and 4 subzonal markers were recognized as potentially cosmopolitan biohorizons. The achieved resolution is comparable for the three biozonations and higher subdivision is possible only at regional level and in restricted time intervals. Moreover, nannofossil events were proved to be extremely useful to biostratigraphically constrain paleoceanographic events of the Late Albian-Early Turonian interval. Namely, Oceanic Anoxic Event 1d, the Mid-Cenomanian Event and Oceanic Anoxic Event 2 were successfully characterized in the studied sequences.

Chapter 1

Introduction

The term calcareous nannoplankton was first introduced by Lohman (1909) to describe planktonic organism very small (< 63 microns). The term calcareous nannofossils now is used for fossil remains smaller than 30 microns, and is referred to the remains of haptophyte algae, i.e. the group of calcareous nannoplankton known as coccolithophores. These organisms are marine, unicellular, flagellate phytoplankton, characterized by a cell-wall covering of coccoliths (forming a coccosphere), which are readily preserved as fossils, either completely or in a disaggregate state as individual coccoliths (Bown & Young, 1998a).

The oldest nannofossil is of Middle Triassic age (Erba et al., 2013) and calcareous nannoplankton became diversified and abundant and therefore rock-forming since Jurassic times. Due to their great abundance, rapid evolutionary lineages and cosmopolitan life of calcareous nannoplankton, nannofossils are exceptionally useful for biostratigraphic analysis. Moreover, because of their small size, they can be studied from minute rock fragments. Upper Cretaceous lithologies like limestone, chalk and marlstone are rich in nannofossils, geographically widespread and well preserved.

Objectives and general outline of this study

My Ph.D. project is focused on the revision of nannofossil biostratigraphic events in the Upper Cretaceous. More specifically, it aims at refine the uppermost Albian-lowermost Campanian zonal schemes by the investigation of selected sections from different sedimentary basins in order to assess nannofossil bioevents across latitudes. The results will be compared to those from other sections to test reliability of bioevents and discriminate global, regional or local events. I also correlate and calibrate nannofossil bioevents with other fossil groups (in particular planktonic formaniferal biozones) and discuss the use of nannofossil biostratigraphy across Late Cretaceous stage boundaries.

To perform this study, samples from different parts of the world have been analyzed in order to obtain a record of the variability in calcareous nannofossil assemblages across latitudes. Sites and sections studied are: DSDP Site 463 (Mid-Pacific Mountains – Pacific Ocean), ODP Site 763 (Exmouth Plateau – Indian Ocean), ODP Site 1138 (Kerguelen Plateau – Indian Ocean), ODP Site 1261 (Demerara Rise – Atlantic Ocean), Monte Petrano (Umbria-Marche Basin – Italy), Clote de Chevalier (Vocontian Basin – France), Rock Canyon, Pueblo (Western Interior Basin – Colorado), Tarfaya Core (Tarfaya Basin – Morocco). These localities have been chosen also because they are dated with various stratigraphic tools – like $\delta^{13}C$ curves and/or other fossil groups like planktonic foraminifera and macrofossils – providing the means for nannofossil calibrations.

In Chapter 2 I present an overview of the available calcareous nannofossil biozonations for the Late Cretaceous time interval.

In Chapter 3 I describe the sample preparation techniques and the abundance and preservation criteria adopted for calcareous nannofossil investigations.

In Chapter 4 results are reported separately for each studied section/site.

In Chapter 5 I discuss calcareous nannofossil data, testing the reliability of bioevents through different sections. A comprehensive discussion of the literature is also aimed at the assessment of nannofossil biohorizon in the Late Albian – earliest Campanian interval.

The conclusions are compiled in Chapter 6.

In the Appendices I present: a short description of every species encountered in my samples with principal diagnostic characters and observations from my own (Appendix 1); the taxonomic list of all taxa encountered in this study (Appendix 2); calcareous nannofossil plates (Appendix 3).

Tables and calcareous nannofossil range charts of every investigated section (Appendices 4-13) are compiled in the attached CD.

Chapter 2

Calcareous nannofossil biozonations of the Upper Cretaceous

First studies on Upper Cretaceous calcareous nannofossils have been performed since the beginning of the twentieth century. Arkhangelsky (1912) was the first who focused on the systematics of this fossil group followed, almost 40 years later, by Deflandre (1952, 1959), Gorka (1957) and Vekshina (1959). In the 1960s, first attempts to compile an Upper Cretaceous biostratigraphy were done by Stradner (1963), Stover (1966) and Reinhardt (1966) in European sections and Stratotypes, whilst in the US Gartner (1968), Bukry (1969) and Cepek & Hay (1969) published tentative biozonations using calcareous nannofossils analyzed in stage stratotype sections of the Upper Cretaceous. The first complete analysis of Upper Cretaceous nannofossil assemblages was done by Manivit (1971). She proposed a zonation for the Aptian to "Danian" interval based on sections from France, with a tentative correlation between Europe and the United States using also ammonite and planktonic foraminiferal zones.

The Deep Sea Drilling Project (DSDP) started a new era also for calcareous nannofossil biostratigraphy. The data collected from the various oceans at all latitudes provided a systematic knowledge of nannofossil distribution and new zonations were established as a function of bioevents (Roth, 1973; Thierstein, 1974; Martini, 1976). Thierstein (1976), using a dataset based both on land and DSDP sections, presented a detailed zonation for the Early Jurassic through Late Cretaceous time interval, suggesting a tentative correlation with the magnetic reversal scale. He also recognized that certain taxa showed evidence of paleoenvironmental restrictions, which caused diachroneity.

Contributions from Verbeek (1977) and Sissingh (1977, 1978) completed the investigations of European Stratotypes suggesting new zonations based on the section of El Kef in western Tunisia, calibrated with nannofossil assemblages of the stage-stratotypes. Roth (1978), compiled his

biozonation based on DSDP material, focusing his attention on oceanic species and introducing Oceanic stages.

In the 1980s and 1990s, calcareous nannofossil studies were performed by several authors who analyzed sections from different parts of the world, thus giving a wide geographic coverage both offshore and onshore. Crux (1982) worked on sections from SE England providing a sort of correlation between nannofossil bioevents and macrofossil zones of northern Europe. Perch-Nielsen (1985) implemented Sissingh (1977) zonation with a number of useful events. Monechi & Thierstein (1985) correlated nannofossils and planktonic foraminifera with magnetostratigraphy in the Campanian-Maastrichtian interval of the Gubbio area. Bralower (1988) analyzed the Cenomanian/Turonian boundary interval in different regions of the Western Interior, Europe and Tunisia. In 1995, Bralower et al. produced a combined scheme for the entire Upper Cretaceous by integrating nannofossils with planktonic foraminifera; they revised Roth's (1978) zonation integrating additional nannofossil data, Western Interior bentonite isotopic ages and the geomagnetic polarity timescale.

After the Symposium on Cretaceous Stage Boundaries held in Copenhagen in 1983 and the follow-up conference of Brussels in 1995, nannofossil studies focused on the refinement and integration with other fossil groups and proposed stage boundaries (see summary of Burnett,1996). Burnett (1998) presented an Upper Cretaceous zonation correlated with European and American macrofossil zones. She integrated old and new bioevents from both oceanic and shelf paleoenvironments and separated three paleobiogeographical areas (provinces), highlighting provincialism of species particularly during the Campanian-Maastrichtian. Her studies were implemented in a successive paper (Lees, 2002) where she reanalyzed samples from DSDP and ODP sites in the Indian Ocean.

The above-mentioned zonations have been applied to several sections/sites and nannofossil biostratigraphy was calibrated, in many cases, with isotopic stratigraphy, ammonite and planktonic foraminiferal zonations A summary of papers documenting Upper Cretaceous calcareous nannofossils is presented in Tab.2.1 (Appendix 4, see CD attached).

Biozonations of Sissingh (1977) and Roth (1978), implemented by Perch-Nielsen (1985) and Bralower et al. (1995) respectively, and the scheme of Burnett (1998) are widely applied but they left several open questions about calibration of events, correlation with other fossil groups and provincialism of different species. Here I present the analysis of the four available biozonations for nannofossil biostratigraphy of the Late Cretaceous.

2.1 Sissingh, 1977

Sissingh (1977) presented a zonation for the Upper Cretaceous principally based on the Tunisian section of Dyr el Kef, correlating nannofossil bioevents with data from French Stratotypes. He integrated his data with nannofossil assemblages of several sections from France and New Jersey (U.S.) and also on industrial well spot-samples from Oman, Turkey and the North Sea region. He also noticed the incomplete nature of the stratotype sections. Biozones follow an alphanumerical notation (CC#) and are predominantly based on earliest occurrences of selected taxa, identifiable with light microscope, with relatively high abundance. Total range of species are used, where possible, to define zonal or sub-zonal boundaries. Less reliable events are used for subzones (Fig.2.1.1).

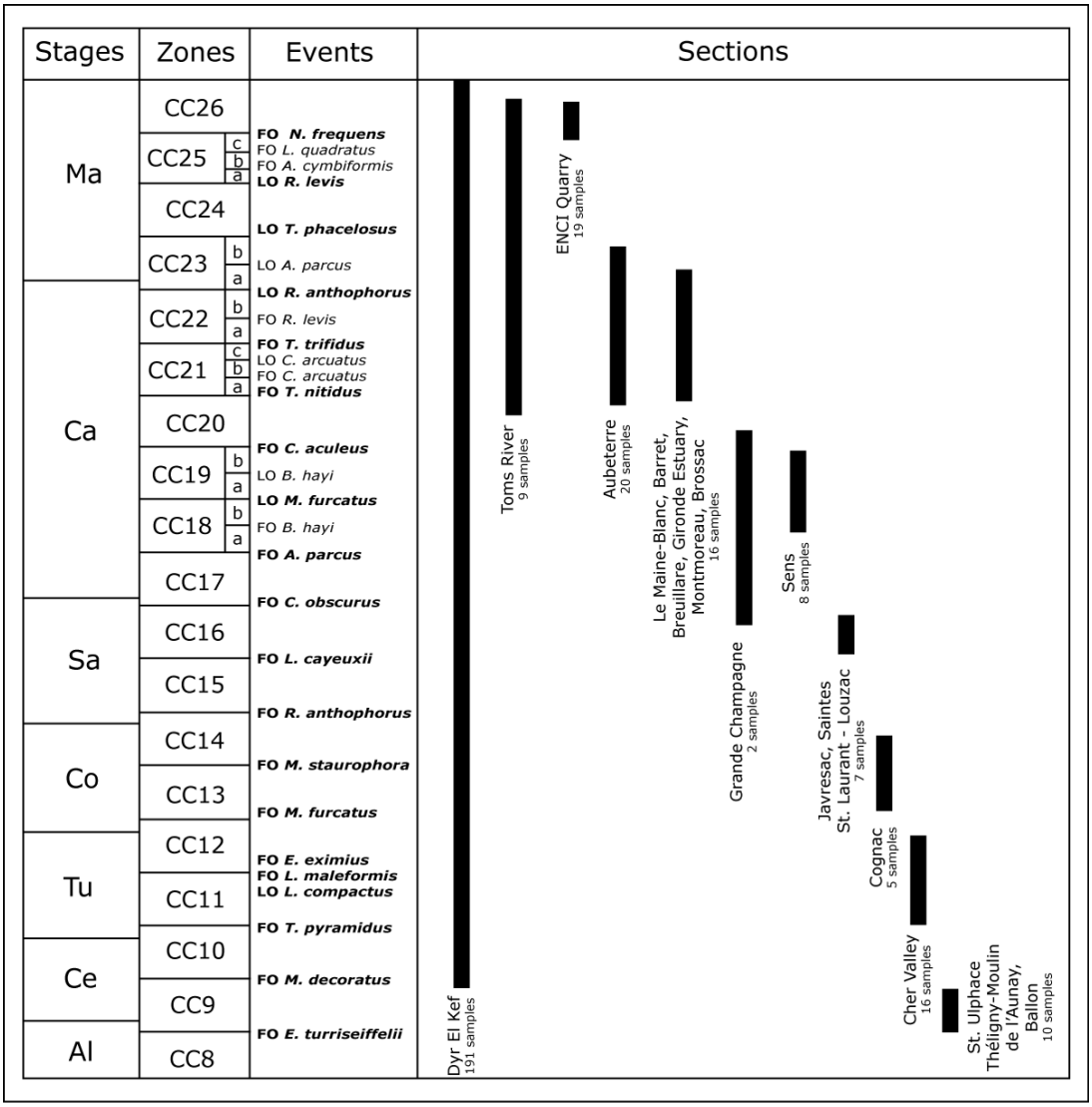

Fig.2.1.1 Biozonation of Sissingh (1977) with the studied sections. Zonal markers are indicated in bold. Age assignements after Sissingh (1978). Nannofossil zones are arbitrarily given equal lengths/duration and, therefore, Stages are not in scale

He correlated nannofossil bioevents with planktonic foraminiferal zones based on the analyses of foraminiferal contents in the same samples from el Kef he used for his own results (Postuma, 1971 and unpublished data). In 1978, Sissingh presented a partial revision of some events and zonal dating based on the revised ages of planktonic foraminiferal zones of Van Hinte (1976).

Events

The nannofossil events used by Sissingh (1977) as zonal and subzonal markers are here discussed, reporting the occurrence in the studied sections, the age assignements and the correlation with planktonic foraminiferal bizonation (Sissingh , 1977; 1978).

- FO of *Microrhabdulus decoratus* (base CC10): El Kef; age assignment: Late Cenomanian; planktonic foraminiferal zone: *R. cushmani.*
- FO of *Tetralithus pyramidus* (= *Quadrum gartneri* – base CC11): El Kef, Cher Valley, Kansas (Cepek & Hay, 1969); age assignment: Early Turonian; planktonic foraminiferal zone: *R. cushmani-G. helvetica*.
- FO of *Lucianorhabdus maleformis* (base CC12): El Kef, Central Pacific (Roth, 1973), Indian Ocean (Thierstein, 1974); age assignment: Late Turonian; planktonic foraminiferal zone: *G. helvetica.*
- FO of *Eiffellithus eximius* (base CC12): mentioned but not documented
- LO of *Lucianorhabdus compactus* (base CC12): LO in the basal Turonian Stratotype.
- FO of *Marthasterites furcatus* (base CC13): El Kef, Central Pacific (Roth, 1973), Indian Ocean (Thierstein, 1974); age assignment: Early Coniacian; planktonic foraminiferal zone: *G. schneegansi.*
- FO of *Micula staurophora* (base CC14): El Kef, Indian Ocean (Thierstein, 1974); age assignment: Late Coniacian; planktonic foraminiferal zone: *G. schneegansi*.
- FO of *Reinhardtites anthophorus* (base CC15): El Kef; age assignment: Early Santonian,; planktonic foraminiferal zone: *G. concavata/G. carinata.*
- FO of *Lucianorhabdus cayeuxii* (base CC16): El Kef, Saintes, Javresac, St.Laurent-Louzac, Gimeux, Alabama (Cepek & Hay, 1969); age assignment: Late Santonian; planktonic foraminiferal zone: *G. concavata/G. carinata.*
- FO of *Calculites obscurus* (base CC17): El Kef, Netherlands, Oman, Alabama (Cepek & Hay, 1969); age assignment: earliest Campanian; planktonic foraminiferal zone: *G. elevata* (basal).

- FO of *Aspidolithus parcus* (base CC18a): El Kef, Genté, Oman, Great Britain, Alabama (Cepek & Hay, 1969), Central Pacific (Roth, 1973); age assignment: earliest Campanian; planktonic foraminiferal zone: *G. elevata.*
- FO of *Bukryaster hayi* (base CC18b): El Kef; age assignment: Early Campanian; planktonic foraminiferal zone: *G. elevata.*
- LO of *Marthasterites furcatus* (base CC19a): El Kef, Oman, Alabama (Cepek & Hay, 1969), Central Pacific (Roth, 1973); age assignment: Early Campanian; planktonic foraminiferal zone: *G. elevata.*
- LO of *Bukryaster hayi* (base CC19b): El Kef; age assignment: Early Campanian; planktonic foraminiferal zone: *G. elevata.*
- FO of *Ceratolithoides aculeus* (base CC20): Toms River, Aubeterre, Oman, Alabama (Cepek & Hay, 1969), Central Pacific (Roth, 1973); age assignment: Early Campanian; planktonic foraminiferal zone: *G. elevata.*
- FO of *Tetralithus nitidus* (= *Uniplanarius gothicus* – base CC21a): El Kef, Aubeterre, Gironde, Estuary, Montmoreau, Brossac, Turkey, Oman, Central Pacific (Roth, 1973); age assignment: Late Campanian; planktonic foraminiferal zone: *G. elevata.*
- FO of *Ceratolithoides arcuatus* (base CC21b): El Kef; age assignment: Late Campanian; planktonic foraminiferal zone: *G. elevata.*
- LO of *Ceratolithoides arcuatus* (base CC21c): El Kef; age assignment: Late Campanian; planktonic foraminiferal zone: *G. elevata.*
- FO of *Tetralithus trifidus* (= *Uniplanarius trifidus* – base CC22a): El Kef, Gironde/Estuary, Aubeterre, Toms River, Turkey, Oman, Central Pacific (Roth, 1973); age assignment: Late Campanian; planktonic foraminiferal zone: *G. elevata.*
- FO of *R. levis* (base CC22b): El Kef, Toms River, Barret; age assignment: Late Campanian; planktonic foraminiferal zone: *G. calcarata.*
- LO of *Reinhardtites anthophorus* (base CC23a): El Kef, Toms River, Netherlands, Great Britain, Central Pacific (Roth, 1973), Alabama (Cepek & Hay, 1969); age assignment: latest Campanian; planktonic foraminiferal zone: *G. calcarata.*
- LO of *Aspidolithus parcus* (base CC23b): El Kef; age assignment: Early Maastrichtian; planktonic foraminiferal zone: *G. gansseri*. Remarks: present in one sample at El Kef above LO *T. phacelosus* (base CC24).
- LO of *Tranolithus phacelosus* (*Tranolithus orionatus* – base CC24): El Kef, Aubeterre, Denmark, Great Britain, Central Pacific (Roth, 1973); age assignment: Early Maastrichtian; planktonic foraminiferal zone: *G. gansseri*.

- LO of *Reinhardtites levis* (base cc25a): El Kef, Denmark; age assignment: Early Maastrichtian; planktonic foraminiferal zone: *G. mayaroensis*. Remarks: present in a sample with *A. cymbiformis* (base CC25b) e *L. quadratus* (base CC25c) at El Kef.
- FO of *Arkhangelskiella cymbiformis* (base CC25b): El Kef, Denmark; age assignment: Late Maastrichtian; planktonic foraminiferal zone: *G. mayaroensis.*
- FO of *Lithraphidites quadratus* (base CC25c): El Kef, Toms River, Maastricht; age assignment: Late Maastrichtian; planktonic foraminiferal zone: *G. mayaroensis.*
- FO of *Nephrolithus frequens/Micula murus* (base CC26): El Kef, Toms River, Maastricht; age assignment: Late Maastrichtian, boreal and tropical preference respectively; planktonic foraminiferal zone: *G. mayaroensis.*

Perch-Nielsen (1979, 1985), implemented Sissingh (1977) zonation by adding numerous events to extend the application of his zonation to a large variety of areas and latitudes (Fig.2.1.2).

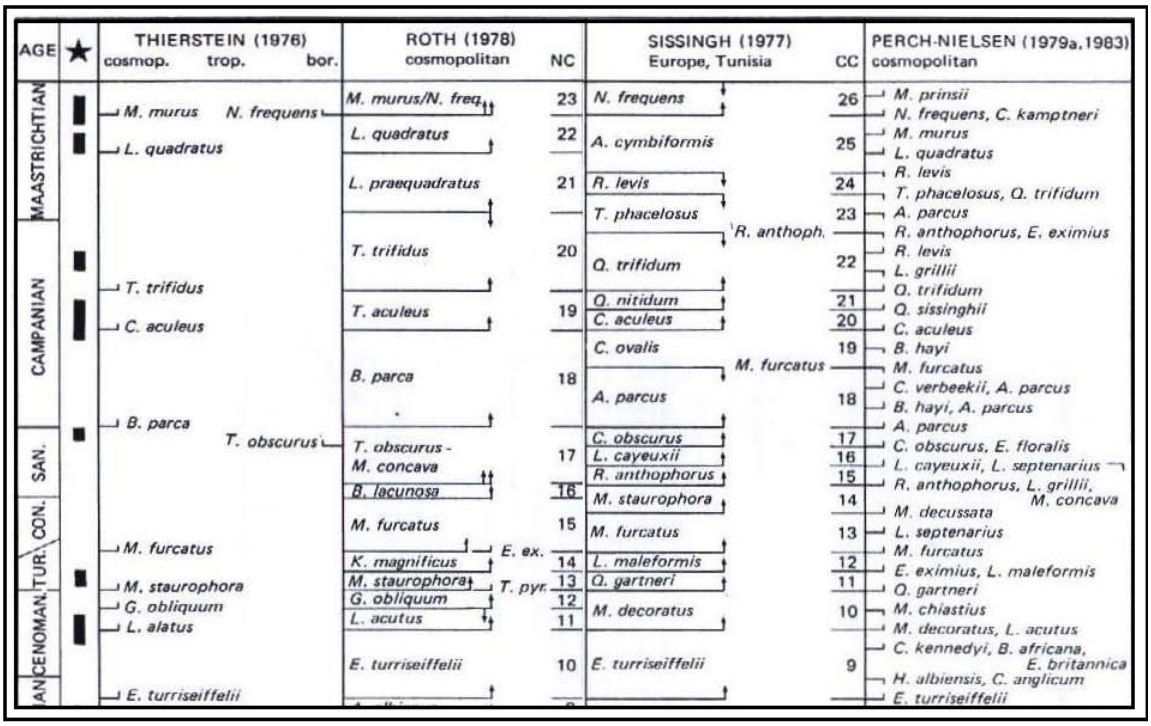

Fig.2.1.2 Correlation of Cretaceous zonal schemes and their correlation with the stratotypes of the Stages (Perch-Nielsen, 1985)

She added:

- five events defining three subzones within the CC9 around the Albian/Cenomanian boundary: LO of *Hayesites albiensis* (base of CC9b), FO of *Calculites anfractus* (base of

CC9b), FO of *Corollithion kennedyi* (base of CC9c), LO of *Braarudosphaera africana* (base of CC9c), LO of *Watznaueria britannica* (base of CC9c),

- one event in the CC10 around the Cenomanian/Turonian boundary: LO of *Helenea chiastia* (base of CC10b)
- one event in the CC13 zone around the Turonian/Coniacian boundary: FO of *Lithastrinus septenarius* (base of CC13b).

She also suggested FO of *Lithastrinus grillii*, LO of *L. septenarius* and LO of *L. grillii* as additional markers for bases of CC15, CC16 and CC22b, respectively.

2.2 Roth, 1978

Roth (1978), presented a zonation for the Upper Cretaceous principally based on data collected during DSDP Legs and following data of Roth (1973), Thierstein (1973, 1974, 1976), Bukry (1975), and Verbeek (1976). His selection of zonal and subzonal marker species was principally based on the bioevents evaluated by Thierstein (1976). Biozones follow an alphanumerical notation (NC#) and are predominantly based on earliest occurrences of marker taxa (Fig.2.2.1). He also introduced Oceanic stages, correlated, although with a wide error-range, to classical Upper Cretaceous stages comparing his data with those presented by Manivit (1971), Thierstein (1976) and Verbeek (1976).

The Oceanic stages of Late Cretaceous age are:

- **Tenerifian**: corresponding to Cenomanian-Early Turonian interval. It includes nannofossil zones NC11, NC12. From FO of *L. acutum* to FO of *T. pyramidus* (*Q. gartneri*).
- **Naturalistian**: corresponding to Middle-Late Turonian interval. It includes nannofossil zones NC13, NC14. From FO of *T. pyramidus* (*Q. gartneri*) to FO of *M. furcatus*.
- **Howlandian**: corresponding to Coniacian-Santonian interval. It includes nannofossil zones NC15, NC16, NC17. From FO of *M. furcatus* to FO of *B. parca*.
- **Bermudan**: corresponding to Campanian-Maastrichtian interval. It includes nannofossil zones NC18, NC19, NC20, NC21, NC22, NC23. From FO of *B. parca* to the extinction of Cretaceous nannofossils.

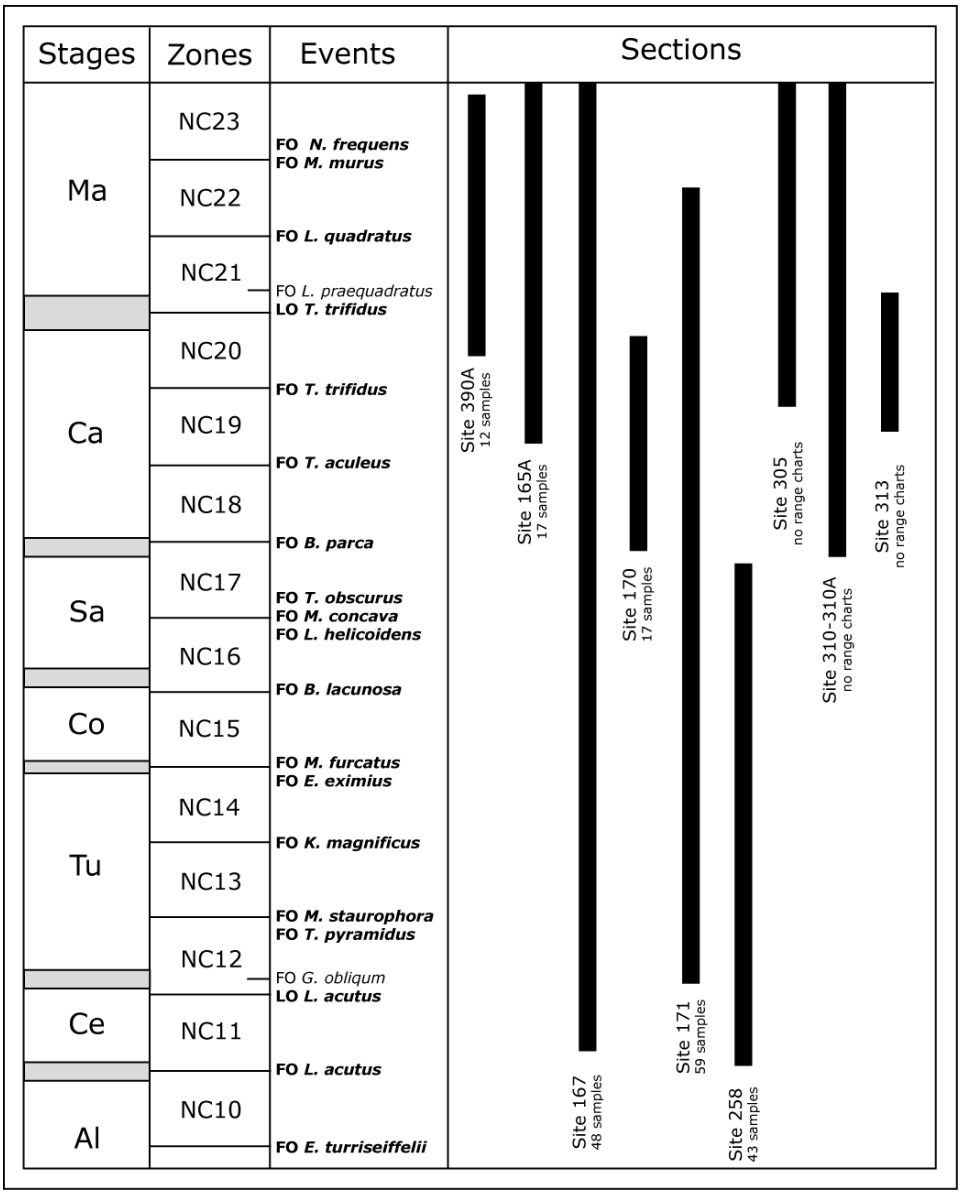

Fig.2.2.1 Biozonation of Roth (1978) with the studied sections. Zonal markers are indicated in bold. Age assignment after (Roth, 1978). Nannofossil zones are arbitrarily given equal lengths/duration and, therefore, Stages are not in scale

Events

The nannofossil events used by Roth (1978) as zonal and subzonal markers are here discussed, reporting the occurrence in the studied sections and the age assignements (Roth, 1978).

- FO of *Lithraphidites acutus* (base NC11): DSDP sites 167, 258, 305, 310; age assignment: basal Cenomanian.
- LO of *Lithraphidites acutus* (base NC12): DSDP sites 167, 258; age assignment: Late Cenomanian.

- FO of *Gartnerago obliquum* (basal NC12): DSDP sites 167, 171, 258; age assignment: Early Turonian.
- FO of *Tetralithus pyramidus* (= *Quadrum gartneri* – base NC13): DSDP sites 167, 171, 258; age assignment: Early Turonian.
- FO of *Kamptnerius magnificus* (base NC14): DSDP Site 258; age assignment: Late Turonian.
- FO of *Eiffellithus eximius* (base NC15): DSDP sites 167, 171; age assignment: Turonian/Coniacian boundary interval.
- FO of *Marthasterites furcatus* (base NC15): DSDP sites 167, 258; age assignment: Turonian/Coniacian boundary interval.
- FO of *Broinsonia lacunosa* (= *Aspidolithus parcus expansus*, base NC16): DSDP Site 258; age assignment: Coniacian.
- FO of *Tetralithus obscurus* (= *Calculites obscurus* – base NC17): DSDP Site 167; age assignment: Middle Santonian.
- FO of *Micula concava* (base NC17): age assignment: Middle Santonian.
- FO of *Lithraphidites helicoidens* (base NC17): DSDP Site 258; age assignment: Middle Santonian.
- FO of *Broinsonia parca* (base NC18): DSDP sites 167, 170, 171, 310; age assignment: basal Campanian.
- FO of *Tetralithus aculeus* (= *Ceratolithoides aculeus* – base NC19): DSDP sites 165, 167, 170, 171; age assignment: Early Campanian.
- FO of *Tetralithus trifidus* (base NC20): DSDP sites 165, 167, 170, 171, 305, 310, 313, 390; age assignment: Late Campanian.
- LO of *Tetralithus trifidus* (base NC21): DSDP sites 165, 167, 171, 305, 310, 313, 390; age assignment: Campanian/Maastrichtian boundary interval.
- FO of *Lithraphidites praequadratus* (lower NC21): species defined in Roth, 1978; age assignment: Campanian/Maastrichtian boundary interval.
- FO of *Lithraphidites quadratus* (base NC22): DSDP sites 165, 171, 390; age assignment: Middle Maastrichtian.
- FO of *Nephrolithus frequens/Micula murus* (base NC23): DSDP sites 165, 167, 305, 310, 390; age assignment: Late Maastrichtian.

2.3 Bralower et al., 1995

Bralower et al. (1995) presented an integrated scheme with nannofossil and planktonic foraminiferal bioevents, principally based on Roth's (1978) zonation and upon a literature survey of numerous DSDP/ODP and land sections as well as partial reinvestigation of parts of these sequences. Improved stratigraphic resolution of Upper Cretaceous zones, additional nannofossil events were introduced in the biozonazion of Roth (1978) to define subzones (indicated by the alphanumerical notation NC*# – Fig.2.3.1).

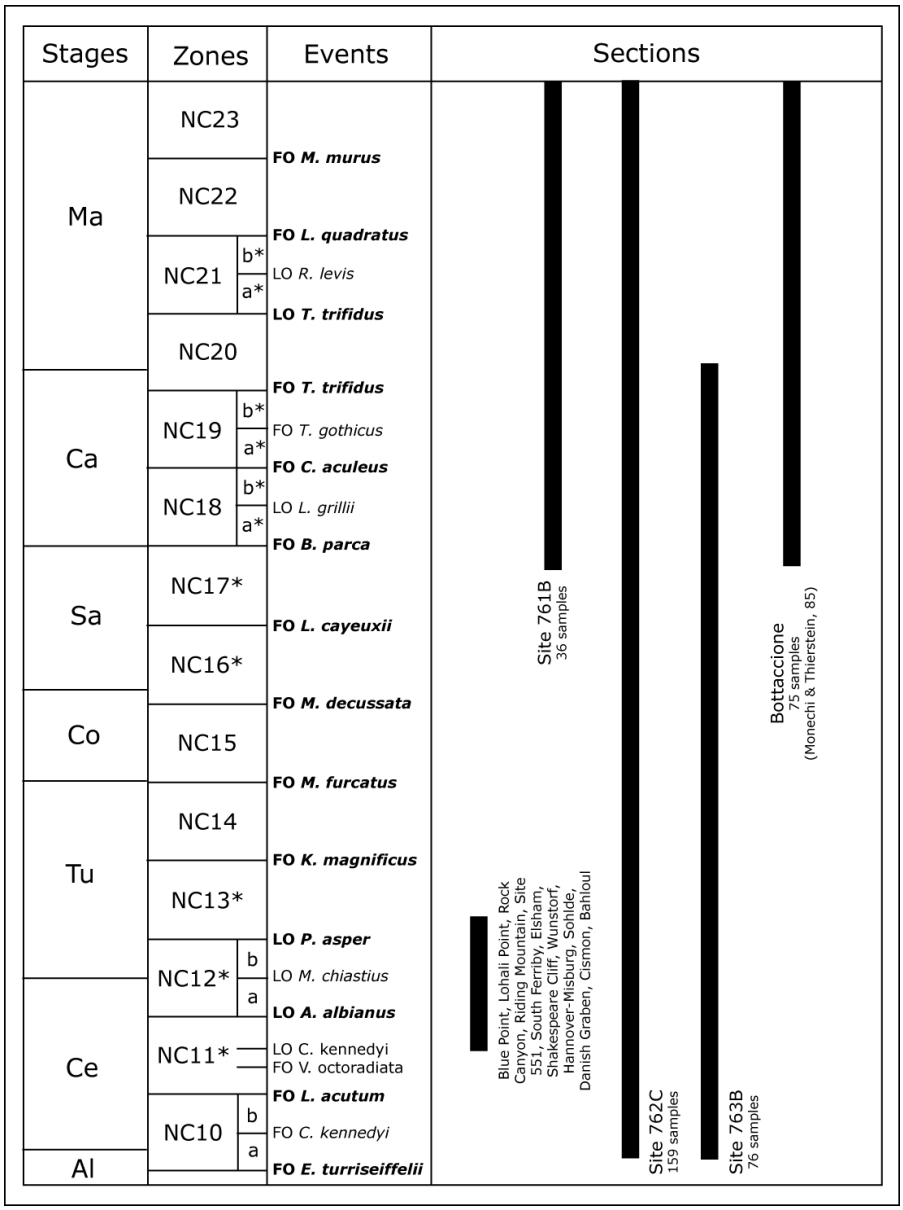

Fig.2.3.1 Biozonation of Bralower et al. (1995) with the studied sections. Zonal markers are indicated in bold. Age assignements after Bralower et al. (1995). Nannofossil zones are arbitrarily given equal lengths/duration and, therefore, Stages are not in scale

Correlations between Late Cretaceous calcareous nannofossil and planktonic foraminiferal zones are based on investigations of sections in the South Atlantic, South Pacific, eastern Indian Oceans (Leckie, 1984; Wiegand, 1984; Bralower & Siesser, 1992) and Western Interior Basin (Leckie, 1985; Bralower, 1988). Analyzes of the Gubbio sequences allowed correlations between calcareous nannofossil bioevents and magnetochrons and planktonic foraminiferal zones (Monechi & Thierstein, 1985; Premoli Silva & Sliter, 1995). Correlations with macrofossil zones, stage designation, and $^{40}Ar/^{39}Ar$ ages follow Obradovich's (1993) analyses in Western Interior Basin. In several cases, correlations between Western Interior macrofossil zones and European stage boundaries are indirect, for this reason fourteen of the seventeen original localities discussed in Obradovich and Cobban (1975) were investigated for calcareous plankton assemblages, although no range charts were published.

Events

The nannofossil events used by Bralower et al. (1995) as zonal and subzonal markers are here discussed, reporting the occurrence in the studied sections, the age assignements and the correlation with planktonic foraminiferal bizonation (Bralower et al., 1995).

- FO of *Corollithion kennedyi* (base NC10b): ODP sites 762, 763; age assignment: basal Cenomanian; planktonic foraminiferal zone: middle *R. brotzeni.*
- FO of *Lithraphidites acutus* (base NC11*): ODP Site 763; age assignment: Early Cenomanian; planktonic foraminiferal zone: upper *R. brotzeni.*
- LO of *Axopodorhabdus albianus* (base NC12a*): Rock Canyon, Riding Mountain, Lohali Point, South Ferriby, Elsham Quarry, Shakespeare Cliff, Wunstorf Quarry, Söhlde Quarry, Hannover Quarry, Danish Graben, Cismon, Bahloul, DSDP Site 551, ODP sites 762, 763; age assignment: latest Cenomanian; planktonic foraminiferal zone: *R. cushmani/W. archeocretacea* boundary interval.
- LO of *Microstaurus chiastius* (base NC12b*): Rock Canyon, Riding Mountain, Blue Point, Lohali Point, South Ferriby, Elsham Quarry, Shakespeare Cliff, Wunstorf Quarry, Söhlde Quarry, Hannover Quarry, Cismon, Bahloul, DSDP Site 551, ODP sites 762, 763; age assignment: Cenomanian/Turonian boundary interval; planktonic foraminiferal zone: middle *W. archeocretacea.*
- LO of *Parhabdolithus asper* (= *Rhagodiscus asper* – base NC13*): Rock Canyon, Riding Mountain, Blue Point, Lohali Point, South Ferriby, Elsham Quarry, Shakespeare Cliff, Wunstorf Quarry, Söhlde Quarry, Hannover Quarry, Danish Graben, Cismon, Bahloul,

DSDP Site 551, ODP sites 762, 763; age assignment: Early Turonian; planktonic foraminiferal zone: *W. archeocretacea/H. helvetica* boundary interval.

- FO of *Kamptnerius magnificus* (base NC14): ODP sites 762, 763; age assignment: Late Turonian; planktonic foraminiferal zone: *H. helvetica/M. sigali* boundary interval.
- FO of *Marthasterites furcatus* (base NC15): ODP sites 762, 763; age assignment: Coniacian; planktonic foraminiferal zone: *M. sigali*.
- FO of *Micula decussata* (= *Micula staurophora* – base NC16*): ODP sites 762, 763; age assignment: Late Coniacian; planktonic foraminiferal zone: lower *D. concavata*.
- FO of *Lucianorhabdus cayeuxii* (base NC17*): ODP sites 762, 763; age assignment: Late Santonian; planktonic foraminiferal zone: *D. asymetrica.*
- FO of *Broinsonia parca* (base NC18a*): ODP sites 761, 762, 763, Bottaccione; age assignment: basal Campanian; planktonic foraminiferal zone: coincident with LO of *D. asymetrica.*
- LO of *Lithastrinus grillii* (base NC18b*): ODP sites 761, 762, 763, Bottaccione; age assignment: Early Campanian; planktonic foraminiferal zone: *G. elevata*. Remarks: in all sections the species is still present after FO of *C. aculeus* – base NC19a*.
- FO of *Ceratolithoides aculeus* (base NC19a*): ODP sites 761, 762, Bottaccione; age assignment: Early Campanian; planktonic foraminiferal zone: middle *G. ventricosa.*
- FO of *Tetralithus gothicus* (= *Uniplanarius gothicus* – base NC19b*): ODP sites 761, 762, 763, Bottaccione; age assignment: Early Campanian; planktonic foraminiferal zone: upper *G. ventricosa.*
- FO of *Tetralithus trifidus* (base NC20): ODP sites 761, 762, 763, Bottaccione; age assignment: Late Campanian; planktonic foraminiferal zone: coincident with FO *G. calcarata.*
- LO of *Tetralithus trifidus* (base NC21a*): ODP sites 761, 762, Bottaccione; age assignment: Early Maastrichtian; planktonic foraminiferal zone: middle *G. gansseri.*
- LO of *Reinhardtites levis* (base NC21b*): ODP sites 761, 762; age assignment: Early Maastrichtian; planktonic foraminiferal zone: upper *G. gannsseri.*
- FO of *Lithraphidites quadratus* (base NC22): ODP sites 761, 762, Bottaccione; age assignment: Early Maastrichtian; planktonic foraminiferal zone: lower *A. mayaroensis.*
- FO of *Micula murus* (base NC23): ODP sites 761, 762, Bottaccione; age assignment: Late Maastrichtian; planktonic foraminiferal zone: upper *A. mayaroensis.*

2.4 Burnett, 1998

Burnett (1998) presented a zonation defined by an high number of events recognized in different paleobiogeographic areas and from both oceanic and shelf paleoenvironments. Biozones follow an alphanumerical notation (UC#) and are based on first and last occurrences of selected species. She distinguished provincialism of several taxa and presented three different zonations for separate regions (tethyan-intermediate – TP; austral – AP; boreal – BP). Her TP zonation is a compilation of literature data, principally from Sissingh (1977) and Perch-Nielsen (1985) (Fig.2.4.1). Her nannofossil data come from numerous sections, including: Belgium, Bulgaria, Czech Republic, Denmark, England, France, Germany, The Netherlands, North Sea, Poland, Russia, South Africa, USA, Australia, Pakistan, Indian, Atlantic and Pacific oceans (Burnett, 1988; Burnett et al., 1992a, b; Kennedy et al., 1992; Gale et al., 1996; Burnett & Whitham, 1999; Lees, 2002 and unpublished data). Calibration is obtained by direct correlations with macrofossil zones in Europe and United States which were used to define Upper Cretaceous stages and substages (Burnett, 1996).

Events

The nannofossil events used by Burnett (1998) as zonal and subzonal markers are here discussed, reporting the occurrence in the studied sections, the age assignements and the correlation with macrofossil bizonations (Burnett, 1998).

- FO of *Corollithion kennedyi* (base UC1a): Trunch Borehole, Mont Risou, DSDP and ODP sites 258, 765; age assignment: basal Cenomanian; macrofossil zone: *M. mantelli*, subzone *N. carcitanense*; planktonic foraminiferal zone: *R. globotruncanoides.*
- LO of *Watznaueria britannica* (base UC1b): DSDP and ODP sites 258, 765; age assignment: Early Cenomanian; macrofossil zone: *M. mantelli*, subzone *N. carcitanense.*
- LO of *Gartnerago chiasta* (base UC1c): DSDP Site 258; age assignment: Early Cenomanian; macrofossil zone: *M. mantelli*, subzone *N. carcitanense*.
- FO of *Kamptnerius magnificus* (base UC1d): Trunch Borehole, DSDP and ODP sites 258, 550, 765; age assignment: Early Cenomanian (in S England); macrofossil zone: *M. mantelli*, subzone *N. carcitanense.* Remarks: in all sites this taxon has its FO in Early Turonian.
- FO of *Helicolithus anceps* (base UC1d): Trunch Borehole, Kent, DSDP and ODP sites 258, 550, 765; age assignment: Early Cenomanian; macrofossil zone: *M. mantelli*, subzone *N. carcitanense.*

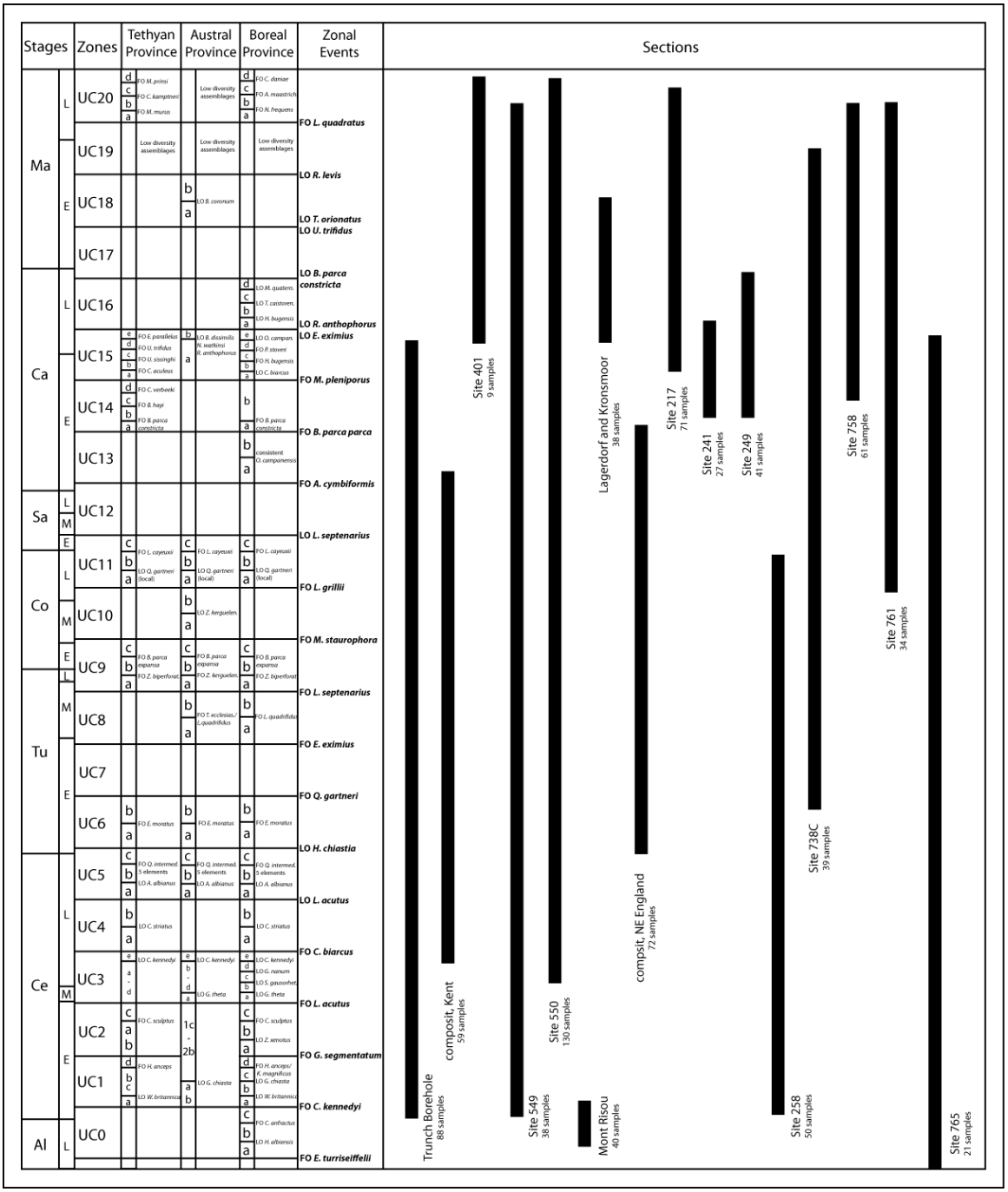

Fig.2.4.1 Biozonation of Burnett (1998) with the studied sections. Zonal markers are indicated in bold. Age assignements after Burnett (1998). Nannofossil zones are arbitrarily given equal lengths/duration and, therefore, Stages are not in scale

- FO of *Gartnerago segmentatum* (base UC2a): DSDP and ODP sites 258, 765; age assignment: Early Cenomanian; macrofossil zone: basal *M. dixoni*.
- LO of *Zeugrhabdotus xenotus* (base UC2b): not present in published range charts; age assignment: Early Cenomanian; macrofossil zone: *M. dixoni*.

- FO of *Cylindralithus sculptus* (base UC2c): ODP Site 765; age assignment: Early Cenomanian; macrofossil zone: *M. dixoni*.
- FO of *Lithraphidites acutus* (base UC3a): Trunch Borehole, DSDP and ODP sites 258; age assignment: basal Middle Cenomanian; macrofossil zone: basal *A. rhotomagense*.
- LO of *Gartnerago theta* (base UC3b): DSDP Site 258; age assignment: Middle Cenomanian: macrofossil zone: *A. rhotomagense.*
- LO of *Staurolithites gausorhethium* (base UC3c): not present in published range charts; age assignment: Late Cenomanian; macrofossil zone: *C. guerangeri*.
- LO of *Gartnerago nanum* (base UC3d): Trunch Borehole, Kent, DSDP sites 258, 549, 550; age assignment: Late Cenomanian; macrofossil zone: *C. guerangeri*.
- LO of *Corollithion kennedyi* (base UC3e): Trunch Borehole, Kent, DSDP and ODP sites 258, 765; age assignment: Late Cenomanian; macrofossil zone: *C. guerangeri*.
- FO of *Cylindralithus biarcus* (= *Rotelapillus biarcus* – base UC4a): Trunch Borehole, DSDP and ODP sites 550, 765; age assignment: Late Cenomanian; macrofossil zone: *M. geslinianum*. Remarks: reported from latest Albian at DSDP Site 258.
- LO of *Cretarhabdus striatus* (base UC4b): ODP Site 765; age assignment: Late Cenomanian; macrofossil zone: *M. geslinianum*.
- LO of *Lithraphidites acutus* (base UC5a): Trunch Borehole, Kent, DSDP and ODP sites 258; age assignment: Late Cenomanian; macrofossil zone: *M. geslinianum*.
- LO of *Axopodorhabdus albianus* (base UC5b): Trunch Borehole, Kent, DSDP and ODP sites 258, 765; age assignment: Late Cenomanian; macrofossil zone: *M. geslinianum*.
- FO of *Quadrum intermedium*-5 (base UC5c): NE England, DSDP and ODP sites 258, 765; age assignment: latest Cenomanian; macrofossil zone: *N. juddii*.
- LO of *Helenea chiastia* base UC6a): Kent, DSDP and ODP sites 258, 549, 550, 765; age assignment: basal Turonian; macrofossil zone: *I. labiatus* - *W. devonense*.
- FO of *Eprolithus moratus* (= *Eprolithus eptapetalus* – base UC6b): Kent, NE England, DSDP and ODP sites 258, 549, 550, 765; age assignment: Early Turonian; macrofossil zone: *I. labiatus*.
- FO of *Quadrum gartneri* (base UC7): Trunch Borehole, Kent, NE England, DSDP and ODP sites 258, 549, 550, 738, 765; age assignment: Early Turonian; macrofossil zone: *I. labiatus*.
- FO of *Eiffellithus eximius* (base UC8a): Trunch Borehole, Kent, NE England, DSDP and ODP sites 258, 549, 550, 738, 765; age assignment: Early Turonian; macrofossil zone: *I. labiatus*.
- FO of *Thierstenia ecclesiastica* (base UC8bAP): DSDP and ODP sites 258, 738; age assignment: Middle Turonian; not identified in an MF-dated sequence

- FO of *Lucianorhabdus quadrifidus* (base UC8b): Trunch Borehole, Kent, NE England, DSDP and ODP sites 549, 550, 738; age assignment: Middle Turonian; macrofossil zone: *T. lata*.
- FO of *Lithastrinus septenarius* (base UC9a): NE England, DSDP and ODP sites 258, 738 (species present in one sample), 765; age assignment: Middle Turonian; macrofossil zone: *T. lata*.
- FO of *Z. biperforatus* (base UC9b): Trunch Borehole, Kent, NE England, DSDP and ODP sites 258, 549, 550 (species present in two samples), 765; age assignment: Late Turonian; macrofossil zone: *H. planus*.
- FO of *B. parca expansa* (base UC9c): NE England, DSDP and ODP sites 258, 738, 765; age assignment: Early Coniacian; macrofossil zone: *M. cortestudinarium*.
- FO of *M. staurophora* (base UC10): Trunch Borehole, Kent, NE England, DSDP and ODP sites 258, 549, 550, 738, 765; age assignment: Middle Coniacian; macrofossil zone: *M. cortestudinarium.*
- LO of *Z. kerguelensis* (base UC10bAP): DSDP and ODP sites 258, 738, 756; age assignment: Middle Coniacian; not identified in an MF-dated sequence.
- FO of *Lithastrinus grillii* (base UC11a): Trunch Borehole, Kent, NE England, DSDP and ODP sites 549, 550, 761, 765; age assignment: Late Coniacian; macrofossil zone: *M. coranguinum.*
- LO of *Q. gartneri* (base UC11b): Trunch Borehole, Kent, Lagerdorf and Kronsmoor, NE England, DSDP and ODP sites 258, 549, 550, 738, 761, 765; age assignment: Late Coniacian; macrofossil zone: *M. coranguinum*.
- FO of *Lucianorhabdus cayeuxii* (base UC11c): Trunch Borehole, NE England, DSDP and ODP sites 549, 550, 738, 761, 765; age assignment: Late Coniacian; macrofossil zone: *M. coranguinum.*
- LO of *Lithastrinus septenarius* (base UC12): NE England, ODP sites 738, 761, 765; age assignment: Early Santonian; macrofossil zone: uppermost *M. coranguinum.*
- FO of *Arkhangelskiella cymbiformis* (base UC13): Kent, NE England, DSDP and ODP sites 550, 761, 765; age assignment: basal Campanian; macrofossil zone: *G. granulata - G. quadrata - O. pillula*.
- FO of *Broinsonia parca parca* (base UC14a): Trunch Borehole, NE England, DSDP and ODP sites 549, 550, 738, 761, 765; age assignment: lower Early Campanian; macrofossil zone: *lingua/quadrata - O. pillula.*
- FO of *Broinsonia parca constricta* (base UC14b): ODP sites 761, 765; age assignment: lower Early Campanian; macrofossil zone: *lingua/quadrata - O. pillula*.

- FO of *Bukryaster hayi* (base UC14cTP): not present in published range charts; age assignment: lower Early Campanian; not identified in an MF-dated sequence.
- FO of *Ceratolithoides verbeeki* (base UC14dTP): ODP sites 761, 765; age assignment: lower Early Campanian; not identified in an MF-dated sequence.
- FO of *Misceomarginatus pleniporus* (base UC15a): ODP sites 738, 758; age assignment: upper Early Campanian; macrofossil zone: *O. pillula/G. senonensis* - *G. quadrata*?.
- LO of *Cylindralithus biarcus* base (UC15bBP): Trunch Borehole, DSDP and ODP sites 217, 549, 758, 761; age assignment: upper Early Campanian; macrofossil zone: *G. senonensis*.
- FO of *Heteromarginatus bugensis* (base UC15cBP): Trunch Borehole, Lagerdorf and Kronsmoor; age assignment: upper Early Campanian; macrofossil zone: *conica/gracilis.*
- FO of *Praediscosphaera stoveri* (base UC15dBP): Trunch Borehole, Lagerdorf and Kronsmoor, DSDP and ODP sites 549, 550, 765; age assignment: lower Late Campanian; macrofossil zone: *basiplana/spiniger* - *B. mucronata*.
- LO of *Orastrum campanensis* (base UC15eBP): Trunch Borehole, Lagerdorf and Kronsmoor; age assignment: upper Late Campanian; macrofossil zone: *B. polyplocum* - *B. mucronata*.
- FO of *Ceratolithoides aculeus* (base UC15bTP): DSDP and ODP sites 217, 549, 550, 761, 765; age assignment: upper Early Campanian; not identified in an MF-dated sequence.
- FO of *Uniplanarius sissinghi* (base UC15cTP): not present in published range charts; age assignment: Early/Late Campanian boundary interval; not identified in an MF-dated sequence.
- FO of *Uniplanarius trifidus* (base UC15dTP): DSDP and ODP sites 217, 241, 401, 549, 550, 738, 758, 761, 765; age assignment: Early/Late Campanian boundary interval; not identified in an MF-dated sequence.
- FO of *Eiffellithus parallelus* (base UC15eTP): DSDP and ODP sites 217, 249, 758, 761, 765; age assignment: lower Late Campanian; not identified in an MF-dated sequence.
- LO of *Biscutum dissimilis* (base UC15bAP): DSDP and ODP sites 217, 738; age assignment: upper Late Campanian; not identified in an MF-dated sequence.
- LO of *Eiffellithus eximius*/LO of *Reinhardtites anthophorus* (base UC16): Trunch Borehole, Lagerdorf and Kronsmoor, DSDP and ODP sites 217, 241, 401, 549, 550, 738, 758, 761; age assignment: upper Late Campanian; macrofossil zone: *grimmensis/granulosus* - *B. mucronata*.

- LO of *Heteromarginatus bugensis* base (UC16bBP): Trunch Borehole, Lagerdorf and Kronsmoor; age assignment: upper Late Campanian; macrofossil zone: *grimmensis/granulosus* - *B. mucronata*.
- LO of *Tortolithus caistorensis* base (UC16cBP): Lagerdorf and Kronsmoor; age assignment: upper Late Campanian; macrofossil zone: *B. lanceolata*.
- LO of *Misceomarginatus quaternarius* (base UC16dBP): not present in published range charts; age assignment: upper Late Campanian; macrofossil zone: *B. lanceolata*.
- LO of *Broinsonia parca constricta* (base UC17): DSDP and ODP sites 217, 758, 761; age assignment: latest Campanian; macrofossil zone: *B. lanceolata*.
- LO of *Tranolithus orionatus* /LO of *Uniplanarius trifidus* (base UC18): Lagerdorf and Kronsmoor, DSDP and ODP sites 217, 401, 549, 550, 738, 758, 761; age assignment: upper Early Maastrichtian; macrofossil zone: *B. sumensis* - Zone 4.
- LO of *Biscutum coronum* (base UC18bAP): DSDP and ODP sites 217, 738, 758, 761; age assignment: upper Early Maastrichtian; macrofossil zone: *B. sumensis*.
- LO of *Reinhardtites levis* (base UC19): DSDP and ODP sites 401, 549, 550, 738, 761; age assignment: upper Early Maastrichtian; macrofossil zone: *B. sumensis* - Zone 5.
- FO of *Lithraphidites quadratus* (base UC20): DSDP and ODP sites 217, 401, 549, 550, 761; age assignment: lower Late Maastrichtian; macrofossil zone: *tegulatus/junior* - Zone 8.
- FO of *Nephrolithus frequens* (base UC20bBP): DSDP and ODP sites 217, 401, 549, 550, 761; age assignment: lower Late Maastrichtian; macrofossil zone: *argentea/junior* - Zone 8.
- FO of *Arkhangelskiella maastrichtiana* (base UC20cBP): DSDP and ODP sites 217, 761; age assignment: lower Late Maastrichtian; macrofossil zone: *argentea/junior* - Zone 8.
- FO of *Cribrosphaerella daniae* (base UC20dBP): DSDP and ODP sites 217, 761; age assignment: upper Late Maastrichtian; macrofossil zone: *baltica/danica* - Zone 10.
- FO of *Micula murus* (base UC20bTP): DSDP and ODP sites 217, 401, 549, 550, 761; age assignment: upper Late Maastrichtian; not identified in an MF-dated sequence.
- FO of *Ceratolithoides kamptneri* (base UC20cTP): DSDP Sites 217; age assignment: upper Late Maastrichtian; not identified in an MF-dated sequence.
- FO of *Micula prinsii* (base UC20dTP): DSDP sites 401, 550; age assignment: latest Maastrichtian; not identified in an MF-dated sequence.

2.5 Comparison between the four nannofossil zonations

The nannofossil zonations are here considered relative to the time scale of Gradstein et al. (2012) (Fig.2.5.1). Out of a total of 82 events used in the zonations by Sissingh (1977), Roth (1978) revised by Bralower et al. (1995) and Burnett (1988), ten bioevents are present in all zonations, namely: the FO of *E. turriseiffeli*, the FO of *C. kennedyi* [this species was defined by Crux (1981) after publication of Sissingh (1977) and Roth (1978) zonations and then added to Sissingh (1977) zonation by Perch-Nielsen (1985)], the FO of *M. staurophora*, the FO of *A. parcus parcus*, the FO of *C. aculeus*, the FO of *U. trifidus*, the LO of *U. trifidus*, the FO of *L. quadratus*, the FOs of *N. frequens* and *M. murus*.

The FO of *Q. gartneri* is used by all Authors except Bralower et al. (1995), although this bioevent was added by Tsikos et al. (2004) in a revised zonation following Roth's zones.

Four events are present in three zonations, namely: the FO of *L. acutus*, the LO of *H. chiastia*, the FO of *M. furcatus* and the LO of *R. levis*.

Most other zonal markers can be correlated between at least two zonations with the exception of six events (FO of *G. segmentatum*, FO of *R. biarcus*, FO of *L. septenarius*, LO of *L. septenarius*, FO of *A. cymbiformis*, FO of *M. pleniporus*) adopted exclusively by Burnett (1998); two events (FO of *M. decoratus*, LO of *M. furcatus*) are used exclusively by Sissingh (1977), and one (LO of *R. asper*) in the zonation of Bralower et al. (1995) (Tab.2.2, Appendix 5, see CD attached).

Looking at the resolution, it is possible to notice that Roth (1978) and Bralower et al. (1995) adopted less bioevents to separate their zones and subzones compared to Sissingh (1977) and Burnett (1998). Burnett (1998) added numerous events observed in the North Sea area, trying to achieve a higher stratigraphic resolution expecially of time intervals characterized by few nannofossil events such as the Early Cenomanian and the Late Campanian. It is also interesting to notice the high number of bioevents reported in the Cenomanian/Turonian boundary interval. (Fig.2.5.1). For the Early Turonian to Late Campanian time interval, zonations of Sissingh (1977) and Burnett (1998) are comparable, probably because Burnett (1998) incorporated in her zonation the data presented by Sissingh (1977) and Perch-Nielsen (1985). The resolution of the zonation of Roth (1978) revised by Bralower et al. (1995), remains lower except in the Cenomanian/Turonian boundary interval and in the Maastrichtian.

The zonation of Burnett (1998) include the majority of the events present in the other zonations with the exception of few zonal and some subzonal markers, namely: the LO of *R. asper* and the

FO of *K. magnificus* in the Turonian; the FO of *C. obscurus* and the LO of *E. floralis* in the Santonian; the LOs of *M. furcatus*, *B. hayi*, *L. grillii* and the FO and LO of *C. arcuatus* in the Early-Middle Campanian.

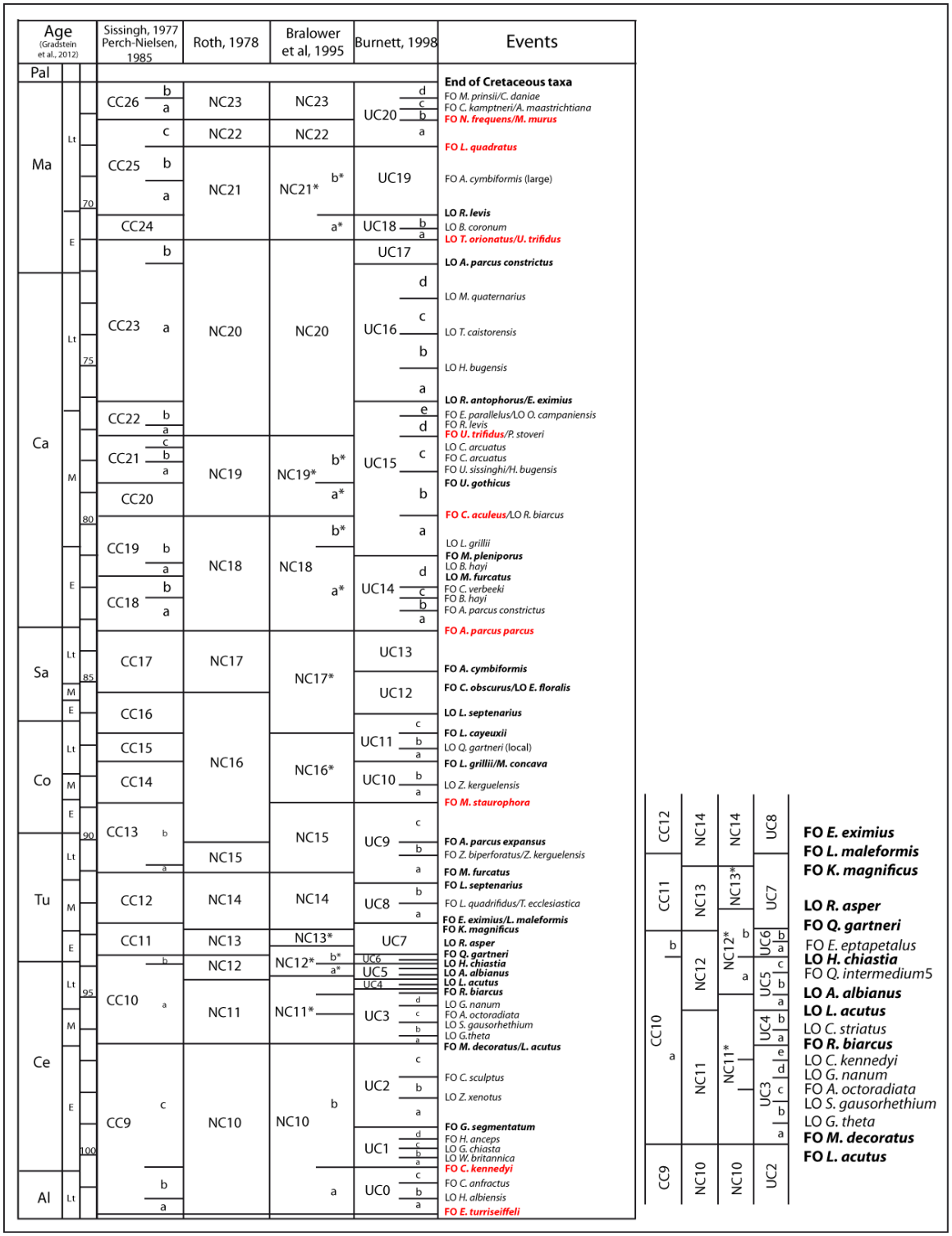

Fig.2.5.1 Correlation between zonations of Sissingh (1977), Roth (1978), Bralower et al. (1995) and Burnett (1998). Nannofossil events adopted by all Authors are marked in red. Time scale after Gradstein et al. (2012)

Chapter 3

Materials and methods

3.1 Studied sections

To perform this study, samples from different parts of the world have been analyzed in order to assess nannofossil biostratigraphy in various sedimentary basins across latitudes (Fig.3.1.1): Mid-Pacific Mountains (DSDP Leg 62, Site 463), Exmouth Plateau (ODP Leg 122, Site 763), Kerguelen Plateau (ODP Leg 183, Site 1138), Demerara Rise (ODP Leg 207, Site 1261), Umbria-Marche Basin (Monte Petrano), Vocontian Basin (Clote de Chevalier), Western Interior Basin (Pueblo), and Tarfaya Basin (Tarfaya Core). The stratigraphical interval sampled with individual section is shown in Fig.3.1.2.

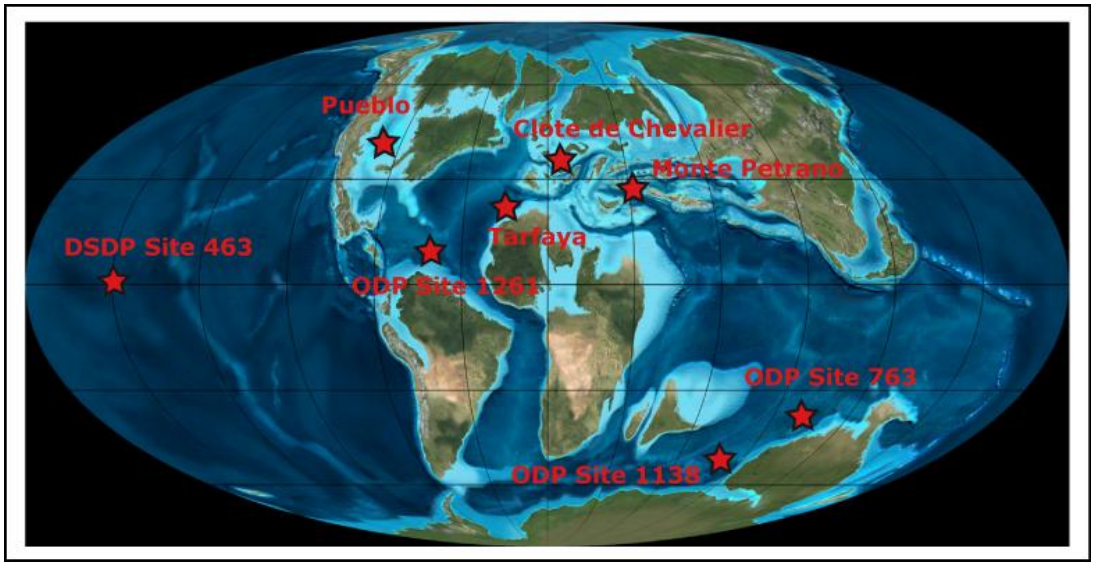

Fig.3.1.1: Location of the studied sections in a paleogeographic reconstruction at 90 Ma (Time Scale Creator, https://engineering.purdue.edu/Stratigraphy/tscreator/index/index.php)

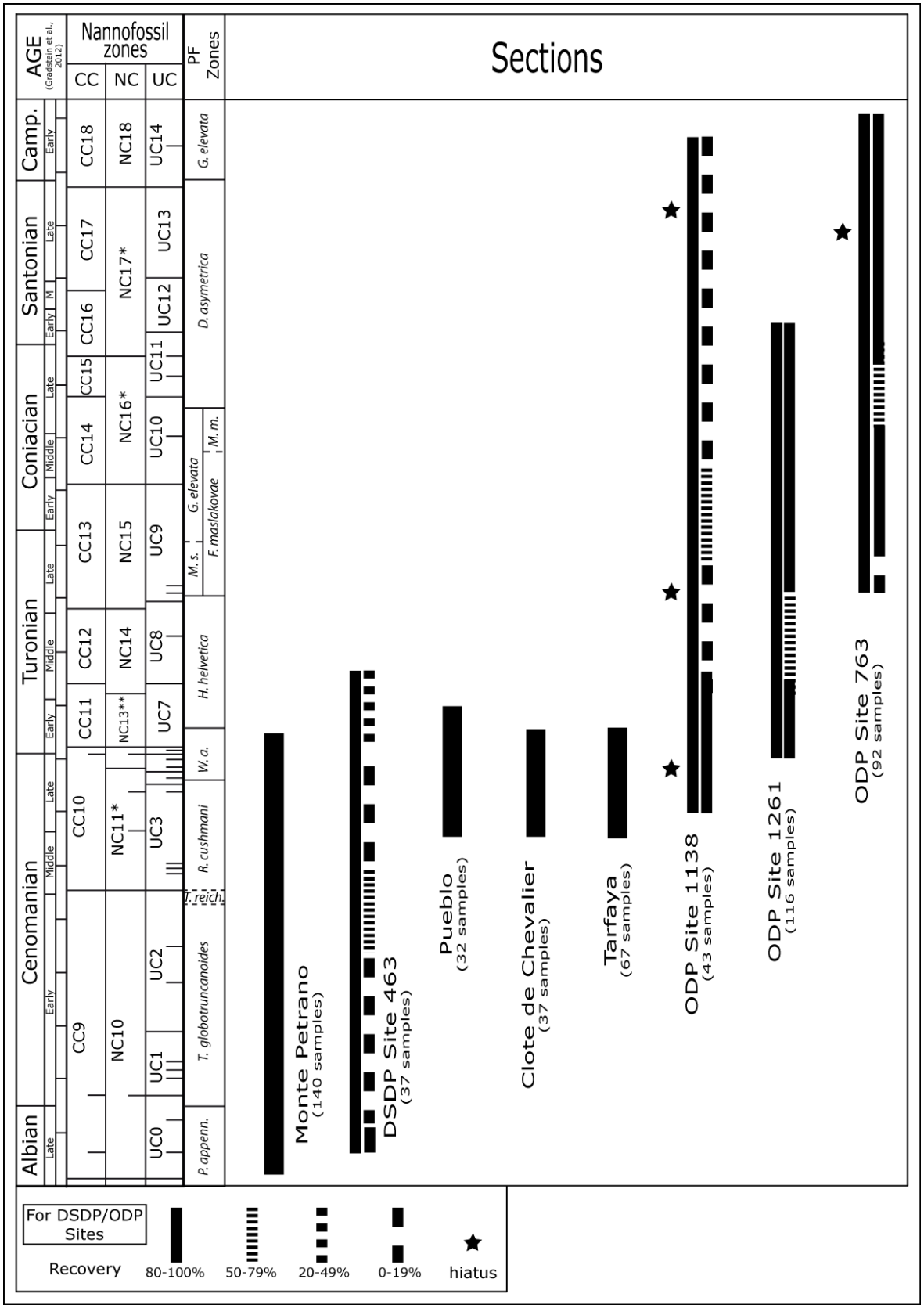

Fig.3.1.2: Summary of the stratigraphic intervals studied

3.2 Sample preparation technique

Calcareous nannofossil biostratigraphic investigation has been performed on a total of 564 smear slides analyzed using standard light microscope techniques under cross polarizers and transmitted light at 1250X magnification. Smear slides from DSDP Site 463, ODP Site 1261, Clote de Chevalier, Pueblo and Tarfaya Core were already available at the University of Milan. A total of 275 smear slides were prepared following the procedures described in Perch-Nielsen (1985) and Bown & Young (1998b). Two different methodologies have been used:

- Samples from ODP Site 1138 and Monte Petrano were prepared powdering into a mortar a small amount of rock material with few drops of bi-distilled water and posed onto a glass coverslip. Using a toothpick, the suspension was repeatedly smeared along the coverslip until the required thickness of smear is achieved and dried rapidly on a hotplate. The coverslip was affixed to a glass slide with Norland Optical Adhesive, and cured by exposure to UV light for a few minutes.
- Samples from ODP Site 763, almost entirely consisting of chalk, were prepared scraping a few grams of rock from a cleaned sample-surface onto a glass cover-slip. After adding a drop of bi-distilled water the suspension was treated as described above.

3.3 Preservation and abundance analysis

Abundances of all the nannofossil taxa identified in this study, provided on the nannofossil range-charts, were determined over two traverses of each slide and coded as follows (Bown & Young, 1998b; Lees, 2002):

A = abundant (more than 11 specimens per field of view)
C = common (1-10 specimens per field of view)
F = few to frequent (1 specimen per 2-20 fields of view)
R = rare (1 specimen per more than 20 fields of view)

Due to calcite dissolution and/or overgrowth, preservation of calcareous nannofossils may vary significantly. Thus, to characterize preservation, a simple code system has been adopted as described (Lees, 2002; Tremolada, 2002):

VG = very good preservation (no evidence of dissolution and/or overgrowth, no alteration of primary morphological characteristics. All specimens are identifiable to the species level)

G = good preservation (little or no evidence of dissolution and/or overgrowth, primary morphological characteristics only slightly altered, most specimens are identifiable to the species level)

M = moderate preservation (some evidence of dissolution and/or overgrowth, primary morphological characteristics somewhat altered, most specimens are identifiable to the species level)

P = poor preservation (overgrowth and/or dissolution is extensive, making identification of some specimens difficult)

VP = very poor preservation (severely etched and/or overgrown, primary morphological characteristics largely destroyed, fragmentation has occurred, and specimens are often unidentifiable at the species and/or generic level)

Estimates of the total calcareous nannofossil abundance, compared to that of other biogenic particles and inorganic components, were recorded as follows (Lees, 2002; Tremolada, 2002, Hardas & Mutterlose, 2006):

H = high (more than 51% of all particles)

M = moderate (11%-50% of all particles)

L = low (1%-10% of all particles)

VL = very low (less than 1% of all particles)

Chapter 4

Results

4.1 Monte Petrano – Italy

Geographical setting and lithology

The Monte Petrano section is located not far from the top of the Petrano Mountain and the Moria village (43°30’24.89’’N, 12°36’49.02’’E) in the Umbria-Marche Basin (Fig.4.1.1). The Mesozoic Umbria-Marche Basin is exposed in the Central Apennines fold and thrust belt and evolved from a carbonate shelf setting in Triassic-Early Jurrassic time into a pelagic environment which extended to the Paleogene (Alvarez et al., 1977).

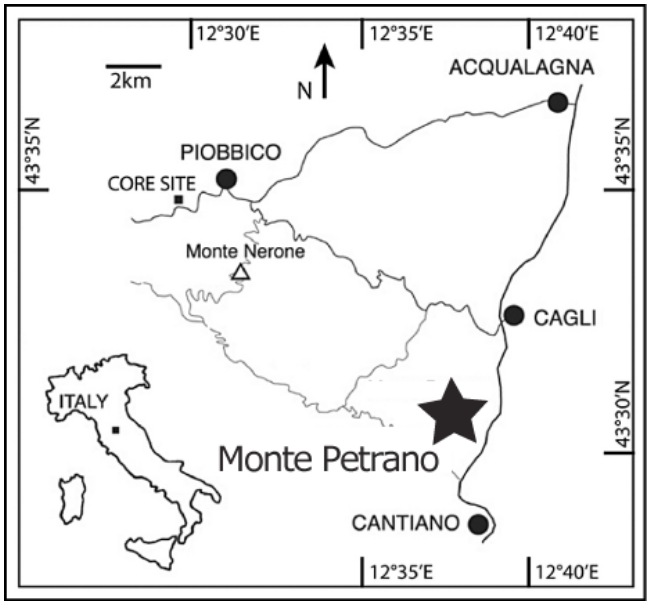

Fig.4.1.1: Location of Monte Petrano section – Italy
(after Giorgioni et al., 2012)

The studied interval is 70 m thick and corresponds to the so called Scaglia Bianca Formation, a calcareous pelagic sequence resulting from lithification of nannofossil-planktonic foraminiferal oozes deposited at a water depth of about 1500-2000m (Arthur and Premoli Silva, 1982; Kuhnt,

1990). It consists mostly of yellowish gray limestones, with a few pink to reddish limestone beds, numerous chert bands, and several black marlstone layers (Gambacorta, 2014). The most prominent feature of this section is the presence of organic-rich black shales constituting the Bonarelli Level that represents the Oceanic Anoxic Event 2 (OAE 2). Studied samples were collected by Gambacorta (2014) for his Ph.D. thesis.

Previous studies

This outcrop has never been studied in detail, except for its lowermost part studied by Giorgioni et al. (2012). They presented a high-resolution carbonate carbon isotope record of the Albian interval of the Marne a Fucoidi Formation (Central Apennines, Italy) which underlies the Scaglia Bianca Formation.

Results

Nannofossil investigation was performed on 140 samples from the interval between 0 and 70 m above the base of the Scaglia Bianca Formation. I produced a semi-quantitative range chart of all taxa (Tab.4.1, Appendix 6, see CD attached). Preservation of nannofossils is generally poor-moderate and total abundance varies from very low to medium. Zonal and subzonal markers identified are listed below from the oldest to the youngest:

- FO of *M. decoratus* (sample MP24; 24 m above the base of the Scaglia Bianca Formation)
- FO of *C. sculptus* (sample MP33.5; 33.5 m above the base of the Scaglia Bianca Formation)
- FO of *C. kennedyi* (sample MP34; 34 m above the base of the Scaglia Bianca Formation)
- FO of *H. anceps* (sample MP34.5; 34.5 m above the base of the Scaglia Bianca Formation)
- FO of *L. acutus* (sample MP38; 38 m above the base of the Scaglia Bianca Formation)
- LO of *S. gausorhethium* (sample MP47.5; 47.5 m above the base of the Scaglia Bianca Formation)
- LO of *C. kennedyi* (sample MP65; 65 m above the base of the Scaglia Bianca Formation, uppermost sample before the Bonarelli Level)
- LO of *A. albianus* (sample MP65; 65 m above the base of the Scaglia Bianca Formation, uppermost sample before the Bonarelli Level)
- LO of *L. acutus* (sample MP65; 65 m above the base of the Scaglia Bianca Formation, uppermost sample before the Bonarelli Level)
- LO of *H. chiastia* (sample MP65; 65 m above the base of the Scaglia Bianca Formation, uppermost sample before the Bonarelli Level)
- FO of *Q. intermedium*-5 (sample MP66.5; 66.5 m above the base of the Scaglia Bianca Formation, lowermost sample above the Bonarelli Level)

- FO of *Q. gartneri* (sample MP66.5; 66.5 m above the base of the Scaglia Bianca Formation, lowermost sample above the Bonarelli Level)
- FO of *E. eptapetalus* (sample MP68; 68 m above the base of the Scaglia Bianca Formation)

All these events were used to determine biozones and subzones after the three zonations adopted (Fig.4.1.2). In particular:

Following Burnett (1998), zones and subzones UC0-UC3d and UC7 were recognized. The absence of carbonate in the Bonarelli Level prevented the identification of zones and subzones UC3e-UC6. UC0a/UC0b and UC0b/UC0C subzonal boundaries were approximated using the total range of *C. stenostaurion* as reported by Burnett (1998). Rarity of subzonal marker *G. chiasta* prevented the placement of the UC1b/UC1c boundary. The FO of *H. anceps* allowed to place UC1a-c/UC1d-2 subzonal boundary. *G. segmentatum* occurs above FO of *Q. gartneri*, at a higher level than reported by Burnett (1998), thus preventing the placement of UC1d/UC2 boundary. *Z. xenotus* and *G. nanum* were not recorded in the studied interval, their absence prevented the subdivision of subzones UC2a/UC2b and UC3c/UC3d. *C. sculptus* occurs below the FO of *C. kennedyi*, at a lower level than reported by Burnett (1998), thus preventing the placement of UC2b/UC2c boundary.

Following Bralower et al. (1995), zones and subzones NC10-NC11* and NC12b*-NC13** were identified. The absence of carbonate in the Bonarelli Level prevented the identification of zone NC12a*.

Following Sissingh (1977), zones CC9-CC11 were identified. Zonal marker *M. decoratus* has its FO below FO of *C. kennedyi*, at a lower level than reported by Sissingh (1977) and Perch-Nielsen (1985), thus preventing the placement of CC9b/CC9c subzonal boundary. Burnett (1998) noticed that a thin form of *M. decoratus* occurs sporadically in the Albian.

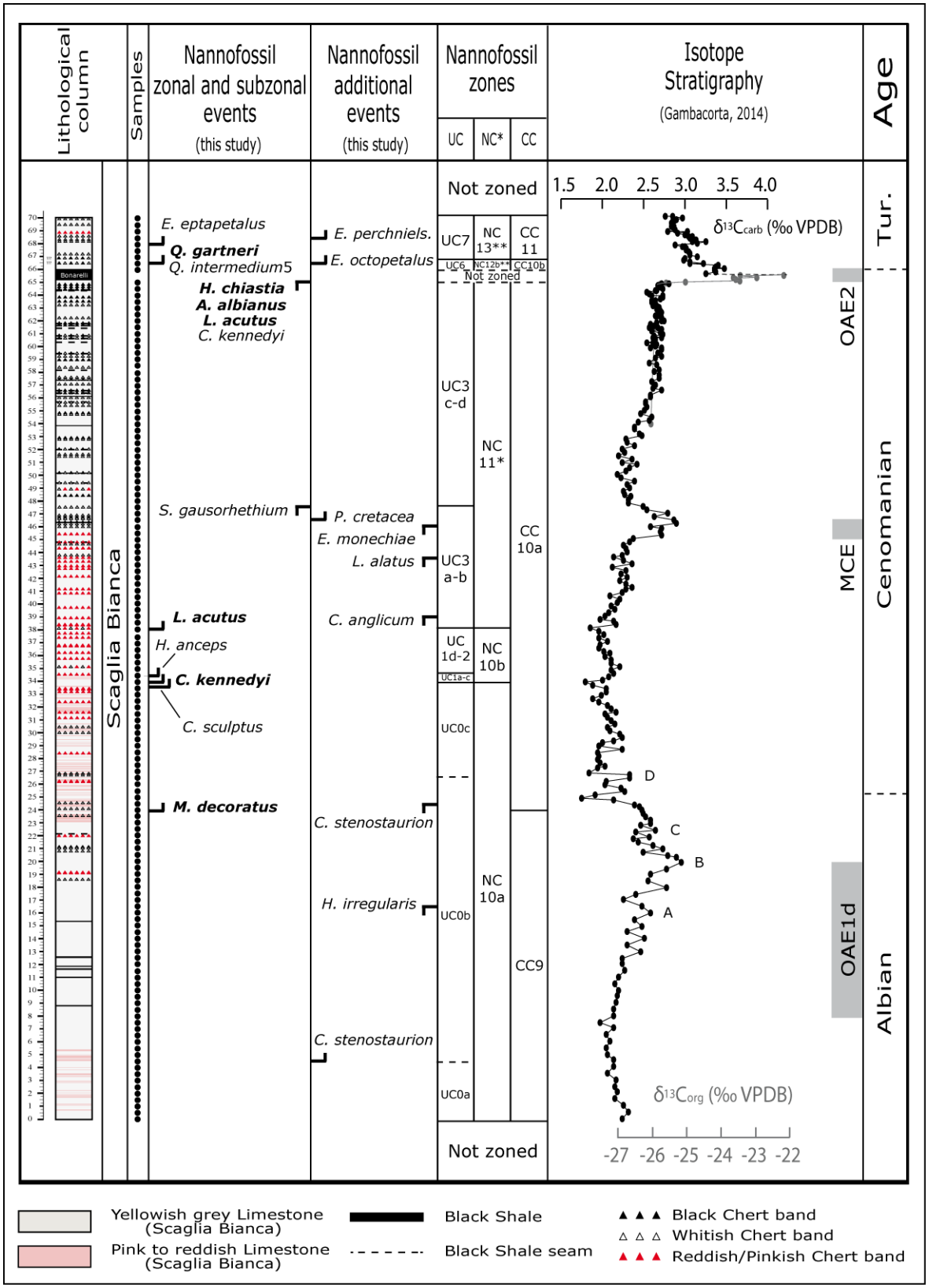

Fig.4.1.2: Calcareous nannofossil bioevents and zones/subzones of the Monte Petrano section. Lithostratigraphy and isotope stratigraphy after Gambacorta (2014)

Calcareous nannofossil assemblages

A total of 110 taxa were observed in the studied section. Based on semiquantitative abundances, nannofossil assemblages were characterized to separate the following intervals, from oldest to youngest:

Interval A: from sample MP0 to sample MP33.5. The first part of this interval (samples MP0 to MP12) shows an assemblage characterized by a low number of calcareous nannofossils and only few taxa occurs frequently: *B. constans* and *W. barnesiae* are the most common taxa and frequent *R. crenulata, R. achlyostaurion, W. manivitiae* and *Z. diplogrammus* are present. Moving upwards *B. constans, W. barnesiae, W. manivitiae* become common and become the dominant taxa. Frequent *C. nudus, E. turriseiffelii, R. crenulata, R. achlyostaurion, Z. diplogrammus* and rare to frequent *E. gorkae, D. ignotus, R. surirella, T. orionatus* and *Z. embergeri* were observed. *C.* cf. *C. percensis, C. ehrenbergii, H. chiastia, M. pemmatoidea, R. angustus, R. asper, W. biporta* and *Z. howei* are rare but occur regularly in the assemblage.

Interval B: from sample MP34 to sample MP40. This interval is still dominated by the same taxa of Interval A, but an increase in abundance of *E. floralis, L. carniolensis* and *R. angustiforata* was observed. *A. terebrodentarius, C. kennedyi* and *C. sculptus* start to occur in the assemblage in this interval.

Interval C: from sample MP40.5 to sample MP65. *B. constans, W. barnesiae, W. manivitiae* remain the dominant taxa, but large specimens of *B. constans* become rarer and more sporadic as well as *D. ignotus, R. angustus* and *Z. noeliae*. *C. nudus, E. turriseiffelii, R. crenulata, R. achlyostaurion, Z. diplogrammus* are still frequent.

Bonarelli Level: without carbonate.

Interval D: from sample MP66.5 to the top of the studied section. *W. barnesiae* and *W. manivitiae* are the dominant taxa. A sharp decrease in abundance is recorded principally by *B. constans* but also *R. surirella, R. achlyostaurion* and *R. asper*. Frequent *E. floralis, Z. diplogrammus* and rare to frequent *A. terebrodentarius, C. nudus, E. turriseiffelii, E. octopetalus, P. cretacea, P. ponticula, R. crenulata, Z. embergeri* and *Z. howei* were observed.

Chronostratigraphy

Stage boundaries were placed using calcareous nannofossil events and $\delta^{13}C$ isotopic stratigraphy presented by Gambacorta (2014). The comparison is summarized in Fig.4.1.2:

The Albian/Cenomanian boundary was placed following the $\delta^{13}C$ anomaly as discussed for the Cenomanian GSSP at Mont Risou (France) by Kennedy et al. (2004).

As discussed by Tsikos et al. (2004) the Cenomanian/Turonian boundary, in absence of ammonite biostratigraphy, can be placed using the $\delta^{13}C$ isotopic anomaly across OAE2. Specifically, at the GSSP Pueblo section, the base of the Turonian closely correlates with the end of the C isotopic plateau phase. In practice the "C" peak closely follows the Cenomanian/Turonian boundary. Also the FO of *Q. gartneri* has been proved to occur in the basal Turonian (e.g. Tsikos et al., 2004).

4.2 DSDP Site 463

Geographical setting and lithology

DSDP Site 463 is situated in the western part of the Mid-Pacific Mountains (21°21.01' N; 174°40.07' E; present water depth 2525 m, Fig.4.2.1). The Mid-Pacific Mountains consist of several segments thought to be part of an ancient fracture-zone-ridge-crest system that separated the North and South Pacific Plates during the Early Cretaceous and constitute one of the large aseismic rises in the central and northern Pacific Ocean (Larson, 1976).

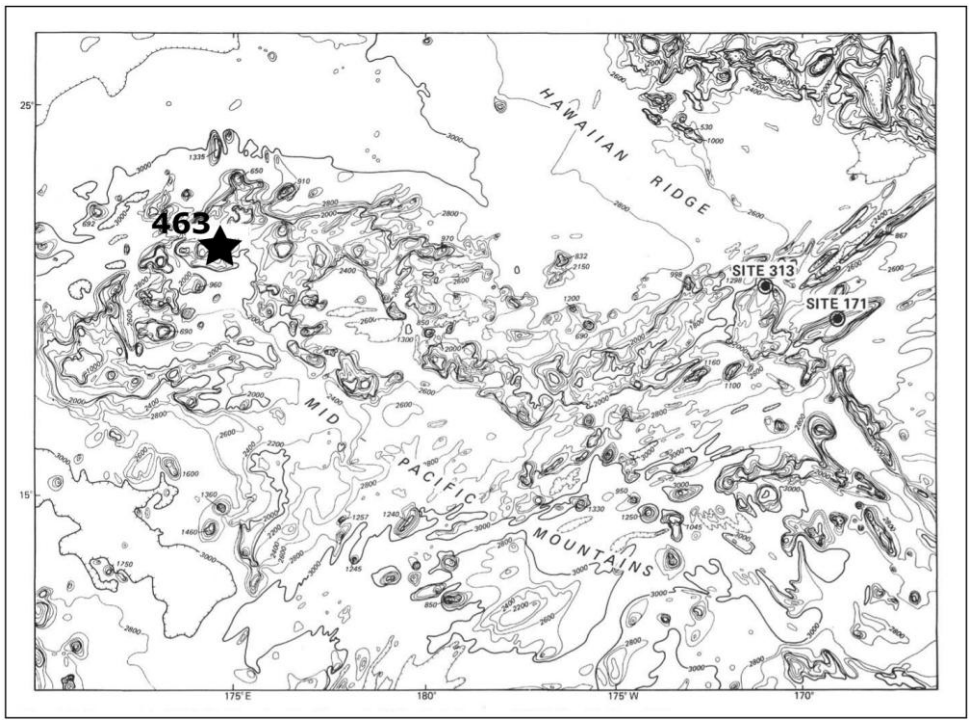

Fig.4.2.1: Location of DSDP Site 463. Other sites drilled on the Mid-Pacific Mountains are also reported (Shipboard Scientific Party, 1981)

At DSDP Site 463 a 822 m-thick sequence of Pleistocene to Barremian sediments was recovered; the igneous basement was not reached. The studied interval goes from 252 to 424 mbsf, of middle Turonian to latest Albian age (Shipboard Scientific Party, 1981). The Cretaceous

sediments analyzed in this work belong to the lithologic Subunit IB, consisting of white to very light grey foraminifer and nannofossil-bearing chalk (Shipboard Scientific Party, 1981).

Previous studies

Previous studies on nannofossils of DSDP Site 463 were presented in the Volume of Leg 62 by Čepek (1981) and Roth (1981). Čepek (1981) performed a biostratigraphic study on Mesozoic calcareous nannoplankton of DSDP Site 463 recognizing a Turonian to Santonian assemblage from Core 25 to Core 37, but zones were not identified for the lack of index species. A latest Albian to Cenomanian interval was recognized in Cores 38 to 50 and assigned to the *Lithraphidites alatus* nannofossil zone as defined by Roth (1973) and modified by Čepek (1981) himself. Roth (1981) presented a study on paleoceanographic implications of mid-Cretaceous calcareous nannoplankton recovered during Leg 62. He also suggested that Cores 38 to 48 belong to his NC11 zone of latest Albian to basal Turonian age. Foraminiferal investigation was performed by Boersma (1981), who described faunas occurring at DSDP Site 463. Sliter (1995) compared the Cretaceous record of sites drilled during ODP Leg 143 to sequences recovered at selected sites in the central Pacific Ocean. He noticed a similar pattern of pelagic sedimentation and determined hiatuses in the Albian/Cenomanian boundary interval, in the Middle Cenomanian and in the Late Turonian.

Results

Nannofossil investigation was performed on 37 samples from the interval between 424.67 and 252.78 mbsf. I produced a semi-quantitative range chart of all taxa (Tab.4.2, Appendix 7, see CD attached). Preservation of nannofossils is generally moderate and total abundance varies from medium to high. Zonal and subzonal markers identified are listed below from the oldest to the youngest:

- LO of *G. chiasta* (sample 62-463-48-1, 51-53; 424.01 mbsf)
- FO of *C. sculptus* (sample 62-463-43-5, 63-65; 382.63 mbsf)
- FO of *L. acutus* (sample 62-463-43-5, 63-65; 382.63 mbsf)
- LO of *S. gausorhethium* (sample 62-463-43-1, 20-22; 376.20 mbsf)
- LO of *C. striatus* (sample 62-463-43-1, 20-22; 376.20 mbsf)
- FO of *Q. intermedium*-5 (sample 62-463-43-1, 20-22; 376.20 mbsf)
- FO of *M. decoratus* (sample 62-463-38-1, 3-6; 328.53 mbsf)
- LO of *A. albianus* (sample 62-463-38-1, 3-6; 328.53 mbsf)
- LO of *L. acutus* (sample 62-463-38-1, 3-6; 328.53 mbsf)
- LO of *H. chiastia* (sample 62-463-38-1, 3-6; 328.53 mbsf)
- FO of *R. biarcus* (sample 62-463-35-1, 1-3; 300.01 mbsf)
- FO of *E. eptapetalus* (sample 62-463-35-1, 1-3; 300.01 mbsf)

- FO of *Q. gartneri* (sample 62-463-35-1, 1-3; 300.01 mbsf)
- LO of *R. asper* (sample 62-463-33-1, 89-91; 281.89 mbsf)
- FO of *E. eximius* (sample 62-463-30-2, 33-35; 254.33 mbsf)

All these events have been integrated with previous data presented by Čepek (1981) to determine biozones and subzones after the three zonations adopted (Fig.4.2.2). In particular:

Following Burnett (1998), zones and subzones UC0, UC3a-b, UC5a and UC7-8a were recognized. Scarcity of recovery made impossible a better accuracy and other zonal boundaries (zones and subzones) were approximated.

Following Bralower et al. (1995), all the zonal markers were recognized and zones NC10-NC13** were identified. As far as subzones are concerned, the absence of *C. kennedyi* in the studied interval prevented the subdivision of zone NC10 into subzones NC10a and NC10b.

Following Sissingh (1977), all the zonal and subzonal markers were recognized and zones CC9-CC12 were identified.

Calcareous nannofossil assemblages

In total 135 species of calcareous nannofossil were observed in the studied section. Based on semiquantitative abundances, nannofossil assemblages were characterized to separate the following intervals, from oldest to youngest:

Interval A: from sample 62-463-48-1, 117-126 to sample 62-463-38-1, 3-6. The assemblage is characterized by common to abundant *B. constans, W. barnesiae, W. manivitiae,* representing the dominant taxa, and frequent to common *C. ehrenbergii, C. nudus, E. turriseiffelii, P. columnata, R. crenulata, R. surirella, R. achlyostaurion* and *Z. diplogrammus.* Other frequent taxa are *E. gorkae, E. floralis, L. carniolensis, M. pemmatoidea, P. ponticula, R. angustus, R. asper, T. orionatus* and *Z. embergeri.* Core 48 contains rare to frequent *C. stenostaurion, G. chiasta, L. alatus* and *S mutterlosei*.

Interval B: from sample 62-463-35-1, 1-3 to the top of the studied interval. This interval is still dominated by *W. barnesiae* with common *P. cretacea* and frequent to common *E. turriseiffelii, E. floralis, P. ponticula, R. crenulata* and *W. manivitiae.* A sharp decrease in abundance of *B. constans, C. ehrenbergii, F. oblongus* and *R. surirella* is noticed. *A. terebrodentarius, B. ambiguus, C. exiguum, E. eptapetalus, M. decoratus,* and *Q. gartneri* become consistently present and frequent in the assemblage. From Core 30 upwards frequent *E. eximius* occur in the assemblage.

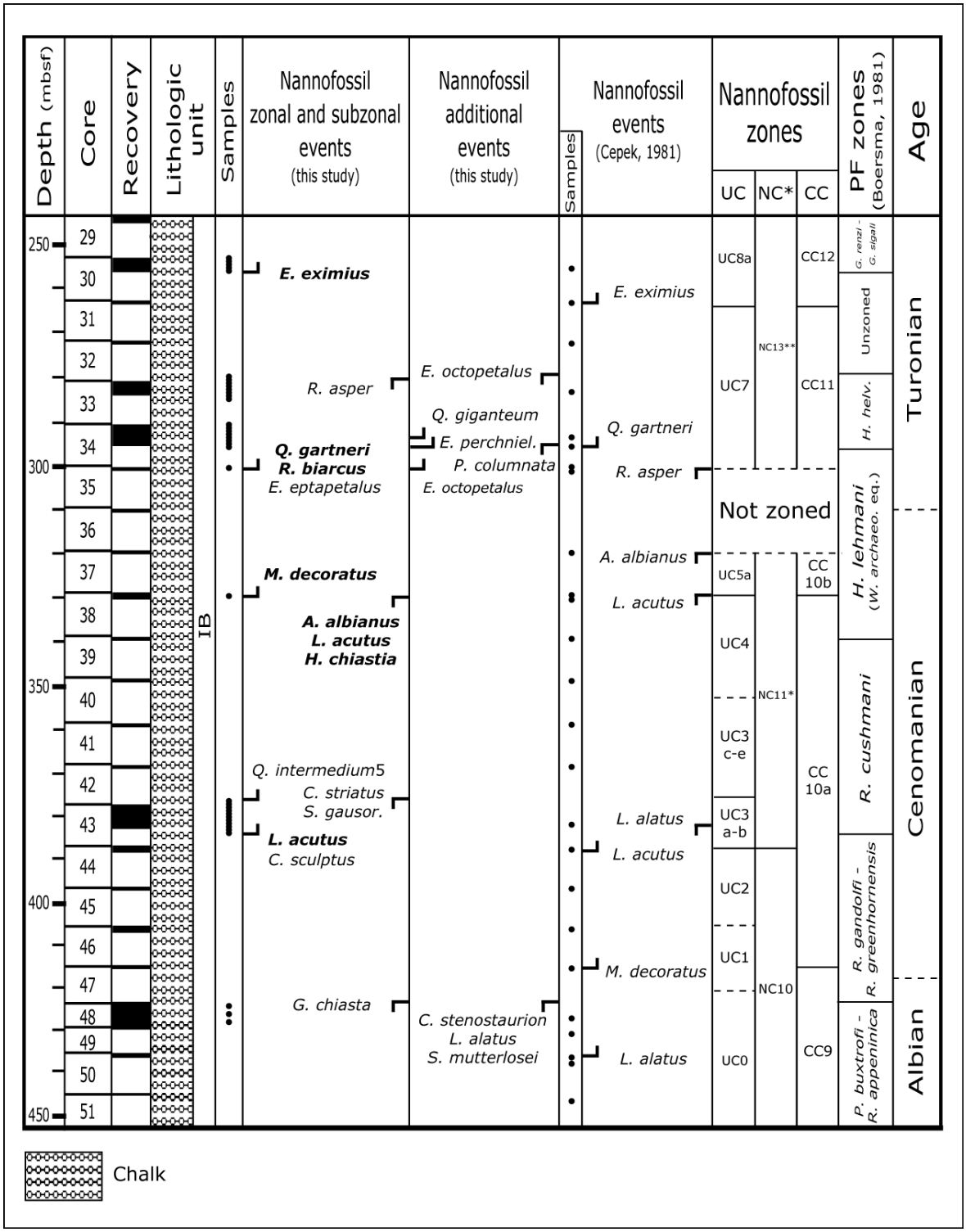

Fig.4.2.2: Calcareous nannofossil bioevents and zones/subzones at DSDP Site 463. Lithostratigraphy after Shipboard Scientific Party (1981); planktonic foraminiferal zones after Boersma (1981)

Chronostratigraphy

To place stage boundaries I integrated my own data with those presented by Čepek (1981) and Boersma (1981). The comparison is summarized in Fig.4.2.2:

The Albian/Cenomanian boundary was placed between FO of *R. gandolfi* and FO of *M. decoratus.* FO of *R. gandolfi* was reported below the Albian/Cenomanian boundary at the GSSP section for the base of the Cenomanian Stage (Kennedy et al., 2004).

The Cenomanian/Turonian boundary was placed at the FO of *Q. gartneri* as suggested by Tsikos et al. (2004). End of rotaliporids, in Core 38, is another useful datum to place the Cenomanian/Turonian boundary in the *H. lehmani* zone (zonation of Van Hinte, 1976) which corresponds to the *W. archaeocretacea* zone (Bolli, 1966; Caron, 1985; Kennedy et al., 2005).

4.3 Rock Canyon – Pueblo

Geographical setting and lithology

The Rock Canyon section is located in south central Colorado near Pueblo, along the Arkansas River (Fig.4.3.1). During the Cretaceous, this location layed in the Western Interior Seaway, a shallow inland sea that extended from the Gulf of Mexico to the Arctic Ocean, with water depths ranging to about 1500 m (Kauffman & Caldwell, 1993; Kennedy et al., 2005).

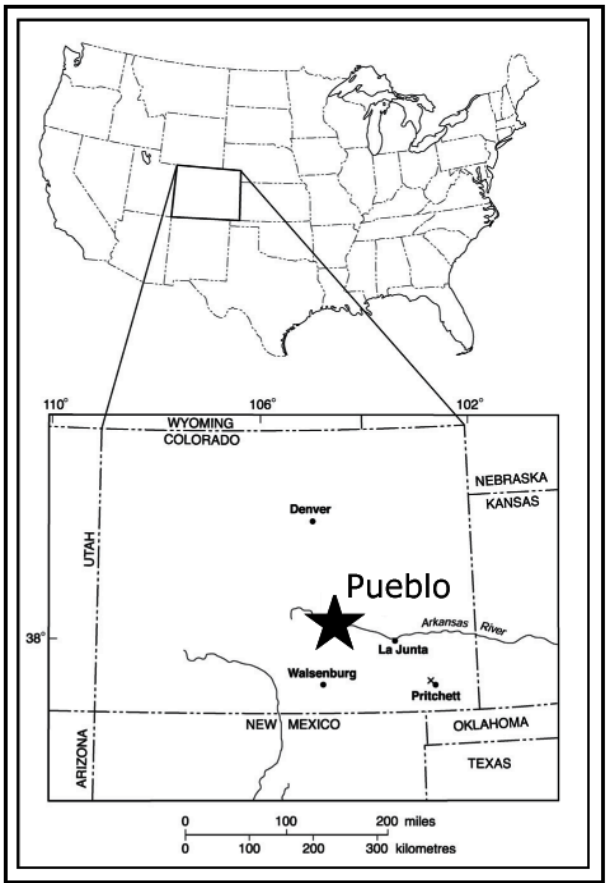

Fig.4.3.1: Location of Rock Canyon section near Pueblo - Colorado (after Kennedy et al., 2005)

The studied interval corresponds to the Bridge Creek Limestone Member of the Greenhorn Limestone Formation and consists in 10.20 m of gray shaly limestones, interbedded with calcareous shale and bentonite layers (Kennedy et al., 2000; 2005). Studied samples were collected by Snow et al. (2005) for their work on trace element abundances in the Rock Canyon Anticline.

Previous studies

The section at the Rock Canyon Anticline was ratified in 2003 as the global boundary stratotype section and point (GSSP) for the base of the Turonian Stage on account of its completeness and well-established bio- and chemostratigraphy (Kennedy et al., 2005). Previous studies on nannofossils in the Pueblo section were published by Watkins (1985), Bralower (1988) and Watkins et al. (1993). Watkins (1985) performed a biostratigraphic and paleoecological study, highlighting that the Bridge Creek Member belongs to the *L. acutum-Q. gartneri* zones of Manivit et al. (1977). He noticed also the scarcity of several biostratigraphically important taxa, suggesting that fresh-water influx was an important factor in restricting nannofossil occurrence and diversity. Bralower (1988) studied the Cenomanian/Turonian boundary interval in numerous sections from Europe, North America and Tunisia. He proposed a detailed nannofossil zonation for this interval consisting of three zones, two subzones and nine additional biohorizons. At Rock Canyon, he reported the FO of *Q. gartneri* well below the beginning of the isotopic positive shift of the $\delta^{13}C$ anomaly. Watkins et al. (1993) presented a synthesis of nannofossil studies of the Western Interior Basin, recognizing eight biostratigraphic events occurring across the Cenomanian/Turonian boundary. Tsikos et al. (2004) placed the FO of *Q. gartneri* at Pueblo, just above the end of the positive shift of $\delta^{13}C$, in the lowermost Turonian.

Results

Nannofossil investigation was performed on 32 samples from the interval between 30 and 1020 cm from the base of the Bridge Creek Limestone Member. I produced a semi-quantitative range chart of all taxa (Tab.4.3, Appendix 8, see CD attached). Preservation of nannofossils is generally poor to moderate and total abundance varies from very low to medium. Zonal and subzonal markers identified are listed below, from the oldest to the youngest:

- LO of *C. striatus* (sample RC50, 0.5 m above the base of the Bridge Creek Limst. Member)
- LO of *H. chiastia* (sample RC400, 4 m above the base of the Bridge Creek Limst. Member)
- FO of *Q. gartneri* (sample RC500, 5 m above the base of the Bridge Creek Limst. Member)
- FO of *E. eptapetalus* (sample RC670, 6.7 m above the base of the Bridge Creek Limst. Member)
- LO of *R. asper* (sample RC870, 8.7 m above the base of the Bridge Creek Limst. Member)

All these events have been integrated with previous data presented by Watkins (1985), Bralower (1988) and Tsikos et al (2004) to determine biozones and subzones after the three zonations adopted (Fig.4.3.2). In particular:

Following Burnett (1998), all the zonal markers were recognized and zones UC4-UC7 were identified. Only in zone UC4 subzonal boundary event could be identified. The absence of *A. albianus* and *Q. intermedium*-5 in my samples prevented the subdivision of zone UC5 into subzones UC5a, UC5b and UC5c. LO of *A. albianus* was recorded by Bralower (1988) and Tsikos et al. (2004) below LO of *L. acutus*, this sequence of events is different relative to the scheme of Burnett (1998). FO of *E. eptapetalus* occurs above FO of *Q. gartneri*, higher than reported by Burnett (1998), thus preventing the placement of UC6a/Uc6b subzonal boundary.

Following Bralower et al. (1995), all the zonal and subzonal markers were identified and zones NC11-NC13** were identified.

Following Sissingh (1977), all the zonal and subzonal markers were identified and zones CC10-CC11 were identified.

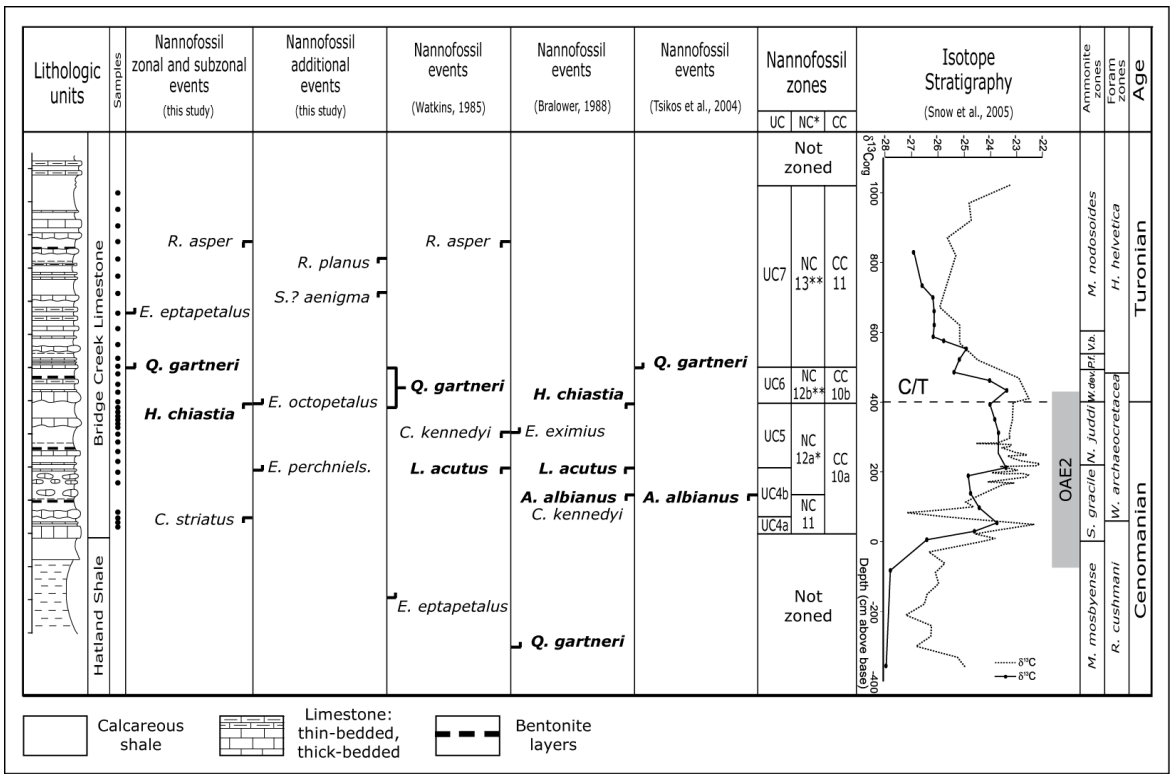

Fig.4.3.2: Calcareous nannofossil bioevents and zones/subzones of the Rock Canyon section. Lithostratigraphy, ammonites and planktonic foraminiferal zones and ages after Kennedy et al. (2005); isotope stratigraphy after Snow et al. (2005)

Calcareous nannofossil assemblages

A total of 108 taxa were observed in the studied section. Based on semiquantitative abundances, nannofossil assemblage can be separated in the following intervals, from oldest to youngest:

Interval A: from sample RC30 to sample RC400. The assemblage comprises frequent to common *B. constans, P. cretacea, W. barnesiae, W. manivitiae*, rare to frequent *D. ignotus, E. gorkae, E. turriseiffelii, E. floralis, H. trabeculatus, P. columnata, P. ponticula, R. angustiforata, R. crenulata, R. surirella, R. achlyostaurion, T. minimus, T. orionatus, T. salillum, Z. diplogrammus, Z. embergeri, Z. howei, Z. scutula*.

Interval B: from sample RC420 to sample RC570. The assemblage is similar to that of Interval A, but an increase in the relative abundance of *H. trabeculatus* and *P. columnata* was observed.

Interval C: from sample RC670 to the top of the studied interval. The assemblage is still dominated by the same taxa of Intervals A and B, although it records an increase in the relative abundance of *C. ehrenbergii, G. segmentatum, T. minimus,* whilst *Z. embergeri* becomes rarer.

Chronostratratigraphy

The Cenomanian/Turonian boundary was placed 4 m above the base of the Bridge Creek Limestone Member, at the lowest occurrence of the ammonite *Watinoceras devonense* (boundary event for the base of the Turonian) as reported by Kennedy et al. (2005) and Snow et al (2005).

4.4 Clote de Chevalier – France

Geographical setting and lithology

Calcareous nannofossil biostratigraphic investigations of Clote de Chevalier section are part of an integrated litho-, chemo- and biostratigraphic study of this section located in the Vocontian Basin (France). The study is still on going, and no informations about lithostratigraphy are available. Samples were provided by Hugh Jenkyns (Dept. of Earth Sciences, Oxford University, UK) to E. Erba and M.R. Petrizzo (Univ. of Milan) to investigate nannofossil and planktonic foraminiferal biostratigraphy. The Vocontian Basin forms a part of the hemipelagic intrashelf basin of the European Tethyan passive margin (Wilpshaar et al., 1997). Major tectonic changes occurred in this basin at the beginning of the Late Cretaceous, with transition from dominant extensional regime until the Albian, to dominant compression or transpression from the Cenomanian (e.g. Fries and Parize, 2003).

Results

Nannofossil investigation was performed on 37 samples from an interval of 34.80 m. I produced a semi-quantitative range chart of all taxa (Tab.4.4, Appendix 9, see CD attached). Preservation of nannofossils is generally poor-moderate to moderate and total abundance varies from low-medium to medium-high. Zonal and subzonal markers identified are listed below from the oldest to the youngest:

- LO of *C. kennedyi* (sample slt360; 3.6 m)
- FO of *R. biarcus* (sample slt480; 4.8 m)
- LO of *C. striatus* (sample slt780; 7.8 m)
- LO of *L. acutus* (sample slt1260; 12.6 m)
- LO of *A. albianus* (sample slt1470; 14.7 m)
- LO of *H. chiastia* (sample slt1740; 17.4 m)
- FO of *Q. intermedium*-5 (sample slt2370; 23.7 m)
- FO of *E. eptapetalus* (sample slt2490; 24.9 m)
- FO of *Q. gartneri* (sample slt2490; 24.9 m)

Zones and subzones after the three zonations adopted are reported below (Fig.4.4.1):

Following Burnett (1998), zones and subzones UC3d-UC7 were identified. All the zonal and subzonal markers were recognized but a different sequence of events (the FO of *Q. intermedium*-5 occurs above the LO of *H. chiastia*, and *E. eptapetalus* has its FO in the same sample of the FO of *Q. gartneri*) related to Burnett (1998) scheme prevented the subdivision of subzones UC5b/UC5c and UC6a/UC6b.

Following Bralower et al. (1995), all the zonal and subzonal markers were recognized and zones NC11-NC13** were identified.

Following Sissingh (1977), all the zonal and subzonal markers were recognized and zones CC10-CC11 were identified.

Calcareous nannofossil assemblages

A total of 119 taxa were observed in the studied section. Based on semiquantitative abundances, nannofossil assemblage can be separated in the following intervals, from oldest to youngest:

Interval A: from sample slt0 to sample slt570. The assemblage comprises common *W. barnesiae*, representing the dominant taxa, and frequent to common *B. constans, E. turriseiffelii, R. achlyostaurion* and *W. manivitiae*. Other frequent taxa are *E. floralis, H. trabeculatus, P. cretacea,*

P. ponticula, R. angustiforata, R. crenulata, T. orionatus, Z. diplogrammus, Z. embergeri, Z. howei and *Z. noeliae.*

Interval B: from sample slt690 to sample slt1980. The assemblage is similar to that of Interval A, but shows a decrease in the abundance of *B. signata*, *C. fossilis*, *C.* cf. *C. percensis*, *G. segmentatum*, *S. horticus* and *T. minimus*. In this interval *T. gabalus* and *Z. erectus* (large form) are present in a more continuous way.

Interval C: from sample slt2070 to the top of the studied interval. The assemblage is still dominated by the same taxa of Intervals A and B, although ther is an increase in the relative abundance of *A. brooksii, E. gorkae, E. perchnielseniae, H. trabeculatus, M. decoratus, S. horticus* and *T. orionatus*.

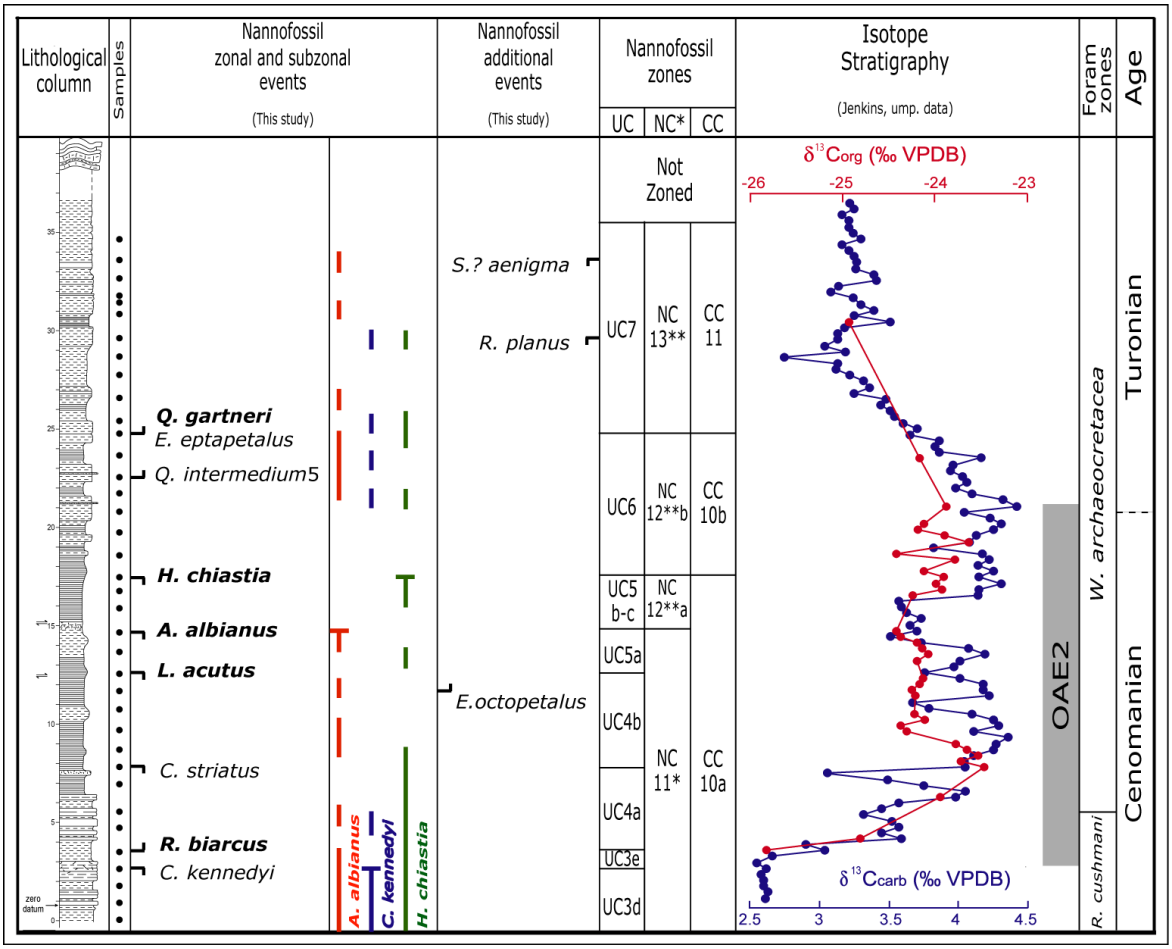

Fig.4.4.1: Calcareous nannofossil bioevents and zones/subzones of the Clote de Chevalier section. Lithostratigraphy, isotope stratigraphy after Gale and Jenkyns (unpublished data); planktonic foraminiferal zones after Falzoni and Petrizzo (unpublished data)

Chronostratigraphy

The Cenomanian/Turonian boundary was placed at the end of the positive shift of $\delta^{13}C$ curve as discussed by Tsikos et al. (2004) and highlighted at the Turonian GSSP (Kennedy et al., 2005).

4.5 Tarfaya Core (S57) – Morocco

Geographical setting and lithology

The Tarfaya Core (S57) is located in South-West Morocco (Fig.4.5.1). It was drilled by Shell during exploration in the late 1970s to early 1980s and logged and sampled in October 2001 at the Ocean Drilling Program Core Repository in Bremen, Germany, where it is currently stored (Tsikos et al., 2004). The Mesozoic Tarfaya Basin extends along the coast of southern Morocco between 28° N and 24° N and is part of the western margin of the Sahara platform, which has been tectonically stable since the Cretaceous (Keller et al., 2008).

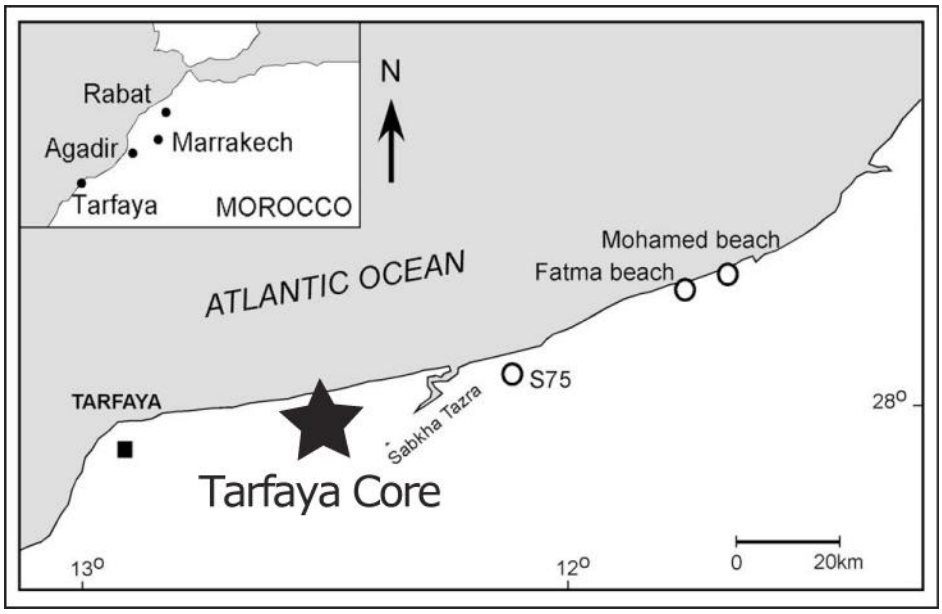

Fig.4.5.1: Location of Tarfaya Core section – Morocco (after Tantawy, 2008)

The studied interval comprises 37 m of organic-rich calcareous sediments, characterized by rhythmic alternations of decimetre-scale, dark- and light-coloured layers separated by gradational contacts (Tsikos et al., 2004). Studied samples were collected by Tsikos et al. (2004) for their work on carbon-isotope stratigraphy in the OAE2 interval.

Previous studies

Tsikos et al. (2004) presented detailed carbon-isotope stratigraphy for OAE2 from three localities (Eastbourne, England; Gubbio, Italy; Tarfaya, Morocco) compared with data from Pueblo. At Tarfaya they recognized the LO of *A. albianus* in the first part of the positive shift of $\delta^{13}C$ curve and they used the FO of *Q. gartneri*, just above the end of the C isotopic anomaly, to approximate the Cenomanian/Turonian boundary.

Results

Nannofossil investigation was performed on 67 samples from the interval between 23.41 and 59.61 mbs. I produced a semi-quantitative range chart of all taxa (Tab.4.5, Appendix 10, see CD attached). Preservation of nannofossils is generally poor-moderate to moderate and total abundance varies from very low-low to medium-high. Zonal and subzonal markers identified are listed below, from the oldest to the youngest:

- LO of *C. kennedyi* (sample T20, 56.00 mbs)
- LO of *A. albianus* (sample T30, 54.08 mbs)
- LO of *L. acutus* (sample T43, 51.47 mbs)
- FO of *Q. intermedium*-5 (sample T58, 48.42 mbs)
- FO of *E. eptapetalus* (sample T59, 48.23 mbs)
- LO of *H. chiastia* (sample T73, 42.27 mbs)
- FO of *Q. gartneri* (sample T74, 42.07 mbs)

All these events have been integrated with previous data presented by Tsikos et al (2004) to determine biozones and subzones after the three zonations adopted (Fig.4.5.2). In particular:

Following Burnett (1998), zones and subzones UC3d-UC7 were identified. The boundary between zones UC3 and UC4 could not be placed for the absence of the marker *R. biarcus* in the assemblage. As far as subzones are concerned, only the boundaries between subzones UC3d/UC3e and UC5b/UC5c could be identified. Also, the occurrence of *C. striatus* in one sample prevented the subdivision of subzones UC4a/UC4b. The boundary between subzones UC5a/UC5b is indicated by the LO of *A. albianus*; I found this event below the LO of *L. acutus*, in a reversed sequence relative to the scheme of Burnett (1998). The FO of *E. eptapetalus* occurs before the LO of *H. chiastia*, at lower level than reported by Burnett (1998), thus preventing the placement of UC6a/Uc6b subzonal boundary.

Following Bralower et al. (1995), all the zonal and subzonal markers were identified and zones NC11-NC13** were identified.

Following Sissingh (1977), all the zonal and subzonal markers were identified and zones CC10-CC11 were identified.

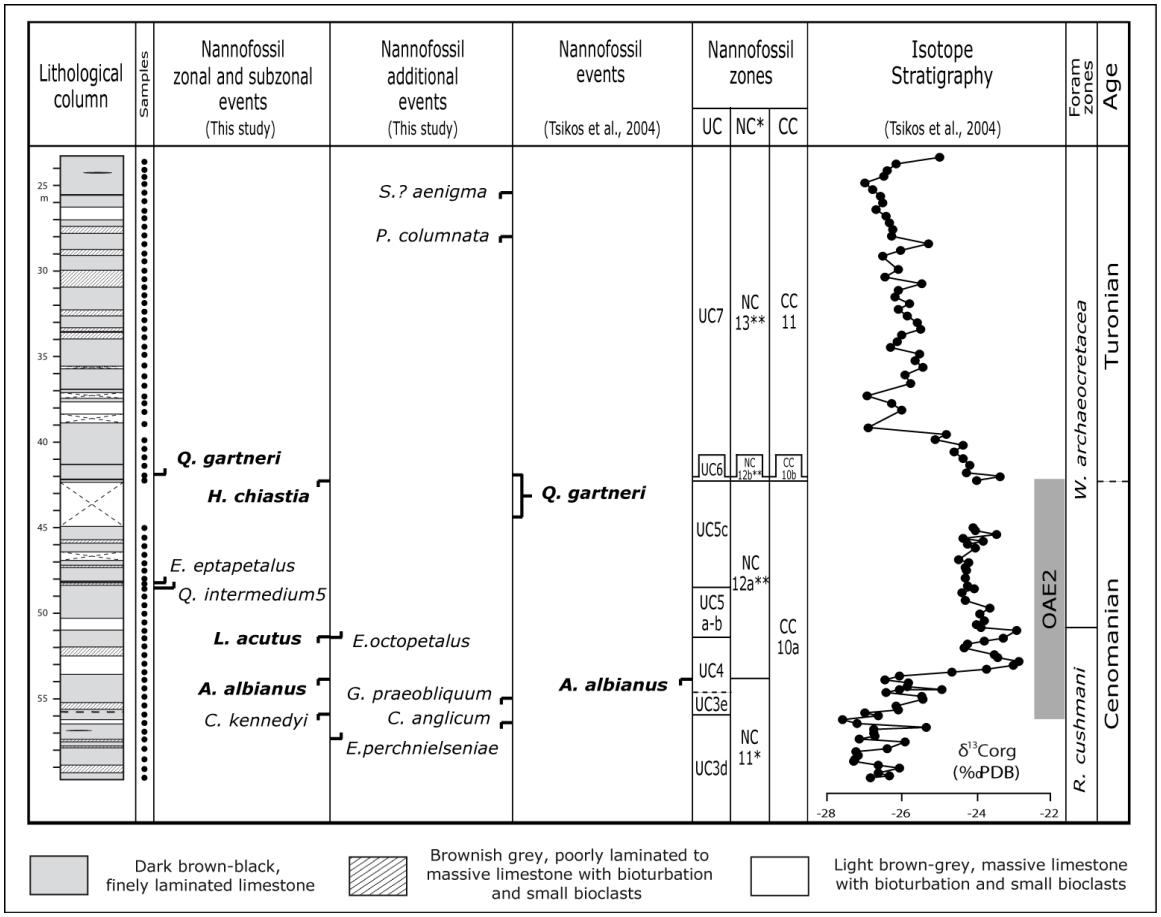

Fig.4.5.2: Calcareous nannofossil bioevents and zones/subzones in the Tarfaya Core section. Lithostratigraphy, isotope stratigraphy and planktonic foraminiferal zones after Tsikos et al. (2004).

Calcareous nannofossil assemblages

A total of 105 taxa were observed in the studied section. Based on semiquantitative abundances, nannofossil assemblage can be separated in the following intervals, from oldest to youngest:

Interval A: from sample T1 to sample T28. The assemblage comprises frequent to common *W. barnesiae, Z. howei*, frequent *E. floralis, W. manivitiae*, rare to frequent *B. constans, E. gorkae, E. turriseiffelii, H. trabeculatus, P. cretacea, R. planus, R. angustiforata, R. crenulata, R. achlyostaurion, T. orionatus, Z. bicrescenticus, Z. diplogrammus, Z. scutula*.

Interval B: from sample T30 to sample T73. The assemblage shows a decrease in total abundance of nannofossils with a reduction of species richness. *W. barnesiae, W. manivitie* and *Z. howei* remain the dominant taxa although become less common. *S. halfanii* and *T. decorus* become rarer and sporadic.

Interval C: from sample T74 to the top of the studied interval. The assemblage is similar to that of Interval B and is still dominated by the same taxa, although there is a decrease in species richness: *A. terebrodentarius, A. enormis, C. ehrenbergii, L. armilla, P. columnata, P. ponticula, P.*

spinosa, R. angustiforata, R. crenulata, R. surirella, R. angustus, R. asper, S. ellipticus, S. laffittei, S. achylosus, T. gabalus, Z. embergeri, Z. erectus are still present in the assemblage but become rarer and sporadic.

Chronostratratigraphy

The Cenomanian/Turonian boundary was placed at the end of the positive shift of $\delta^{13}C$ curve as reported by Tsikos et al. (2004).

4.6 ODP Site 1138

Geographical setting and lithology

ODP Site 1138 is situated on the central Kerguelen Plateau (53°33'S, 75°58'E; present water depth 1141 m, Fig.4.6.1), a large igneous province (LIP) formed in Cretaceous time (Shipboard Scientific Party, 2000).

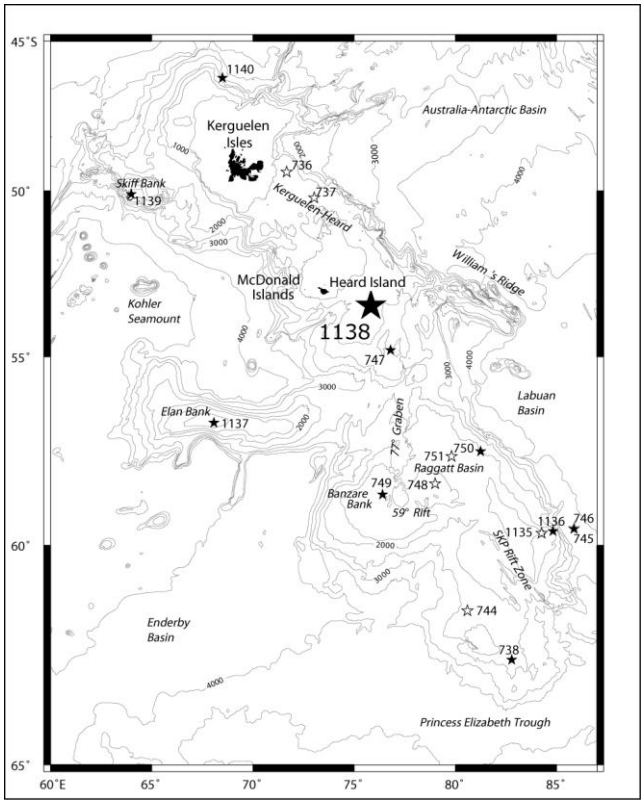

Fig.4.6.1: Location of ODP Site 1138.
Other sites drilled on the Kerguelen Plateau are also reported
(after Shipboard Scientific Party, 2000)

In Hole ODP 1138A a 689 m-thick sequence of Pleistocene to Cenomanian sediments overlying 144 m of volcanic basement was recovered. The studied interval goes from 580 to 700 mbsf, of Early Campanian to Late Cenomanian age (Shipboard Scientific Party, 2000). The youngest

Cretaceous sediments analyzed in this work belong to the lithologic Subunit IIIB, consisting of white to very light grey foraminifer-bearing chalk. The underlying Unit IV consists of cyclic alternations of light grey foraminifer-bearing chalk with grey through greenish-grey to black intervals of nannofossil claystone. The dark grey to black nannofossil claystone beds become increasingly prominent in the lower portion of Core 67R and increasingly black and clay-rich toward the base. The darkest interval, occurring at the base of Unit IV (Core 69R-6) with a high organic carbon content (2.24% total weight), seems to represent the sedimentary expression of the Cenomanian-Turonian Oceanic Anoxic Event (OAE 2). Unit V consists of glauconite-bearing to glauconitic calcareous sandstones. Unit VI consists predominantly of dark brown silty claystone with interbedded sandstone and conglomerate with no nannofossil content (Shipboard Scientific Party, 2000).

Previous studies

Paleontological data from ODP Site 1138 have been presented in the ODP volume of Leg 183, indicating a Maastrichtian to Turonian assemblage of nannofossils and foraminifers from Core 52 to Core 71 (Shipboard Scientific Party, 2000). The nannofossil zonation used for the Upper Cretaceous during Leg 183 is the one of Watkins et al. (1996), a high-latitude scheme developed for the Southern Ocean based on DSDP/ODP successions throughout this region. Foraminifer zonation is based on Cita et al.'s (1997) Upper Cretaceous biostratigraphy for the Southern Ocean. Petrizzo (2001) and Holbourn & Kuhnt (2002) presented data on planktonic and benthic foraminifera, respectively, to improve the Southern Ocean foraminifer biozonation and to evaluate how faunal changes are linked to sedimentary and palaeoenvironmental changes on the Kerguelen Plateau.

Results

Nannofossil investigation was performed on 43 samples from the interval between 689.78 and 592.96 mbsf, the same studied by Petrizzo (2001) to determine planktonic foraminiferal biozonation. I produced a semi-quantitative range chart of all taxa (Tab.4.6, Appendix 11, see CD attached). Preservation of nannofossils is generally moderate-good and total abundance varies from low to medium. Zonal and subzonal markers identified are listed below, from the oldest to the youngest:

- LO of *A. albianus* (sample 183-1138A-69R-6, 75-77; 657.82 mbsf)
- LO of *L. acutus* (sample 183-1138A-69R-6, 75-77; 657.82 mbsf)
- LO of *C. kennedyi* (sample 183-1138A-69R-6, 75-77; 657.82 mbsf)
- FO of *A. octoradiata* (sample 183-1138A-69R-5, 13-15; 655.70 mbsf)
- FO of *Q. intermedium*-5 (sample 183-1138A-69R-4, 119-120; 655.29 mbsf)

- FO of *E. eptapetalus* (sample 183-1138A-69R-6, 119-120; 655.29 mbsf)
- FO of *Q. gartneri* (sample 183-1138A-69R-4, 51-53; 654.60 mbsf)
- LO of *R. asper* (sample 183-1138A-69R-3, 41-43; 653.00 mbsf)
- FO of *K. magnificus* (sample 183-1138A-68R-4, 25-27; 644.91 mbsf)
- FO of *E. eximius* (sample 183-1138A-68R-1, 119-121; 641.59 mbsf)
- FO of *L. septenarius* (sample 183-1138A-67R-2, 68-70; 632.79 mbsf)
- LO of *L. septenarius* (sample 183-1138A-67R-1, 76-79; 631.46 mbsf)
- FO of *A. parcus expansus* (sample 183-1138A-66R-4, 72-75; 626.32 mbsf)
- FO of *M. staurophora* (sample 183-1138A-66R-4, 72-75; 626.32 mbsf)
- FO of *R. anthophorus* (sample 183-1138A-66R-4, 72-75; 626.32 mbsf)
- FO of *L. cayeuxii* (sample 183-1138A-66R-4, 72-75; 626.32 mbsf)
- FO of *A. parcus parcus* (sample 183-1138A-65R-1, 75-78; 612.25 mbsf)
- FO of *R. levis* (sample 183-1138A-65R-1, 75-78; 612.25 mbsf)
- FO of *A. parcus constrictus* (sample 183-1138A-63R-1, 76-78; 592.96 mbsf)

All these events have been integrated with previous data presented by Shipboard Scientific Party (2000) to determine biozones and subzones after the three zonations adopted (Fig.4.6.2). In particular:

Following Burnett (1998), zones and subzones UC3b, UC6b-UC9a, UC11c-UC12 and UC14 were recognized. Sample 183-1138A-69R-5, 13-15 is attributed to subzones UC3c-UC6a: the absence of markers prevents a better subdivision of this interval. Subzones UC9b-UC11b were not recognized as the uppermost sample from Core 67 belongs to subzone UC9a and the lowermost sample of Core 66R contains *L. cayeuxii* with no *L. septenarius,* which define zone UC12. The boundary between zones UC12 and UC13 could not be placed for the absence of the marker *A. cymbiformis* in the assemblage.

Following Bralower et al. (1995), zones NC11-NC15 and NC17*-NC18 were recognized. Zone NC16 was not recognized as the uppermost sample from Core 67 belongs to zone NC15 and the lowermost sample from Core 66R belongs to zone NC17. The boundary between zones NC14 and NC15 could not be placed for the absence of the marker *M. furcatus* in the assemblage.

Following Sissingh (1977), zones CC10-CC13, CC16 and CC18 were recognized. Zones CC14-CC15 were not recognized as the uppermost sample from Core 67 belongs to subzone CC13b and the lowermost sample from Core 66R belongs to zone CC16. The CC12/CC13 and CC16/CC17 zonal boundaries could not be placed for the absence of markers *M. furcatus* and *C. obscurus* in the assemblage.

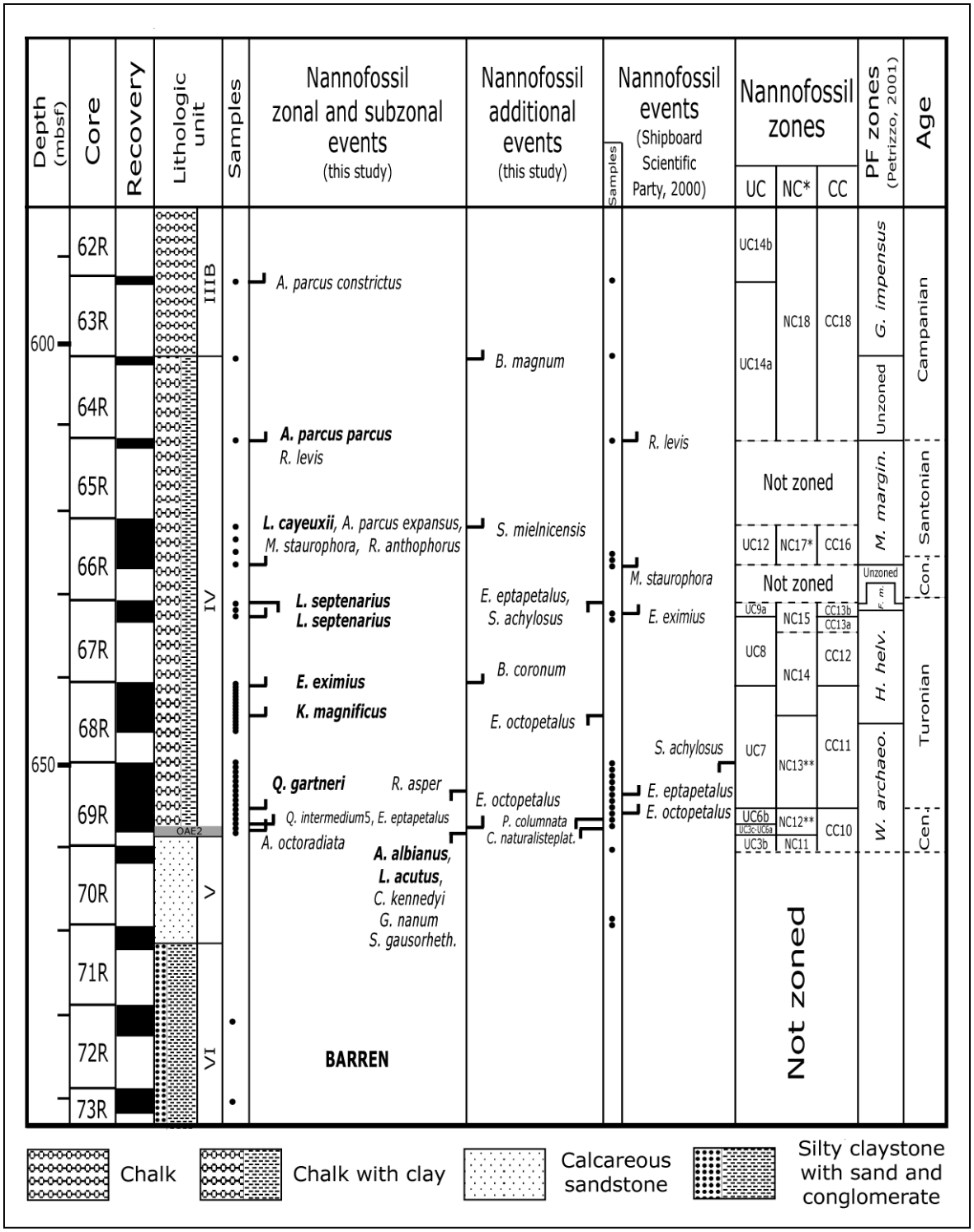

Fig.4.6.2: Calcareous nannofossil bioevents and zones/subzones at ODP Site 1138. Lithostratigraphy after Shipboard Scientific Party (2000); planktonic foraminiferal zones after Petrizzo (2001)

Calcareous nannofossil assemblages

Samples 183-1138A-73R-2, 47-50 and 183-1138A-72R-1, 5-7 do not contain calcareous nannofossils. From sample 183-1138A-69R-6, 75-77 upwards 160 taxa were observed in the studied section. Based on semiquantitative abundances, nannofossil assemblages can be separated in the following intervals, from oldest to youngest:

Interval A: sample 183-1138A-69R-6, 75-77. The assemblage is characterized by common *B. constans, R. parvidentatum, Z. noeliae,* representing the dominant taxa, and frequent *E. gorkae, E. turriseiffelii, E. floralis, H. trabeculatus, W. barnesiae, W. manivitiae, Z. noeliae* and *Z. scutula.* This sample contains also rare to frequent *A. albianus, C. kennedyi, G. nanum, L. acutus, S gausorhethium* and *C. naturalisteplateauensis*.

Interval B: from sample 183-1138A-69R-5, 13-15 to sample 183-1138A-68R-1, 75-78. The assemblage is characterized by frequent to common, *H. trabeculatus, P. cretacea, W. barnesiae, W. manivitiae,* and *Z. scutula* which become dominant taxa as well as *B. constans* and *Z. noeliae,* whilst *R. parvidentatum* shows a low decrease in abundance. Other frequent taxa are *A. octoradiata, E. gorkae, G. segmentatum* and *T. salillum*; *K. magnificus* become frequent in the assemblage from sample 183-1138A-68R-3, 120-122.

Interval C: from sample 183-1138A-67R-2, 68-70 to sample 183-1138A-67R-1, 76-79. The assemblage is similar to that of Interval B and still dominated by the same taxa. However *E. eximius* and *L. septenarius* are frequent in this interval whilst *E. gorkae* become rare and sporadic.

Interval D: from sample 183-1138A-66R-4, 72-75 to the top of the studied interval. Changes in the assemblage comprise: *M. staurophora* is the dominant taxon, *A. parcus expansus* becomes consistently present and frequent in the assemblage as well as *H. anceps. E. eximius, G. segmentatum, P. cretacea, W. barnesiae* and *W. manivitiae* are still frequent and *K. magnificus* increase in abundance whilst *B. constans, Z. noeliae* and *Z. scutula* become rarer. No more *E. floralis, E. eptapetalus, L. septenarius, S. achylosus* and *T. salillum* have been noticed.

Chronostratigraphy

Nannofossil investigation was performed on the same samples studied by Petrizzo (2001) to determine planktonic foraminiferal biozonation (Fig.4.6.2). To place stage boundaries I integrated my own data with those presented by Petrizzo (2001):

The Cenomanian/Turonian boundary was placed at FO of *Q. gartneri* as suggested by Tsikos et al., (2004). In the same sample, the LO of *G. bentonensis* was reported by Petrizzo (2001): this event may be used to approximate the Cenomanian/Turonian boundary as indicated by Kennedy et al., (2005).

The Turonian/Coniacian boundary was placed in the no-recovery interval of Core 66R as suggested by the presence of *S. achylosus* and by the absence of *A. parcus expansus* and *M. staurophora* in the uppermost sample of Core 67R. The uppermost range of *S. achylosus* is given as Early Cenomanian by Perch-Nielsen (1985), but it has been recorded in the Turonian of the

Naturaliste Plateau at DSDP Site 258 by Thierstein (1974), Watkins et al. (1996), Burnett (1998) and Lees (2002).

The Coniacian/Santonian boundary was placed above the FO of *L. cayeuxii* (Gale et al., 2007; Howe et al., 2007; Melinte & Lamolda, 2007) in the *M. marginata* planktonic foraminiferal zone after the FO of *H. papula*, a useful event to identify the Coniacian/Santonian boundary in the Southern Ocean record (Petrizzo, 2003).

The Santonian/Campanian boundary was placed at the FO of *A. parcus parcus* which falls very close to the end of Chron 34N as reported by Bralower et al. (1995).

4.7 ODP Site 1261

Geographical setting and lithology

ODP Site 1261 is situated on the dipping northwest-facing slope of Demerara Rise. (9°2.9168′N, 54°19.0384′W; present water depth 1899 m, Fig.4.7.1). Demerara Rise is a prominent submarine plateau located at ~5°N off the coasts of Suriname and French Guyana and is built on rifted continental crust of Precambrian and early Mesozoic age (Shipboard Shientific Party, 2004). ODP Site 1261 is the shallowest site of those forming the paleoceanographic depth transect across Demerara Rise.

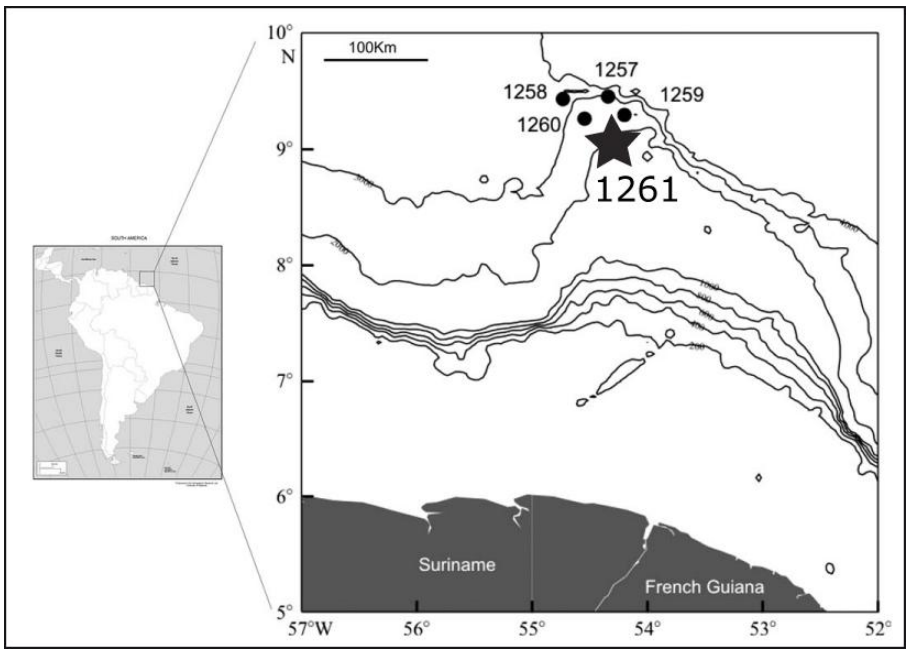

Fig.4.7.1: Location of ODP Site 1261.
Other sites drilled on the Demerara Rise during Leg 207 are also reported
(after Hardas & Mutterlose, 2006)

In Hole 1261A a 478 m-thick sequence of Pleistocene to Cenomanian sediments was recovered; the igneous basement was not reached. The upper 230 m interval was only recovered by six spot cores. The studied succession goes from 564.20 to 635.40 mbsf, of Late Cenomanian to Santonian age (Shipboard Scientific Party, 2004). The Cretaceous sediments analyzed in this work belong to the lithologic Unit IV, consisting of black, finely laminated claystone with organic matter to olive-gray laminated clayey limestone and clayey chalk with nannofossils. The two major lithologies in Unit IV, laminated claystone and laminated nannofossil chalk and limestone, show cyclic alternations and gradational contacts over a centimeter to decimeter scale (Shipboard Scientific Party, 2004).

Previous studies

The shipboard examination of calcareous nannofossils and planktonic foraminifera from core catcher samples was supplemented by additional samples from the cores, thus allowing to identify an apparently continuous Upper Cenomanian to Santonian interval from Core 50R to 41R. The Sissingh (1977) zonation was applied and zones CC10-CC14 were identified. The zonation used for Cretaceous planktonic foraminifers is based on the tropical zonal schemes of Caron (1985) and Sliter (1989) (KS Zones) with modifications by Bralower et al. (1993, 1995, 1997) and Premoli Silva and Sliter (1995, 1999). Previous studies on the sediments from ODP Leg 207 were also presented by Erbacher et al. (2005) on carbon isotope stratigraphy across the Cenomanian/Turonian boundary interval and by Hardas & Mutterlose (2006, 2007) who performed high-resolution biostratigraphic analysis and paleoecological studies on calcareous nannofossils in the same interval.

Results

Nannofossil investigation was performed on 116 samples from the interval between 635.40 and 564.20 mbsf, the same studied by Tamagnini (2007). I integrated her data with my own to produce a semi-quantitative range chart of all taxa (Tab.4.7, Appendix 12, see CD attached). Preservation of nannofossils is generally moderate and total abundance varies from very low-low to medium-high. Zonal and subzonal markers identified are listed below from the oldest to the youngest:

- FO of *E. eptapetalus* (sample 207-1261A-47R-5, 140-141; 628.57 mbsf)
- FO of *Q. intermedium*-5 (sample 207-1261A-47R-5, 140-141; 628.57 mbsf)
- LO of *H. chiastia* (sample 207-1261A-47R-5, 140-141; 628.57 mbsf)
- FO of *Q. gartneri* (sample 207-1261A-47R-5, 50-51; 627.57 mbsf)
- FO of *K. magnificus* (sample 207-1261A-46R-1, 40-41; 612.20 mbsf)
- FO of *E. eximius* (sample 207-1261A-45R-2, 90-91; 604.60 mbsf)
- FO of *L. septenarius* (sample 207-1261A-45R-1, 80-81; 603.00 mbsf)

- FO of *A. parcus expansus* (sample 207-1261A-44R-3, 120-121; 596.80 mbsf)
- FO of *Z. biperforatus* (sample 207-1261A-43R-2, 50-51; 585.00 mbsf)
- FO of *M. furcatus* (sample 207-1261A-43R-1, 60-61; 583.60 mbsf)
- FO of *M. staurophora* (sample 207-1261A-42R5, 100-101; 580.40 mbsf)
- FO of *R. anthophorus* (sample 207-1261A-42R-3, 140-141; 577.80 mbsf)
- FO of *L. grillii* (sample 207-1261A-41R-7, 20-21; 573.00 mbsf)
- LO of *Q. gartneri* (sample 207-1261A-41R-5, 60-61; 570.40 mbsf)
- FO of *L. cayeuxii* (sample 207-1261A-41R-3, 140-141; 568.20 mbsf)

All these events have been integrated with previous data presented by Shipboard Scientific Party, (2004) and by Hardas & Mutterlose (2006) to determine biozones and subzones after the three zonations adopted (Fig.4.7.2). In particular:

Following Burnett (1998), all the zonal markers were recognized and zones UC5-UC11 were identified. The UC6a/UC6b subzonal boundary could not be placed becouse *E. eptapetalus* and *H. chiastia* occur in the same sample. The occurrence of *Z. biperforatus* above the FO of *A. parcus expansus*, at a higher level than reported by Burnett (1998), prevented the subdivision of subzones UC9a and UC9b.

Following Bralower et al. (1995), all the zonal and subzonal markers were recognized and zones NC11*-NC17* were identified.

Following Sissingh (1977), all the zonal and subzonal markers were recognized and zones CC10-CC16 were identified.

Calcareous nannofossil assemblages

A total of 142 taxa were observed in the studied section. Based on semiquantitative abundances, nannofossil assemblages were characterized to separate the following intervals, from oldest to youngest:

Interval A: from sample 207-1261A-48R-3, 140-141.5 to sample 207-1261A-46R-1, 80-81. The assemblage is characterized by frequent to common *B. constans, C. signum, E. turriseiffelii, P. cretacea, W. barnesiae Z. howei* and *Z. noeliae,* representing the dominant taxa and frequent *E. floralis, P. ponticula, P. spinosa, R. angustus, S. ellipticus* and *Z. diplogrammus*.

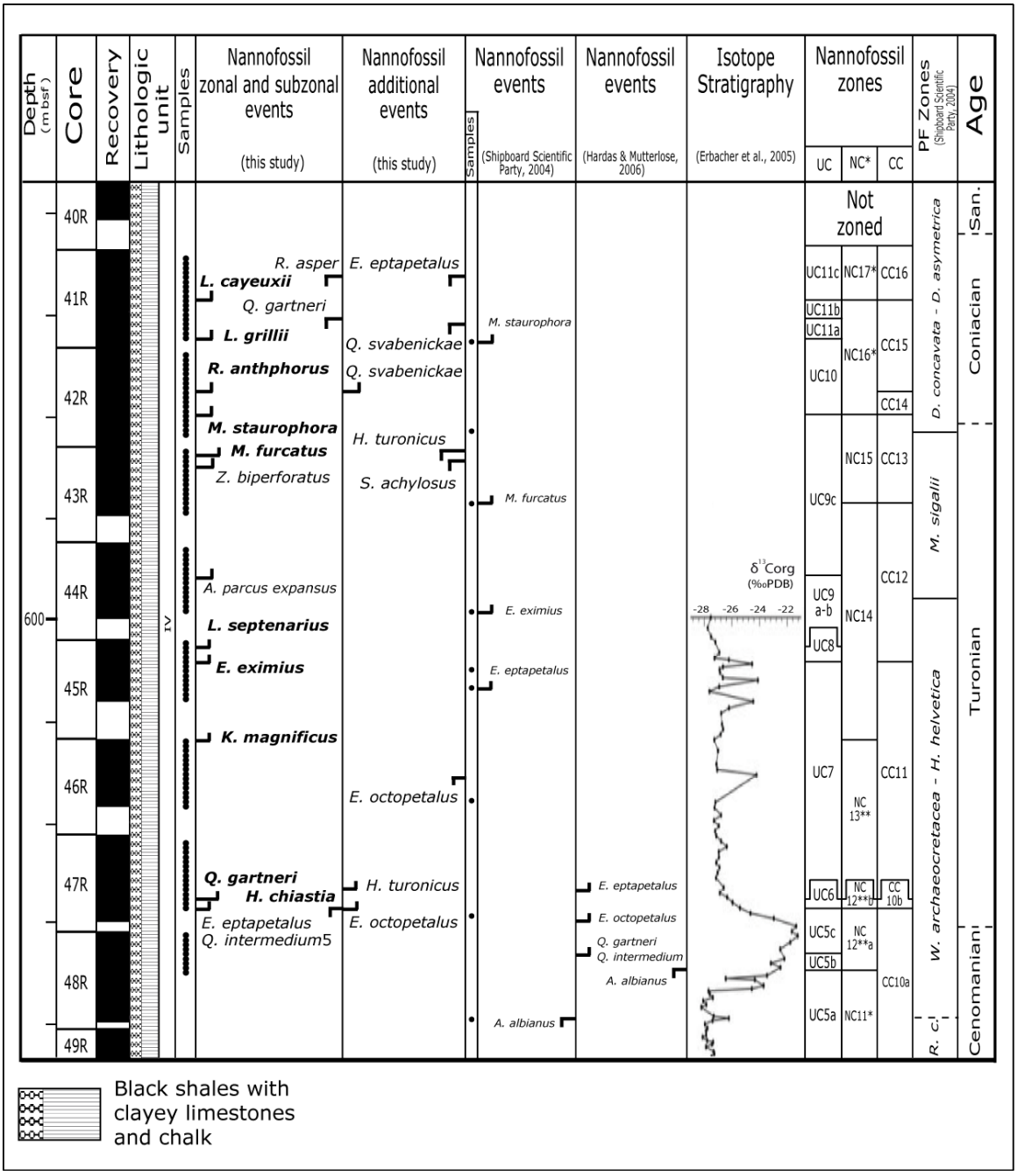

Fig.4.7.2: Calcareous nannofossil bioevents and zones/subzones at ODP Site 1261. Lithostratigraphy and planctonic foraminiferal zones after Shipboard Scientific Party (2004); isotopic stratigraphy after Erbacher et al. (2005)

Interval B: from sample 207-1261A-46R-1, 40-41 to sample 207-1261A-43R-4, 10-11. The assemblage is similar to that of Interval A, although *Z. howei* and *Z. noeliae* show a low decrease in abundance, remaining frequent but no more dominant and *T. salillum* starts to become continuously frequent to common in the assemblage. Along with previously recorded taxa, this interval shows a decrease in the occurrences of *C. litterarius, E. keio, G. coronadventis, R. planus, R. asper, R. crenulatus* and *T. stradneri* which become more sporadic whilst *G. segmentatum, L. quadricuspis, Q. gartneri, R. coronatus* and *T. orionatus* are present in a more frequent and continuous way.

Interval C: from sample 207-1261A-43R-3, 100-101 to sample 207-1261A-42R-6, 50-51. This interval shows an increase of total abundance and a rise in species richness, *P. cretacea* and *W. barnesiae* become common to abundant. The assemblage is still dominated by the same taxa of Intervals A and B and it records an increase in the relative abundance of *A. furtivus, A. parcus expansus, G. obliquum,L. armilla, M. simplex* and *O. robinsonii. M. furcatus* starts to occur in this interval, becoming frequent soon after its FO. *E. eptapetalus, L. quadricuspis, S. ellipticus* and *S. halfani* instead, show a decrease in their relative abundance.

Interval D: from sample 207-1261A-42R-5, 140-141 to the top of the studied interval. The assemblage is characterized by frequent to common *C. signum, M. staurophora, P. cretacea, P. spinosa* and *W. barnesiae* representing the dominant taxa. *A. parcus expansus, B. constans, B. ambiguous, E. eximius, E. gorkae, E. turriseiffelii, G. segmentatum, L. septenarius, M. pemmatoidea, M. belgicus, M. decoratus, T. minimus* and *T. salillum* are consistently present and frequent in the assemblage as well as *G. obliquum* and *L. armilla* whilst *B. signata* and *S. crux* become more sporadic.

Chronostratratigraphy

To place stage boundaries I integrated my own data with those presented by Shipboard Scientific Party (2004), Erbacher et al. (2005) and Hardas & Mutterlose (2006):

The Cenomanian/Turonian boundary was placed at the end of the positive shift of $^{13}\delta C$ curve as discussed by Tsikos et al. (2004) and highlighted at the Turonian GSSP (Kennedy et al., 2005).

The Turonian/Coniacian boundary was placed between the FO of *M. furcatus* and the FO of *M. staurophora* after the LO of *S. achylosus* in the *G. elevata* PF zone as suggested by Lees (2008), Walaszczyk et al. (2010) and Gradstein et al. (2012).

4.8 ODP Site 763

Geographical setting and lithology

ODP Site 763B is situated on the western part of the central Exmouth Plateau (20°35’S, 112°12’E; present water depth 1367 m, Fig.4.8.1), a thinned, subsided and sediment-starved continental block about 20 km thick, representing a passive continental margin with a wide continent/ocean transition (Wilcox & Exon, 1976; Haq et al., 1992).

In Hole 763B a 653.5 m-thick sequence of Eocene to Berriasian sediments was recovered; the igneous basement was not reached. The studied interval goes from 313 to 364 mbsf, of Early Campanian to Late Turonian age (Shipboard Scientific Party, 1990). The Cretaceous sediments

analyzed in this work belong to the lithologic Subunits IIIB and IIIC. The upper IIIB Subunit consists of green-gray to light green-gray foraminifer-nannofossil chalk, the underlying Subunit IIIC consists of gray-green and green-gray colour-banded nannofossil chalk with clay. The contact between Subunits IIIB and IIIC at 353.0 mbsf corresponds approximately to a condensed interval or a hiatus (Shipboard Scientific Party, 1990).

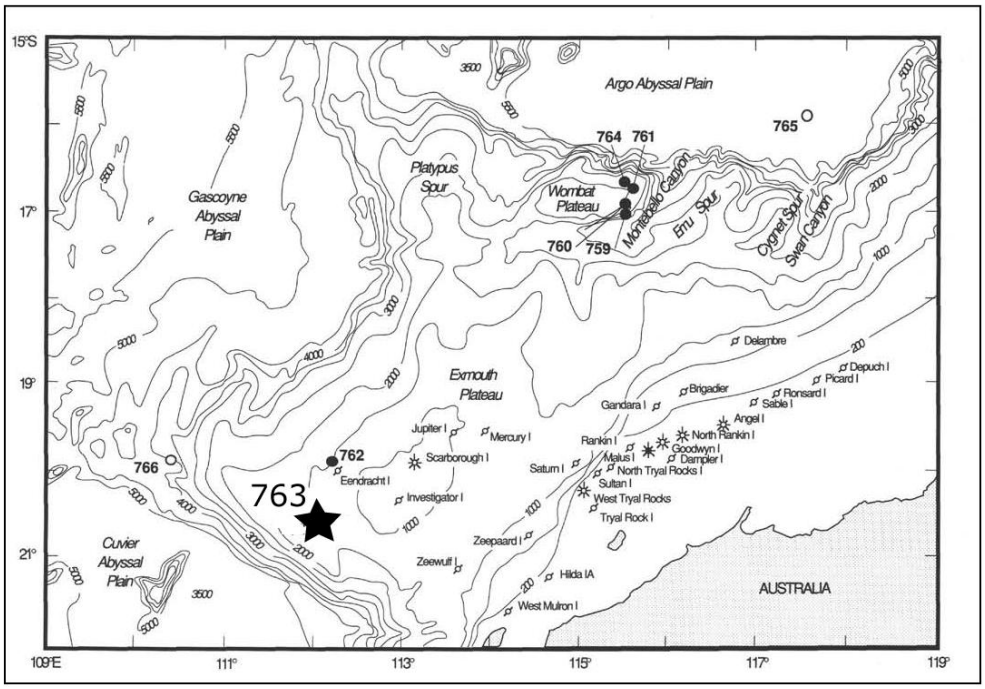

Fig.4.8.1: Location of ODP Site 763. Other sites drilled on the Exmouth Plateau are also reported (after Shipboard Scientific Party, 1990)

Previous studies

Previous studies on nannofossils of Site 763 were presented by Bralower & Siesser (1992) in the ODP volume of Leg 122. They performed a biostratigraphic study of Cretaceous calcareous nannofossils of Exmouth and Wombat Plateaus. An apparently continuous Upper Aptian to Upper Campanian interval was recognized in Hole 763B, from Core 43X to Core 8X. The Sissingh (1977) and Roth (1978) zonations were applied and zones CC7-CC22 and NC6-NC20, respectively, were identified. Foraminiferal investigation was performed by Wonders (1992), who described faunas occurring at ODP Site 763. Petrizzo (2000) presented new data on planktonic foraminifera from this site and from other southern mid-high latitudes sections to improve the Southern Ocean planktonic foraminiferal biozonation.

Results

Nannofossil investigation was performed on 92 samples from the interval between 364.22 and 313.72 mbsf, the same studied by Petrizzo (2000) to determine planktonic foraminiferal biozonation. I produced a semi-quantitative range chart of all taxa (Tab.4.8, Appendix 13, see CD

attached). Preservation of nannofossils is generally moderate and total abundance varies from low to medium-high. Zonal and subzonal markers identified are listed below from the oldest to the youngest:

- FO of *M. furcatus* (sample 122-763B-20X-2, 56-58; 363.06 mbsf)
- FO of *L. septenarius* (sample 122-763B-20X-2, 40-42; 362.92 mbsf)
- FO of *Z. biperforatus* (sample 122-763B-19X-CC, 15-17; 360.97 mbsf)
- FO of *A. parcus expansus* (sample 122-763B-19X-5, 140-142; 358.92 mbsf)
- FO of *M. staurophora* (sample 122-763B-19X-2, 76-78; 353.78 mbsf)
- FO of *L. grillii* (sample 122-763B-18X-2, 70-72; 344.22 mbsf)
- LO of *L. septenarius* (sample 122-763B-17X-4, 86-88; 337.88 mbsf)
- FO of *L. cayeuxii* (sample 122-763B-17X-1, 19-21; 332.71 mbsf)
- LO of *E. floralis* (sample 122-763B-16X-4, 139-141; 328.91 mbsf)
- FO of *A. cymbiformis* (sample 122-763B-16X-2, 16-18; 324.68 mbsf)
- FO of *A. parcus parcus* (sample 122-763B-15X-6, 10-12; 320.92 mbsf)
- FO of *R. levis* (sample 122-763B-15X-4, 56-58; 318.56 mbsf)
- FO of *A. parcus constrictus* (sample 122-763B-15X-1, 86-88; 314.38 mbsf)

All these events have been integrated with previous data presented by Bralower & Siesser (1992) to determine biozones and subzones after the three zonations adopted (Fig.4.8.2). In particular:

Following Burnett (1998), all the zonal markers were recognized and zones UC8-UC14 were identified. Only in zones UC9 and UC14 subzonal boundary events could be identified. As far as subzones are concerned, the absence of *Z. kerguelensis* prevented the subdivision of zone UC10 into subzones UC10a and UC10b. Subzones UC11a, UC11b and UC11c were not separated, because the sequence of events is different relative to the scheme of Burnett (1998).

Following Bralower et al. (1995), all the zonal markers were recognized and zones NC14-NC18* were identified.

Following Sissingh (1977), zones CC12-CC18 were identified. The boundary between zones CC16 and CC17could not be placed for the absence of the marker *C. obscurus* in the assemblage, I therefore approximate this boundary at the extinction level of *E. floralis,* as suggested by Perch-Nielsen (1985).

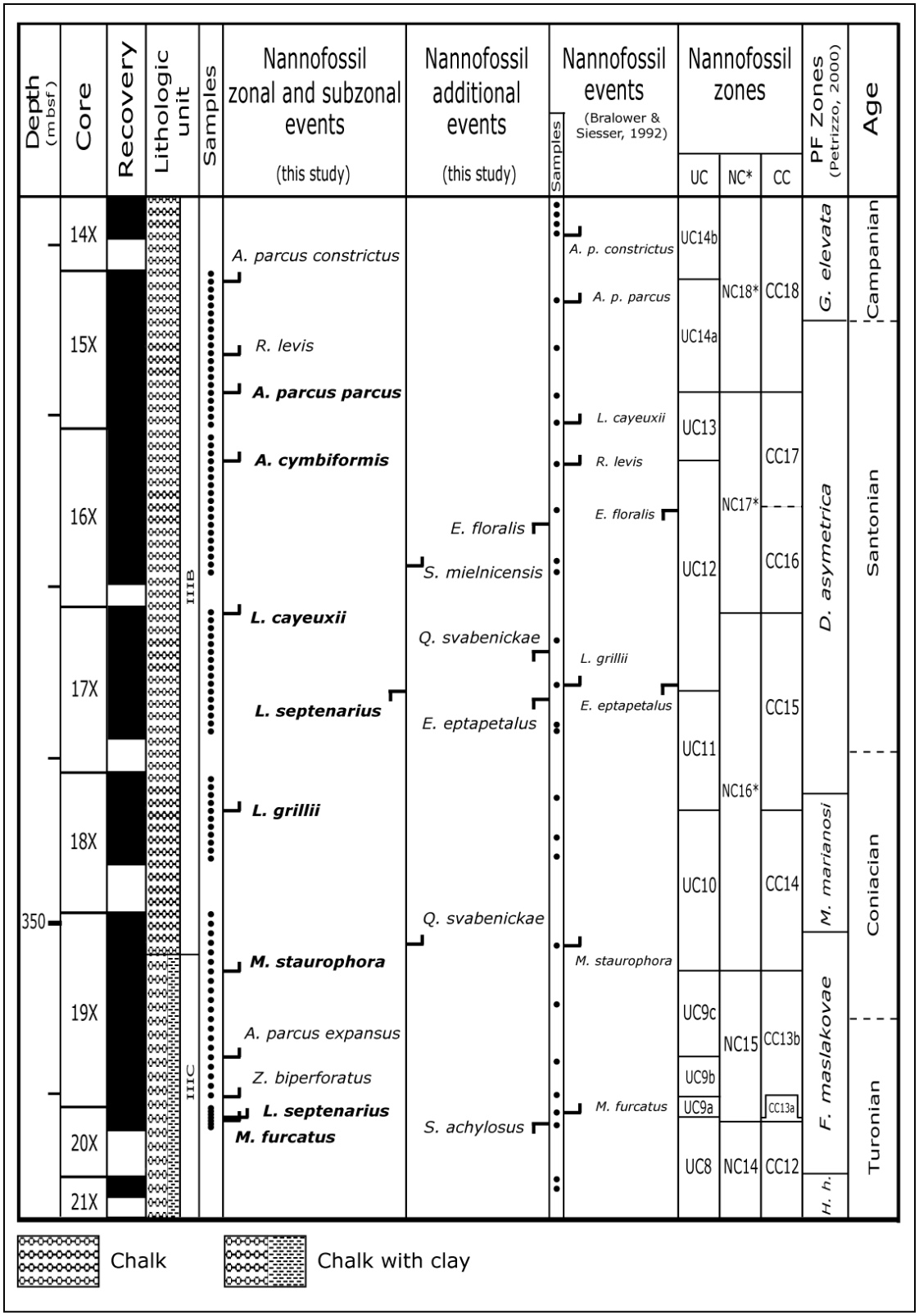

Fig.4.8.2: Calcareous nannofossil bioevents and zones/subzones at ODP Site 763.
Lithostratigraphy after Shipboard Scientific Party (1990); planktonic foraminiferal zones after Petrizzo (2000).

Calcareous nannofossil assemblages

A total of 117 taxa were observed in the studied section. Based on semiquantitative abundances, nannofossil assemblages were characterized to separate the following intervals, from oldest to youngest:

Interval A: from sample 122-763B-20X-CC, 20-22 to sample 122-763B-19X-2, 120-122. The assemblage is characterized by frequent to common *W. barnesiae* and *W. manivitiae,* representing the dominant taxa and frequent *E. eximius*, *E. floralis*, *P. cretacea*, *P. ponticula* and *Q. gartneri*.

Interval B: from sample 122-763B-19X-2, 76-78 to sample 122-763B-18X-4, 116-118 The assemblage is similar to that of Interval A and still dominated by *Watznaueria*, however, the genus *Micula* become frequent soon after the first occurrence of *M. staurophora*.

Interval C: from sample 122-763B-18X-4, 62-64 to sample 122-763B-17X-5, 91-93. *W. barnesiae* and *W. manivitiae,* still dominate the assemblage while *E. eximius*, *P. cretacea,* and *P. ponticula* are frequent (similar to intervals A and B). *C. ehrenbergii* increase in abundance from rare to frequent as well as *M. cubiformis*, *M. staurophora* and *M. swastika.* In this interval *E. floralis* and *Q. gartneri* show a decrease in abundance becoming rare and sporadic.

Interval D: from sample 122-763B-17X-5, 50-52 to sample 122-763B-16X-5, 140-142. The assemblage is characterized by frequent to common *W. barnesiae, W. manivitiae, M cubiformis*, *M. staurophora, E. eximius*, *C. ehrenbergii*, *P. cretacea,* and *P. ponticula*, which become dominant taxa. *A. parcus expansus* become consistently present and frequent in the assemblage as well as *L. grillii* and *G. segmentatum* whilst *K. magnificus* become sporadic.

Interval E: from sample 122-763B-16X-5, 70-72 to the top of the studied interval. *W. barnesiae W. manivitiae, P. cretacea* and *M. staurophora* are the dominant taxa with frequent *A. parcus expansus, H. anceps, C. ehrenbergii, E. eximius, L. grillii, M cubiformis, P. ponticula.* The regular occurrence of *L. cayeuxii*, the increase of *R.* cf. *R. levis* and the decrease in abundance of *M. furcatus* and *M. belgicus* have been noticed.

Chronostratratigraphy

Nannofossil investigation was performed on the same samples studied by Petrizzo (2000) to determine planktonic foraminiferal biozonation and data were integrated to place stage boundaries:

The Turonian/Coniacian boundary was placed between the FO of *A. parcus expansus* and the FO of *M. staurophora* in the *F. maslakovae* planktonic foraminiferal zone as suggested by Lees (2008) and Walaszczyk et al. (2010).

The Coniacian/Santonian boundary was placed between the FO of *L. grillii* and the LO of *L. septenarius* in the *D. asymetrica* planktonic foraminiferal zone. The FO of *L. cayeuxii* is supposed to be the last nannofossil event of the Coniacian (Gale et al., 2007; Howe et al., 2007; Melinte & Lamolda, 2007) but in Hole 763B it occurs at a higher level. I found this event in sample 122-763B-17X-1, 19-21, although other specimens possibly related to this species occur in lower samples. High occurrence of *L. cayeuxii* in this section may be justified by the increase in abundance of the species in Middle Santonian as indicated by Hampton et al. (2007).

The Santonian/Campanian boundary was placed at the end of *D. asymetrica* planktonic foraminiferal zone which corresponds to the beginning of Chron 33R in the nearby ODP Site 762 (Petrizzo, 2000; Petrizzo et al., 2011).

Chapter 5

Discussion

In this chapter my results are compared to the available nannofossil biozonation of the Late Albian-Early Campanian time interval and relative to data documented in the literature. The nannofossil events (zonal and subzonal markers are discussed to evaluate their reproducibility in different sedimentary basins and/or at different paleo-latitudes. Moreover, additional potential events are discussed in comparison with zonal and subzonal markers. Nannofossil characterization of stage boundaries is examined to provide information for potential future application and evaluation of reliability.

5.1 Calcareous nannofossil events: reproducibility and reliability

Summarizing my results, a total of 17 zonal and 4 subzonal markers have been recognized as reported in Fig. 5.1.1.

A few nannofossil biohorizons used in the zonal schemes were not identified due to their absence or extreme rarity in the studied sections, or because were found at significantly different stratigraphic level relative to the timing attribution in adopted zonations. The following section is the discussion (from oldest to youngest) of the reasons for not using such bioevents. Events used for zonal boundaries are in bold.

- LO of *H. albiensis*. Due to potential taxonomic discrepancy, this taxon was not identified in the studied material. However, the LO of *H. irregularis* occurs in the studied section at similar stratigraphic level. It might well be that the two apparently different biohorizons are actually the same event.
- FO of *C. anfractus*. This taxon was never observed in the studied sections.
- LO of *W. britannica*. This taxon is extremely rare in the studied sections and, therefore, considered not reliable as marker.

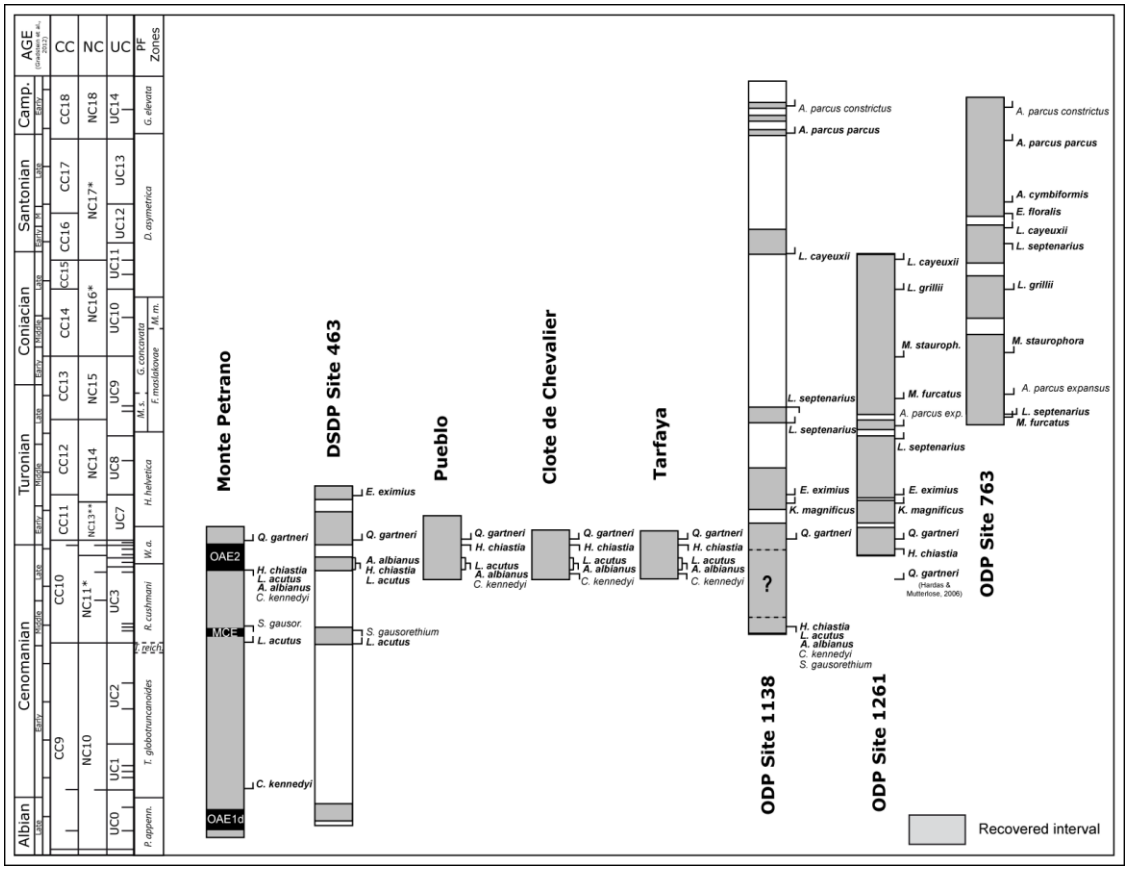

Fig.5.1.1 Zonal and subzonal events recognized in the studied interval. Zonal markers are indicated in bold

- LO of *G. chiasta*. This taxon is extremely rare in the studied sections and, therefore, considered not reliable as marker.
- FO of *H. anceps*. This taxon is extremely rare in the studied sections and, therefore, considered not reliable as marker.
- **FO of *G. segmentatum***. In the studied sections, this taxon was consistently observed in stratigraphic levels younger than early Cenomanian.
- LO of *Z. xenotus*. This taxon was never observed in the studied sections.
- FO of *C. sculptus*. In the studied sections this taxon was detected below the FO of *C. kennedyi*, in stratigraphic levels older than late Early Cenomanian.
- **FO of *M. decoratus*.** Extremely rare specimens of this taxon were observed in the lowermost Cenomanian of the Monte Petrano section, significantly before the known age of its FO and, therefore, was not used as marker. However, it should be noticed that after an interval of absence, the beginning of the continuous range was detected at a stratigraphic level consistent with the FO as reported in biozonations.
- LO of *G. theta*. This taxon was never observed in the studied sections.
- FO of *A. octoradiata*. This taxon is extremely rare in the studied sections and, therefore, considered not reliable as marker.

- LO of *G. nanum*. In the studied material this species displays sparse distribution and very low abundances.
- **FO of *R. biarcus***. This taxon is extremely rare in the studied sections and, therefore, considered not reliable as marker.
- LO of *C. striatus*. This taxon is extremely rare in the studied sections and, therefore, considered not reliable as marker.
- FO of *Q. intermedium*. The FO of this taxon was found at different stratigraphic levels in the studied sections and, consequently, is disregarded as subzonal event.
- FO of *E. eptapetalus* (= *E. moratus*). The FO of this taxon was found at different stratigraphic levels in the studied sections and, consequently, is disregarded as subzonal event.
- **LO of *R. asper*.** This taxon becomes rare above the Albian and therefore its disappearance level could not be determined in sections just covering the Cenomanian/Turonian boundary interval. Moreover, *R. asper* was found through the Turonian at ODP Site 1261.
- **FO of *L. maleformis*.** This taxon is extremely rare in the studied sections and, therefore, considered not reliable as marker.
- FO of *L. quadrifidus*. This taxon is extremely rare in the studied sections and, therefore, considered not reliable as marker.
- FO of *T. ecclesiastica*. This taxon is extremely rare in the studied sections and, therefore, considered not reliable as marker.
- FO of *Z. biperforatus*. This taxon is rare in the first portion of its stratigraphic range and the FO was found at different levels in the studied sections.
- FO of *Z. kerguelensis*. This taxon is absent in the studied sections.
- LO of *Z. kerguelensis*. This taxon is absent in the studied sections.
- **FO of *M. concava*.** This taxon is extremely rare in the studied sections and, therefore, considered not reliable as marker.
- LO of *Q. gartneri*. The stratigraphic position of this event was indicated by Burnett (1998) as Late Coniacian with the remark that this biohorizon has a local validity. However, Burnett (1998) did not specify the area where she found the LO of *Q. gartneri*. In the studied sections *Q. gartneri* was observed up to the lowermost Campanian.
- **FO of *C. obscurus*.** This taxon is absent in the studied sections.

Most zonal and subzonal events have been identified and are here reported from oldest to youngest. Events used for zonal boundaries are in bold. Figure 5.1.2 illustrates the reproducibility of zonal and subzonal events in the late Albian to early Campanian. The Cenomanian/Turonian interval is characterized by several nannofossil events that are detailed in Figs. 5.1.3 and 5.1.4.

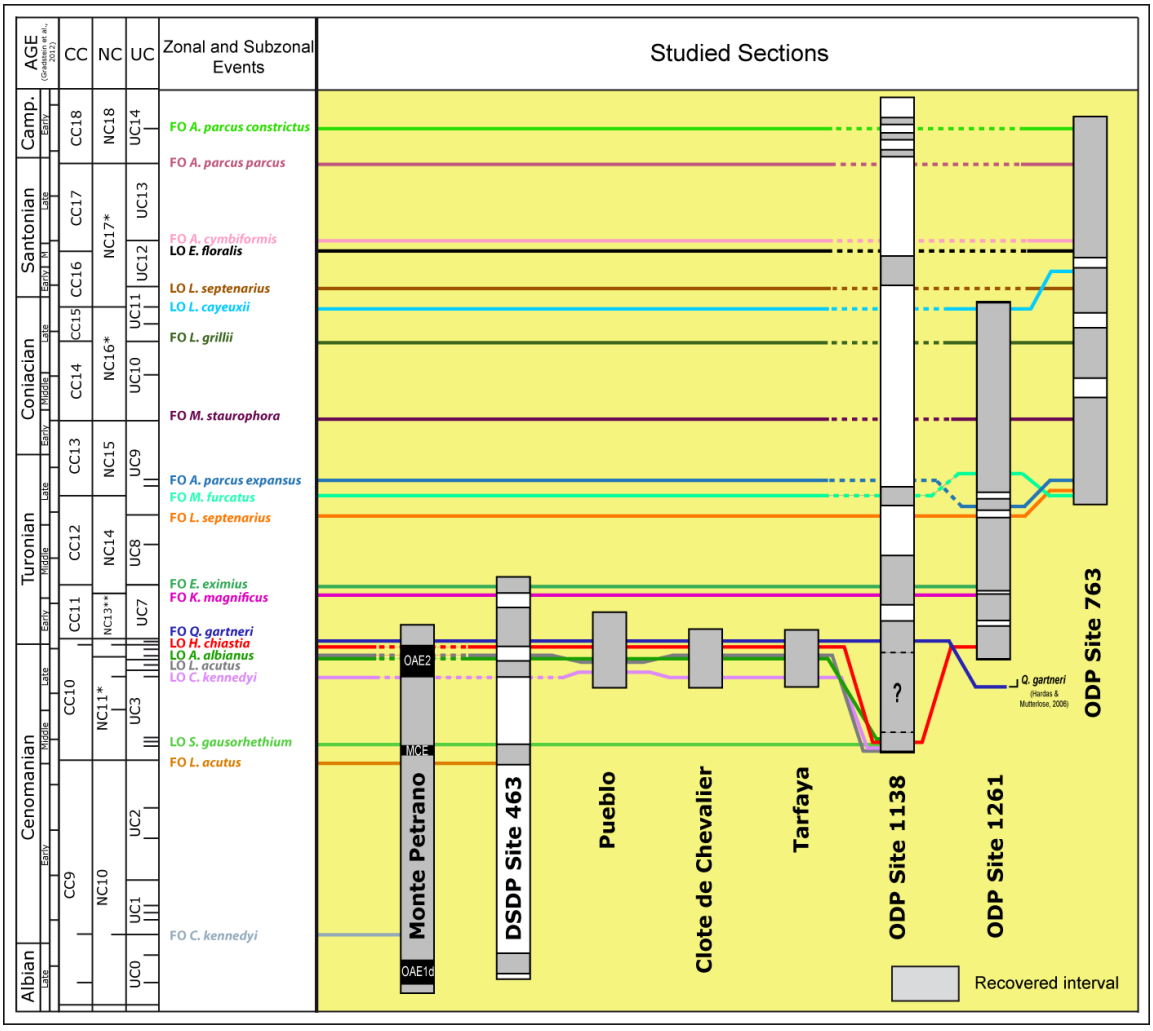

Fig.5.1.2 Correlation of zonal and subzonal selected bioevents through the studied sections

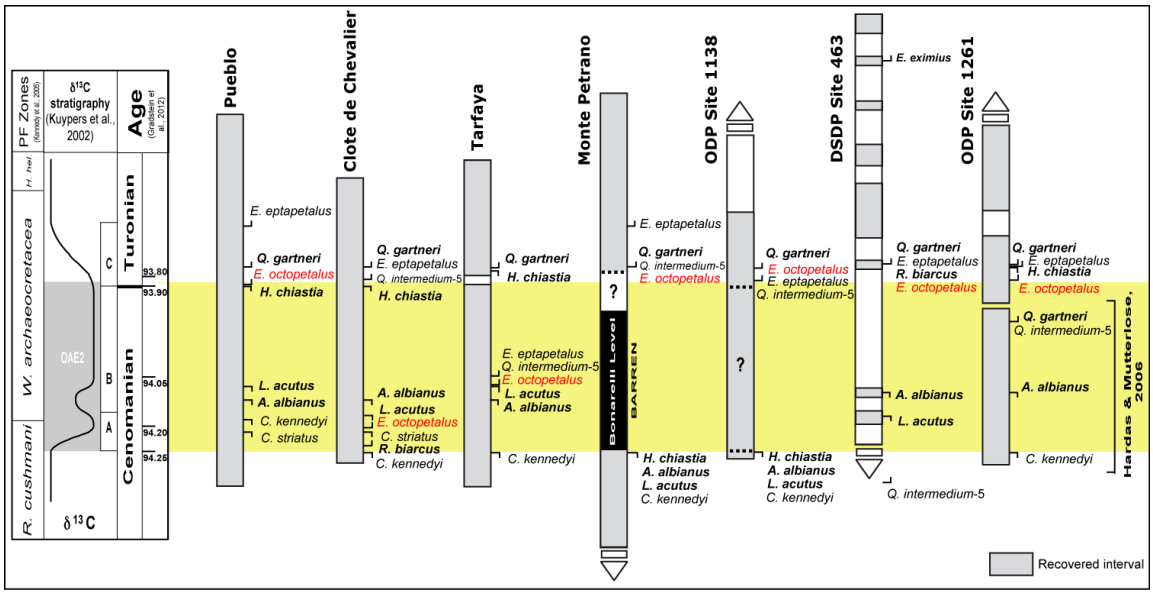

Fig.5.1.3 Zonal (bold) and subzonal (regular) events recognized in the Cenomanian/Turonian boundary interval. Additional bioevent is indicated in red

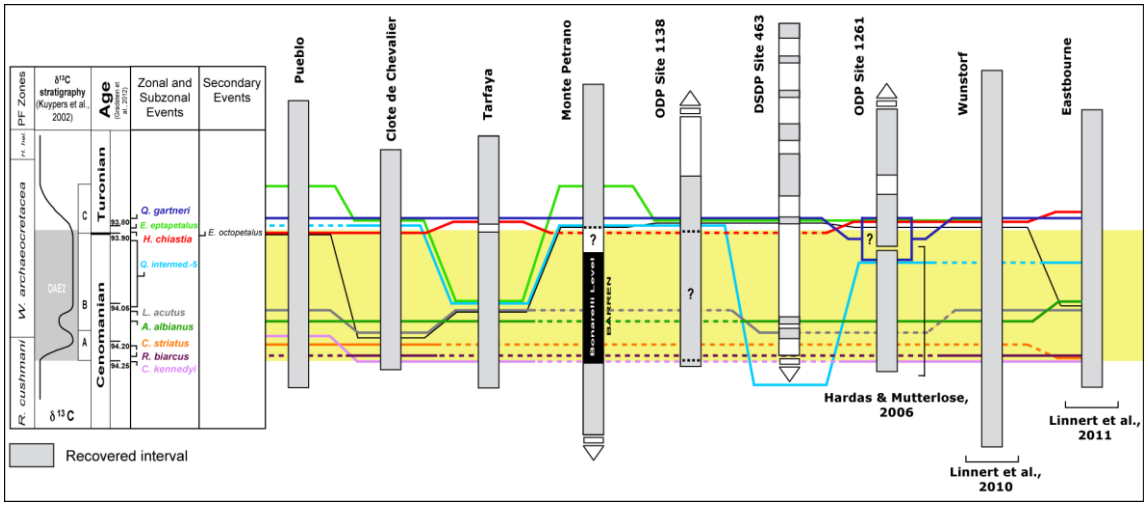

Fig.5.1.4 Correlation of zonal, subzonal and secondary bioevents in the Cenomanian/Turonian boundary interval in the studied sections and two other sections selected for their well-established integrated bio-chemostratigraphy

- **FO of *E. turriseiffelii.*** This event is Late Albian in age and occurs before the analyzed time interval. In fact this taxon is present from the lowermost sample studied.
- **FO of *C. kennedyi.*** This event was found in coeval levels (earliest Cenomanian) in the studied sections.
- **FO of *L. acutus*.** This event was found in coeval levels (Middle Cenomanian) in the studied sections.
- LO of *S. gausorhethium.* This event was found in coeval levels (Middle Cenomanian) in the studied sections.
- LO of *C. kennedyi*. This event was found in coeval levels (Late Cenomanian) in the studied sections. In particular the LO of *C. kennedyi* correlates with the onset of the $\delta^{13}C$ positive excursion associated with OAE 2. In one studied section, similarly to data reported for the Lower Saxony Basin (Linnert et al., 2010), this taxon was observed in the interval above its LO.
- **LO of *L. acutus* and LO of *A. albianus*.** These events were found in coeval levels (Late Cenomanian) in the studied sections. In particular their LOs correlate with the first part of the $\delta^{13}C$ positive excursion associated with OAE 2, between peaks A and B. However, the order of these two events is not systematically reproduced. In one studied section, similarly to data reported for the Lower Saxony Basin (Linnert et al., 2010), *A. albianus* was observed in the interval above its LO.
- **LO of *H. chiastia.*** This event was found in coeval levels (latest Cenomanian) in the studied sections. In particular the LO of *H. chiastia* correlates with the uppermost part of the "plateau" of the $\delta^{13}C$ positive excursion associated with OAE 2. In one studied section, similarly to data reported for the Lower Saxony Basin (Linnert et al., 2010), this taxon was observed in the interval above its LO.

- **FO of *Q. gartneri.*** This event was found in coeval levels (earliest Turonian) in the studied sections. In particular the FO of *Q. gartneri* is observed slightly above the end of the $\delta^{13}C$ positive excursion (peak C) associated with OAE 2.
- **FO of *K. magnificus.*** This event was found in coeval levels (Middle Turonian) in the studied sections.
- **FO of *E. eximius.*** This event was found in coeval levels (Middle Turonian) in the studied sections.
- **FO of *L. septenarius.*** This event was found in coeval levels (Middle Turonian) in the studied sections.
- **FO of *M. furcatus.*** This event was found in coeval levels (Late Turonian) in the studied sections.
- FO of *A. parcus expansus.* This event was found in coeval levels (Late Turonian) in the studied sections.
- **FO of *M. staurophora.*** This event was found in coeval levels (Middle Coniacian) in the studied sections.
- **FO of *L. grillii.*** This event was found in coeval levels (Late Coniacian) in the studied sections.
- **FO of *L. cayeuxii.*** This event was found in the Coniacian/Santonian interval of the studied sections. However, its position relative to the LO of *L. septenarius* is variable (before or after).
- **LO of *L. septenarius.*** This event was found in coeval levels (earliest Santonian) in the studied sections.
- **LO of *E. floralis.*** This event was found in coeval levels (Middle Santonian) in the studied sections.
- **FO of *A. cymbiformis.*** This event was found in coeval levels (early-Late Santonian) in the studied sections.
- **FO of *A. parcus parcus.*** This event was found in coeval levels (uppermost Santonian or base of Campanian, see discussion in chapter 5.2) in the studied sections.
- FO of *A. parcus constrictus.* This event was found in coeval levels (Early Campanian) in the studied sections.

5.2 Calcareous nannofossil events and Cenomanian-Campanian stage boundaries

Here the nannofossil events discussed in section 5.1 are examined in the context of stage boundary definitions. Specifically, for each stage boundary the data documented for GSSP sections

and/or presented for GSSP proposals are reported. Then the result of my investigation are compared to provide information about the applicability of nannofossil events also based on literature screening.

Albian/Cenomanian boundary interval

The Mont Risou section in southeast France was chosen as GSSP for the base of the Cenomanian (Tröger & Kennedy, 1996; Gale et al., 1996; Kennedy et al., 2004). The basal boundary criterion selected by the Cenomanian Working Group is the FO of the planktonic foraminifer *Thalmanninella globotruncanoides* (*Rotalipora globotruncanoides* or *Rotalipora brotzeni* of some studies – Fig.5.2.1).

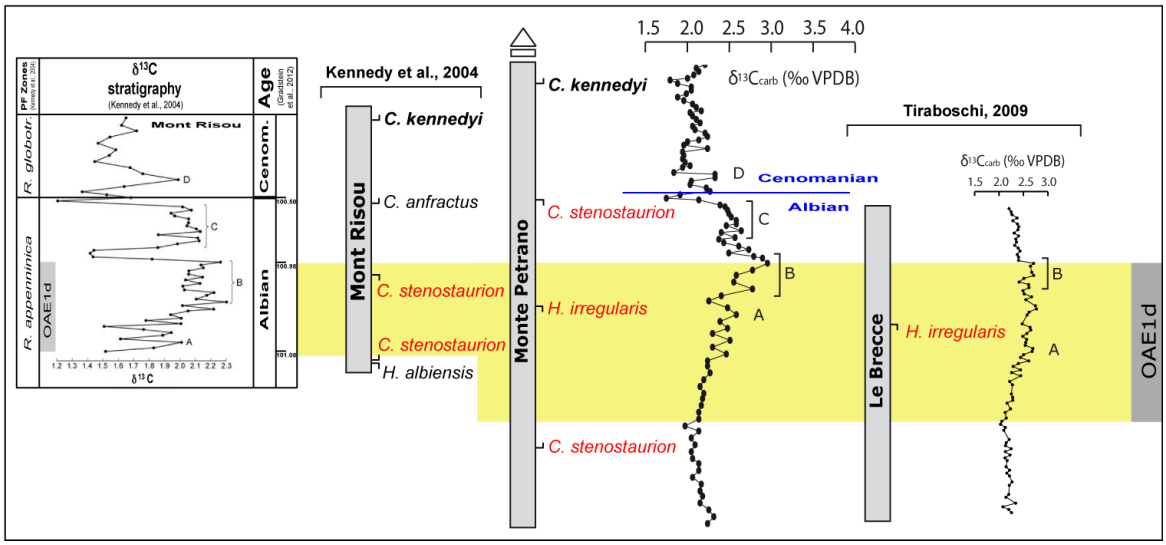

Fig.5.2.1 Zonal (bold) and subzonal (regular) events recognized in the Albian/Cenomanian boundary interval. Additional bioevents are indicated in red

In the Mont Risou section, nannofossil investigations allowed to recognize two bioevents below the boundary and one above, namely: the LO of *H. albiensis*, the FO of *C. anfractus* and the FO of *C. kennedyi* (Fig.5.2.1). The LO of *H. albiensis*, a rare species, occurs just below the isotopic point A of the $\delta^{13}C$ positive shift associated with the Breistroffer Level, representing the sedimentary expression of the OAE1d (Gale et al., 1996; Kennedy et al., 2004).

In available zonations, the LO of *H. albiensis* was reported by Perch-Nielsen (1985) as subzonal marker for CC9a/CC9b boundary and used by Burnett (1998) in her zonation to subdivide UC0a from UC0b. At Mont Risou, this event is followed by the FO of *C. anfractus* just below the Albian/Cenomanian boundary, between isotopic interval C and point D (Gale et al., 1996; Kennedy et al., 2004). This bioevent is used by Burnett (1998) to place UC0b/UC0c subzonal boundary. Above the Albian/Cenomanian boundary the first event recognized is the FO of *C. kennedyi*, above the isotopic point D, near the top of the Mont Risou section (Gale et al., 1996; Kennedy et al., 2004). The FO of *C. kennedyi* is used by Bralower et al. (1995) and Burnett (1998) as an earliest

Cenomanian biohorizon. This species was defined by Crux (1981), after publication of Sissingh (1977) and Roth (1978) works and then added to Sissingh's scheme (1977) by Perch-Nielsen (1985) to place CC9b/CC9c subzonal boundary.

Two of the studied sections comprise the Albian/Cenomanian boundary interval, but only Monte Petrano shows a complete record, at DSDP Site 463 the boundary falls in a no-recovery interval. Compared to the Mont Risou section, only the FO of *C. kennedyi* was identified at Monte Petrano, occurring above the isotopic point D (Fig.5.2.1). Three additional events were also observed in the Monte Petrano section, namely: the FO of *C. stenostaurion*, the LO of *H. irregularis* and the LO of *C. stenostaurion*. The FO and the LO of *C. stenostaurion* were reported at Mont Risou, the first below the isotopic point A and the second at the end of the interval that represents the isotopic peak B (Gale et al., 1996; Kennedy et al., 2004). At Monte Petrano I identified a slightly longer total range for this taxon, due to the wider extension of the section below OAE1d.

The LO of *H. irregularis* seems to have potential biostratigraphic significance, at least at regional level in the Umbria-Marche Basin. At the Le Brecce section, studied by Tiraboschi (2009), the extinction datum of this taxon falls slightly above the isotopic point A. At the same level, following the $\delta^{13}C$ isotopic curve, this bioevent was observed at Monte Petrano (Fig.5.2.1). At Mont Risou, *H. irregularis* was not reported, but looking at the extinction datum of *H. albiensis* it is possible that this difference is due to taxonomic discrepancy and that the same species was given different taxonomic interpretation. If this is correct, then the extinction datum of *H. irregularis* (= *H. albiensis*) falls around the isotopic point A also at Mont Risou (Fig.5.2.1).

At low-latitudes, the FO of *C. stenostaurion*, the LO of *H. irregularis* and the LO of *C. stenostaurion* might be reliable events. The OAE1d falls within the stratigraphic interval covered by these three bioevents. At low latitudes, the LO of *H. irregularis* is of latest Albian age, just before the Albian/Cenomanian boundary. The FO of *C. kennedyi* is the first, widely adopted and easily recognizable, post-boundary bioevent. The age of this biohorizon should be revised as earliest Cenomanian.

Cenomanian/Turonian boundary interval

The Turonian Working Group placed the base of the Turonian at the FO of the ammonite *Watinoceras devonense*. Its GSSP is at Rock Canyon Anticline, Pueblo (Colorado – Bengtson et al., 1996; Kennedy et al., 2005). The major carbon isotope anomaly is characterized by a complex curve, with "C" peak (coinciding with the end of the plateu and preceding the recovery decrease) occurring just above the boundary. Tsikos et al. (2004) proposed to use the $\delta^{13}C$ excursion for stratigraphic characterization, and specifically the "C" peak to identify the base of the Turonian.

Previous studies on calcareous nannofossils in the Pueblo section were published by Watkins (1985), Bralower (1988) and Watkins et al. (1993) as discussed in chapter 4.3. Further information were given by Kennedy et al. (2000; 2005) with the definition of the GSSP (Fig.5.2.2).

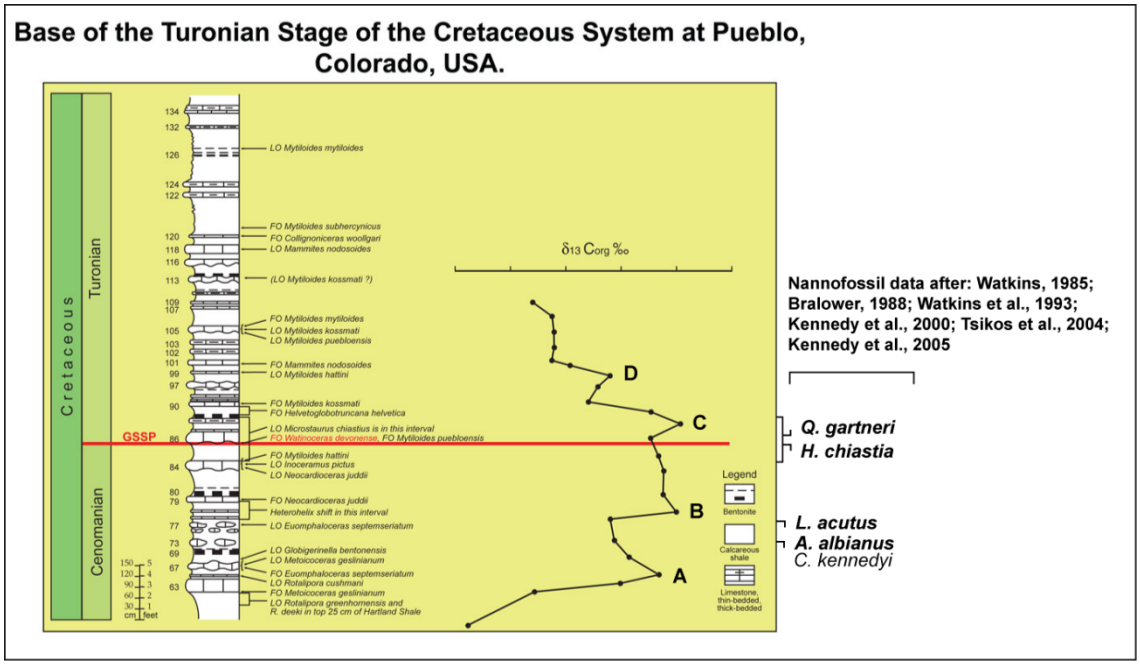

Fig.5.2.2 Calcareous nannofossil data at the Turonian GSSP. Lithostratigraphy, isotope stratigraphy, biostratigraphy from https://engineering.purdue.edu/Stratigraphy/gssp/logturon.htm

In the Pueblo section, nannofossil investigation allowed to recognize five bioevents: four last occurrences and one first occurrence (Fig.5.2.2). The LOs of *C. kennedyi* and *A. albianus* were reported by Bralower (1988) and Tsikos et al. (2004) between the isotopic peaks A and B of the positive shift of the $\delta^{13}C$ curve. The LO of *L. acutus* was observed by Watkins (1985) and Bralower (1988) slightly below the isotopic point B. The LO of *H. chiastia* and the FO of *Q. gartneri* were reported by Watkins (1985), Bralower (1988), Kennedy et al. (2000; 2005) and Tsikos et al. (2004) in the interval around the Cenomanian/Turonian boundary, in close proximity of the isotopic peak C (Fig.5.2.2). All these bioevents were adopted by Sissingh (1977), Bralower et al. (1995) and Burnett (1998) in their zonations to characterize the Cenomanian/Turonian boundary interval.

Seven of the studied sections comprise the Cenomanian/Turonian boundary interval, but only three of them show a complete record as well as correlations with chemo- and planktonic foraminiferal bio-stratigraphy (Pueblo, Clote de Chevalier and Tarfaya). One of these sections is the reinvestigation of the Turonian GSSP. All the five bioevents reported in the GSSP were identified in the studied sections, additionally four zonal and subzonal markers and a secondary bioevent reported in the three Cretaceous zonations were recognized within this time interval. They are: the FO of *R. biarcus*, the LO of *C. striatus* and the FOs of *Q. intermedium*-5, *E. octopetalus* and *E. eptapetalus* (Fig.5.1.3).

The correlation among the studied sections shows that only five of the reported bioevents occur, relative to the $\delta^{13}C$ curve, at the same stratigraphic position. They are: the LOs of *C. kennedyi*, *A. albianus*, *L. acutus*, *H. chiastia* and the FO of *Q. gartneri*, the same five events reported in the GSSP section. *R. biarcus* and *C. striatus* are too rare to be suitable as biostratigraphic markers, whilst the FOs of *Q. intermedium*-5, *E. octopetalus* and *E. eptapetalus* have been found at different stratigraphic levels in the studied sections and in previous studies (Fig.5.1.4). A summary of the global and regional bioevents recognized in the Cenomanian/Turonian boundary interval is given in Fig.5.2.3.

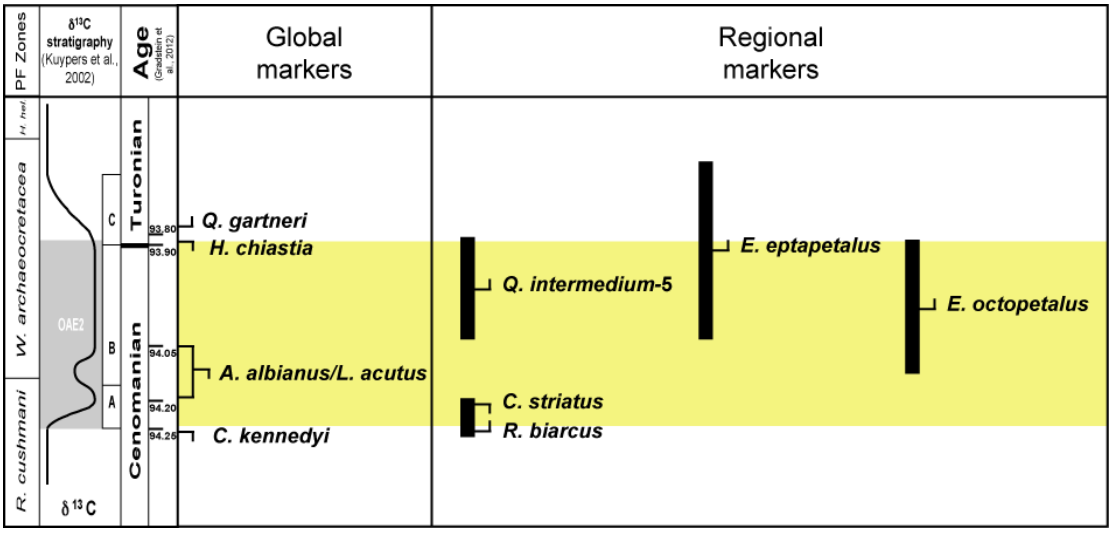

Fig.5.2.3 Summary of zonal, subzonal and secondary bioevents in the Cenomanian/Turonian boundary interval. The range of the position of secondary events shows their unsuitability as stratigraphic marker at global scale

Turonian/Coniacian boundary interval

The proposed marker for the base of the Coniacian is the FO of inoceramid bivalve *Cremnoceramus deformis erectus* (*C. rotundatus – sensu* Tröger *non* Fiege – of some studies). The Coniacian GSSP is not yet defined, but a composite GSSP of Salzgitter-Salder Quarry (Germany) and Słupia Nadbrzeżna (Poland) was proposed (Walaszczyk et al., 2010). Nannofossil investigations in the GSSP proposed sections were carried out by Lees (2008) and then summarized by Walaszczyk et al. (2010) in the GSSP proposal. The nannofossil event closest to the boundary is the LO of *H. turonicus* (Lees, 2008; Walaszczyk et al., 2010). At Salzgitter-Salder Quarry and Słupia Nadbrzeżna, nannofossil assemblage is characterized by the presence of regular *A. parcus expansus*, *Z. biperforatus* and *M. furcatus*, these three taxa have their first occurrence below the boundary whilst *M. staurophora* is absent in both successions (Lees, 2008; Walaszczyk et al., 2010) (Fig.5.2.4). The FO of *M. furcatus* was used by both Sissingh (1977) and Bralower et al. (1995) to place CC12/CC13 and NC14/NC15 zonal boundaries, respectively. The FOs of *Z. biperforatus* and *A. parcus expansus* were used by Burnett (1998) as subzonal boundaries in her UC9 zone. All these events were reported by Lees (2008) from different regions: she identified in

sequence the FO of *Z. biperforatus*, the FO of *M. furcatus*, the FO of *A. parcus expansus*, the LO of *H. turonicus* below the boundary and the FO of *M. starophora* above (in Czech Republic); the FO of *M. furcatus*, the FO of *A. parcus expansus*, the LO of *H. turonicus* below the boundary and the FOs of *Z. biperforatus* and *M. staurophora* above (in England). At Bottaccione (Tremolada, 2002), *Z. biperforatus*, *A. parcus expansus* and *H. turonicus* were not reported and the Turonian/Coniacian boundary was approximate to the FO of *M. furcatus*.

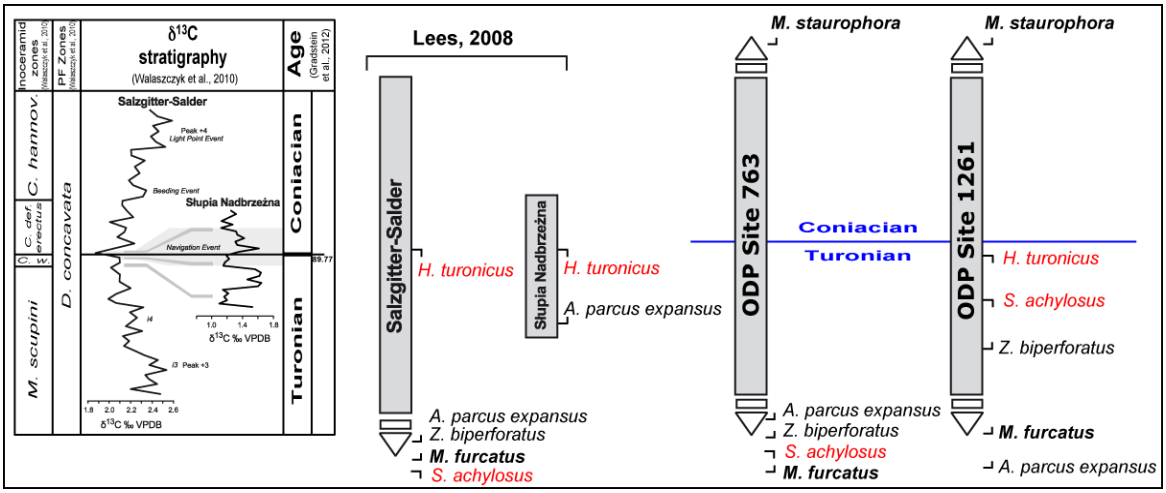

Fig.5.2.4 Zonal (bold) and subzonal (regular) events recognized in the Turonian/Coniacian boundary interval. Additional bioevents are indicated in red

Three of the studied sections comprise the Turonian/Coniacian boundary interval, but only ODP Sites 763 and 1261 show a complete record whilst at ODP Site 1138, almost the entire Coniacian is missing (Fig.5.2.4). *H. turonicus* was not identified at ODP Site 763, and its absence from other sections in the Indian Ocean (Lees, 2002) leads to argue that this taxon may be latitudinally restricted and absent at Austral palaeolatitudes. I recognized the FO of *Z. biperforatus* at different levels at ODP sites 763 and 1261. Lees (2008) reported this taxon below or above the boundary in the different sections, so it should be used with caution to define the Turonian/Coniacian boundary. The FOs of *M. furcatus* and *A. parcus expansus* were always found below the boundary (Fig.5.2.4). The sequence of these two events is not always the same, perhaps because of the rarity of both taxa at the beginning of their range. Additionally, I noticed the LO of *S. achylosus*, a taxon considered to extinguish in the Middle Turonian (Thierstein, 1974; Watkins et al., 1996; Burnett, 1998), close to the LO of *H. turonicus* at ODP Site 1261 (Fig.5.2.4). A similar datum was reported by Lees (2008) from Langdon Stairs (England).

In sections where *H. turonicus* is identified, its extinction datum seems to fall at, or really close to, the Turonian/Coniacian boundary. At Austral palaeolatitudes, or where this taxon is absent, the Turonian/Coniacian boundary interval may be constrained by the FOs of *M. furcatus*, *A. parcus expansus* (below) and the FO of *M. staurophora* (above).

Coniacian/Santonian boundary interval

The GSSP candidate for the Santonian Stage is the Olazagutía Quarry section (Spain); the boundary marker is the FO of the inoceramid *Cladoceramus undulatoplicatus* which appearance datum is reported above the FOs of *L. grillii* and *L. cayeuxii* and below the LO of *L. septenarius*, in the *Dicarinella asymetrica* planktonic foraminiferal zone, in particular in the *Sigalia carpatica* subzone (Lamolda & Paul, 2007) (Fig.5.2.5). The same sequence of events reported at Olazagutía Quarry was determined in several sections (Gale et al., 2007; Howe et al., 2007; Melinte & Lamolda, 2007; Melinte-Dobrinescu, 2010). At Bottaccione (Tremolada, 2002) no specimens of *L. grillii* and *L. septenarius* were reported, *L. cayeuxii* has its first occurrence between FOs of *D. asymetrica* and *Sigalia* sp. (Premoli Silva & Sliter, 1995; Tremolada, 2002), which seems correlatable with the proposed GSSP. The FO of *L. cayeuxii* was reported in all available zonations, whilst the two other events were not indicated by Bralower et al. (1995). The LO of *L. septenarius* was added by Perch-Nielsen (1985) to Sissingh's (1977) scheme at the same level of the FO of *L. cayeuxii*.

Two of the studied sections comprise the Coniacian/Santonian boundary interval and one ends just below the boundary (Fig.5.2.5). All the markers reported from the proposed GGSP section were identified excepted at ODP Site 1138 where *L. grillii* was not observed (Fig.5.2.5). At ODP Site 763 the FO of *L. cayeuxii* have been identified above the LO of *L. septenarius* and at ODP Site 1261, *L. septenarius* is still present in the uppermost sample (Fig.5.2.5). At ODP Site 1138 no samples with both *L. cayeuxii* and *L. septenarius* were observed. The FO of *L. cayeuxii* above the LO of *L. septenarius* seems to be confirmed at Austral palaeolatitudes by Lees (2002) who reported the sequence of these two bioevents in the same order recognized at ODP Site 763 (this work).

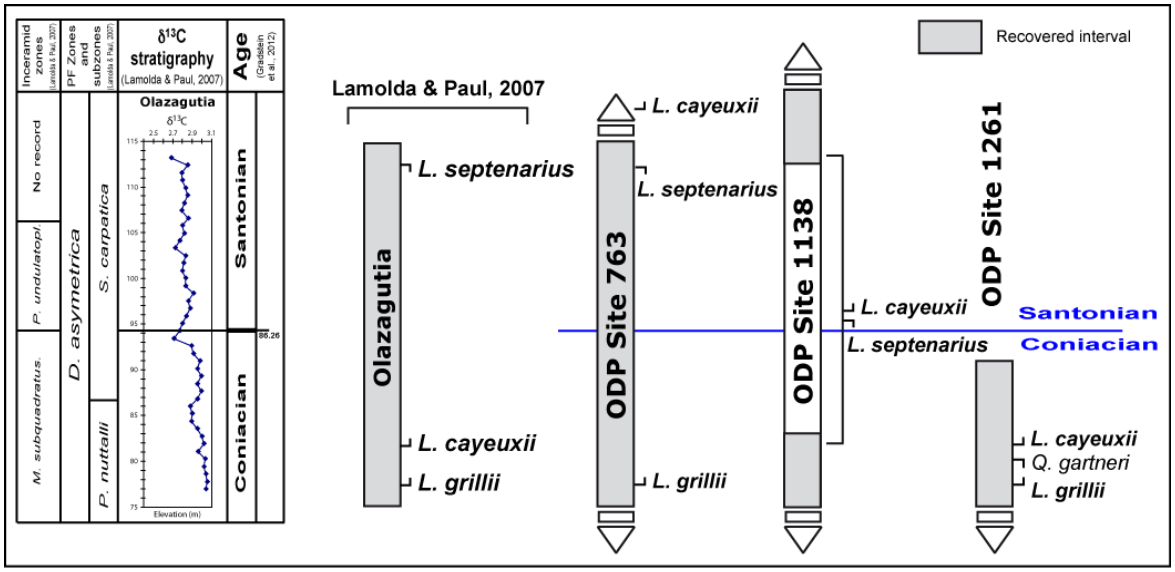

Fig.5.2.5 Zonal (bold) and subzonal (regular) events recognized in the Coniacian/Santonian boundary interval

Santonian/Campanian boundary interval

The base of the Campanian Stage has not yet been formally defined. Two boundary events were proposed: the LO of crinoid *Marsupites testudinaris* and the end of the normal-polarity Chron C34n (Alvarez et al., 1977; Gale et al., 2008; Petrizzo et al., 2011). In this study I use the proposition of the end of magnetochron C34n to place the base of the Campanian. The FO of *A. parcus parcus* has been widely used to approximate the Santonian/Campanian boundary as it falls in close proximity of the magnetic boundary, near the LO of the planktonic foraminifer *Dicarinella asymetrica* (Thierstein, 1976; Roth, 1978; Monechi & Thierstein, 1985; Bralower & Siesser, 1992; Bralower et al., 1995; Premoli Silva & Sliter, 1995; Tremolada, 2002; Petrizzo et al., 2011). In the Bottaccione section (Italy), where integrated bio-magneto-stratigraphy is available (e.g. Monechi & Thierstein, 1985), the FO of *A. parcus parcus* is preceded by the FO of *A. cymbiformis* (Tremolada, 2002) and is followed by the FO of *A. parcus constrictus* (Gardin et al., 2001) (Fig.5.2.6).

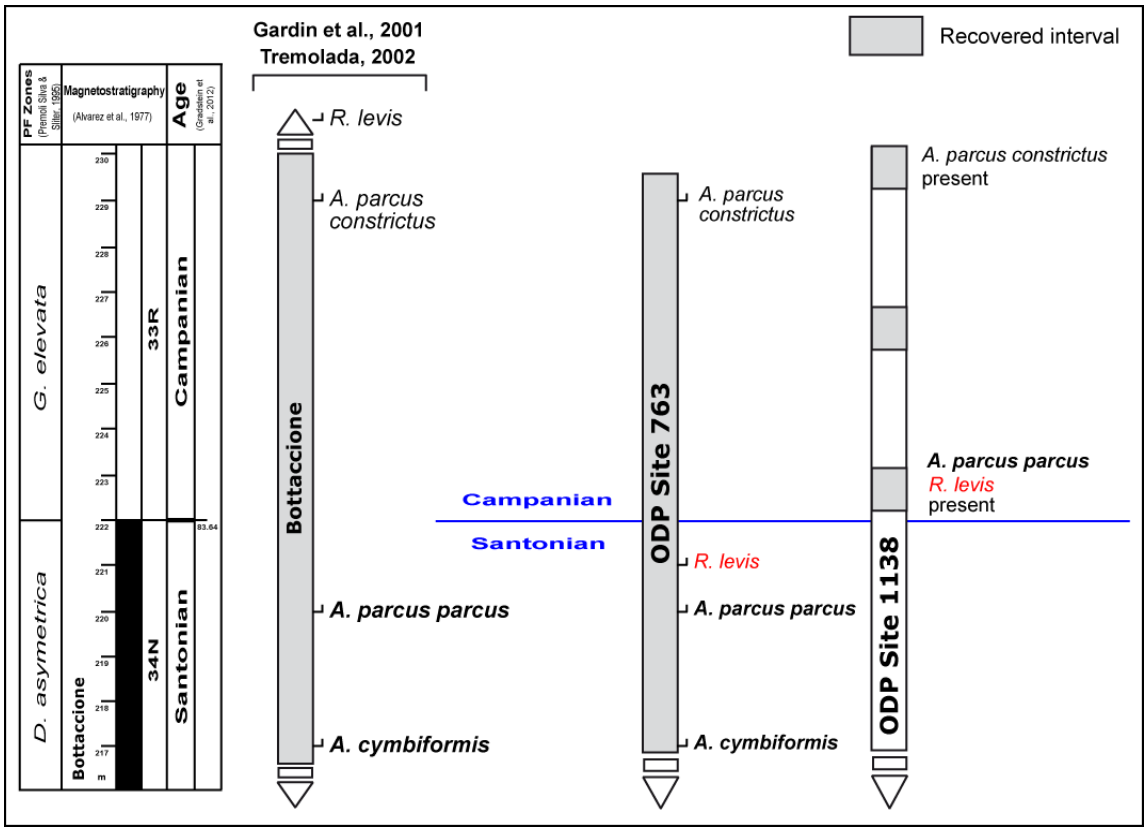

Fig.5.2.6 Zonal (bold) and subzonal (regular) events recognized in the Santonian/Campanian boundary interval

Two of the studied sections comprise the Coniacian/Santonian boundary interval (Fig.5.2.6). The FO of *A. parcus parcus* was identified at ODP Site 763; this event is preceded by the FO of *A. cymbiformis* and followed by the FO of *A. parcus constrictus*. Scarcity of recovery at ODP Site 1138 prevented the identification of the FO of *A. cymbiformis*. The FOs of *A. cymbiformis*, *A. parcus parcus* and *A. parcus constrictus* were reported in the same order in South England

(Hampton et al., 2007), thus giving a cosmopolitan value to these biostratigraphic markers, from Austral to Boreal palaeolatitudes.

I recognized the FO of *R. levis* at ODP Site 763 slightly above the FO of *A. parcus parcus* and below the FO of A. *parcus constrictus* (Fig.5.2.6). This datum is different from what reported by Sissingh (1977) and Perch-Nielsen (1985) and also from what reported by Gardin et al. (2001) at Bottaccione who placed this event well above the FO of *A. parcus constrictus*. As also reported by Bralower & Siesser (1992) for ODP sites 761-763 and by Lees (2002) for ODP sites 217, 249, 738, 758, *R. levis* seems to have its appearance datum quite earlier in the Indian Ocean.

Chapter 6

Conclusions

For the Late Cretaceous time interval three nannofossil biozonations are available. They were originally established for different paleobiogeographic areas (Oceanic sites, Southern Europe and Northern Africa sections, North-West Europe, high Southern latitudes) and have been applied to several case studies. A total of 48 zonal and subzonal events constitute the base for up to 14 biozones in the Late Albian to Early Campanian interval. Screening of individual zonations (Sissingh, 1977; Roth, 1978; Bralower et al., 1995; Burnett, 1998) including analyses of range charts (when available) and independent data used for age assignment, was preparatory for a detail comparison of individual events and zones/subzones.

The different time resolution of the three zonations is mainly due to a higher number of nannofossil biohorizons in Burnett (1998). Numerous events observed in the North Sea area, were added to achieve a higher stratigraphic resolution especially in the Early Cenomanian and Late Campanian interval characterized by few nannofossil events in Roth (1978) - Bralower et al. (1995) and partially in Sissingh (1977).

The Cenomanian/Turonian boundary interval is punctuated by several bioevents in all the zonations. For the Early Turonian to Late Campanian time interval, zonations of Sissingh (1977) and Burnett (1998) are comparable, probably because Burnett (1998) incorporated in her zonation the data presented by Sissingh (1977) and Perch-Nielsen (1985). The resolution of the zonation of Roth (1978) revised by Bralower et al. (1995), remains lower except in the Cenomanian/Turonian boundary interval and in the Maastrichtian.

The zonation of Burnett (1998) includes the majority of the events present in the other zonations with the exception of few zonal and some subzonal markers.

This study was focused on the nannofossil biostratigraphic analyses of eight sections covering the Late Albian to Early Campanian interval. Sections/Sites were selected based on chemo-bio-

stratigraphy available to constrain the age of nannofossil events relative to stages, C-isotope anomalies and Oceanic Anoxic Events (OAE)s.

Nannofossil assemblages were investigated in smear slides using polarizing light microscope and semi-quantitative characterization of preservation, total abundance and individual taxon abundance were compiled.

Most of the observed taxa are unambiguously described in the literature, but some taxonomic revision has been applied to cases of potential misidentification and discrepant attribution. Taxonomic appendices comprise the list of all identified taxa and remarks based on personal observation. Also, photographic plates are provided for all zonal/subzonal markers and some other common species.

The detailed results obtained for each section/site were compared to previous studies of the same successions (when available) and to biostratigraphic investigations of other areas documented in the literature. This comparison resulted in an evaluation of the reproducibility, sinchroneity or diachroneity of individual event.

Results were compared to the available nannofossil biozonation of the Late Albian-Early Campanian time interval. The observed nannofossil biohorizons (zonal, subzonal and secondary markers) were evaluated to assess the applicability of biozonations in the study areas. A total of 17 zonal and 4 subzonal markers have been recognized, whereas 26 biohorizons could not be used due to their absence or extreme rarity in the studied sections, or because were found at significantly different stratigraphic level relative to the timing attribution in adopted zonations. A few potential additional events were recognized and further investigations will assess their applicability.

Nannofossil events were examined in the context of stage boundary definition. Specifically, for each stage boundary the data documented for GSSP sections and/or presented for GSSP proposals were analyzed and the result of my investigation were used to provide information about the applicability of nannofossil events.

The major conclusion of my Ph.D. work is the applicability of the three zonations and the recognition of 21 zonal/subzonal events on a total of 48. The achieved resolution is comparable for the three biozonations; higher subdivision is possible only at regional level and in restricted time intervals. Moreover, nannofossil events were proved to be extremely useful to biostratigraphically constrain paleoceanographic events of the Late Albian-Early Turonian interval. Namely, OAE1d, MCE and OAE2 were successfully characterized in all the studied sequences.

References

Alvarez, W., Arthur, M.A., Fisher, A.G., Lowrie, W., Napoleone, G., Premoli Silva, I., Roggentheim, W.M., 1977. Upper Cretaceous-Paleocene magnetic stratigraphy at Gubbio, Italy. Type section for the Late Cretaceous-Paleocene geomagnetic reversal time scale. *Geol. Soc. Am. Bull.*, 88, 383-389.

Arthur, M.A., Premoli Silva, I., 1982. Development of widespread organic carbon-rich strata in Mediterranean Tethys. In: Schlanger, S.O., Cita, M.B. (Eds.), *Nature and Origin of Cretaceous Carbon-rich Facies*. 7-54.

Applegate, J.L., Bergen, J.A., 1988. Cretaceous calcareous nannofossil biostratigraphy of sediments recovered from the Galicia margin, ODP Leg 103. In: Boillot, G., Winterer, E. L., et al. (Eds.), *Proceedings of the Ocean Drilling Program, Scientific Results*,103, 293-348.

Arkhangelsky, A. D., 1912. Upper Cretaceous deposits of East European Russia: *Mater. Geol. Russ.*, 25.

Bauer, J., Marzouk, A.M., Steuber T., Kuss, J., 2001. Lithostratigraphy and biostratigraphy of the Cenomanian–Santonian strata of Sinai, Egypt. *Cretaceous Research*, 22 , 497–526.

Bengtson, P., Cobban, W.A., Dodsworth, P., Gale, A.S., Kennedy, W.J., Lamolda, M.A., Matsumoto, T., (…), Tröger, K.-A., 1996. The Turonian Stage and substage boundaries. *Bulletin de l'Institut Royal des Sciences Naturelles de Belqique, Sciences de la Terre*, 66 (SUPPL.), 69-70

Blair, S.A., Watkins, D.K., 2009. High-resolution calcareous nannofossil biostratigraphy for the Coniacian/Santonian Stage boundary, Western Interior Basin. *Cretaceous Research*, 30, 367–384.

Blechschmidt, G., 1979. Biostratigraphy of calcareous nannofossils: Leg 47B, Deep Sea Drilling Project. In: Sibuet, J.-C, Ryan, W.B.F, et al. (Eds.), *Initial Reports of the Deep Sea Drilling Project*, 47, 2, 327-360.

Boersma, A., 1981. Cretaceous and Early Tertiary foraminifers from Deep Sea Drilling Project Leg 62 sites in the central Pacific. In: Thiede, J., Vallier, T.L., et al. (Eds.), *Initial Reports of the Deep Sea Drilling Project*, 62, 377- 396.

Bolli, H.M., 1966. Zonation of Cretaceous to Pliocene marine sediments based on planktonic Foraminifera. *Asoc. Venezoelana Geologia, Mineria y Petroleo Bol. Inf.*, 9, 3-32.

Bown, P.R., 2006. Early to mid-Cretaceous calcareous nannoplankton from the northwest Pacific Ocean, Leg 198, Shatsky Rise. In: Bralower, T.J., Premoli Silva, I., Malone, M.J. (Eds.), *Proceedings of the Ocean Drilling Program, Scientific Results*,198, 1-82.

Bown, P.R., and Young, J.R., 1997. Mesozoic calcareous nannoplankton classification. *Journal of Nannoplankton Research*, 19, 21–36.

Bown, P.R., and Young, J.R., 1998a. Introduction. In: Bown, P.R. (Ed.), Calcareous Nannofossil Biostratigraphy. Chapman and Hall, London, 132–199.

Bown, P.R., and Young, J.R., 1998b. Techniques. In: Bown, P.R. (Ed.), Calcareous Nannofossil Biostratigraphy. Chapman and Hall, London, 132–199.

Bralower, T.J., 1988. Calcareous nannofossil biostratigraphy and assemblages of the Cenomanian–Turonian boundary interval: implications for the origin and timing of oceanic anoxia. *Paleoceanography* 3, 275–316.

Bralower, T.J., Bergen, J.A., 1998. Cenomanian-Santonian calcareous nannofossil biostratigraphy of a transect of cores drilled across the Western Interior Seaway. In: Dean, W.E., Arthur, M.A. (Eds.), Stratigraphy and Paleoenvironments of the Cretaceous Western Interior Seaway, USA, vol. 6. *Society for Economic Paleontology and Mineralogy Concepts in Sedimentology and Paleontology*, 159–177.

Bralower, T.J., Leckie, R.M., Sliter, W.V., Thierstein, H.R., 1995. An integrated Cretaceous microfossil biostratigraphy. In: Berggren, W.A., Kent, D.V., Aubry, M.-P., Hardenbol, J. (Eds.), *Geochronology, Time Scales and Global Stratigraphic Correlation. Society of Economic Paleontologists and Mineralogists*, Special Publication, 54, 65-79.

Bralower, T.J., Fullagar, P.D., Paull, C.K., Dwyer, G.S., Leckie, R.M., 1997. Mid-Cretaceous strontium-isotope stratigraphy of deep-sea sections. *Geol. Soc. Am. Bull*., 109, 1421–1442.

Bralower, T.J., Siesser, W.J., 1992. Cretaceous calcareous nannofossil biostratigraphy of Sites 761, 762 and 763, Exmouth and Wombat Plateaus, northwest Australia. In: von Rad, U., Haq, B. U., et al. (Eds.), *Proceedings of the Ocean Drilling Program, Scientific Results*, 122, 529-556.

Bralower, T.J., Sliter, W.V., Arthur, M.A., Leckie, R.M., Allard, D., Schlanger, S.O., 1993. Dysoxic/anoxic episodes in the Aptian-Albian (Early Cretaceous). In: Pringle, M., Sager, W.W., Sliter, W.V., Stein, S. (Eds.), *The Mesozoic Pacific: Geology, Tectonics, and Volcanism*. American Geophysical Union Monograph, 77, 5-37.

Bukry, D., 1969. Upper Cretaceous coccoliths from Texas and Europe. *Univ. Kansas Paleontol. Contrib.*, 51, 1-79.

Bukry, D., 1973a. Low-latitude coccolith biostratigraphic zonation, In: Edgar, N. T., Saunders, J. B., et al. (Eds.), *Initial Reports of the Deep Sea Drilling Project*, 15, 685-703.

Bukry, D., 1973b. Coccolith stratigraphy, eastern equatorial Pacific, Leg 16, Deep Sea Drilling Project. In: van Andel, T. H., Heath, G. R., et al. (Eds.), *Initial Reports of the Deep Sea Drilling Project*, 16, 653-711.

Bukry, D., 1974. Coccolith stratigraphy, offshore Western Australia, Deep Sea Drilling Project Leg 27. In: Veevers, J. J., Heirtzler, J. R., et al. (Eds.), *Initial Reports of the Deep Sea Drilling Project*, 27, 623-630.

Bukry, D., 1975. Coccoliths and silicoflagellate stratigraphy, Northwestern Pacific ocean, Deep Sea Drilling Project Leg 32. In: Larson, R. L., Moberly, R., et al. (Eds.), *Initial Reports of the Deep Sea Drilling Project*, 32, 677-701.

Bukry, D., 1976. Coccolith stratigraphy of the Manihiki Plateau, Central Pacific, Deep Sea Drilling Project, Site 111. In: Jackson, E. D., Schlanger, S., et al. (Eds.), *Initial Reports of the Deep Sea Drilling Project*, 33, 493-501.

Bukry, D., Bramlette, M. N., 1970. Coccolith age determinations, Deep Sea Drilling Project Leg 3. In: Maxwell, E., von Herzen, R., et al. (Eds.), *Initial Reports of the Deep Sea Drilling Project*, 3, 589-611.

Burnett, J.A., 1988. North-west European Late Cretaceous calcareous nannofossils: Biostratigraphy and selected evolutionary lineages. *Ph.D. Thesis*, University College London.

Burnett, J.A., 1996. Nannofossils and Upper Cretaceous (sub-)stage boundaries - state of the art. *Journal of Nannoplankton Research*, 18, 23-32.

Burnett, J.A., 1997. New species and new combinations of Cretaceous nannofossils, and a note on the origin of Petrarhabdus (Deflandre) Wind & Wise. *Journal of Nannoplankton Research*, 19, 133-146.

Burnett, J.A., 1998. Upper cretaceous. In: Bown, P.R. (Ed.), *Calcareous Nannofossil Biostratigraphy*. Chapman and Hall, London, 132–199.

Burnett, J.A., Hancock, J.M., Kennedy, W.J., Lord, A.R., 1992a. Macrofossil, planktonic foraminiferal and nannofossil zonation at the Campanian/Maastrichtian boundary. *Newsletters on Stratigraphy*, 27, 157-172.

Burnett, J.A., Kennedy, W.J., Ward, P.D., 1992b. Maastrichtian nannofossil biostratigraphy in the Biscay region (south western France, northern Spain). *Newsletters on Stratigraphy*, 26, 145-155.

Burnett, J.A., Whitham, F., 1999. Correlation between the nannofossil and macrofossil biostratigraphies and the lithostratigraphy of the Upper Cretaceous of NE England. *Proceedings of the Yorkshire Geological Society*, 52, 371-381.

Campbell, R.J., Howe, R.W., Rexilius, J.P., 2004. Middle Campanian–lowermost Maastrichtian nannofossil and foraminiferal biostratigraphy of the northwestern Australian margin. *Cretaceous Research*, 25, 827–864.

Caron, M., 1985. Cretaceous planktonic foraminifera. In: Bolli, H.M., Saunders, J.B., Perch-Nielsen, K. (Eds.), *Plankton Stratigraphy*. Cambridge University Press, Cambridge, 17-86.

Catanzariti, R., Ellero, A., Levi, N., Ottria, G., Pandolfi, L., 2007. Calcareous nannofossil biostratigraphy of the Antola Unit succession (Northern Apennines, Italy): new age constraints for the Late Cretaceous Helminthoid Flysch. *Cretaceous Research*, 28, 841-860.

Cavalier-Smith, T., 1981. Eukaryote kingdoms: seven or nine? *BioSystems*, 10, 93-114.

Cavalier-Smith, T., 1986. The Kingdom Chromista: Origins and systematics. *Progress in Phycological Research*, 4, 309-344.

Čech, S., Hradecká, L., Svobodová, M., Švábenická, L., 2005. Cenomanian and Cenomanian-Turonian boundary in the southern part of the Bohemian Cretaceous Basin, Czech Republic. *Bulletin of Geosciences*, 80, 321-354.

Cepek, P., 1978. Mesozoic calcareous nannoplankton of the eastern North Atlantic, Leg 41. In: Lancelot, Y., Seibold, E., et al. (Eds.), *Initial Reports of the Deep Sea Drilling Project*, 41, 667-687.

Čepek, P., 1981. Mesozoic calcareous-nannoplankton stratigraphy of the central north Pacific (Mid-Pacific Mountains and Hess Rise), Deep Sea Drilling Project Leg 62. In: Thiede, J., Vallier, T.L., et al. (Eds.), *Initial Reports of the Deep Sea Drilling Project*, 62, 397-418.

Cepek, P., Hay, W.W., 1969. Calcareous nannoplankton and biostratigraphic subdivision of the Upper Cretaceous. *Gulf Coast Assoc. Geol. Soc. Trans.*, 19, 323-336.

Cita, M.B., Coccioni, R., Edwards, A.R., Monechi, S., Morgans, H.E.G., Strong, C.P., Watkins, D.K., and Webb, P.-N., 1997. Nannofossils and foraminifera. In: Hannah, M.J., Raine, J.I. (Eds.), *Southern Ocean Late Cretaceous/Early Cenozoic Biostratigraphic Datums*. Inst. Geol. Nucl. Sci., Sci. Rep., 4, 5-10.

Cita, M.B. and Gartner, S., 1971. Deep sea Upper Cretaceous from the Western North Atlantic: *2ndPlank. Conf. Proc*, 1, 287-319.

Corbett, M.J., Watkins, D.K., 2013. Calcareous nannofossil paleoecology of the mid-Cretaceous Western Interior Seaway and evidence of oligotrophic surface waters during OAE2. *Palaeogeography, Palaeoclimatology, Palaeoecology*, 392, 510-523.

Crux, J.A., 1981. New calcareous nannofossil taxa from the Cretaceous of South East England. *Neues Jahrbuch für Geologie und Paläontologie, Monatshefte*, 1981, 633-640.

Crux, J.A., 1982. Upper Cretaceous (Cenomanian to Campanian) calcareous nannofossils. In: Lord, A.R. (Ed.), *A Stratigraphical Index of Calcareous Nannofossils*. British Micropalaeontological Society Series. Ellis Horwood Limited, Chichester, 81-135.

Crux, J.A., 1991. New calcareous nannofossil taxa from the Cretaceous of South East England. *Neues Jahrbuch für Geologie und Palaöntologie*, Monatshefte, 1981, 633-640.

Deflandre, G., 1952. Classe des Coccolithophoridés (Coccolithophoridae Lohmann, 1902). *Traité de zoologie. Anatomie, systematique biologie, 1, part 1, Phylogenie. Protozoaires: généralités. Flagellés* (ed. P.P. Grassé). Masson et Cie (Paris), 439-470.

Deflandre, G., 1959. Sur le nannofossiles calcaires et leur Systématique. *Revue de Micropaléontologie*, 2, 127-152.

De Romero, L.M., Truskowski, I.M., Bralower, T.J., Bergen, J.A., Odreman, O., Zachos, J.C., Galea-Alvarez, F.A., 2003. An integrated calcareous microfossil biostratigraphic and carbon-isotope stratigraphic framework for the La Luna Formation, Western Venezuela. *Palaios*,18, 349–366.

Desmares, D., Grosheny, D., Beaudoin, B., Gardin, S., Gauthier-Lafaye, F., 2007. High resolution stratigraphic record constrained by volcanic ash beds at the Cenomanian-Turonian boundary in the Western Interior Basin, USA. *Cretaceous Research*, 28, 561-582.

Do Monte Guerra, R., Tokutake, L.R., Fauth, G., 2010. Upper Campanian nannofossils from a core of well 2-RSS-1, Pelotas Basin, Brazil. *Rev. bras. paleontol*., 13, 181-188.

Do Monte Guerra, R., Tokutake, L.R., Fauth, G., 2012. Cretaceous calcareous nannofossils from Pelotas Basin, Brazil: Biostratigraphic and paleoecological inferences. *Journal of South American Earth Sciences*, 36, 55-71.

Erba, E., 2004. Calcareous nannofossils and Mesozoic anoxic events. *Marine Micropaleontology*, 52, 85–106.

Erba, E., Covington, J.M., 1992. Calcareous nannofossil biostratigraphy of Mesozoic sediments recovered from the western Pacific, Leg 129. In: Larson, R. L., Lancelot, Y., et al. (Eds.), *Proceedings of the ODP, Scientific Results*, 129, 179-187.

Erba, E., Da-Yong, J., Tintori, A., Motani, R., 2013. The oldest calcareous nannofossil: Middle Triassic coccoliths from China. *INA14 abstracts*, Reston, Virginia.

Erba, E., Premoli Silva, I., Watkins, D.K., 1995. Cretaceous calcareous plankton biostratigraphy of Sites 872 through 879. In: Haggerty, J.A., Premoli Silva, I., Rack, F, and McNutt, M.K. (Eds.), *Proceedings of the Ocean Drilling Program, Scientific Results*, 144, 157-169.

Erbacher, J., Friedrich, O., Wilson, P.A., Birch, H., Mutterlose, J., 2005. Stable organic carbon isotope stratigraphy across Oceanic Anoxic Event 2 of Demerara Rise, western tropical Atlantic. *Geochemistry, Geophysics, Geosystems* 6, Q06010. doi:10.1029/2004GC000850.

Eshet, Y., Almogi-Labin, A., 1996. Calcareous nannofossils as paleoproductivity indicators in upper cretaceous organic-rich sequences in Israel. *Marine Micropaleontology*, 29, 37–61.

Farouk, S., Faris, M., 2012. Late Cretaceous calcareous nannofossil and planktonic foraminiferal bioevents of the shallow-marine carbonate platform in the Mitla Pass, west central Sinai, Egypt. *Cretaceous Research*, 33, 50-65.

Fernando, A.G.S., Takashima, R., Nishi, H., Giraud, F., Okada, H., 2010. Calcareous nannofossil biostratigraphy of the Thomel Level (OAE2) in the Lambruisse section, Vocontian Basin, southeast France. *Geobios*, 43, 45–57.

Fernando, A.G.S., Nishi, H., Tanabe, K.,Moriya, K., Iba, Y., Kodama, K., Murphy, M.A., Okada, H., 2011. Calcareous nannofossil biostratigraphic study of forearc basin sediments: Lower to Upper Cretaceous Budden Canyon Formation (Great Valley Group), northern California, USA. *Island Arc*, 20, 346-370.

Fiorentino, A., 1995. Calcareous nannofossil stratigraphy of Maastrichtian sections in Israel**.** *Cretaceous Research*, 16, 327-341.

Fries, G., Parize, O., 2003. Anatomy of ancient passive margin slope systems: Aptian gravity-driven deposition on the Vocontian palaeomargin, western Alps, south-east France. *Sedimentology*, 50, 1231-1270.

Gale, A.S., Kennedy, W.J., Burnett, J.A., Caron, M., Kidd, B.E., 1996. The Late Albian to Early Cenomanian succession at Mont Risou near Rosans (Drome , SE France): an integrated study (ammonites, inoceramids, planktonic foraminifera, nannofossils, oxygen and carbon isotopes). *Cretaceous Research*, 17 , 515-606.

Gale, A.S., Kennedy, W.J., Petrizzo, M.R., Lees, J.A., Walaszczyk, I., 2007. An integrated study (inoceramid bivalves, ammonites, calcareous nannofossils, planktonic foraminifera, stable carbon isotopes) of the Ten Mile Creek section, Lancaster, Dallas County, north Texas, a candidate Global boundary Stratotype Section and Point for the base of the Santonian Stage. *Acta Geologica Polonica*, 57, 2, 113-160.

Gale, A.S., Hancock, J.M., Kennedy, W.J., Petrizzo, M.R., Lees, J.A., Walaszczyk, I., Wray, D.S., 2008. An integrated study (geochemistry, stable oxygen and carbon isotopes, nannofossils, planktonic foraminifera, inoceramid bivalves, ammonites and crinoids) of the Waxahachie Dam Spillway section, north Texas: a possible boundary stratotype for the base of the Campanian Stage. *Cretaceous Research*, 29, 131-167.

Gambacorta, G., 2013. Paleoceanographic and paleoclimatic reconstructions of the late Albian - early Turonian (Late Cretaceous) time interval: from an unstable to a stable ocean. *Ph.D. Thesis*, Università degli Studi di Milano.

Gardin, S., Del Panta, F., Monechi, S., Pozzi, M., 2001. A tethyan reference record for the Campanian and Maastrichtian stages: the Bottaccione Section (Central Italy); review of data and new calcareous nannofossil results. In: Odin, G.S. (Eds.), *The Campanian-Maastrichtian boundary*, Elsevier Science B. V., 745-757.

Gartner Jr., S., 1968. Coccoliths and Related Calcareous Nannofossil from Upper Cretaceous Deposits of Texas and Arkansas, 48. *University of Kansas Paleontological Contributions*, 48, 1-56.

Gartner, S., 1974. Nannofossil biostratigraphy, Leg 22, DSDP. In: C. yon der Borch, J.G. Sclater, et al. (Eds.), *Initial Reports of the Deep Sea Drilling Project*, 22, 577-599.

Gebhardt, H., 2001. Calcareous nannofossils from the Nkalagu Formation type locality (Middle Turonian to Coniacian, southern Nigeria): biostratigraphy and palaeo-ecologic implications. *Journal of African Earth Sciences*, 32, 3, 391-402.

Gertsch, B., Adatte, T., Keller, G., Tantawy, A.A.A.M., Berner, Z., Mort, H.P., Fleitmann, D., 2010. Middle and late Cenomanian oceanic anoxic events in shallow and deeper shelf environments of western Morocco. *Sedimentology*, 57, 1430-1462.

Giorgioni, M., Weissert, H., Bernasconi, S.M., Hochuli, P.A., Coccioni, R., Keller, C.E., 2012. Orbital control on carbon cycle and oceanography in the mid-Cretaceous greenhouse. *Paleoceanography*, 27, art. no. PA1204.

Giraud, F., Reboulet, S., Deconinck, J.F., Martinez, M., Carpentier, A., Bréziat, C., 2013. The Mid-Cenomanian Event in southeastern France: Evidence from palaeontological and clay mineralogical data. *Cretaceous Research*, 46, 43-58.

Gorka, H. 1957. Les Coccolithophorides du Maestrichtian supérieur de Pologne: *Acta Paleont. Polonica*, 2, 235-284.

Gradstein, F.M., Ogg, J.G., Schmitz, M.D., Ogg, G.M., 2012.The Geologic Time Scale, 2, 801-853.

Hadavi,F., Senemari, S., 2010. Calcareous Nannofossils from the Gurpi Formation (Lower Santonian-Maastrichtian), Faulted Zagros Range, Western Shiraz, Iran. *Stratigraphy and Geological Correlation*, 18, 166–178.

Hampton, M.J., Bailey, H.W., Gallagher, L.T., Mortimore, R.N., Wood, C.J., 2007. The biostratigraphy of Seaford Head, Sussex, southern England; an international reference section for the basal boundaries for the Santonian and Campanian Stages in chalk facies. *Cretaceous Research*, 28, 43-60.

Haq, B.U., Boyd, R.L., Exon, N.F., von Rad, U., 1992. Evolution of the central Exmouth Plateau: a post-drilling perspective. In: von Rad, U., Haq, B.U., et al. (Eds.), *Proceedings of the Ocean Drilling Program, Scientific Results*, 122, 801-808.

Hardas, P., Mutterlose, J., 2006. Calcareous nannofossil biostratigraphy of the Cenomanian/Turonian boundary interval of ODP Leg 207 at the Demerara Rise. *Revue de Micropaléontologie*, 49, 165–179.

Hardas, P., Mutterlose, J., 2007. Calcareous nannofossil assemblages of Oceanic Anoxic Event 2 in the equatorial Atlantic: Evidence of an eutrophication event. *Marine Micropaleontology*, 66, 52–69.

Hardas, P., Mutterlose, J., Friedrich, O., Erbacher, J., 2012. The Middle Cenomanian Event in the equatorial Atlantic: The calcareous nannofossil and benthic foraminiferal response. *Marine Micropaleontology*, 96-97, 66-74.

Hattner, J.G., Wind, F.H. & Wise, S.W., 1980. The Santonian-Campanian boundary: comparison of nearshore-offshore calcareous nannofossil assemblages. *Cahiers de Micropaléontologie*, 3, 9-26.

Hibberd, D.J., 1976. The ultrastructure and taxonomy of the Chrysophyceae and Prymnesiophyceae (Haptophyceae): a survey with some new observations on the ultrastructure of the Chrysophyceae. *Botanical Journal of the Linnaen Society*, 72, 55-80.

Hill, M.E., 1976. Lower Cretaceous calcareous nannofossils from Texas and Oklahoma. *Palaeontographica Abteilung B*, 156, 103-179.

Holburn, A., Kuhnt, W., 2002. Cenomanian-Turonian palaeoceanographic change on the Kerguelen Plateau: a comparison with Northern Hemisphere records. *Cretaceous research*, 23, 333-349.

Howe, R.W., Sikora, P.J., Gale, A.S., Bergen, J.A., 2007. Calcareous nannofossil and planktonic foraminiferal biostratigraphy of proposed stratotypes for the Coniacian/Santonian boundary: Olazagutia, northern Spain; Seaford Head, southern England; and Ten Mile Creek, Texas, USA. *Cretaceous Research*, 28, 61-92.

Jeremiah, J., 1996. A proposed Albian to lower Cenomanian nannofossil biozonation for England and the North Sea Basin. *Journal of Micropalaeontology*, 15, 97-129.

Jiménez Berrocoso, A., MacLeod, K.G., Huber, B.T., Lees, J.A., Wendler, I., Bown, P.R., Mweneinda, A.K., Isaza Londoño, C., Singano, J.M., 2010. Lithostratigraphy, biostratigraphy and chemostratigraphy of Upper Cretaceous sediments from southern Tanzania: Tanzania drilling project sites 21–26. *Journal of African Earth Sciences*, 57, 47-69.

Karakitzios, V., Tsikos, H., Van Breugel, Y., Koletti, L., Sinninghe Damsté, J.S., Jenkins, H.C., 2007. First evidence for the Cenomanian–Turonian oceanic anoxic event (OAE2, 'Bonarelli' event) from the Ionian Zone, western continental Greece. *International Journal of Earth Sciences*, 96, 343-352.

Kauffman, E.G., Caldwell, W.G.E., 1993. The Western Interior Basin in Space and Time. In: Caldwell, W.G.E., Kauffman, E.G. (Eds.), *Evolution of the Western Interior Basin. Geological Association of Canada, Special Paper*, 39, 1-30.

Kedzierski, M., 2008. Calcareous nannofossil and inoceramid biostratigraphies of a Middle Turonian to Middle Coniacian section from the Opole Trough of SW Poland. *Cretaceous Research*, 29, 451-467.

Keller, G., Adatte, T., Berner, Z., Chellai, E.H., Stueben, D., 2008. Oceanic events and biotic effects of the Cenomanian-Turonian anoxic event, Tarfaya Basin, Morocco. Cretaceous Research, 29, 976-994.

Kennedy, W.J., Gale, A.S., Lees, J.A., Caron, M., 2004.The Global Boundary Stratotype Section and Point (GSSP) for the base of the Cenomanian Stage, Mont Risou, Hautes-Alpes, France. *Episodes*, 27, 21-32.

Kennedy, W.J., Hansotte, M., Bilotte, M., Burnett, J., 1992. Ammonites and Nannofossils from the Campanian of Nalzen (Ariège, France). *Geobios*, 25, 2, 263-278.

Kennedy, W.J., Walaszczyk, I., Cobban, W.A., 2005. The Global Boundary Stratotype Section and Point for the base of the Turonian Stage of the Cretaceous: Pueblo, Colorado, U.S.A. *Episodes*, 28, 2, 93-104.

Kennedy, W.J., Walaszezyk, I., Cobban, W.A., 2000. Pueblo, Colorado, USA, candidate Global Boundary Stratotype Section and Point for the base of the Turonian Stage of the Cretaceous and for the base of the middle Turonian Substage, with a revision of the Inoceramidae (Bivalvia). *Acta Geologica Polonica*, 50, 295-334.

Kuhnt, W., 1990. Agglutinated foraminifera of western Mediterranean Upper Cretaceous pelagic limestones (Umbrian Apennines, Italy, and Betic Cordillera, southern Spain). *Micropaleontology*, 36, 297-330.

Ladner, B.C., Wise, S.W.,Jr., 2001. Calcareous nannofossil biostratigraphy of Upper Cretaceous to Paleocene sediments from Leg 173, Iberia Abyssal Plain, Sites 1067-1069. In: Beslier, M.-O., Whitmarsh, R.B., Wallace, P.J., Girardeau, J. (Eds.), *Proceedings of the Ocean Drilling Program, Scientific Results*, 173, 1-50 (CD-ROM).

Lamolda, M.A., Gorostidi, A., Martinez, R., Lopez, G., Peryt, D., 1997. Fossil occurrences in the Upper Cenomanian-Lower Turonian at Ganuza, northern Spain: an approach to Cenomanian/Turonian boundary chronostratigraphy. *Cretaceous Research,* 18, 331–353.

Lamolda M.A., Paul, C.R.C., 2007. Carbon and oxygen stable isotopes across the Coniacian/Santonian boundary at Olazagutia, northern Spain. *Cretaceous Research*, 28, 37-45.

Larson, R.L., 1976. Late Jurassic and Early Cretaceous evolution of the western central Pacific Ocean. *Journal of Geomagnetism and Geoelectricity*, 28, 219-239.

Lauer, G., 1974. Evolutionary trends in the Arkhangelskiellaceae (calcareous nannoplankton) of the Upper Cretaceous of central Oman, S.E. Arabia. *In*: D. Noel and K. Perch-Nielsen, *Report on the Consultant Group on Calcareous Nannoplankton*, Kiel, September 5-7. Arch. Sci. Geneve, 28 (2), 259-262.

Leckie, R.M., 1984. Mid-Cretaceous Planktonic Foraminiferal Biostratigraphy off Central Morocco, Deep Sea Drilling Project Leg 79, Sites 545 and 547. In: Hinz, K., Winterer, E.L., et al (Eds.), *Initial Reports of the Deep Sea Drilling Project*, 79, 579-620.

Leckie, R.M., 1985. Foraminifera of the Cenomanian-Turonian boundary interval, Greenhorn Formation, Rock Canyon Anticline, Pueblo, Colorado. In: Pratt, L.M., Kauffman, E.G., Zelt, F.B. (Eds.), *Fine-grained Deposits and Biofacies of the CretaceousWestern Interior Seaway: Evidence of Cyclic Sedimentary Processes*. Society of Economic Paleontologists and Mineralogists Field Trip Guidebook, 4, 139-149.

Lees, J.A., 2002. Calcareous nannofossil biogeography illustrates palaeoclimate change in the Late Cretaceous Indian Ocean. *Cretaceous Research*, 23, 537–634.

Lees, J.A., 2007. New and rarely reported calcareous nannofossils from the Late Cretaceous of coastal Tanzania: outcrop samples and Tanzania Drilling Project Sites 5, 9 and 15. *Journal of Nannoplankton Research*, 29, 39-65.

Lees, J.A., 2008. The calcareous nannofossil record across the Late Cretaceous Turonian/Coniacian boundary, including new data from Germany, Poland, the Czech Republic and England. *Cretaceous Research*, 29, 40-64.

Lees, J.A., Bown, P.R., 2006. Upper Cretaceous calcareous nannofossil biostratigraphy, ODP Leg 198 (Shatsky Rise, northwest Pacific Ocean). In: Bralower, T.J., Premoli Silva, I., and Malone, M.J. (Eds.), *Proceedings of the Ocean Drilling Program, Scientific Results*, 198, 1–60. doi:10.2973/odp.proc.sr.198.114.2005.

Linnert, C., Mutterlose, J., 2009. Biometry of the Late Cretaceous *Arkhangelskiella* group: ecophenotypes controlled by nutrient flux. *Cretaceous Research*, 30, 1193-1204.

Linnert, C., Mutterlose, J., Erbacher, J., 2010. Calcareous nannofossils of the Cenomanian/Turonian boundary interval from the Boreal Realm (Wunstorf, northwest Germany). *Marine Micropaleontology*, 74, 38–58.

Linnert, C., Mutterlose, J., Mortimore, R., 2011. Calcareous nannofossils from Eastbourne (Southeastern England) and the paleoceanography of the Cenomanian-Turonian boundary interval. *Palaios*, 26, 298-313.

Lohman, H., 1909. Die Gehause und Gallertblasen der Appendicularien und ihre Bedeutung fur die Erforschung des Lebens in Meer. *Verhandlungen Deutsche Zoologische Geselleschaft*, 19, 200-239.

Luciani, V., Cobianchi, M., 1999. The Bonarelli Level and other black shales in the Cenomanian–Turonian of the northeastern Dolomites (Italy): calcareous nannofossil and foraminiferal data. *Cretaceous Research*, 20, 135–167.

Manivit, H., 1971. Nannofossiles calcaires du Crétacé Français (Aptien-Maestrichtion). Essai de Biozonation appuyée sur les stratotypes. *Thése Doctorat d'Etat*, Université de Paris.

Manivit, H., 1984. Paleogene and upper Cretaceous calcareous nannofossils from Deep Sea Drilling Project Leg 74 (South Atlantic). In: Moore, T. C , Jr., Rabinowitz, P. D., et al., (Eds.), *Initial Reports of the Deep Sea Drilling Project*, 74, 475-499.

Manivit, H., Perch-Nielsen K., Prins, B., and Verbeek, J. W., 1977. Mid-Cretaceous calcareous nannofossil biostratigraphy. *Proc. Koninkl. Nederl. Akad. Wehettschappen*, Amsterdam, B80, 3, 169-181.

Mao, S., Wise, S.W.Jr., 1993. Mesozoic calcareous nannofossils from Leg 130. *In*: Berger, W.H., Kroenke, L.W., Mayer, L.A., et al. (Eds.), *Proceedings of the Ocean Drilling Program, Scientific Results*, 130, 85-92.

Martini, E., 1976. Cretaceous to Recent nannoplankton from the central Pacific Ocean (DSDP Leg 33). In: Schlanger, S. O., Jackson, E. D., et al. (Eds.), *Initial Reports of the Deep Sea Drilling Project*, 33, 383-424.

Melinte, M.C., Jipa, D., 2005. Campanian–Maastrichtian marine red beds in Romania: biostratigraphic and genetic significance. *Cretaceous Research*, 26, 49-56.

Melinte, M.C., Lamolda, M.A., 2007. Calcareous nannofossil biostratigraphy of the Coniacian/Santonian boundary interval in Romania and comparison with other European regions. *Cretaceous Research*, 28, 119-127.

Melinte-Dobrinescu, M.C., 2010. Lithology and biostratigraphy of Upper Cretaceous marine deposits from the Haţeg region (Romania): Palaeoenvironmental implications. *Palaeogeography, Palaeoclimatology, Palaeoecology*, 293, 283-294.

Melinte-Dobrinescu, M.C., Bojar, A.-V., 2008. Biostratigraphic and isotopic record of the Cenomanian–Turonian deposits in the Ohaba-Ponor section (SW Haţeg, Romania). *Cretaceous Research*, 29, 1024-1034.

Melinte-Dobrinescu, M.C., Bojar, A.-V., 2010. Late Cretaceous carbon- and oxygen isotope stratigraphy, nannofossil events and paleoclimate fluctuations in the Haţeg area (SW Romania). *Palaeogeography, Palaeoclimatology, Palaeoecology*, 293, 295-305.

Monechi, S., Thierstein, H., 1985. Late Cretaceous-Eocene Nannofossil And Magnetostratigraphic Correlations Near Gubbio, Italy. *Marine Micropaleontology*, 9, 419-440.

Moran, M.J., 1992. Biostratigraphy of Upper Cretaceous and Paleogene calcareous nannofossils from Leg 123, northeastern Indian Ocean. In: Gradstein F. M., Ludden, J. N., et al. (Eds.), *Proceedings of the Ocean Drilling Program, Scientific Results*, 123, 381-405.

Mortimer, C.P., 1987. Upper Cretaceous calcareous nannofossil biostratigraphy of the southern Norwegian and Danish North Sea area. *Abhandlungen der Geologische Bundesanstalt* (Wien), 39, 143-175.

Nederbragt, A.J., Fiorentino, A., 1999. Stratigraphy and paleoceanography of the Cenomanian-Turonian boundary event in Oued Mellegue, north-western Tunisia. *Cretaceous Research*, 20, 47-62.

Noel, 1970. Coccolithes crétacés: la craie campanienne du Bassin de Paris: *Centre Nat. Rech. Sci.*, Paris, 129.

Obradovich, J.D., 1993. A Cretaceous time-scale. In: Caldwell, W. G. E. and Kauffman, E. G., (Eds.), *Evolution of the Western Interior Basin*: St. Johns, Geological Association of Canada Special Paper 39, 379-396.

Obradovich, J.D. Cobban, W.H., 1975. A time-scale for the late Cretaceous of the Western Interior of North America: *Geol. Assoc. Canada Spec. Paper*, 13, 31-54.

Odin, G.S., Lamaurelle, M.A., 2001. The global Campanian-Maastrichtian stage boundary. *Episodes*, 24, 229-236.

Okada, H., Thierstein, H.R., 1979. Calcareous nannoplankton-Leg 43, Deep Sea Drilling Project. In: Tucholke, B.E., Vogt, P.R., et al. (Eds.), *Initial Reports of the Deep Sea Drilling Project*, 43, 507-573.

Olfer'ev, A.G., Beniamovski, V.N., Vishnevskaya, V.S., Ivanov, A.V., Kopaevich, L.F., Pervushov, E.M., Sel'tser, V.B., Tesakova, E.M., Kharitonov, V.M., Shcherbinina, E.A., 2007. Upper Cretaceous Deposits in the Northwest of Saratov Oblast, Part 1: Litho- and Biostratigraphic Analysis of the Vishnevoe Section. *Stratigraphy and Geological Correlation*, 15, 610-655.

Paul, C.R.C., Lamolda, M.A., Mitchell, S.F., Vaziri, M.R., Gorostidi, A., Marshall, J.D., 1999. The Cenomanian/Turonian boundary at Eastbourne (Sussex, UK): a proposed European reference section. *Palaeogeography, Palaeoceanography, Palaeoecology*, 150, 83–121.

Pearson, P.N., Nicholas, C.J., Singano, J.M., Bown, P.R., Coxall, H.K., van Dongen, B.E., Huber, B.T., Karega, A., Lees, J.A., MacLeod, K., McMillan, I.K., Pancost, R.D., Pearson, M., Msaky, E., 2006. Further Paleogene and Cretaceous sediment cores from the Kilwa area of coastal Tanzania: Tanzania Drilling Project Sites 6–10. *Journal of African Earth Sciences*, 45, 279-317.

Perch-Nielsen, K., 1972. Remarks on the Late Cretaceous to Pleistocene coccoliths from the North Atlantic. In: Laughton, A. S., Berggren, W. A., et al. (Eds.), *Initial Reports of the Deep Sea Drilling Project*, 12, 1003-1069.

Perch-Nielsen, K., 1977. Albian to Pleistocene Calcareous Nannofossils from the Western South Atlantic, DSDP Leg 39. In: Supko, P.R., Perch-Nielsen, K, et al. (Eds.), *Initial Reports of the Deep Sea Drilling Project*, 39, 699-823.

Perch-Nielsen, K., 1979. Calcareous nannofossils from the Cretaceous between the North Sea and the Mediterranean. In: Wiedmann, J. (Ed.), *Aspekte der Kreide Europas*. Int. Union Geol. Sci., A6, 223–272.

Perch-Nielsen, K., 1984. Validation of new combinations. *INA newsletters*, 6, 42-46.

Perch-Nielsen, K., 1985. Mesozoic calcareous nannofossils. *In*: Bolli, H.M., Saunders, J.B., Perch-Nielsen, K. (Eds.), *Plankton Stratigraphy*. Cambridge University Press, Cambridge, 329–427.

Percival, S.F., 1984. Late Cretaceous to Pleistocene Calcareous Nannofossils from the South Atlantic, Deep Sea Drilling Project Leg 73. In: Hsii, K.J., LaBrecque, J.L., et al. (Eds.), *Initial Reports of the Deep Sea Drilling Project*, 73, 391-424.

Pérez-Rodríguez, I., Lees, J.A.,Larrasoaña, J.C., Arz, J.A., Arenillas, I., 2012. Planktonic foraminiferal and calcareous nannofossil biostratigraphy and magnetostratigraphy of the uppermost Campanian and Maastrichtian at Zumaia, northern Spain. *Cretaceous Research*, 37, 100-126.

Persico, D., Villa, G., 2002. Problematic side views of Eprolithus: comparison with Micula decussata. *Journal of Nannoplankton Research*, 24, 15-25.

Petrizzo, M.R., 2000. Upper Turonian-lower Campanian planktonic foraminifera from southern mid-high latitudes (Exmouth Plateau, NW Australia): biostratigraphy and taxonomic notes. *Cretaceous Research*, 21, 479-505.

Petrizzo, M.R., 2001. Late Cretaceous planktonic foraminifera from Kerguelen Plateau (ODP Leg 183): new data to improve the Southern Ocean biozonation. *Cretaceous Research*, 22, 829-855.

Petrizzo, M.R., 2003. Late Cretaceous planktonic foraminiferal bioevents in the Tethys and in the Southern Ocean record: an overview. *Journal of Foraminiferal Research*, 33, 330-337.

Petrizzo, M.R., Falzoni, F., Premoli Silva, I., 2011. Identification of the base of the lower-to-middle Campanian *Globotruncana ventricosa* Zone: Comments on reliability and global correlations. *Cretaceous Research*, 32, 387-405.

Pospichal, J.J., Wise Jr., S.W.,1990. Calcareous nannofossils across the K–T boundary, ODP Hole 690C, Maud Rise, Weddell Sea. *Proceedings of the Ocean Drilling Program, Scientific Results*, 113, 515–532.

Postuma, J.A., 1971. Manual of plantonic Foraminifera. Elseviers Publishing Company, Amsterdam, 1-420.

Premoli Silva, I., Sliter, WV., 1995. Cretaceous planktonic foraminiferal biostratigraphy and evolutionary trends from the Bottaccione section, Gubbio, Italy. *Palaeontogr. Ital*, 82, 1-89.

Premoli Silva, I., Sliter, W.V., 1999. Cretaceous paleoceanography: Evidence from planktonic foraminiferal evolution. *Geol. Soc. Am.* Spec. Paper, 332, 301-328.

Proto Decima, F., Medizza, F., Todesco, L., 1978. Southeastern Atlantic Leg 40 calcareous nannofossils. In: Bolli, H.M., Ryan, W.B.F., et al. (Eds.), *Initial Reports of the Deep Sea Drilling Project*, 40, 571-634.

Reboulet, S., Giraud, F., Colombié, C., Carpentier, A., 2013. Integrated stratigraphy of the Lower and Middle Cenomanian in a Tethyan section (Blieux, southeast France) and correlations with Boreal basins. *Cretaceous Research*, 40, 170-189.

Reinhardt, P., 1966. Zur Taxonomie und Biostratigraphie des fossilen Nannoplankton aus dem Malm, der Kreide und dem Alttertiär Mitteleuropas. Freiberger Forschungshefte, C196, 5-109.

Resiwati, P., 1991. Upper Cretaceous calcareous nannofossils from Broken Ridge and Ninetyeast Ridge, Indian Ocean. In: Weissel, J., Peirce, J., Taylor, E., Alt, J., et al. (Eds.), *Proceedings of the Ocean Drilling Program, Scientific Results*, 121, 141-170.

Robaszynski, F., Caron, M., Dupuis, C., Amédro, F., Gonzalez Donoso, J.-M., Linares, D., Hardenbol, J., Gartner, S., Calandra, F., Deloffre, R., 1990. A tentative integrated stratigraphy in the Turonian of Central Tunisia: Formations, zones and sequential stratigraphy in the Kalaat Senan area. *Bull. Centres Rech. Explor.-Prod. Elf-Aquitaine*, 14, 213-384.

Roth, P.H., 1973. Calcareous nannofossils. In: Winterer, E.L., Ewing, J.I., et al., (Eds.), *Initial Reports of the Deep Sea Drilling Project*, 17, 695–795.

Roth, P.H., 1978. Cretaceous nannoplankton biostratigraphy and oceanography of the northwestern Atlantic Ocean. In: Benson, W.E., Sheridan, R.E., et al., (Eds.), *Initial Reports of the Deep Sea Drilling Project*, 44, 731–759.

Roth, P.H., 1981. Mid-Cretaceous calcareous nannoplankton from the central Pacific: implications for paleoceanography. In: Thiede, J., Vallier, T.L., et al. (Eds.), *Initial Reports of the Deep Sea Drilling Project*, 62, 471-490.

Roth, P.H., Thierstein, H., 1972. Calcareous nannoplankton: Leg 14 of the Deep Sea Drilling Project. In: Hayes, D.E., Pimm, A.C., et al. (Eds.), *Initial Reports of the Deep Sea Drilling Project*, 14, 421-485.

Sasaran, L., Balc, R., Sasaran, E., 2005. Sedimentologic and micropaleontological study of an Upper Cretaceous (Santonian-Campanian) regressive facies development – from basin to upper slope sediments (Gilau Mountains, Plescuta Valley, NW Romania). *Acta Paleontologica Romanie*, 5, 441-450.

Schroder-Adams, C.J., Leckie, D.A., Bloch, J., Craig, J., McIntyre, D.J., Adams, P.J., 1996. Paleoenvironmental changes in the Cretaceous (Albian to Turonian) Colorado Group of western Canada: microfossil , sedimentological and geochemical evidence. *Cretaceous Research*, 17, 311-365.

Scopelliti, G., Bellanca, A., Erba, E., Jenkyns, H.C., Neri, R., Tamagnini, P., Luciani, V., Masetti, D., 2008. Cenomanian-Turonian carbonate and organic-carbon isotope records, biostratigraphy and provenance of a key section in NE Sicily, Italy: palaeoceanographic and palaeogeographic implications. *Palaeogeography, Palaeoclimatology, Palaeoecology*, 265, 59-77.

Shafik, S., 1975. Nannofossil Biostratigraphy of the Southwest Pacific, Deep Sea Drilling Project, Leg 30. In: Andrews, J.E., Packham, G., et al. (Eds.), *Initial Reports of the Deep Sea Drilling Project*, 30, 549-598.

Shamrock, J.L., Watkins, D.K., 2009. Evolution of the Cretaceous calcareous nannofossil genus Eiffellithus and its biostratigraphic significance. *Cretaceous Research*, 30, 1083-1102.

Shipboard Scientific Party, 1981. Site 463: Western Mid-Pacific Mountains. *In* Thiede, J., Vallier, T.L., et al. (Eds.), *Initial Reports of the Deep Sea Drilling Project*, 62, 33-156.

Shipboard Scientific Party, 1990. Site 763. In: von Rad, U., Haq, B.U., et al. (Eds.), *Proceedings of the Ocean Drilling Program, Initial Reports*, 122, 289-352.

Shipboard Scientific Party, 2000. Site 1138. In: Coffin, M.F., Frey, F.A., Wallace, P.J., et al. (Eds.), *Proceedings of the Ocean Drilling Program, Initial Reports*, 183, 1-205.

Shipboard Scientific Party, 2004. Site 1261. In Erbacher, J., Mosher, D.C., Malone, M.J., et al. (Eds.), *Proceedings of the Ocean Drilling Program, Initial Reports*, 207, 1-103.

Sissingh, W., 1977. Biostratigraphy of Cretaceous calcareous nannoplankton. *Geol. Mijnbouw*, 56, 37–65.

Sissingh, W., 1978. Microfossil biostratigraphy and stage-stratotypes of the Cretaceous. *Geol. Mijnbouw*, 57, 433–440.

Sliter, W.V., 1989. Biostratigraphic zonation for Cretaceous planktonic foraminifers examined in thin sections. Journal of Foraminiferal Research, 19, 1-19.

Sliter, W.V., 1995. Cretaceous Planktonic Foraminifers from Sites 865, 866, and 869: A Synthesis of Cretaceous Pelagic Sedimentation in the Central Pacific Ocean Basin. In: Winterer, E.L., Sager, W.W., Firth, J.V., and Sinton, J.M. (Eds.), *Proceedings of the Ocean Drilling Program, Scientific Results*, 143, 15-30.

Snow, L.J., Duncan, R.A., Bralower, T.J., 2005. Trace element abundances in the Rock Canyon Anticline, Pueblo, Colorado, marine sedimentary section and their relationship to Caribbean plateau construction and oceanic anoxic event 2. *Paleoceanography*, 20, PA3005. doi:10.1029/2004PA001093.

Stover, L.E, 1966. Cretaceous coccoliths and associated nannofossils from France and the Netherlands: *Micropaleontology*, 12, 133-167.

Stradner, H., 1963. New contributions to Mesozoic stratigraphy by means of nannofossils: *Sixth World Petrol Congr. Proc.* (Frankfurt a. M.) sect. 1, paper 4.

Stradner, H., and Steinmetz, J., 1984. Cretaceous calcareous nannofossils from the Angola Basin, Deep Sea Drilling Project Site 530. In: Hay, W.W., Sibuet, J.-C., et al. (Eds.), *Initial Reports of the Deep Sea Drilling Project,* 75, 565-649.

Švábenická, L., 2012. Nannofossil record across the Cenomanian-Coniacian interval in the Bohemian Cretaceous Basin and Tethyan foreland basins (Outer Western Carpathians), Czech Republic. *Geologica Carpathica*, 63, 3, 201-217.

Tamagnini, P., 2007. Calcareous nannofossils as tracers of paleoceanographic changes associated to Oceanic Anoxic Event 2: records from the Tethys and Atlantic Oceans. *Ph.D. Thesis*, Università degli Studi di Milano.

Tantawy, A.A., 2008. Calcareous nannofossil biostratigraphy and paleoecology of the Cenomanian – Turonian transition at Tazra, Tarfaya Basin, southern Morocco. *Cretaceous Research*, 29, 995-1007.

Thibault, N., 2010. Biometric analysis of the Arkhangelskiella group in the upper Campanian-Maastrichtian of the Stevns-1 borehole, Denmark: Taxonomic implications and evolutionary trends. *Geobios*, 43, 639-652.

Thibault, N., Gardin, S., 2010. The calcareous nannofossil response to the end-Cretaceous warm event in the Tropical Pacific. *Palaeogeography, Palaeoclimatology, Palaeoecology*, 291, 239-252.

Thierstein, H.R., 1973. Lower Cretaceous calcareous nannoplankton biostratigraphy. *Abhandlungen der Geologischen Bundesandsalt,* 29, 1-52.

Thierstein, H.R., 1974. Calcareous nannoplankton - Leg 26, DSDP. In: T.A. Davis, B.P. Luyendyk et al. (Eds.), *Initial Reports of the Deep Sea Drilling Project*, 26, 619-668.

Thierstein, H.R., 1976. Mesozoic calcareous nannoplankton biostratigraphy of marine sediments. *Marine Micropaleontology,* 1, 325–362.

Thierstein, H.R., Manivit, H., 1981. Calcareous-Nannofossil Biostratigraphy, Nauru Basin, Deep Sea Drilling Project Site 462, and Upper Cretaceous Nannofacies. In: Larson, R.L., Shlanger, S., et al. (Eds.), Initial Reports of the Deep Sea Drilling Project, 61, 475-494.

Tiraboschi, D., 2009. Variazioni quantitative del nannoplancton calcareo durante il Cretacico medio: paleoecologia, paleoceanografia e produzione di carbonato in condizioni di anossia globale ed eccesso di ρCO2. *Ph.D. Thesis*, Università degli Studi di Milano.

Tremolada, F., 2002. Aptian to Campanian calcareous nannofossil biostratigraphy from the Bottaccione Section, Gubbio, central Italy. *Rivista Italiana di Paleontologia e Stratigrafia*, 108, 441-456.

Tröger, K.-A., Kennedy, W.J., 1996. The Cenomanian Stage. *Bulletin de l'Institut Royal des Sciences Naturelles de Belgique, Sciences de la Terre*, 66, 57-68.

Tsikos, H., Jenkyns, H.C., Walsworth-Bell, B., Petrizzo, M.R, Forster, A., Kolonic, S., Erba, E., Premoli Silva, I., Baas, M., Wagner, T., Sinninghe Damste J.S., 2004. Carbon-isotope stratigraphy recorded by the Cenomanian–Turonian Oceanic Anoxic Event: correlation and implications based on three key localities. *Journal of the Geological Society*, London, 161, 711–719.

Van Hinte, J.E., 1976. A Cretaceous time scale: *Am. Assoc. Petrol.Geol*., 60, 498-516.

Varol, O., 1989. Quantitative analysis of the *Arkhangelskiella cymbiformis* group biostratigraphic usefulness in the North Sea Area. *J. Micropalaeont.*, 8, 131-134

Varol, O., 1992. Taxonomic revision of the Polycyclolithaceae and its contribution to Cretaceous biostratigraphy. *Newsletters on Stratigraphy*, 27, 93-127.

Vekshina, V.N., 1959. Coccolithophoridae of the Maastrichtian deposits of the West Siberian lowland. *Trudy Sib. nauchno_issled. Inst. Geol. Geofiz. Mineral Resour.,* **2**, 56–81.

Verbeek, J.W., 1976. Upper Cretaceous calcareous nannoplankton zonation in a composite section near El Kef, Tunesia. I and II: *Koninkl. Nederl. Akad. Wettenschappen, Amsterdam, Proc,* ser. B, 79, 129-148.

Verbeek, J.W., 1977. Calcareous nannoplankton biostratigraphy of Middle and Upper Cretaceous deposits in Tunisia, southern Spain and France. *Utrecht Micropaleontological Bulletin* 16, 1–157. 12pl.

Wagreich, M., 1992. Correlation of Late Cretaceous calcareous nannofossil zones with ammonite zones and planktonic foraminifera: the Austrian Gosau sections. *Cretaceous Research*, 13, 505-516.

Wagreich, M., Bojar, A.-V., Sachsenhofer, R.F., Neuhuber, S., Egger, E., 2008. Calcareous nannoplankton, planktonic foraminiferal, and carbonate carbon isotope stratigraphy of the Cenomanian–Turonian boundary section in the Ultrahelvetic Zone (Eastern Alps, Upper Austria). Cretaceous Research, 29, 965-975.

Wagreich, M., Summesberger, H., Kroh, A., 2010. Late Santonian bioevents in the Schattau section, Gosau Group of Austria – implications for the Santonian–Campanian boundary stratigraphy. *Cretaceous Research*, 31, 181-191

Walaszczyk, I., Wood, C.J., Lees, J.A., Peryt, D., Voigt, S., Wiese, F., 2010. The Salzgitter-Salder Quarry (Lower Saxony, Germany) and Słupia Nadbrzeżna river cliff section (central Poland): a proposed candidate composite Global Boundary Stratotype Section and Point for the base of the Coniacian Stage (Upper Cretaceous). *Acta Geologica Polonica*, 60, 445-477.

Watkins, D.K., 1985. Biostratigraphy and paleoecology of calcareous nannofossils in the Greenhorn Marine Cycle. In: Pratt, L.M., Kauffman, E.G., Zelt, F.B. (Eds.), Fine-grained deposits and biofacies of the Cretaceous Western Interior Seaway: Evidence of cyclic sedimentary processes, 4. *Society of Economic Paleontologists and Mineralogists*, Field Trip Guidebook, Tulsa, 151–156.

Watkins, D.K., 1992. Upper Cretaceous nannofossils from Leg 120, Kerguelen Plateau, Southern Ocean. In: Wise, S.W., Schlich, R., et al. (Eds.), *Proceedings of the Ocean Drilling Program,* Scientific Results, 120, 343-370.

Watkins, D.K., 1996. Upper Cretaceous calcareous nannofossil biostratigraphy and paleoecology of the southern ocean. In: A. Moguilevky and R. Whatley (Eds.), *Microfossils and Oceanic Enviroments*, University of Wales, Aberystwyth press, 355–381.

Watkins, D.K., Bowdler, J.L., 1984. Cretaceous calcareous nannofossils from Deep Sea Drilling Project Leg 77, southeast Gulf of Mexico. In: Buffler, R. T., Schlager, W., et al., (Eds.), *Initial Reports of the Deep Sea Drilling Project*, 77: Washington (U.S. Govt. Printing Office), 649-674.

Watkins, D.K., Bralower, T.J., Covington, J.M., Fisher, C.G., 1993. Biostratigraphy and paleoecology of the Upper Cretaceous calcareous nannofossils in the Western Interior Basin, North America. In: Caldwell, W.G.E., Kauffman, E.G. (Eds.), *Evolution of the Western Interior Basin. Geological Association of Canada, Special Paper,* 39, 521–537.

Watkins, D.K., Self-Trail, J.M., 2005. Calcareous nannofossil evidence for the existence of the Gulf Stream during the late Maastrichtian. *Paleoceanography*, 20, PA3006, doi:10.1029/2004PA001121

Watkins, D.K., Shafik, S., Shin, I., 1998. Calcareous nannofossils from the Cretaceous of the Deep Ivorian Basin. In: Mascle, J., Lohmann, G.P., and Moullade, M. (Eds.), *Proceedings of the Ocean Drilling Program, Scientific Results*, 159, 319-333.

Watkins, D.K., Verbeek, J.V., 1988. Calcareous nannofossil biostratigraphy from Leg 101, Northern Bahamas. In: Austin, J.A., Jr., Schlager, W., et al. (Eds.), *Proceedings of the Ocean Drilling Program, Scientific Results,* 101, 63-85.

Watkins, D.K., Wise, S.W., Jr., Pospichal, J.J., Crux, J., 1996. Upper Cretaceous calcareous nannofossil biostratigraphy and paleoceanography of the Southern Ocean. *In* Moguilevsky, A., and Whatley, R. (Eds.), *Microfossils and Oceanic Environments:* Univ. of Wales (Aberystwyth Press), 355-381.

Wei, W., Thierstein, H.R., 1991. Upper Cretaceous and Cenozoic calcareous nannofossil of the Kerguelen Plateau (Southern Indian Ocean) and Prydz Bay (East Antarctica). In: Barron, J., Larsen, B., et al. (Eds.), *Proceedings of the Ocean Drilling Program, Scientific Results,* 119, 467-493.

Wiegand, G.E., 1984. Cretaceous nannofossils from the Northwest African Margin, Deep Sea Drilling Project, Leg 79. In: Hinz, K., Winterer, E.L., et al (Eds.), *Initial Reports of the Deep Sea Drilling Project,* 79, 563-578.

Wilcox, J.B., Exon, N.F., 1976. The regional geology of the Exmouth Plateau. *Australian Petroleum Exploration Association Journal,* 16, 1-11.

Wilpshaar, M., Leereveld, H., Visscher, H., 1997. Early Cretaceous sedimentary and tectonic development of the Dauphinois Basin (SE France). *Cretaceous Research,* 18, 457-468.

Wind, F. H., and Wise, S. W., Jr., 1983. Correlation of Upper Campanian-Lower Maestrichtian calcareous nannofossil assemblages in drill and lower piston cores from the Falkland Plateau, Southwest Atlantic Ocean. In: Ludwig, W. J., Krasheninnikov, V. A., et al. (Eds.), *Initial Reports of the Deep Sea Drilling Project,* 71, 551-563.

Wise, S. W., Jr., 1983. Mesozoic and Cenozoic calcareous nannofossils recovered by Deep Sea Drilling Project Leg 71 in the Falkland Plateau region, Southwest Atlantic Ocean. In: Ludwig, W. J., Krasheninnikov, V. A., et al. (Eds.), *Initial Reports of the Deep Sea Drilling Project,* 71, 481-550.

Wise Jr., S.W., Wind, F.H., 1977. Mesozoic and Cenozoic calcareous nannofossils recovered by DSDP Leg 36 drilling on the Falkland Plateau, southwest Atlantic sector of the Southern Ocean. In: Wise Jr., S.W. (Ed.), *Initial Reports of the Deep Sea Drilling Project*, 36, 269–492.

Wonders, A.A.H., 1992. Cretaceous planktonic foraminiferal biostratigraphy, Leg 122, Exmouth Plateau, Australia. In: von Rad, U., Haq, B.U., et al. (Eds.), *Proceedings of the Ocean Drilling Program, Scientific Results,* 122, 587-599.

Appendices

Appendix 1: Taxonomic description

Appendix 2: Taxonomic list

Appendix 3: Plates

Appendix 4: Tab.2.1 Compilation of the analyzed literature regarding Late Cretaceous calcareous nannofossils

Appendix 5: Tab.2.2 Nannofossil events used as zonal/subzonal markers in the zonations proposed by Sissingh (1977), Roth (1978), Bralower et al. (1995) and Burnett (1998) for the Late Cretaceous

Appendix 6: Tab.4.1 Range chart of Monte Petrano section

Appendix 7: Tab.4.2 Range chart of DSDP Site 463

Appendix 8: Tab.4.3 Range chart of Rock Canyon section

Appendix 9: Tab.4.4 Range chart of Clote de Chevalier section

Appendix 10: Tab.4.5 Range chart of Tarfaya Core section

Appendix 11: Tab.4.6 Range chart of ODP Site 1138

Appendix 12: Tab.4.7 Range chart of ODP Site 1261

Appendix 13: Tab.4.8: Range chart of ODP Site 763

Appendices 1-3 are included.

For appendices 4-13 please contact the author (fabio.russo@unimi.it).

Appendix 1

Taxonomic description

Kingdom **CHROMISTA** Cavalier-Smith, 1981

Division (Phylum) **HAPTOPHYTA** Hibberd *ex* Cavalier-Smith, 1986

Class **PRYMNESIOPHYCEAE** Hibberd, 1976

Subclass **PRYMNESIOPHYCIDAE** Cavalier-Smith, 1986

In this chapter I present a short description of every species encountered in this study. Principal diagnostic characters and observations from my own are provided. A four level order-family-genus-species classification is used, in addition, a set of numbered groupings (1. Heterococcoliths, 2. Holococcoliths, 3. Nannoliths) are used to provide a major organization.

Heterococcoliths

This is the predominant group, usually defined as coccoliths formed of one or more radial cycles of complex and variably shaped crystal-units (Fig.A.1.1).

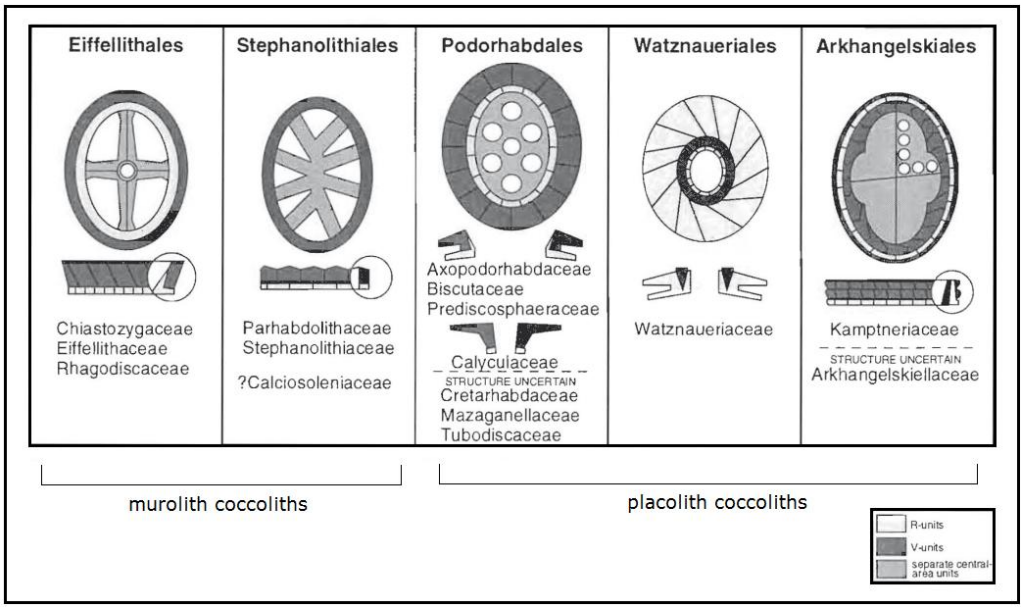

Fig.A.1.1 Proposed heterococcolith orders. Sketches illustrate distal views, and side-views with interpreted cut-away cross sections. Darker-shaded rim-cycles indicate V-units, and lighter-shaded cycles R-units; central-area structures are given a different shade (after Bown & Young, 1998)

These crystal units are termed V-unit (the crystallographic c-axes are vertically oriented) and R-unit (the crystallographic c-axes are radially oriented) and may form clearly separate parts of the rim or may be complexly intergrown, but they always originate as alternating crystal nuclei in the proto-coccolith ring (Bown & Young, 1998).

Order Arkhangelskiales

Tiered placoliths with 3-5 closely appressed "shields". Central-area structures include transverse bars with proximal net; axial or near axial crosses with proximal net; and perforate plates crossed by axial or near axial sutures (Fig.A.1.2).

Genera \ structural elements	general: central cross	general: central plate	general: perforations	general: central net	general: flange	view: distal: knob or spine	view: distal: outer rim	view: distal: inner rim	view: distal: zeugoid rim	view: proximal: outer rim	view: proximal: crown	view: proximal: inner rim	side tiers: 1	side tiers: 2	side tiers: 3 or more
Acaenolithus	●			●		●	●	●		●		●		?	
Arkhangelskiella		●	●				●			●					●
Aspidolithus		●	●				●	●		●				●	
Broinsonia	●						●	●		●				●	
Crucicribrum	●	●	●			●			●						●
Gartnerago	●	●	●				●	●		●	●	●		●	
Kamptnerius		●	●		●		●	●		●	●	●	●		
Misceomarginatus	●	●	●				●	●	●						
Thiersteinia	●	●	●			●	●	●		●					●

Fig.A.1.2 Overview of the order of the Arkhangelskiales (after Perch-Nielsen, 1985)

Family Arkhangelskiellaceae: placoliths made up of a narrow to broad multi-tiered rim and a central area that may be spanned by crossbars or filled by a perforate plate divided by axial sutures.

Genus *Acaenolithus*: This genus has a bicyclic rim with a broad, bright inner cycle and narrow, dark outer cycle. The central area is filled by a net with an axial cross supporting a knob.

A. cenomanicus, Plate I, Fig.A: type species of the genus.

Genus *Arkhangelskiella*: This genus has a bright, unicyclic rim. The central area is filled by a perforate plate with axial sutures. Each of the four segments of the central plate shows a less conspicuous subdivision in two parts of different birefringence.

A. cymbiformis: type species of the genus. The name *A. cymbiformis* has been used to include a variety of forms, because of its large variability in coccolith length, width of the rim and number of perforations.

Remarks: several Authors suggested distinctions in diverse morphotypes or species based on different morphological features (Lauer, 1974; Perch-Nielsen, 1985; Varol, 1989; Burnett, 1997; Linnert & Mutterlose, 2009; Thibault, 2010). In this work I used the distinction suggested by Thibault (2010) and summarized as follow:

***A. cymbiformis* var. N** (= *A. confusa,* Burnett, 1997): it corresponds to small (<8.5 μm length) specimens with a relatively narrow central area and relatively wider rims in relation to the total length of the coccolith. The opening of the central area in these specimens therefore tends to be reduced. The ratio between the central area width and the rim width is less than 0.57.

A. cymbiformis var. SW: it corresponds to medium-sized (8.5-11 μm length) specimens with a narrow central area and a wide rim. The ratio between central area width and the rim width is less than 0.57.

A. cymbiformis var. W (= A. maastrichtiensis, Burnett, 1997): it corresponds to large (>11 μm length) specimens with a wide rim and a slightly more open central area. The ratio between the central area width and the rim width is less than 0.62.

A. cymbiformis var. NT, Plate I, Fig.B: it corresponds to small to very large specimens (6.5 to 14.5 μm) with a widely open central area and a relatively thin rim in relation to the total length of the coccolith. The ratio between the central area width and the rim width is greater than 0.57 for specimens less than 11 μm-long and greater than 0.62 for specimens greater than 11 μm-long.

Genus *Aspidolithus*: This genus has a bright, bicyclic rim. The central area is filled by a perforate plate with axial sutures. Each of the four segments of the central plate shows a less conspicuous subdivision in two parts of different birefringence and appearing like the blades of a windmill.

A. enormis, Plate I, Fig.B: species of *Aspidolithus* with a narrow rim and a central area filled by a perforate plate crossed by axial sutures.

A. furtivus, Plate I, Fig.C: species of *Aspidolithus* with a broad rim and a narrow central area filled by a plate crossed by axial sutures.

Remarks: the central plate may be perforate or imperforate. In very poor preserved specimens only the part around the axial sutures is kept, giving a LM image of axial crossbars. This species differs from *A. enormis* for the dimension of the rim related to the central area.

A. parcus constrictus, Plate I, Fig.D: A subspecies of *Aspidolithus parcus* with a very small central area whose width in distal view is approximately equal to or significantly less than the width of the shield margin. It is spanned by a perforate plate divided by axial sutures. The one to three perforations per quadrant lie approximately parallel to the major axis.

A. parcus expansus, Plate I, Fig.E, F: A subspecies of *Aspidolithus parcus* with a large central area whose width in distal view is approximately twice or more than twice the width of the shield margin. It is spanned by a perforate plate divided by axial sutures. Central area perforations are usually disposed along the major and minor axes. In at least one quadrant perforations extend out along the periphery.

Remarks: I distinguished two morphotypes for this taxon, I called *A. parcus expansus* large (Fig.E), specimens larger than 8 μm and *A. parcus expansus* small (Fig.F) specimens smaller than 8 μm.

A. parcus parcus, Plate I, Fig.G: A subspecies of *Aspidolithus parcus* with a width approximately one to two times the width of the distal margin. It is spanned by a perforate plate divided by axial sutures. Central area perforations lie parallel to the major and minor axes only.

Genus *Broinsonia*: This genus has a bright, bicyclic rim. The central area is spanned by axial crossbars.

B. matalosa, Plate I, Fig.H: species of *Broinsonia* with a two tiered rim in plan view and an open central area spanned by axial crossbars that may support a short spine. The inner edge of the rim is

faintly scalloped whilst the outer one is smooth. Each bar of the cross is composed of two pieces easily recognizable in LM image.

B. signata, Plate I, FigI: species of *Broinsonia* with a two tiered rim in plan view and an open central area spanned by axial crossbars. Each bar of the cross is composed of two pieces easily recognizable in LM image.

Remarks: it differs from *B. matalosa* for the inner edge of the rim that is smooth as the outer one.

Genus *Thiersteinia*: This genus is characterized by a *Broinsonia*-like margin and a wide perforated central area surmounted on the distal surface by a solid spine. The spine is supported by buttresses which form a cross along the major and minor axes of the central area.

T. ecclesiastica: type species of the genus.

Family Kamptneriaceae: Placoliths made up of a narrow to moderately-broad three-tiered rim and a central area that may be spanned by a transverse bar, crossbars or plate, usually with axial sutures and perforations. The rim consists in a narrow, dark outer cycle, a bright median cycle and a dark inner cycle.

Genus *Crucicribrum*: This genus has a narrow rim and a perforated central plate with a central process.

C. anglicum, Plate I, Fig.J: species of *Crucicribrum* with a narrow, slightly wavy and bright median rim, the inner rim cycle shows lower birefringence. The central area is filled by a perforate plate crossed by axial bars and sutures.

C. stenostaurion, Plate I, Fig.K: species of *Crucicribrum* with a narrow, bright median rim cycle and wide central area spanned by a perforated plate and bright, thin axial cross, which are longitudinal and near transverse (rotated by ~10°), and birefringent when the coccolith is at 45° to the polarizing directions.

Remarks: this species was related to *Broinsonia* by Hill (1976) and to *Gartnerago* by Bown (2006), I decided to place it in *Crucicribrum* genus for the aspect of the rim and for the presence of a central cross process overlying a plate that is a typical aspect of *Crucicribrum.*

Genus *Gartnerago*: This genus has a narrow to moderately-broad rim and a central area that may be spanned by a transverse bar, crossbars or plate, usually with axial sutures and perforations. When the central area is filled by a plate, this shield is convex distally and concave proximally.

G. chiasta, Plate I, Fig.L: small and weakly birefringent species of *Gartnerago* with diagonal crossbars.

G. margaritatus, Plate I, Fig.M: species of *Gartnerago* with a thin rim structure and a delicate, axial cross. The central plate contains a thin axial cross that extends to the inner part of the rim. The crossbars may be slightly offset from the major and minor axes and are composed of two thin bar elements.

G. nanum, Plate I, Fig.N: small species of *Gartnerago* with a moderately-broad rim and a small sub-rhomboidal central opening which is filled by a plate surmounted by axial bars and may show a few perforations in each quadrant. The longitudinal bar is often poorly defined.

G. obliquum, Plate I, Fig.O, P: species of *Gartnerago* with a narrow rim and a large central area, filled with a plate pierced by numerous pores; the plate is crossed by sutures, the transverse of which is slightly oblique.

G. praeobliquum, Plate I, Fig.Q: species of *Gartnerago* with a thin rim and a open central area spanned by axial crossbars. Each of the four bars making up the axial cross diverges near the inner margin of the rim and shows a central sutures.

G. segmentatum, Plate I, Fig.R: species of *Gartnerago* with a medium to moderately-broad rim and a central area spanned by a plate. The base plate is slightly arched distally and appears coarsely granular under parallel nicols. It is divided into quadrants by axial sutures, the transverse suture may be slightly oblique.

Genus *Kamptnerius*: This genus has a broad rim that has an asymmetric flange forming a wing and a central area spanned by a perforate plane plate.

K. magnificus, Plate I, Fig.S, T: type species of the genus. The development of the asymmetric rim flange and pores of the central area are extremely variable. The middle part of the central area may show a longitudinal suture with different forms, from four points star (Plate I, Fig.S, *K. sculptus*, Bukry, 1969 of some Authors) to simple line suture (Plate I, Fig.T).

Order Eiffellithales

Elliptical coccoliths with a high wall-like rim composed by two crystal-units (V-unit and R-unit). The distal/outer cycle (V-unit), commonly dominant, is composed of imbricating elements but these features, characterizing this order, are distinguishable only in SEM images. The term loxolith is applied to this rim structure. The central area is spanned by different structures.

Family Chiastozygaceae: loxoliths with variably-developed proximal/inner cycles (R-unit) and a central area spanned by different structures. Rim may appear unicyclic or bicyclic in LM images.

Genus *Ahmuellerella*: This genus has a narrow unicyclic rim and a central area spanned by a plate or a complex axial cross structure. A spine may be present.

A. octoradiata, Plate II, Fig.A: species of *Ahmuellerella* with an axial cross structure displaying 8 axial bars diverging when they approach the rim.

Genus *Amphizygus*: This genus has a bicyclic rim. The central area is spanned by a transverse bar formed from laths which continue around the inner edge of the rim, delineating two circular perforations.

A. brooksii, Plate II, Fig.B, C: type species of the genus. A stem may be observed in the middle of the transverse bar. Length of the long axis less than 8 μm.

Genus *Bukrylithus*: This genus has a narrow unicyclic rim and a central area mostly covered by broad and fibrous axial cross bars.

B. ambiguus, Plate II, Fig.D: type species of the genus. A circular opening is present in the center of cross.

Genus *Chiastozygus*: This genus has a rim which may be unicyclic or bicyclic and a central area spanned by variably constructed diagonal bars.

C. amphipons, Plate II, Fig.E*:* species of *Chiastozygus* with a relatively narrow and weakly birefringent bicyclic rim and a wide central area spanned by diagonal crossbars.

C. bifarius, Plate II, Fig.F**:** species of *Chiastozygus* with a broad bicyclic rim and a small central area spanned by diagonal crossbars disposed at 45° about the long and short axis of the ellipse. Crossbars are broad, with a median suture and support a small stem.

C. litterarius, Plate II, Fig.G: species of Chiastozygus with a relatively broad bicyclic rim and a large central area. Diagonal crossbars are thick and weakly birefringent. A median suture is present on crossbars.

C. platyrhethus, Plate II, Fig.H: species of *Chiastozygus* with a relatively narrow bicyclic rim and a wide central area. Diagonal crossbars are straight and birefringent with a median suture.

***C. synquadriperforatus*:** species of *Chiastozygus* with a relatively broad bicyclic rim and a central area spanned by narrow, asymmetrical crossbars. The short arm of the cross makes a smaller angle with the short axis of the ellipse than the long arm.

Genus *Gorkaea*: This genus has a bicyclic rim. The outer cycle is bright and thin, the inner one is broad and robust. The central area is spanned by a transverse bar constructed of few large elements.

G. pseudanthophorus, Plate II, Fig.I: species of *Gorkaea* with a wide central area. The transverse bar is constructed of two to four elements.

Remarks: this form is distinguished from *Z. embergeri* to be thinner and for the aspect of the transverse bar, straight instead of diamond-shaped.

Genus *Loxolithus*: This genus is constructed by numerous imbricated plates forming an open ring with a wide central area.

L. armilla, Plate II, Fig.J: type species of the genus.

Genus *Placozygus*: This genus has a bicyclic rim exhibiting spiral interference pattern. The central area is spanned by variably constructed transverse bar.

P. fibuliformis, Plate II, Fig.K: species of Placozygus with central area spanned by a bipartite transverse bar formed of two or three elements.

Genus *Reinhardtites*: This genus has a broad rim and a small central area that may be spanned or completely filled by calcite elements and a transverse bar.

R. anthophorus, Plate II, Fig.L: species of *Reinhardtites* with the central area spanned by a bar formed by numerous, small laths creating two circular opening. A massive central process may be present. The stem is longer than the long axis of the coccolith and widens distally to form an inverted cone.

R. levis, Plate II, Fig.M: species of *Reinhardtites* with the central area filled by calcite elements leaving sometimes two small openings at both sides of the central bridge structure. A short spine with a bright, diamond-shaped aspect overlies these elements.

Genus *Staurolithites*: This genus has narrow rim and wide central area spanned by axial crossbars. A spine is usually present.

S.? aenigma: small species of *Staurolithites* with a bicyclic rim and a central area filled by a weakly birefringent plate. A small axial cross, composed of laths, lies on the plate.

S. crux: very simple species of *Staurolithites* with narrow, unicyclic rim and axial crossbars bearing a spine.

S. dicandidula, Plate II, Fig.N: species of *Staurolithites* with a weakly birefringent rim and a bright axial cross divided by longitudinal extinction lines. Arms of the axial cross are straight.

S. ellipticus, Plate II, Fig.O: species of *Staurolithites* with a narrow bicyclic rim and a small central area spanned by broad and tapering axial crossbars. A stem is present at the intersection of the crossbars.

S. elongatus: small species of *Staurolithites* with elongate outline. Axial crossbars are broader than the rim. A stem is present at the intersection of the crossbars.

S. flavus, Plate II, Fig.P, Q: species of *Staurolithites* with a unicyclic rim and a distinctively highly-birefringent axial cross, which become more evident when the coccolith is rotated at 45°.

S. gausorhethium, Plate II, Fig.R: species of *Staurolithites* with a relatively broad rim and a central area spanned by narrow crossbars that may be slightly rotated from axial. The long bar curve when reaching the rim.

S. glaber: species of *Staurolithites* with a narrow outer rim and a broad inner rim. The central area is spanned by thin axial crossbars.

S. halfanii, Plate II, Fig.S, T: small species of *Staurolithites* with a very narrow rim and dark axial cross. A small spine is present with a distinctively birefringent spine top, which appears when the coccolith is rotated.

S. imbricatus, Plate III, Fig.A: species of *Staurolithites* with a bicyclic rim and bright axial cross. The inner rim is usually less conspicuous than the outer one. Crossbars display a distinct median extinction line.

S. laffittei: species of *Staurolithites* with a narrow rim forming a ledge in the inner part and tight, cylindrical axial crossbars.

S. mielnicensis, Plate III, Fig.B: medium to large species of *Staurolithites* with a weakly birefringent rim and an axial cross which widens to the inner edge of the rim. A plug-shaped cross is present at the intersection of the crossbars.

S. minutus: small species of *Staurolithites* with a broad, highly-birefringent rim and a very small central area with a dark axial cross.

S. mutterlosei, Plate III, Fig.C: medium to large sized species of *Staurolithites* with a distinctive bicyclic and equally birefringent rim. The axial cross is bright and may be slightly rotated from axial.

***Staurolithites* sp. 2**, Plate III, Fig.D: species of *Staurolithites* with a bicyclic rim exhibiting spiral interference pattern in the inner one. The outer rim is darker and not always recognizable. Axial crossbars are bipartite and widens approaching the rim.

Genus *Tranolithus*: This genus has an unicyclic to bycyclic rim and a central area spanned by transverse structures made by 2 or 4 disjoint platelets. A spine may be present.

T. gabalus, Plate III, Fig.E: species of *Tranolithus* with narrow rim and a central area spanned transversely by two platelets. Components of central structure and adjacent part of the rim have same optical orientation.

T. minimus, Plate III, Fig.F: small species of *Tranolithus* with narrow rim and a central area filled by a central stem flanked by two triangular platelets which occupy the remaining area.

T. orionatus, Plate III, Fig.G: species of *Tranolithus* with unicyclic rim and a central area spanned by a transverse structure of four quadrangular platelets.

T. salillum, Plate III, Fig.H: species of *Tranolithus* with unicyclic rim and a central area spanned by a transverse structure of four triangular platelets.

Genus *Zeugrhabdotus*: This genus has a variably developed rim which may be unicyclic or bicyclic. The central area is spanned by variably constructed transverse bar, that is usually spine-bearing.

Z. acanthus, Plate III, Fig.I: species of *Zeugrhabdotus* with bicyclic rim exhibiting spiral interference pattern.

Remarks: the inner rim is brighter than the outer one. The central area is spanned by a transverse bar formed by numerous calcite crystals which create an effect of indistinct, tangled elements in LM images under crossed nicols.

Z. bicrescenticus, Plate III, Fig.J: species of *Zeugrhabdotus* with broad, bicyclic rim and narrow central area spanned by a bipartite transverse bar.

Z. biperforatus, Plate III, Fig.K: species of *Zeugrhabdotus* with a broad rim composed of strongly imbricated elements. The central area is nearly closed, spanned by a bipartite transverse bar constructed of numerous calcite elements giving a bright image in LM under crossed nicols.

Z. diplogrammus, Plate III, Fig.L: species of *Zeugrhabdotus* with unicyclic rim and a central area spanned by a bipartite transverse bar with two bright elements appearing at both terminations of the bar when the coccolith is rotated.

Remarks: It differs from *Z. bicrescenticus* for the bright elements of the transverse bar. I called *Z.* cf. *Z. diplogrammus* coccoliths similar to *Z. diplogrammus* with thinner transverse bar and numerous platelets partially filling the rest of the central area. The occurrence of the two bright elements allows to relate this species to *Z. diplogrammus*.

Z. embergeri, Plate III, Fig.M: large and highly birefringent species of *Zeugrhabdotus* with a broad, bicyclic rim. Large, diamond-shaped transverse bar and small to no perforations occupy the central area.

Z. erectus, Plate III, Fig.N: small species of *Zeugrhabdotus* with unicyclic narrow rim and a central area spanned by a simple bar bearing a spine.

Remarks: the holotype length is of 4.9 μm, in my samples I distinguished two different ranges of size for this species: the smaller one has the long axis of the ellipse less than 5 μm, larger specimens have a length of more than 6 μm. In larger specimens the transverse bar is usually broader than the rim.

Z. howei, Plate III, Fig.O: species of *Zeugrhabdotus* with a bar which has a granular appearance when orientated parallel with the polarising directions. At 45° the bar becomes dark but four bright protrusions from the rim may be visible.

Z. noeliae: small species of *Zeugrhabdotus* with a relatively broad bicyclic rim. The outer rim is broader than the inner one. The small central area is spanned by a transverse bar constructed of four elements near the juncture with the inner rim margin and few other crystals that complete the bridge.

Z. praesigmoides, Plate III, Fig.P: bicyclic species of *Zeugrhabdotus* with low birefringent outer rim and wide central area spanned by a transverse bar composed of small blocks and a sigmoidal appearance. The inner cycle is distinctively birefringent and broader than in *Z. sigmoides*, it thins close to the long axis of the ellipse. It is smaller than *Z. sigmoides*.

Z. scutula, Plate III, Fig.Q: species of *Zeugrhabdotus* with low birefringent rim and wide central area spanned by a transverse bar constructed of numerous laths.

Remarks: a brightly birefringent, elongate, diamond-shaped figure is observed on the central portion of the bar when the coccolith is oriented parallel to the polarizing direction. As described by Bergen (1994) it may be related to the genus *Reinhardtites* as the ancestral species of the *R. anthophorus-R. levis* lineage.

Z. sigmoides: species of *Zeugrhabdotus* with bicyclic rim and wide central area spanned by a spine-bearing bar that narrows at both ends. The inner cycle is narrow and bright in XPL and broadens where the bar meets the rim.

Z. trivectis: species of *Zeugrhabdotus* with bicyclic rim with equally developed cycles, the inner rim is brighter than the outer one and exhibits spiral interference pattern. The central area is spanned by a

transverse bar which consists of two or three element bundles oriented at slightly oblique angles to each other.

Family Eiffellithaceae: Clearly bicyclic loxoliths with a well developed proximal/inner cycle (R-unit) and a central area spanned by axial to diagonal crossbars. A spine may be present.

Genus *Eiffellithus*: This genus has a broad and birefringent inner cycle. The central area is spanned by differently oriented crossbars, which are fibrous and usually support a large stem. Crossbars show a median extinction line.

E. angustus, Plate III, Fig.R, S: medium to very large (7.4 to 14 μm) species of *Eiffellithus*. The central area is filled by broad and robust axial crossbars with evident bifurcations on all four terminations. The stem base is composed of four disjunct crystals that rise above the middle, forming a large, diamond shaped opening through the center of the axial cross.

E. eximius, Plate III, Fig.T: species of *Eiffellithus* with the central area filled by axial crossbars (less than 20° from the axes of the ellipse). Longitudinal crossbars may bifurcate at the end whilst along the transversal axis, crossbars taper toward the rim. A stem is present, when it is absent a large opening occurs in the middle of the coccolith.

E. gorkae, Plate IV, Fig.A: small (less than 7 μm) species of *Eiffellithus* with symmetrical diagonal crossbars spanning or completely filling the central area. The cross-bars are of equal length and taper toward the rim. It differs from *E. turriseiffelii* to be smaller.

E.? hancockii, Plate IV, Fig.B: small species of *Eiffellithus*. The outer rim is dark while the inner one is broad and highly birefringent. The central area is very small and spanned by an axial cross not always recognizable.

Remarks: this species is doubtfully assigned to *Eiffellithus* because of its particular inner rim construction that is quite different from other species of *Eiffellithus* or *Staurolithites* (Burnett, 1997).

E. keio, Plate IV, Fig.C: species of *Eiffellithus* with a wide, open central area spanned by diagonal crossbars with bifurcate to trifurcate terminations. Along the major axis of the ellipse, angles displayed by crossbars are more than 45°.

E. monechiae: small (less than 7 μm) species of *Eiffellithus* with the central area spanned by crossbars, the longitudinal one aligned within 20° of the major axis of the ellipse.

E. perch-nielseniae, Plate IV, Fig.D: species of *Eiffellithus* with the central area spanned by asymmetric, diagonal crossbars, the longitudinal one aligned between 20° and 40° of the major axis of the ellipse and taper toward the rim.

E. turriseiffelii, Plate IV, Fig.E: species of *Eiffellithus* with symmetrical diagonal crossbars spanning the central area. The cross-bars are of equal length and terminal morphology, typically tapered to blunt. A square-shaped opening may be observed within the central cross, and tapers away from the center in well-preserved specimens.

Genus *Helicolithus*: This genus has bicyclic rim with a broad and birefringent inner cycle and narrow central area. The central area is filled by broad, variably oriented crossbars.

H. anceps, Plate IV, Fig.F: species of *Helicolithus* with similar birefringence for the two rim cycles. The central area is spanned by symmetrical diagonal crossbars brighter than the rim. In the middle of the coccolith, a perforation is often present.

H. compactus, Plate IV, Fig.G: species of *Helicolithus* with cross bars slightly rotated from the axial position. Each bar of the cross is formed by two elements.

H. trabeculatus, Plate IV, Fig.H: species of *Helicolithus* with symmetrical diagonal crossbars. Each bar of the cross is formed by two elements.

H. turonicus, Plate IV, Fig.I: species of *Helicolithus* with axial crossbars. Each bar of the cross is formed by two elements.

H. varolii, Plate IV, Fig.J: species of *Helicolithus* with axial cross composed of four overlapping elements. These elements are triangle-shaped and contains a median suture that does not span the entire length of the crossbar.

Genus *Tegumentatum*: This genus has a strongly imbricate and birefringent inner rim cycle. The central area is spanned by curving, diagonal cross-bars.

T. stradneri, Plate IV, Fig.K: type species of the genus. The rim appears wide and bright and each crossbar consist of two elongate parts of different crystallographic orientation.

Family Rhagodiscaceae: generally unicyclic loxoliths with a central area filled by a plate of granular calcite that may be spine-bearing, perforate or massive.

Genus *Rhagodiscus*: This genus has an unicyclic low rim and a central area filled by a granular plate which may be perforate and spine-bearing.

R. achlyostaurion, Plate IV, Fig.L: species of *Rhagodiscus* with a large spine in the middle which appears as a bright ring traversed by four sharply defined extinction gyres in the shape of a small X-shaped cross.

R. angustus, Plate IV, Fig.M: elongated species of *Rhagodiscus* with sub-parallel flanks and a short stem that spans the central area.

R. asper, Plate IV, Fig.N: species of *Rhagodiscus* with a relatively wide central area filled by a perforate granular plate. A spine is usually present.

R. indistinctus: medium to large species of *Rhagodiscus* with broad rim and narrow central area spanned by a stem. This species exhibits low birefringence and the spine is often difficult to discern.

R. reniformis, Plate IV, Fig.O: species of *Rhagodiscus* with an irregularly thickened rim and a kidney form.

R. splendens, Plate IV, Fig.P: medium to large species of *Rhagodiscus* with a broad spine, clearly striated in plan-view and with elicoidal arrangement in side-view.

Order Podorhabdales (Fig.A.1.3)

Placoliths usually constructed from two superimposed, appressed shields joined by a tube-cycle (Bown & Young, 1997). Shields elements are typically jointed along radial sutures which display generally no imbrications. LM images have typically low birefringence but high relief in phase contrast.

Family Axopodorhabdaceae: placoliths with two thin shields and a wide central area, spanned by crossbars or plates with variable numbers of perforations. A tall hollow spine is usually present in the centre of the coccolith. Shields elements are often visible in LM images.

Genus *Axopodorhabdus*: This genus has a tall-spine-bearing axial cross.

A. albianus, Plate IV, Fig.Q, R; Plate XI, Fig.P: species of *Axopodorhabdus* with bars that flare when they reach the rim. Cross bars also show a median extinction line.

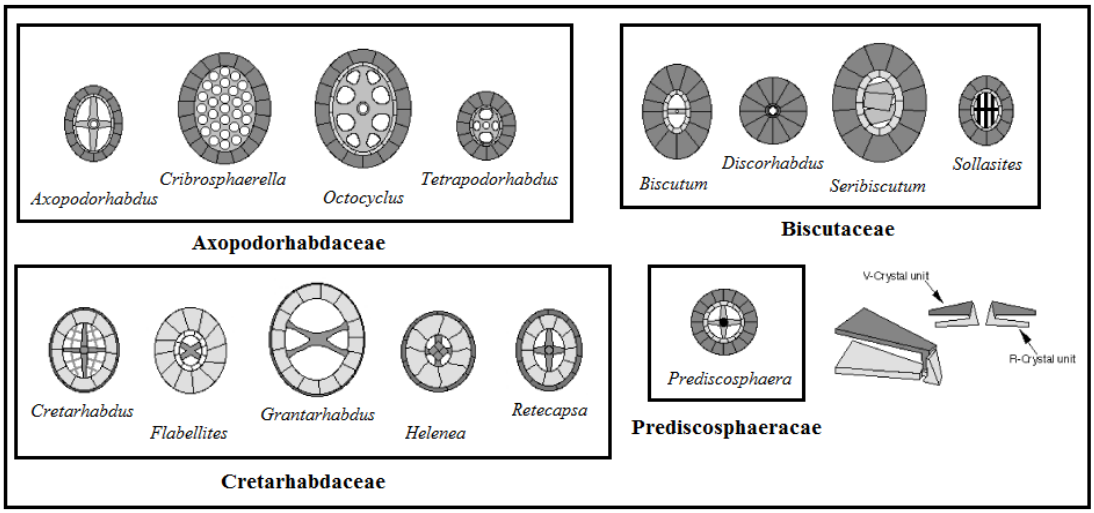

Fig.A.1.3 Genus overview of the Podorhabdales (after Bown & Young, 1997)

Genus *Cribrosphaerella*: This genus has an elliptical to sub-rectangular rim and a central area spanned by a highly perforated plate.

C. ehrenbergii, Plate IV, Fig.S: species of *Cribrosphaerella* with elliptical rim and a multi-perforated central area net.

Genus *Octocyclus*: This genus has a wide central area spanned by eight broad bars that delineate eight large perforations that run either sides of the longitudinal axis. A central spine may be present.

O. reinhardtii, Plate IV, Fig.T: species of *Octocyclus* with no central spine.

Genus *Tetrapodorhabdus*: This genus has a tall-spine-bearing diagonal cross or four offset cross bars.

T. decorus, Plate V, Fig.A, B: species of *Tetrapodorhabdus* with central area spanned by relatively high angle diagonal cross bars that bear a large, flaring and diagnostic spine.

Family Biscutaceae: placoliths with two shields constructed of non-imbricate elements. The relatively narrow central areas are vacant, filled with granular calcite or spanned by variably oriented bars. The LM image is generally dark, but bright inner-cycles are common.

Genus *Biscutum*: This genus has elliptical shields with a bright tube-cycle; the central area may be imperforated or narrow and vacant or spanned by cross or bar (Bown & Young, 1997). Elements of the shield are usually recognizable.

B. constans, Plate V, Fig.C, D, E: variably sized (1.5-8 μm) species of *Biscutum* with numerous elements in the two shields and without any discernible structure inside its birefringent central tube cycle.

Remarks: in this work three dimensional morphotypes have been adopted: small (up to 4 μm), medium (4-6 μm), large (more than 6 μm). Following the holotype descriptions, small specimens may be assigned to *B. dubium* and large specimens may be assigned to *B. ellipticum*.

B. coronum, Plate V, Fig.F: species of *Biscutum* with a large elliptical central area and a diagnostic bright ring surrounding it. Elements of the distal shield are numerous and dextrally oriented, proximal shield elements appear to be radial.

B. dissimilis: species of *Biscutum* with thick massive distal plates and thin, small proximal shield. Long axis extremities are usually dominated by one or two exceptionally broad, massive elements. The central area is small and may be filled or lined by a small number of thick plates.

B. magnum, Plate V, Fig.G: large species of *Biscutum* with a wide central area occupied by numerous inwardly projecting elements.

Remarks: in not well-preserved specimens the elements of the central area are rarely recognizable and it may be distinguished from *B. coronum* for the absence of the bright ring adjacent to the central area.

B. melaniae, Plate V, Fig.H, I: medium to large species of *Biscutum* with a wide dark shield and a small, highly birefringent, closed central area.

Genus *Discorhabdus*: This genus has a circular rim and generally no central-area structures. Radial elements of the rim are usually visible in the LM images.

D. ignotus, Plate V, Fig.J; Plate XI, Fig.R: small species of *Discorhabdus* with closed central area.

Genus *Seribiscutum*: This genus has elliptical shields and a central area spanned by broad platelets. A bright inner-cycle is present.

S. primitivum, Plate V, Fig.K: highly elliptical species of *Seribiscutum* with central area spanned by four platelets that zig-zag across the central area.

Genus *Sollasites*: This genus has elliptical shields and a wide central opening spanned by structures including axial crossbars, multiple longitudinal bars and concentric bars.

S. horticus, Plate V, Fig.L: species of *Sollasites* with a central area spanned by three longitudinal bars and one transverse bar.

Family Prediscosphaeraceae: round and elliptical placoliths with non-imbricated elements in each of the two shields. The central area is spanned by axial or diagonal bars supporting a tall and complex spine. The LM image is bicyclic, with the outer cycle dark, and inner cycle bright.

Genus *Prediscosphaera* (Fig.A.1.4)**:** This genus has the typical aspects of the family description

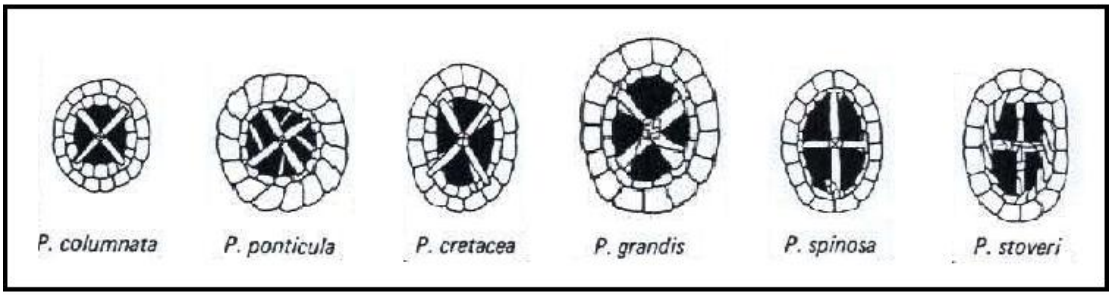

Fig.A.1.4 Species of *Prediscosphaera* adopted in this work (after Perch-Nielsen, 1985)

P. columnata, Plate V, Fig.M: small (5 to 7 μm), circular species of *Prediscosphaera* with a thin outer cycle. The central area is spanned by bars.

P. cretacea, Plate V, Fig.N: elliptical species of *Prediscosphaera*. Diagonal bars span the central area.

P. grandis, Plate V, Fig.O: large (more than 10 μm), elliptical species of *Prediscosphaera*. Diagonal bars span the central area.

Remarks: I called *P.* cf. *P. grandis* fragments of *Prediscosphaera*, related to *P. grandis* for their dimensions.

P. ponticula, Plate V, Fig.P: circular species of *Prediscosphaera* with a thick outer cycle. The central area is spanned by bars. In well preserved specimens, adjunctive bars span the central area.

Remarks: it is distinguishable from *P. columnata* for larger elements of the external shield.

P. spinosa, Plate V, Fig.Q: elliptical species of *Prediscosphaera*. Axial cross bars span the central area.

P. stoveri: elliptical species of *Prediscosphaera* with a broad and bright inner cycle. Axial cross bars span the central area.

Family Cretarhabdaceae: placoliths with a relatively large rim formed by two shield and a central area spanned by different structures. Usually cross bars with adjunctive oblique lateral bars or net. Central spine or process may be present.

Genus *Cretarhabdus*: This genus has a central area spanned by a net that often includes axial cross bars. Spine may be present. Elements of the rim are radially arranged.

C. conicus, Plate V, Fig.R: species of *Cretarhabdus* with a distinct axial cross and a central spine overlying the central area net.

C. striatus, Plate V, Fig.S: species of *Cretarhabdus* with a wide central area and narrow axial cross bars which clearly divide four quadrant. In each quadrant a set of parallel bars extends from the inner margin of the rim to the crossbars. The four quadrants are optically discontinuous.

Genus *Flabellites*:This genus has a central area spanned by small, blocky diagonal cross. Elements of the distal shield are elongated and often extend beyond the elliptical periphery of the coccolith.

F. oblongus, Plate V, Fig.T: species of *Flabellites* with a relatively narrow central area spanned by four blocky elements diagonally disposed.

Genus *Grantarhabdus*:This genus is characterized by a wide central area and diagonal crossbars.

G. coronadventis, Plate VI, Fig.A, B: large species of *Grantarhabdus* with broad crossbars with irregular edge.

Genus *Helenea*: This genus has usually narrow central area, spanned by features which principally display crossbars that may flare when reaching the rim. A stem may be present in the middle. The inner part of the rim is clearly birefringent, creating a bicyclic image.

H. chiastia, Plate VI, Fig.C: broadly elliptical to subcircular species of *Helenea* with a narrow central area spanned by an axial cross that bears a distinctly blocky short spine. The long axis of the central area is less than one-half of the coccolith length.

Genus *Retecapsa*: This genus has a central area spanned by axial bars and adjunctive lateral bars. This genus has similar characters of *Cretarhabdus*, for that reasons some authors include Retecapsids within *Cretarhabdus*, this is not followed here.

R. angustiforata, Plate VI, Fig.D: species of *Retecapsa* with axial crossbars and four additional bars which divide each quadrant at 45°.

R. crenulata, Plate VI, Fig.E: species of *Retecapsa* with axial crossbars and two additional bars in each quadrant.

R. ficula: species of *Retecapsa* with a small central area surrounded by numerous small calcareous fragments displaying an opening in the middle.

R. schizobrachiata, Plate VI, Fig.F: species of *Retecapsa* with a wide central area spanned by axial crossbars which split in two or three branches at their junction with the disc.

R. surirella, Plate VI, Fig.G: species of *Retecapsa* with axial crossbars and three or more additional bars in each quadrant.

Family Tubodiscaceae: elliptical placoliths composed of two narrow shields and a third, narrow, proximally-situated collar cycle that is variable in height. The central-area is broad and open; no central structures have yet been observed. The LM image is dark, although the collar cycle is brighter (Bown & Young, 1997).

Genus *Manivitella*: This genus has a low proximal collar cycle and a wide vacant central area. The outer edge of the rim is raised.

M. pemmatoidea, Plate VI, Fig.H: type species of the genus.

Order Stephanolithiales (Fig.A.1.5)

Coccoliths with a low to high wall-like rim composed by two crystal-units (V-unit and R-unit). The distal/outer cycle (V-unit) is composed of non-imbricating elements but this feature, which characterizes this order, is distinguishable only in SEM images. The term protolith is applied to this rim structure. The central area is spanned by different structures.

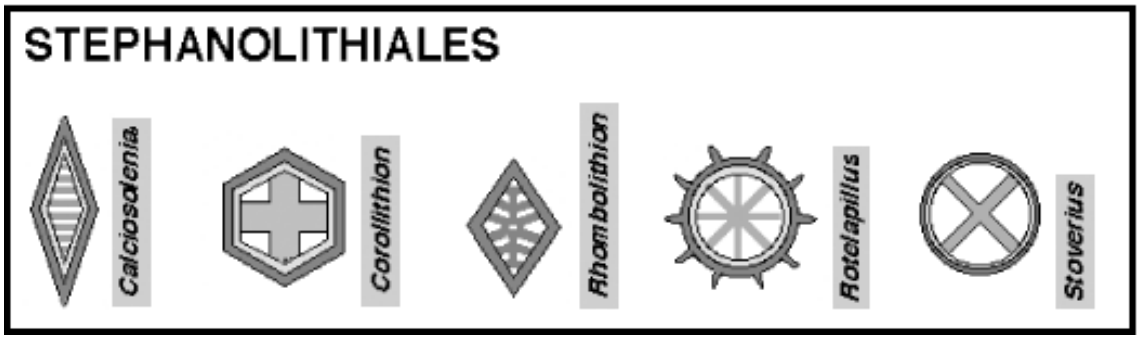

Fig.A.1.5 Genera of Stephanolithiales identified in this work. Darker-shaded rim-cycles indicate V-units, and lighter-shaded cycles R-units; central-area structures are given a different shade (after Bown & Young, 1997)

Family Stephanolithiaceae: protoliths with low rim, the proximal/inner cycle (R-unit) is weakly-developed or vestigial. The central area is spanned by one to numerous bars which sometimes support a central process.

Genus *Calciosolenia*: This genus has a rhombic form, a narrow rim and a small central area spanned by numerous transverse bars.

C. fossilis, Plate VI, Fig.I: small and elongated species of *Calciosolenia*.

Genus *Corollithion*: This genus has a polygonal form, bicyclic rim and a central area spanned by 4-6 bars that may completely fill it.

C. exiguum, Plate VI, Fig.J; Plate XI, Fig.S: species of *Corollithion* with hexagonal to sub-elliptical outline and six radial bars spanning the central area.

C. kennedyi, Plate VI, Fig.K: species of *Corollithion* with sub-square, hexagonal or sub-circular outline and a central area filled by a broad axial cross.

C. madagaskarensis, Plate VI, Fig.L: small species of *Corollithion* with sub-elliptical to hexagonal outline and a central area spanned by a thin diagonal cross.

Remarks: the external part of the rim is wavy which differs it from the species *Anfractus harrisonii*.

C. signum, Plate VI, Fig.M: species of *Corollithion* with sub-square, hexagonal or sub-circular outline and a central area spanned by thin axial cross.

Genus *Rhombolithion*: This genus has a narrow, slightly birefringent, diamond-shaped rim with four or more central-area bars.

R. rombicum, Plate VI, Fig.N: species of *Rhombolithion* with central area spanned by 8 lateral bars that meet at a longitudinal bar.

Genus *Rotelapillus*: This genus has a circular to sub-circular form with bicyclic, high, narrow rim. The inner rim is clearly higher and more distinguishable than the outer one. Focusing on the outer rim, short, lateral spines may be observed. The central area is wide and spanned by bars.

R. asymmetricus, Plate VI, Fig.O: species of *Rotelapillus* with a slightly elliptical central area spanned by a 4-bars structure making small angles (24° to 30°) with the short axis of the ellipse.

Remarks: I placed this species in the genus *Rotelapillus* for the aspect of the inner rim that is higher than in *Stoverius*. Lees & Bown (2006) placed *R. biarcus* in the genus *Rotelapillus* saying that this species has comparable rim structure to other *Rotelapillus* coccoliths, whilst *Cylindralithus* coccoliths have distinctly different rim structure, modified from the placolith *Watznaueria* group, and no central area bars. *Stoverius* has a low rim, whereas that of *Rotelapillus* is high. Perch-Nielsen (1984) placed *R. biarcus, R. coronatus* and *R. asymmetricus* in the genus *Stoverius* instead of *Cylindralithus* restricting this latter genus to forms with an open central area. She also noticed that these three species have an higher wall related to other *Stoverius* species.

R. biarcus, Plate VI, Fig.P: species of *Rotelapillus* with the central area spanned by two arched crossbars.

R. coronatus, Plate VI, Fig.Q: species of *Rotelapillus* with a central area spanned by a 4-bars structure nearly perpendicular each other.

Remarks: I placed this species in the genus *Rotelapillus* for the aspect of the inner rim that is higher than in *Stoverius* as well as *R. asymmetricus*.

R. crenulatus, Plate VI, Fig.R, S: species of *Rotelapillus* with the central area spanned by eight radial bars.

Genus *Stoverius*: This genus has a circular to sub-circular form with bicyclic, low, narrow rim. The central area is wide and spanned by crossbars.

S. achylosus, Plate VI, Fig.T; Plate XI, Fig.T: species of *Stoverius* with bright inner cycle and axial crossbars that meet at 90°.

Order Watznaueriales

Placoliths with proximal and distal shields formed by elements with opposite senses of imbrications. The outer cycle of crystal elements is usually reduced and appears in LM images as a thin, dark line. Central area structures are typically disjunct.

Family Watznaueriaceae: Imbricating placoliths with two shields and a central area which is usually closed or narrow and devoid of central structures or filled by a plug, spanned by bars, axial cross, or grills (Bown & Young, 1997). Highly-birefringent LM image.

Genus *Cyclagelosphaera*: This genus has circular outline and narrow or closed, round central area.

C. margerelii, Plate VII, Fig.A: species of *Cyclagelosphaera* with closed central area slightly raised over the shields structure.

C. reinhardtii: species of *Cyclagelosphaera* with closed central area raised over the shields structure.

C. rotaclypeata, Plate VII, Fig.B: species of *Cyclagelosphaera* with closed central area recessed into the shields structure.

Genus *Cylindralithus*: This genus has a rim modified from the placolith *Watznaueria* group with high, tube-like proximal shield and distinctive side-view images. Central area is usually vacant. Highly birefringent.

C. nudus, Plate VII, Fig.C, D: species of *Cylindralithus* with a small and open central area. A smooth outline may surround the central area.

C. sculptus, Plate VII, Fig.E, F, G, H: species of *Cylindralithus* with a central area that seems closed in proximal view and narrow and surrounded by a large and birefringent outline in distal view.

C. serratus: species of *Cylindralithus* with a wide central area that in well preserved specimens is closed by a delicate porous plate.

Genus *Watznaueria*: This genus has the typical aspects of the family description with central-areas that are typically closed or narrow but may be spanned by transverse bar, bars or grill.

W. barnesiae, Plate VII, Fig.I, J; Plate XI, Fig.M: species of *Watznaueria* with a closed central area. In XPL the extinction gyres meet in the centre of the coccolith, forming a swastika-like extinction pattern, and do not separate on rotation.

W. biporta, Plate VII, Fig.K: large species of *Watznaueria* with two well-defined pores aligned in the long axis of its central area. The pores are separated by a bridge that is optically continuous with the rim.

W. britannica: species of *Watznaueria* with a narrow central area spanned by a transverse bar. The bridge is optically discontinuous with the rim and aligned with the minor axis of the ellipse.

W. fossacinta, Plate VII, Fig.N: species of *Watznaueria* with a narrow central area opening without any structures.

W. manivitiae, Plate VII, Fig.O: Large (more than 9 μm) and highly birifrangent species of *Watznaueria* with a closed central area.

W. ovata, Plate VII, Fig.P: species of *Watznaueria* with a wide, vacant central area.

***W.* sp1,** Plate VII, Fig.L, M: species of *Watznaueria* similar to *W. britannica* with an oblique bridge optically discontinuous with the rim.

Heterococcoliths incertae sedis

Genus *Haqius*: This genus has circular outline, coccoliths are composed of two shields with 40 or more slightly dextrally imbricated elements. The diffuse extinction figure is caused by the slight amount of imbrication. The central area is about one-half of the total diameter, with or without an inner cycle of plates.

H. circumradiatus, Plate VII, Fig.Q, R: type species of the genus.

Remarks: weakly birefringent. Under LM the shields appear pale gray crossed by radial extinction lines, with a darker central region, the numerous individual elements are usually visible.

Genus *Markalius*: This genus has circular outline, it is composed of two shields formed by numerous elements. The central area may be closed or spanned by a bright inner cycle

M. inversus: type species of the genus. Shields are weakly birefringent. The central area is closed, filled by calcite showing high birefringence and a dark cross produced by the orientation of calcite elements.

Genus *Petrarhabdus*: This genus has a circular to elliptical placolith base composed by imbricate elements and a distal structure consisting of a rosette of angular rhombs. The rosette may be developed into a tetralith-like structure with variable size. It may occupy the central area only or may extend beyond the width of the shield.

P. copulatus, Plate VII, Fig.S: type species of the genus. The distal structure is a massive cross of four blocky elements.

Genus *Repagulum*: This genus has elliptical form and is composed by two shields with low birefringence. Each rim cycle consists of very narrow elements forming a fine striated rim. The central area is relatively wide and spanned by bars often indistinguishable in LM image.

R. parvidentatum: type species of the genus.

Remarks: it has a distinctive flaring image when focusing on LM.

Genus *Tortolithus*: This genus has elliptical outline, it is composed by an outer rim of imbricate elements and a central area closed by overlapping plates with a suture in the central area aligned with the long axis of the ellipse.

T. pagei, Plate VII, Fig.T: species of *Tortolithus* with a narrow, scalloped rim cycle.

Holococcoliths

This group is composed of specimens formed by numerous, minute, equidimensional calcite crystallites of simple shape. These crystallites are arranged in precise geometric arrays clearly showing that the location of nucleation is precisely controlled (Bown & Young, 1998).

Family Calyptrosphaeraceae: a morphological taxonomic grouping which embraces coccolithophores which secrete holococcoliths (Bown & Young, 1997).

Genus *Acuturris*: This genus has elongate forms constructed of three adjacent calcite laths tapering to one end and rising from a thin basal disk of 4-5 µm length.

A. scotus, Plate VIII, Fig.A: type species of the genus.

Genus *Calculites*: This genus comprises elliptical form constructed of four blocks which may form a short central projection. It has been argued that *Calculites* represents the basal plate of *Lucianorhabdus* (Burnett, 1998).

C. obscurus: species of *Calculites* with narrow rim and broad wall.

Remarks: in LM images, under crossed-nicols, extinction gyres display different arrangement. If the axes of the ellipse are aligned with the nicols, sutures are diagonal crossbars-like; if the specimen is rotated to 45°, the gyres do not intersect but form arches and short axis blocks seem to be unified, dividing the other two blocks.

C. ovalis: species of *Calculites* with narrow rim and broad wall, sutures are always aligned with the axes of the ellipse.

Remarks: in LM images, under crossed-nicols, extinction gyres do not display different arrangement.

C. percensis, Plate VIII, Fig.B, C: species of *Calculites* with narrow rim and broad wall with a central pore.

Remarks: in LM images, under crossed-nicols, extinction gyres display different arrangement. If the axes of the ellipse are aligned with the nicols, sutures lie on the principal axes of the ellipse; if the specimen is rotated 45°, the gyres do not intersect but form arches and short axis blocks seem to be unified, dividing the other two blocks. In analyzed samples, I observed specimens without central pores. Therefore I named them *C.* cf. *C. percensis*.

Genus *Lucianorhabdus*: This genus has a basal shield of four blocks with a tall, hollow stem. The stem may have different aspects, curved or globular with irregular edge (Fig.A.1.6).

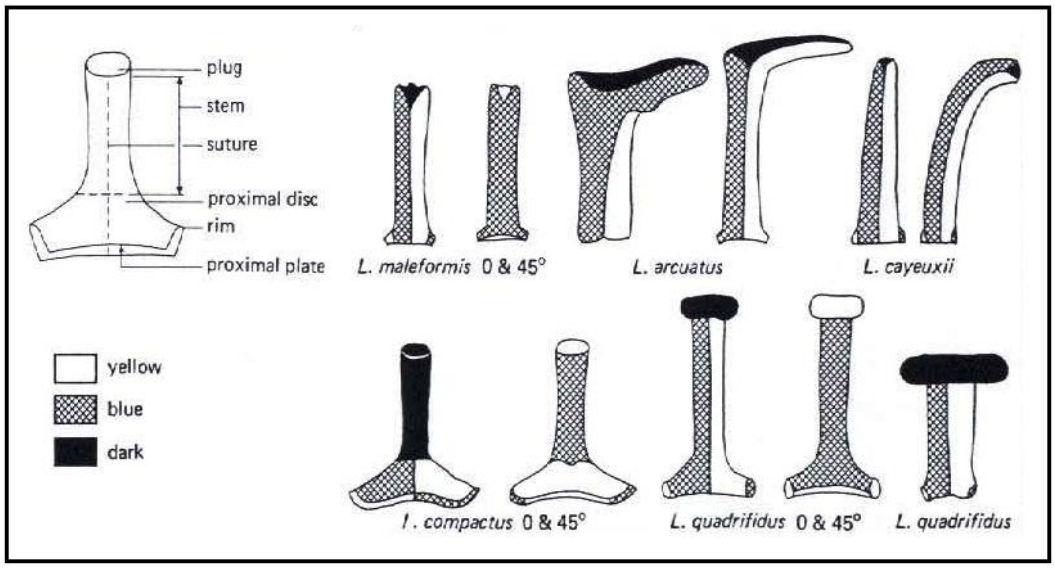

Fig.A.1.6 terminology and optical properties of *Lucianorhabdus* (after Perch-Nielsen, 1985)

L. arcuatus: species of *Lucianorhabdus* with a massive curved process situated at about ¾ of its length from the basal shield. The plug has a rectangular shape and it is placed on one of its vertexes on the top of the stem.

L. cayeuxii, Plate VIII, Fig.D, E: species of *Lucianorhabdus* with irregular shape that may be observed in different form.

L. maleformis, Plate VIII, Fig.F: species of *Lucianorhabdus* with a straight form and four broad basal extensions.

L. quadrifidus, Plate VIII, Fig.G: species of *Lucianorhabdus* with a massive central process terminating in a crown. The plug has a rectangular shape and appears as a sort of "hat" situated on the top of the spine.

Genus *Orastrum*: This genus is composed by one or more calcite plates surrounded by a rim. Specimens with dark plates and bright rim have been placed in this genus (Lees, 2007).

O. robinsonii, Plate VIII, Fig.H: species of *Orastrum* with a wide central area filled by a dark perforated plate and a thick, bright rim.

Genus *Owenia*: This genus has a narrow rim and a central structure of two or four block with, usually, a bridge-shaped structure which may extend into a spine.

O. hillii, Plate VIII, Fig.I, J, K: species of *Owenia* with a central structure consisting in two perforate blocks joined along a transverse suture. A variably developed spine extends distally and may be closed by a distal plug.

Nannoliths

This is an heterogeneous group and includes forms with a wide range of shapes. Most of them show some of the features of heterococcoliths but they are all sufficiently different to make their relationship with coccolithophores uncertain (Bown & Young, 1998).

Family Braarudosphaeraceae: nannoliths constructed from five elements which form an outline that may be pentagonal to starry.

Genus *Braarudosphaera*: This genus has five trapezoidal elements forming a pentalith. Sutures go to the edge of the nannolith.

B. bigelowii, Plate VIII, Fig.L: species of *Braarudosphaera* with pentagonal outline. Sutures do not reach the middle of each side but they run from centre to approximately 3/8 of the way along side of the pentalith.

Family Lepideacassaceae: cylindrical nannoliths with wall constructed from one to several cycles of elements, enclosing a wide central space. An apical process may be present.

Genus *Lepideacassis*: This genus has the typical aspects of the family description.

L. mariae, Plate VIII, Fig.M, N: tall and cylindrical species of *Lepideacassis* tapering at one end. A bifurcating spine may be present.

Family Microrhabdulaceae: elongated, rod-shaped nannoliths with a cruciform or circular cross section.

Genus *Lithraphidites*: This genus has cruciform cross-section and usually variably expanded lateral blades.

L. acutus, Plate VIII, Fig.O, P; Plate XI, Fig.O: species of *Lithraphidites* with four narrow, pointed, triangular blades projected from the center of the rod.

L. alatus, Plate VIII, Fig.Q, R: species of *Lithraphidites* with four blades that taper gradually to an end of the rod

L. carniolensis, Plate VIII, Fig.S: simple species of *Lithraphidites* without extending blades and tapering at both ends.

L. pseudoquadratus: species of *Lithraphidites* with four small, keel like blades projected from the center of the rod.

Remarks: it differs from *L. acutum* in having extensions of a broad flat-topped shape. *L. quadratus* is similar to this species but has wider extensions.

Genus *Microrhabdulus*: This genus has a circular cross-section and it is constructed by superposed calcite elements.

M. belgicus, Plate IX, Fig.A, B: species of *Microrhabdulus* with numerous cycles of sub-rhomboidal and equally spaced nodes.

M. decoratus, Plate IX, Fig.C, D: species of *Microrhabdulus* characterized by superposed calcite elements with alternate optical orientation creating a "chequered" LM image.

M. undosus: species of *Microrhabdulus* characterized by superposed calcite elements with alternate optical orientation and appearing, in LM image, as two lines of rectangular elements that intersect with each other along a wavy line.

Family Nannoconaceae: conical, globular or cylindrical nannoliths composed entirely of spirally-arranged platelets, enclosing an axial cavity or canal.

Genus *Nannoconus*, Plate IX, Fig.E: This genus has the typical aspect of family description.

N. dauvillieri, Plate IX, Fig.F: elongated (12-18 μm) species of *Nannoconus* with a large central cavity and widens to one end.

Family Polycyclolithaceae: nannoliths made up of one or two superposed wall cycles and a central-area which may be closed, open and vacant, or spanned by a diaphragm structure formed by imbricated elements. Each cycle contains the same number of elements in the shape of a ray, petal or brick (Fig.A.1.7).

Genus *Assipetra*: This genus has a sub-rectangular to globular form, it is constructed from two stacks of intergrown irregular rhomboidal plates. These elements may show radial symmetry.

A. terebrodentarius terebrodentarius, Plate IX, Fig.G; Plate XI, Fig.Q: blocky globular subspecies of *Assipetra terebrodentarius*, formed from calcite blocks which are complexly intergrown and may rotate or spiral about a central axis.

A. terebrodentarius youngii, Plate IX, Fig.H: large (more than 7.5 μm) blocky globular subspecies of *Assipetra terebrodentarius*, formed from calcite blocks which are complexly intergrown and may rotate or spiral about a central axis.

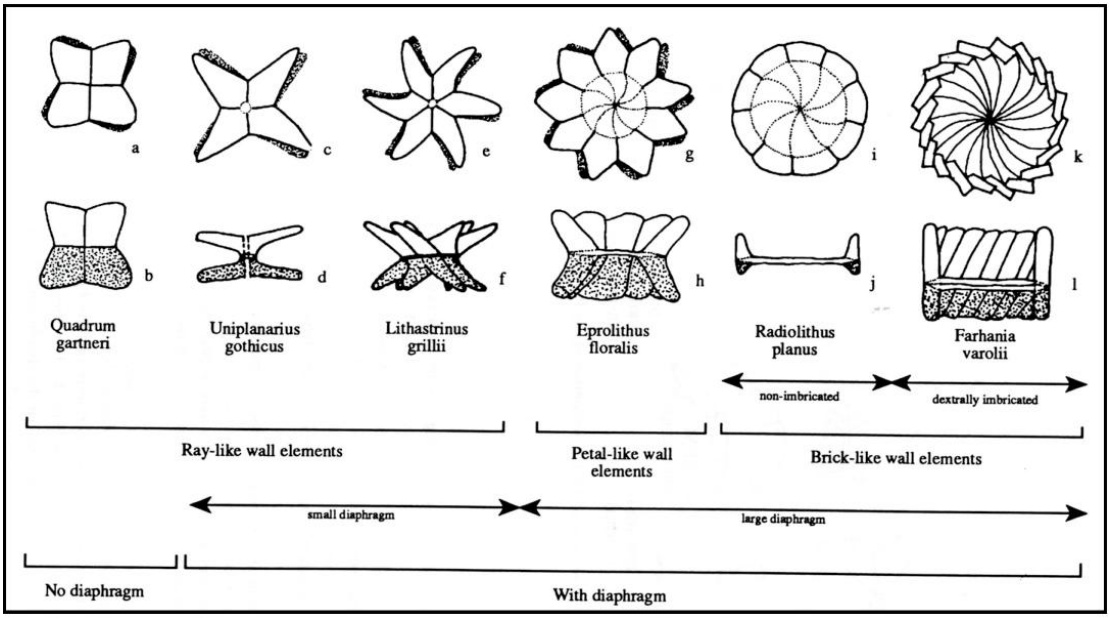

Fig.A.1.7 Overview of the genera in the Polycyclolithaceae (after Varol, 1992)

Genus *Eprolithus*, Plate IX, Fig.I, J: This genus has a wall formed by two cycles of 7-9 non imbricated petal-like elements. A median diaphragm is present in the central opening. Cycles are twisted and elements are slightly inclined. H- to X-shaped in side-view.

E. apertior: species of *Eprolithus* with nine tall (more than 5 μm) elements in each cycle of the wall and widen at both ends. More than half of the total length of the coccolith in plan-view is occupied by the diaphragm.

E. eptapetalus, Plate IX, Fig.K: species of *Eprolithus* with seven elements in each cycle of the wall.

E. floralis, Plate IX, Fig.L, M; Plate XI, Fig.N: species of *Eprolithus* with nine elements in each cycle of the wall.

E. octopetalus, Plate IX, Fig.N: species of *Eprolithus* with eight elements in each cycle of the wall.

Genus *Lithastrinus*: This genus has a wall formed by two cycles of 4-7 non imbricated, curving ray-like elements surrounding a narrow, median diaphragm not discernible in LM. Cycles are strongly twisted and elements are strongly slanting.

L. grillii, Plate IX, Fig.O: species of *Lithastrinus* with six elements in each cycle of the wall.

Remarks: in my samples I called *L.* cf. *L. grillii* specimens with six broad elements and no clear evidence of diaphragm.

L. pentabrachiatus: species of *Lithastrinus* with five elements in each cycle of the wall.

L. quadricuspis, Plate IX, Fig.P, Q: species of *Lithastrinus* with four elements in each cycle of the wall. One cycle has long narrow rays and the other has broader and shorter rays.

L. septenarius, Plate IX, Fig.R: species of *Lithastrinus* with seven elements in each cycle of the wall.

Remarks: in my samples I called *L.* cf. *L. septenarius* specimens with seven broad ray-like elements and no clear evidence of diaphragm.

Genus *Micula*: This genus has a wall formed by two cycles of 4 blocky elements, strongly twisted along their joining surface. In LM images, this genus has a "square" form with sutures spanning entirely or partially the coccolith. No diaphragm is present.

M. adumbrata: species of *Micula* which sutures do not reach the corners of the "square".

M. concava, Plate IX, Fig.S: species of *Micula* with a central depression and extending corners.

M. cubiformis, Plate IX, Fig.T: small species of *Micula* with a central depression.

Remarks: in LM images it is possible to recognize two couple of sutures, diagonal and axial ones.

M. staurophora, Plate X, Fig.A: species of *Micula* composed of four equal-sized, pyramid-shaped blocks in each cycle of the wall. These elements are joined along straight sutures starting from the corners of the "square".

M. swastika, Plate X, Fig.B: species of *Micula* with sutures forming a swastika pattern. Elements of the cycles may protrude slightly from the edge of the "square".

Genus *Quadrum*: This genus has a wall formed by two cycles of 4-9 non-imbricated elements without any central opening or diaphragm. The cycles of the wall are moderately twisted along their joining surface.

Q. eneabrachium, Plate X, Fig.C: species of *Quadrum* with nine elements in each cycle of the wall.

Q. eptabrachium: species of *Quadrum* with seven elements in each cycle of the wall.

Remarks: in my samples I called *Q.* cf. *Q. eptabrachium* specimens larger than the holotype and which seem to have imbricated elements. Some specimens seem to show a sort of diaphragm.

Q. gartneri, Plate X, Fig.D, E, F, G, H: cubiform species of *Quadrum* with four elements in each cycle of the wall. Elements are joined along sutures which go out to the mid-point of the cube edge.

Q. giganteum, Plate X, Fig.I, J, K, L: large (more than 11 μm) species of *Quadrum* with nine elements in each cycle of the wall.

Remarks: in my samples I called *Q.* cf. *Q. giganteum* specimens which seem to have imbricated elements. Some specimens seem to show a sort of diaphragm more evident at parallel nicols. *Rucinolithus* sp. aff. *R.? magnus* Bukry, illustrated in Proto-Decima et al. (1978) and considered by Varol (1992) as synonym of *Q. giganteum*, also seems to show a diaphragm and a sort of imbrications as well as specimens illustrated by Varol (1992) himself. Further studies on this taxon are probably necessary to refine its definition.

Q. intermedium, Plate X, Fig.M, N, O: species of *Quadrum* with four elements of equal size in each cycle of the wall and one to three small ray-like elements inserted in between.

Q. octobrachium, Plate X, Fig.P: small (≈ 4 μm) species of *Quadrum* with eight elements in each cycle of the wall.

Q. svabenickae, Plate X, Fig.Q: species of *Quadrum* with a central depression and four thick elements at the corners.

***Quadrum?* sp. 3**, Plate X, Fig.R, S: doubtful species of *Quadrum* with three or three and one additional elements in each cycle of the wall.

Genus *Radiolithus*: This genus has a relatively thin wall formed by two cycles of 9-16 brick-like elements surrounding a wide central area spanned by an amedian diaphragm. The height of each cycle is unequal and they are twisted along the diaphragm.

R. planus, Plate X, Fig.T: species of *Radiolithus* with a low wall (less than 4 μm height) formed by nine brick-like elements.

R. undosus: species of *Radiolithus* with a low wall (less than 4 μm height) formed by nine brick-like elements in one cycle and nine petal-like elements in the other cycle.

Remarks: similar to *R. planus* in non well-preserved material.

Uncertain polycycloliths

Genus *Hayesites*: This genus has a stellate form with six to eleven dextrally imbricated elements. A multielement central process is generally present.

H. irregularis, Plate XI, Fig.A, B: species of *Hayesites* composed of 6-11 variously shaped elements giving an irregular outline.

Genus *Hexalithus*: This genus has an hexagonal form of six elements.

H. gardetiae, Plate XI, Fig.C: small species of *Hexalithus* with subcircular, scalloped outline.

Genus *Rucinolithus*: This genus has a rosette form with five or more imbricated elements in a single cycle, small additional cycles may be present.

***Rucinolithus* sp. 8 petals**, Plate XI, Fig.D: species of *Rucinolithus* with eight petals, similar to those illustrated by Burnett (1997) from the Lower Campanian of the South Indian Ocean.

Nannoliths incertae sedis

Genus *Ceratolithina*: This genus has a rod common to all species usually rounded at the ends. The rod supports horns or blade-like structures.

C. hamata hamata: species of *Ceratolithina* with a rod bearing two horns of different size and same orientation positioned at the anterior and posterior end of the rod.

C. naturalisteplateauensis, Plate XI, Fig.E: species of *Ceratolithina* with a rod bearing two horns (or a blade and a horn) of different size positioned at the anterior and posterior end of the rod, apparently joined in a unique structure. A small third horn lying in a different orientation is present.

Genus *Liliasterites*: This genus has six rays separated by alternately narrow and wide angles. In well preserved specimens sutures may be observed.

L. angularis, Plate XI, Fig.F: species of *Liliasterites* with tapering and pointed rays.

Genus *Marthasterites*: This genus has three rays originating from a central process. These rays may be straight or slightly arched and may bifurcate at their ends. Weakly birefringent.

M. crassus, Plate XI, Fig.G, H: broad species of *Marthasterites* with short rays bifurcating at their ends.

M. furcatus, Plate XI, Fig.I, J: species of *Marthasterites* with long rays bifurcating at their ends.

M. inconspicuus: species of *Marthasterites* with a triangular shape and slightly concave sides.

M. simplex, Plate XI, Fig.K: species of *Marthasterites* with long rays characterized by cuplike terminations.

Appendix 2

Taxonomic list

Calcareous nannofossil species identified and reported in the distribution charts are here listed following genera and species alphabetical order. References to original desciptions are not given. Synthesis of taxonomic discussion are given by Perch-Nielsen (1985), Burnett (1998) and Lees (2007).

- Genus: *Acaenolithus* Black, 1973

A. cenomanicus Black, 1973

- Genus: *Acuturris* Wind & Wise in Wise & Wind, 1977

A. scotus (Risatti 1973) Wind & Wise in Wise & Wind 1977

- Genus: *Ahmuellerella* Reinhardt, 1964

A. octoradiata (Górka, 1957) Reinhardt & Górka, 1967

- Genus: *Amphizygus* Bukry, 1969

A. brooksii Bukry, 1969

- Genus: *Arkhangelskiella* Vekshina, 1959

A. cymbiformis Vekshina, 1959

A. cymbiformis var. N Varol, 1989

A. cymbiformis var. SW Thibault, 2010

A. cymbiformis var. W Varol, 1989

A. cymbiformis var. NT Varol, 1989

- Genus: *Aspidolithus* Noël, 1969

A. enormis (Shumenko, 1968) Manivit, 1971

A. furtivus (Bukry, 1969) Perch-Nielsen, 1984

A. parcus constrictus (Hattner et al., 1980) Perch-Nielsen, 1984

A. parcus expansus (Wise & Watkins in Wise, 1983) Perch-Nielsen, 1984

A. parcus parcus (Stradner, 1963) Noël, 1969

- Genus: *Assipetra* Roth, 1973

A. terebrodentarius terebrodentarius (Applegate et al. *in* Covington & Wise, 1987) Rutledge & Bergen *in* Bergen, 1994

A. terebrodentarius youngii Tremolada & Erba, 2002

- Genus: *Axopodorhabdus* Wind & Wise in Wise & Wind, 1977

A. albianus (Black, 1967) Wind & Wise in Wise & Wind, 1977

- Genus: *Biscutum* Black in Black & Barnes, 1959

B. constans (Górka, 1957) Black in Black and Barnes, 1959

B. coronum Wind & Wise in Wise & Wind 1977

B. dissimilis Wind & Wise in Wise & Wind 1977

B. magnum Wind & Wise in Wise & Wind 1977

B. melaniae (Górka, 1957) Burnett, 1997

- Genus: *Braarudosphaera* Deflandre, 1947

B. bigelowii (Gran & Braarud, 1935) Deflandre, 1937

- Genus: *Broinsonia* Bukry, 1969

B. matalosa (Stover, 1966) Burnett in Gale et al., 1996

B. signata (Noël, 1969) Noël, 1970

- Genus: *Bukrylithus* Black, 1971

B. ambiguus Black, 1971

- Genus: *Calciosolenia* Gran, 1912

C. fossilis (Deflandre in Deflandre & Fert, 1954) Bown in Kennedy et al., 2000

- Genus: *Calculites* Prins & Sissingh in Sissingh, 1977

C. obscurus (Deflandre, 1959) Prins & Sissingh in Sissingh, 1977

C. ovalis (Stradner, 1963) Prins & Sissingh in Sissingh, 1977

C. percensis Jeremiah, 1996

- Genus: *Ceratolithina* Martini, 1967

C. hamata hamata Martini, 1967

C. naturalisteplateauensis Burnett, 1997

- Genus: *Chiastozygus* Gartner, 1968

C. amphipons (Bramlette & Martini, 1964) Gartner, 1968

C. bifarius Bukry, 1969

C. litterarius (Górka, 1957) Manivit, 1971

C. platyrhethus Hill, 1976

C. synquadriperforatus Bukry, 1969

- Genus: *Corollithion* Stradner, 1962

C. exiguum Stradner, 1961

C. kennedyi Crux, 1981

C. madagaskarensis Perch-Nielsen, 1973

C. signum Stradner, 1963

- Genus: *Cretarhabdus* Bramlette & Martini, 1964

C. conicus Bramlette & Martini, 1964

C. striatus (Stradner, 1963) Black, 1973

- Genus: *Cribrosphaerella* Deflandre in Piveteau, 1952

C. ehrenbergii (Arkhangelsky, 1912) Deflandre in Piveteau, 1952

- Genus: *Crucicribrum* Black, 1973

C. anglicum Black, 1973

C. stenostaurion (Hill, 1976) comb. nov.

- Genus: *Cyclagelosphaera* Noël, 1965

C. margerelii Noël, 1965

C. reinhardtii (Perch-Nielsen, 1968) Romein, 1977

C. rotaclypeata Bukry, 1969

- Genus: *Cylindralithus* Bramlette & Martini, 1964

C. nudus Bukry, 1969

C. sculptus Bukry, 1969

C. serratus Bramlette & Martini, 1964

- Genus: *Discorhabdus* Noël, 1965

D. ignotus (Górka, 1957) Perch-Nielsen, 1968

- Genus: *Eiffellithus* Reinhardt, 1965

E. angustus (Bukry, 1969) Shamrock in Shamrock & Watkins, 2009

E. eximius (Stover, 1966) Perch-Nielsen, 1968

E. gorkae Reinhardt, 1965

E.? hancockii Burnett, 1997

E. keio Shamrock in Shamrock and Watkins, 2009

E. monechiae Crux, 1991

E. perch-nielseniae Shamrock in Shamrock & Watkins, 2009

E. turriseiffelii (Deflandre in Deflandre & Fert, 1954) Reinhardt, 1965

- Genus: *Eprolithus* Stover, 1966

E. apertior Black, 1973

E. eptapetalus Varol, 1992

E. floralis (Stradner, 1962) Stover, 1966

E. octopetalus Varol, 1992

- Genus: *Flebellites* Thierstein, 1973

F. oblongus (Bukry, 1969) Crux in Lord, 1982

- Genus: *Gartnerago* Bukry, 1969

G. chiasta Varol, 1991

G. margaritatus Blair & Watkins, 2009

G. nanum Thierstein, 1974

G. obliquum Stradner, 1963

G. praeobliquum Jakubovski, 1986

G. segmentatum (Stover, 1966) Thierstein, 1974

G. theta (Black in Black & Barnes, 1959) Jakubowski, 1986

- Genus: *Gorkaea* Varol & Girgis, 1994

G. pseudanthophorus (Bramlette & Martini, 1964) Varol & Girgis, 1994

- Genus: *Grantarhabdus* Black, 1971

G. coronadventis (Reinhardt, 1966) Grün in Grün and Allemann, 1975

- Genus: *Haqius* Roth, 1978

H. circumradiatus (Stover, 1966) Roth, 1978

- Genus: *Hayesites* (Manivit, 1971) Applegate et al. in Covington & Wise, 1987

H. irregularis (Thierstein in Roth & Thierstein, 1972) Applegate et al. in Covington & Wise, 1987

- Genus: *Helenea* Worsley, 1971

H. chiastia Worsley, 1971

- Genus: *Helicolithus* Noël, 1970

H. anceps (Górka, 1957) Nöel, 1970

H. compactus (Bukry, 1969) Varol & Girgis, 1994

H. trabeculatus (Górka, 1957) Verbeek, 1977

H. turonicus Varol & Girgis, 1994

H. varolii Blair & Watkins, 2009

- Genus: *Hexalithus* Gardet, 1955

H. gardetiae Bukry, 1969

- Genus: *Kamptnerius* Deflandre, 1959

K. magnificus Deflandre, 1959

- Genus: *Lepideacassis* Black, 1971

L. mariae (Black, 1971) Wind & Wise in Wise & Wind, 1977

- Genus: *Liliasterites* Stradner & Steinmetz, 1984

L. angularis Svabenicka & Stradner in Stradner & Steinmetz, 1984

- Genus: *Lithastrinus* Stradner, 1962

L. grillii Stradner, 1962

L. pentabrachiatus Varol, 1992

L. quadricuspis Farhan, 1987

L. septenarius Forchheimer, 1972

- Genus: *Lithraphidites* Deflandre, 1963

L. acutus Verbeek & Manivit in Manivit et al., 1977

L. alatus Thierstein in Roth & Thierstein, 1972

L. carniolensis Deflandre, 1963

L. pseudoquadratus Crux, 1981

- Genus: *Loxolithus* Noël, 1965

L. armilla (Black in Black & Barnes, 1959) Noel, 1965

- Genus: *Lucianorhabdus* Deflandre, 1959

L. arcuatus Forchheimer, 1972

L. cayeuxii Deflandre, 1959

L. maleformis Reinhardt, 1966

L. quadrifidus Forchheimer, 1972

- Genus: *Manivitella* Thierstein, 1971

M. pemmatoidea (Deflandre in Manivit, 1965) Thierstein, 1971

- Genus: *Markalius* Bramlette & Martini, 1964

M. inversus (Deflandre in Deflandre & Fert, 1954) Bramlette & Martini, 1964

- Genus: *Marthasterites* Deflandre, 1959

M. crassus (Deflandre, 1959) Burnett, 1997

M. furcatus (Deflandre in Deflandre & Fert 1954) Deflandre, 1959

M. inconspicuous Deflandre, 1959

M. simplex (Bukry, 1969) Burnett, 1997

- Genus: *Microrhabdulus* Deflandre, 1959

M. belgicus Hay & Towe, 1963

M. decoratus Deflandre, 1959

M. undosus Perch-Nielsen, 1973

- Genus: *Micula* Vekshina, 1959

M. adumbrata Burnett, 1997

M. concava (Stradner in Martini & Stradner, 1960) Verbeek, 1976

M. cubiformis Forchheimer, 1972

M. staurophora (Gardet, 1955) Stradner, 1963

M. swastika Stradner & Steinmetz, 1984

- Genus: *Nannoconus* Kamptner, 1931

N. dauvillieri Deflandre & Deflandre, 1960

- Genus: *Octocyclus* Black, 1972

O. reinhardtii (Bukry, 1969) Wind & Wise in Wise & Wind, 1977

- Genus: *Orastrum* Wind & Wise in Wise & Wind, 1977

O. robinsonii Lees, 2007

- Genus: *Owenia* Crux, 1991

O. hillii Crux, 1991

- Genus: *Petrarhabdus* Wind & Wise in Wise, 1983

P. copulatus (Deflandre, 1959) Wind & Wise in Wise, 1983

- Genus: *Placozygus* Hoffman, 1970

P. fibuliformis (Reinhardt, 1964) Hoffman, 1970

- Genus: *Prediscosphaera* Vekshina, 1959

P. columnata (Stover, 1966) Perch-Nielsen, 1984

P. cretacea (Arkhangelsky, 1912) Gartner, 1968

P. grandis Perch-Nielsen, 1979

P. ponticula (Bukry, 1969) Perch-Nielsen, 1984

P. spinosa (Bramlette & Martini 1964) Gartner 1968

P. stoveri (Perch-Nielsen, 1968) Shafik & Stradner, 1971

- Genus: *Quadrum* Prins & Perch-Nielsen in Manivit et al., 1977

Q. eneabrachium Varol, 1992

Q. eptabrachium Varol, 1992

Q. gartneri Prins & Perch-Nielsen in Manivit et al., 1977

Q. giganteum Varol, 1992

Q. intermedium Varol, 1992

Q. octobrachium Varol, 1992

Q. svabenickae Burnett, 1997

- Genus: *Radiolithus* Stover, 1966

R. planus Stover, 1966

R. undosus (Black, 1973) Varol, 1992

- Genus: *Reinhardtites* Perch-Nielsen, 1968

R. anthophorus (Deflandre, 1959) Perch-Nielsen, 1968

R. levis Prins & Sissingh in Sissingh, 1977

- Genus: *Repagulum* Forchheimer, 1972

R. parvidentatum (Deflandre & Fert, 1954) Forchheimer, 1972

- Genus: *Retecapsa* Black, 1971

R. angustiforata Black, 1971

R. crenulata (Bramlette & Martini, 1964) Grün in Grün and Allemann, 1975

R. ficula (Stover, 1966) Burnett, 1997

R. schizobrachiata (Gartner, 1968) Grün in Grün and Allemann, 1975

R. surirella (Deflandre & Fert, 1954) Grün in Grün and Allemann, 1975

- Genus: *Rhagodiscus* Reinhardt, 1967

R. achlyostaurion (Hill, 1976) Doeven, 1983

R. angustus (Stradner, 1963) Reinhardt, 1971

R. asper (Stradner, 1963) Reinhardt, 1967

R. indistinctus Burnett, 1997

R. reniformis Perch-Nielsen, 1973

R. splendens (Deflandre, 1953) Verbeek, 1977

- Genus: *Rhombolithion* Black, 1973

R. rombicum (Stradner & Adamiker, 1966) Black, 1973

- Genus: *Rotelapillus* Noël, 1973

R. asymmetricus (Bukry, 1969) comb. nov.

R. biarcus (Bukry, 1969) Lees & Bown, 2006

R. coronatus (Bukry, 1969) comb. nov.

R. crenulatus (Stover, 1966) Perch-Nielsen, 1984

- Genus: *Rucinolithus* Stover, 1966

Rucinolithus sp. 8 Burnett, 1997

- Genus: *Seribiscutum* Filewicz et al. in Wise & Wind, 1977

S. primitivum (Thierstein, 1974) Filewicz et al. in Wise & Wind, 1977

- Genus: *Sollasites* Black, 1967

S. horticus (Stradner et al. in Stradner & Adamiker, 1966) Cepek & Hay, 1969

- Genus: *Staurolithites* Caratini, 1963

S.? aenigma Burnett, 1997

S. crux (Deflandre & Fert, 1954) Caratini, 1963

S. dicandidula Bergen in Bralower & Bergen, 1998

S. ellipticus (Gartner, 1968) Lambert, 1987

S. elongatus (Bukry, 1969) Burnett, 1997

S. flavus Burnett, 1997

S. gausorhethium (Hill, 1976) Varol & Girgis, 1994

S. glaber (Jeremiah, 1996) Burnett, 1997

S. halfanii Lees, 2007

S. imbricatus (Gartner, 1968) Burnett, 1997

S. laffittei Caratini, 1963

S. mielnicensis (Górka 1957) Crux, 1982

S. minutus Burnett, 1997

S. mutterlosei Crux, 1989

Staurolithites sp. 2 Bown, 1998

- Genus: *Stoverius* Perch-Nielsen, 1984

S. achylosus (Stover, 1966) Perch-Nielsen, 1984

- Genus: *Tegumentatum* Thierstein in Roth & Thierstein, 1972

T. stradneri Thierstein in Roth & Thierstein, 1972

- Genus: *Tetrapodorhabdus* Black, 1971

T. decorus (Deflandre in Deflandre & Fert, 1954) Wind & Wise in Wise & Wind, 1977

- Genus: *Thiersteinia* Wise & Watkins in Wise, 1983

T. ecclesiastica Wise & Watkins in Wise, 1983

- Genus: *Tortolithus* Crux, in Lord, 1982

T. pagei (Bukry, 1969) Crux, in Lord, 1982

- Genus: *Tranolithus* Stover, 1966

T. gabalus Stover, 1966

T. minimus (Bukry, 1969) Perch-Nielsen, 1984

T. orionatus Reinhardt, 1966

T. salillum (Noel, 1965) Crux, 1981

- Genus: *Watznaueria* Reinhardt, 1964

W. barnesiae (Black, 1959) Perch-Nielsen, 1968

W. biporta Bukry, 1969

W. britannica (Stradner, 1963) Reinhardt, 1964

W. fossacinta (Black, 1971) Bown in Bown & Cooper, 1989

W. manivitiae Bukry, 1973

W. ovata Bukry, 1969

- Genus: *Zeugrhabdotus* Reinhardt, 1965

Z. acanthus Reinhardt, 1965

Z. bicrescenticus (Stover, 1966) Burnett in Gale et al., 1996

Z. biperforatus (Gartner, 1968) Burnett, 1997

Z. diplogrammus (Deflandre in Deflandre & Fert, 1954) Burnett in Gale et al., 1996

Z. embergeri (Noël, 1958) Perch-Nielsen, 1984

Z. erectus (Deflandre in Deflandre & Fert, 1954) Reinhardt, 1965

Z. howei Bown in Kennedy et al., 2000

Z. noeliae Rod, Hay & Barnard, 1971

Z. praesigmoides Burnett, 1997

Z. scutula (Bergen, 1994) Rutledge & Bown, 1996

Z. sigmoides (Bramlette & Sullivan, 1961) Bown & Young, 1997

Z. trivectis Bergen, 1994

Appendix 3

Plates

Plate I (bar scale: 5μm)

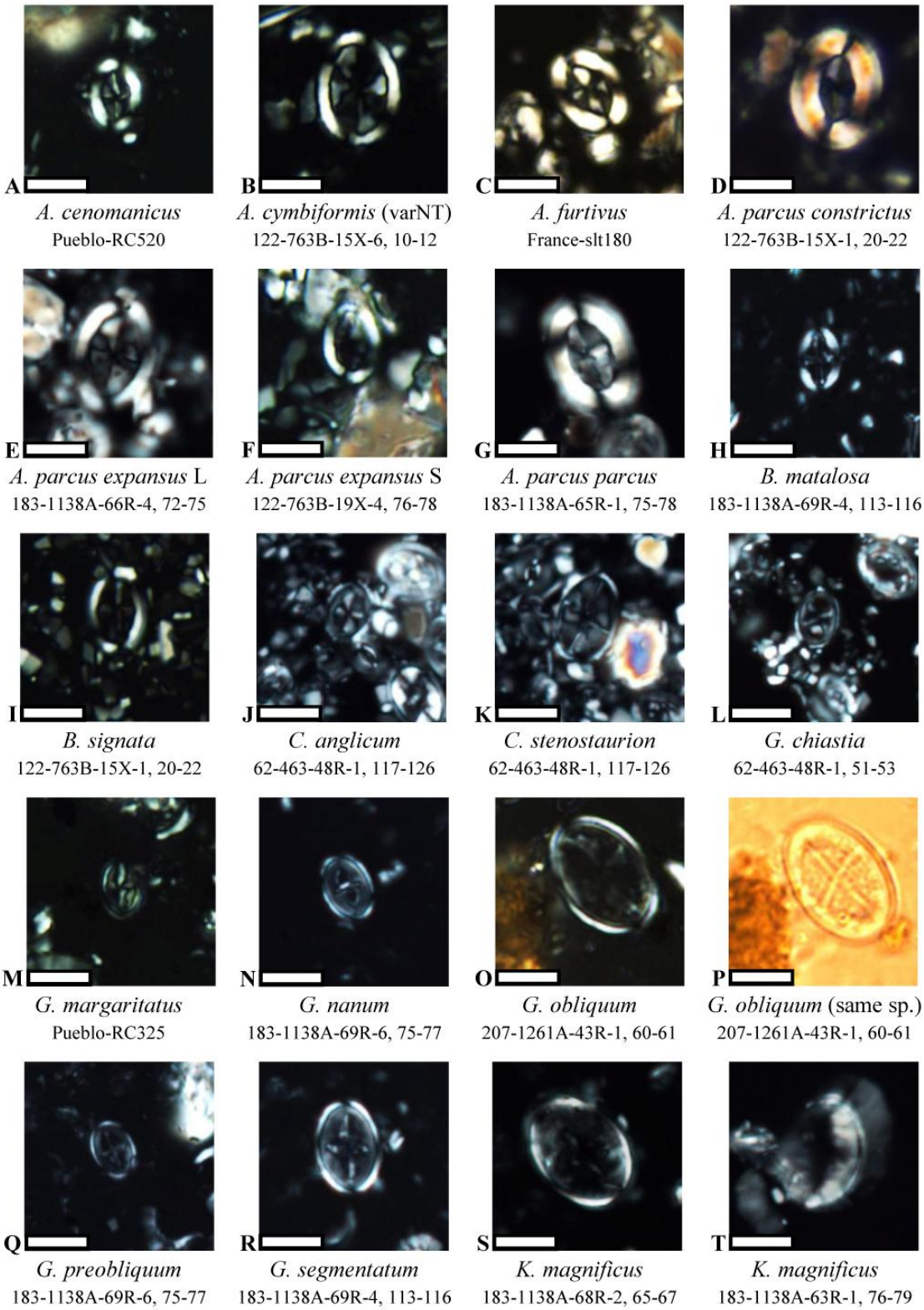

Plate II (bar scale: 5µm)

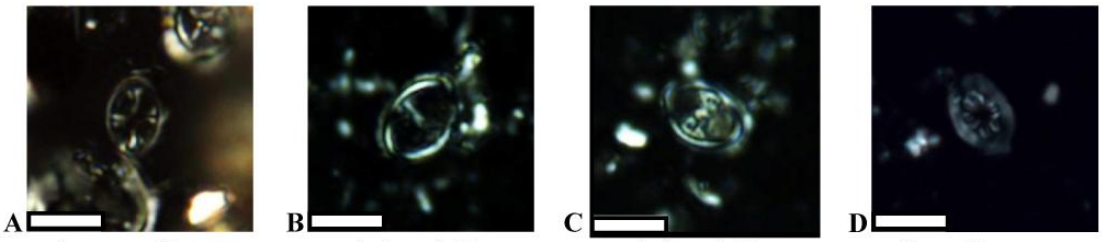

A *A. octoradiata*
207-1261A-41R-5, 20-21

B *A. brooksii*
Pueblo-RC520

C *A. brooksii*
Pueblo-RC670

D *B. ambiguus*
183-1138A-68R-3, 58-61

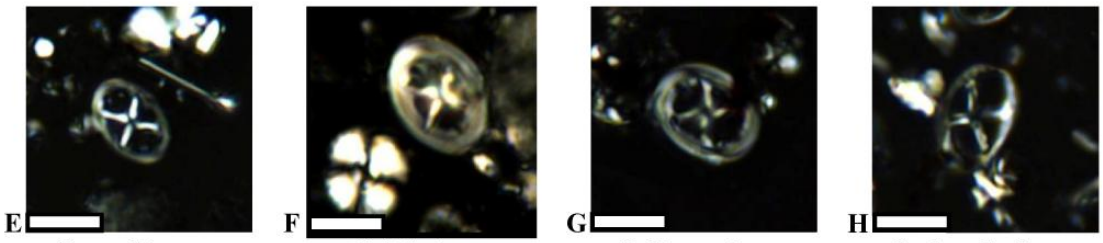

E *C. amphipons*
207-1261A-42R-2, 30-31

F *C. bifarius*
207-1261A-41R-5, 20-21

G *C. litterarius*
207-1261A-45R-3, 20-21

H *C. platyrhethus*
207-1261A-47R-5, 90-91

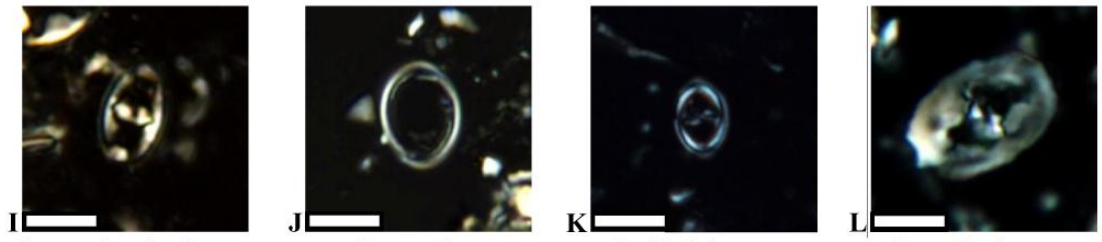

I *G. pseudanthophorus*
207-1261A-44R-2, 90-91

J *L. armilla*
207-1261A-42R-2, 30-31

K *P. fibuliformis*
183-1138A-69R-6, 75-77

L *R. anthophorus*
122-763B-19X-4, 76-78

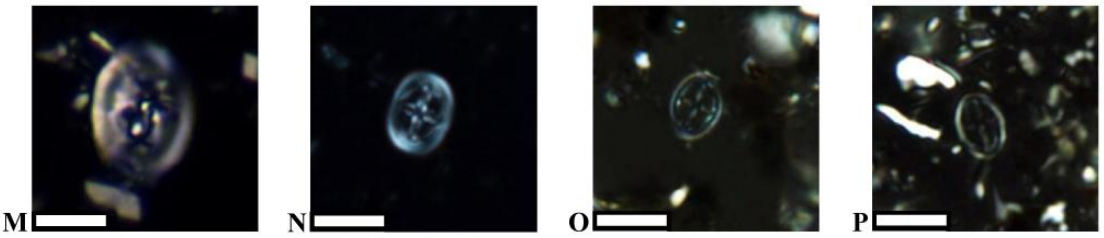

M *R. levis*
122-763B-15X-1, 20-22

N *S. dicandidula*
183-1138A-69R-6, 75-77

O *S. ellipticus*
207-1261A-48R-3, 80-81

P *S. flavus*
207-1261A-41R-6, 130-131

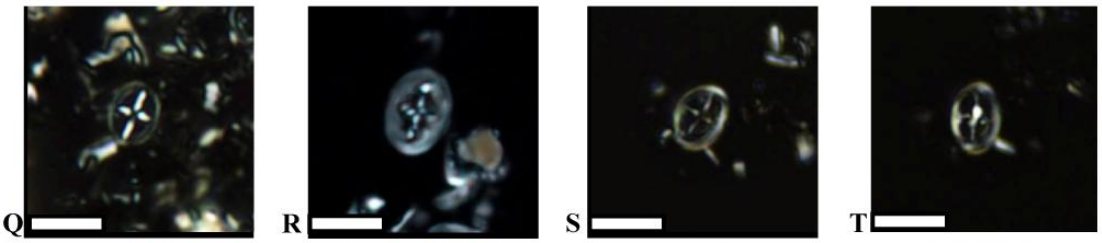

Q *S. flavus*
Same specimen as II – P

R *S. gausorhethium*
62-463-43R-5, 3-5

S *S. halfanii*
207-1261A-41R-3, 140-141

T *S. halfanii*
Same specimen as II – S

Plate III (bar scale: 5µm)

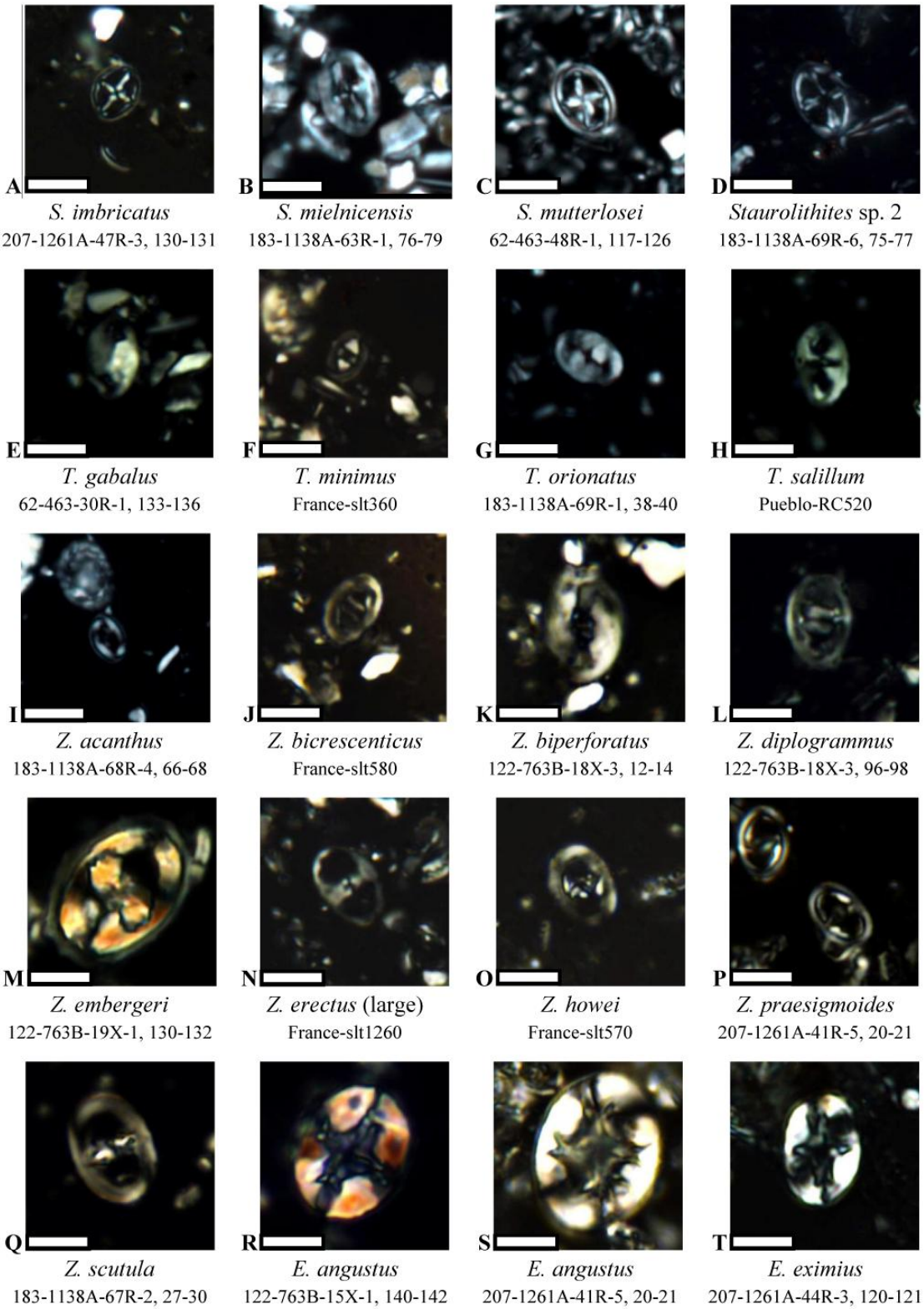

Plate IV (bar scale: 5µm)

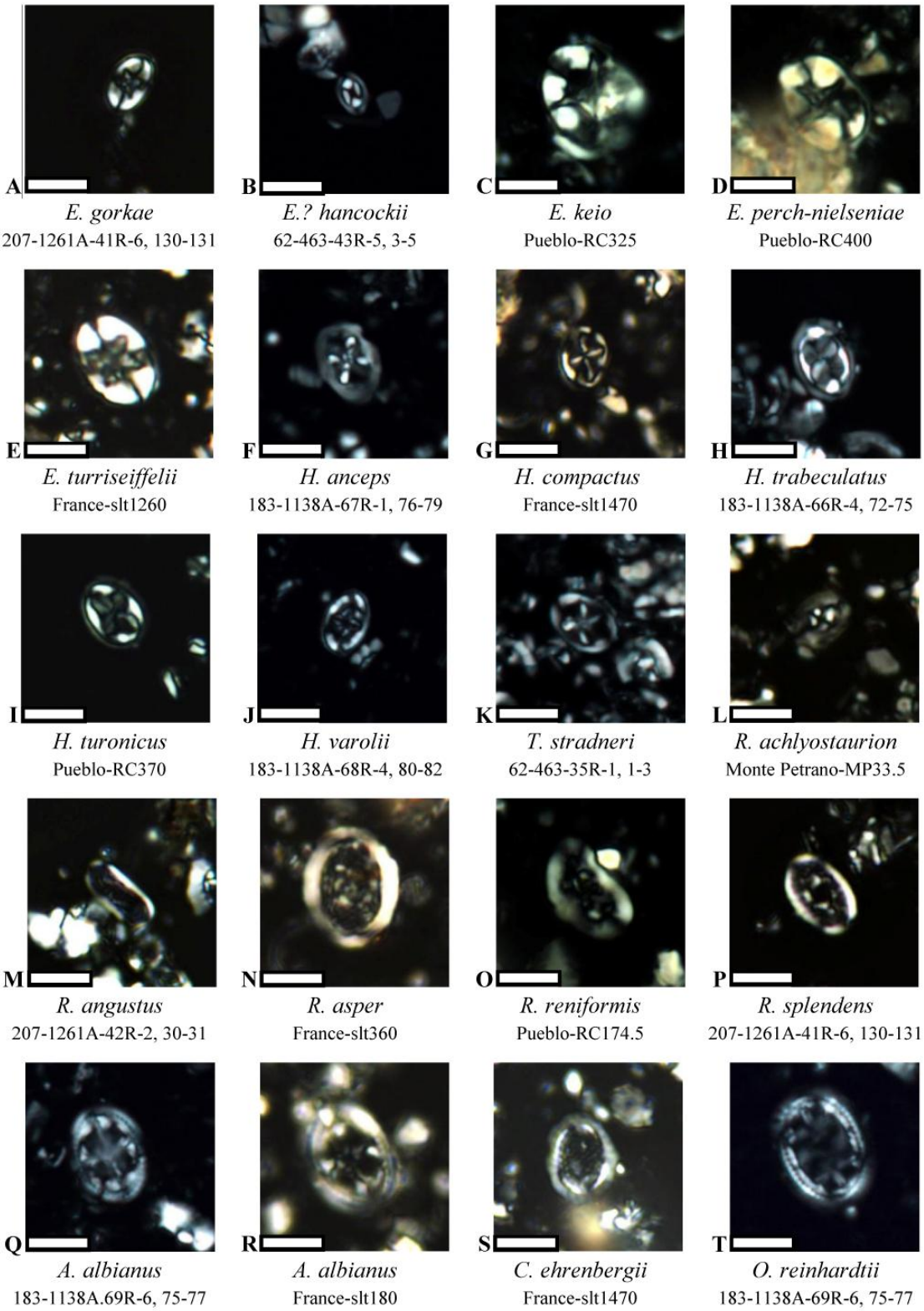

Plate V (bar scale: 5µm)

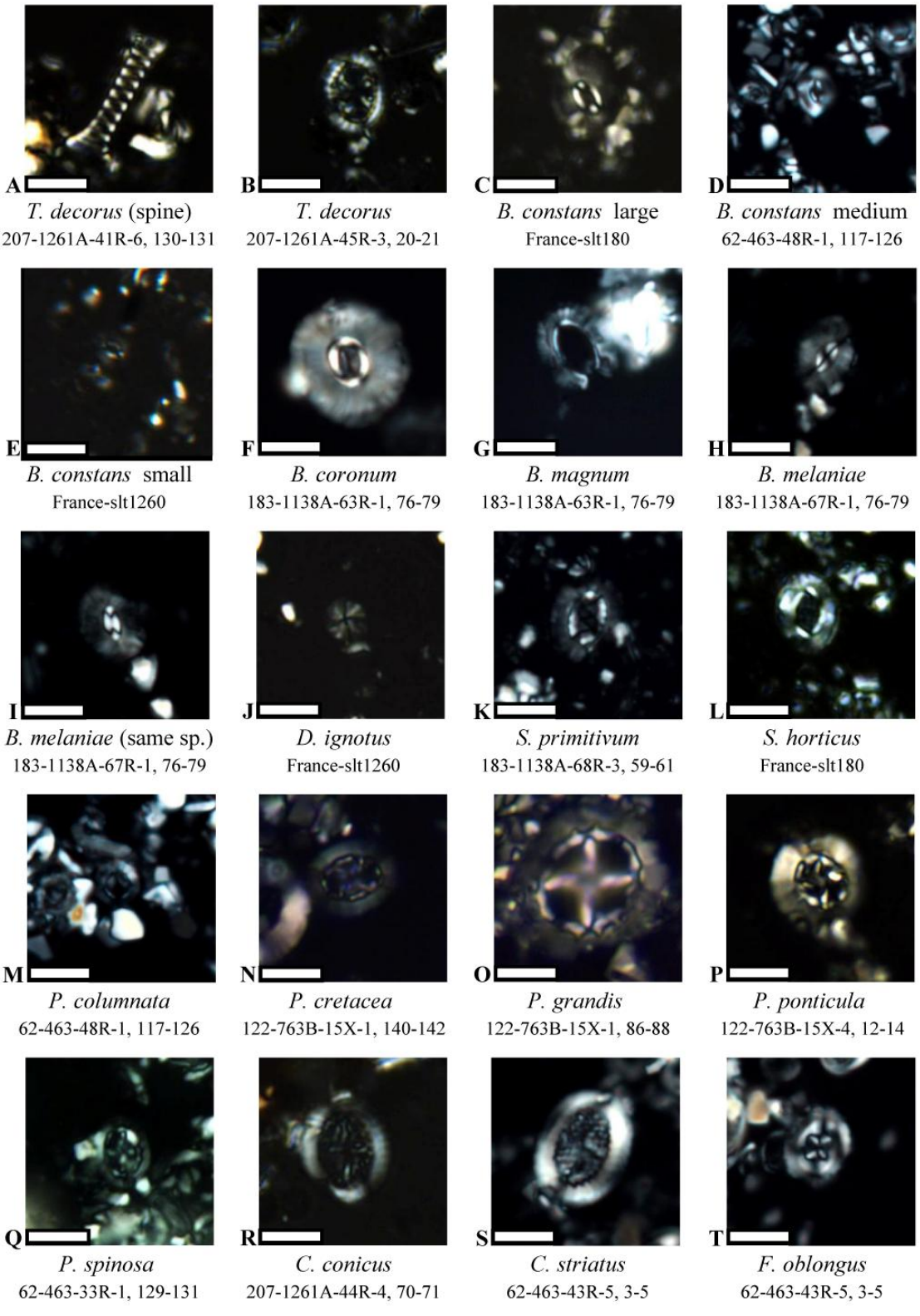

Plate VI (bar scale: 5μm)

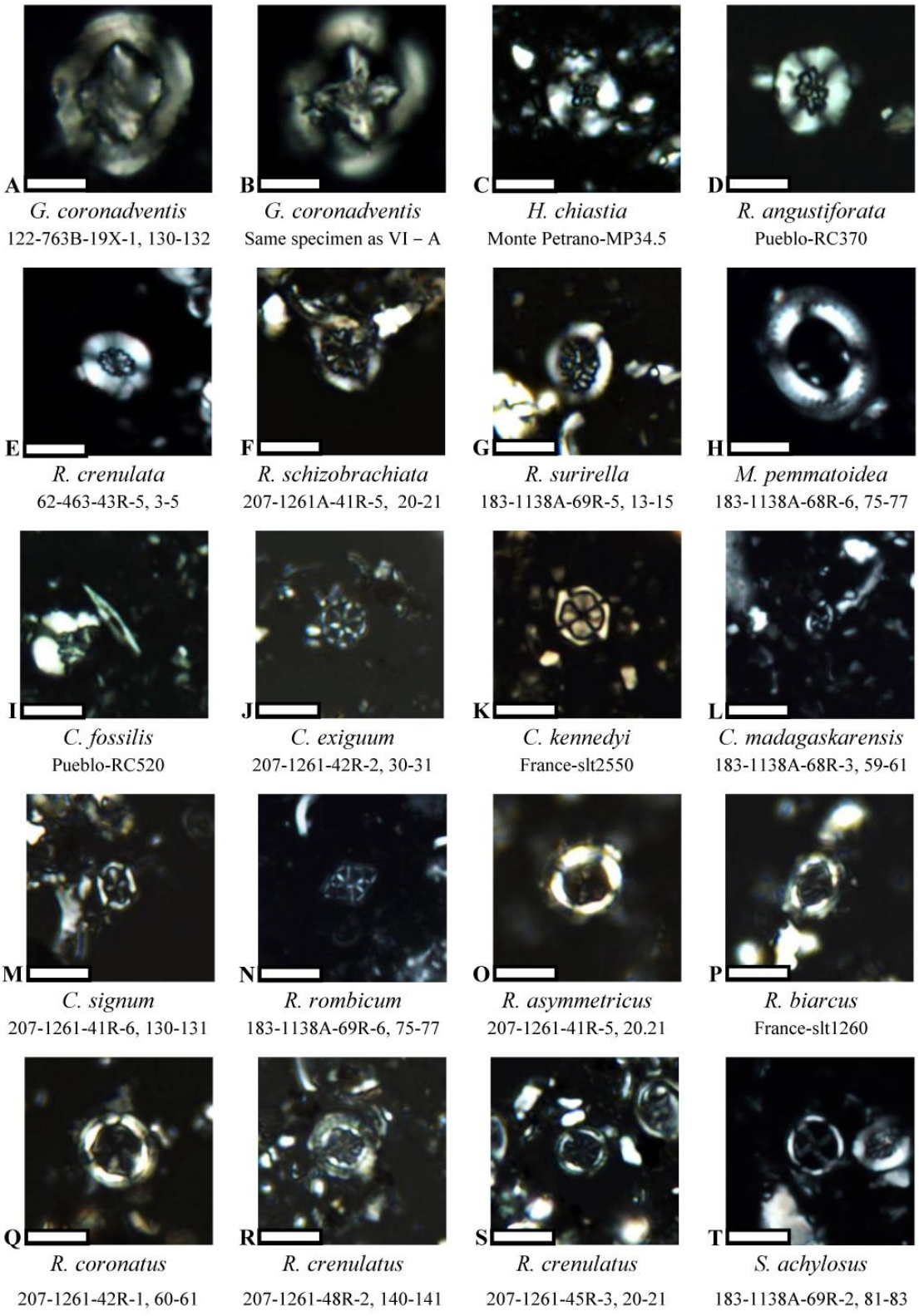

A *G. coronadventis*
122-763B-19X-1, 130-132

B *G. coronadventis*
Same specimen as VI – A

C *H. chiastia*
Monte Petrano-MP34.5

D *R. angustiforata*
Pueblo-RC370

E *R. crenulata*
62-463-43R-5, 3-5

F *R. schizobrachiata*
207-1261A-41R-5, 20-21

G *R. surirella*
183-1138A-69R-5, 13-15

H *M. pemmatoidea*
183-1138A-68R-6, 75-77

I *C. fossilis*
Pueblo-RC520

J *C. exiguum*
207-1261-42R-2, 30-31

K *C. kennedyi*
France-slt2550

L *C. madagaskarensis*
183-1138A-68R-3, 59-61

M *C. signum*
207-1261-41R-6, 130-131

N *R. rombicum*
183-1138A-69R-6, 75-77

O *R. asymmetricus*
207-1261-41R-5, 20.21

P *R. biarcus*
France-slt1260

Q *R. coronatus*
207-1261-42R-1, 60-61

R *R. crenulatus*
207-1261-48R-2, 140-141

S *R. crenulatus*
207-1261-45R-3, 20-21

T *S. achylosus*
183-1138A-69R-2, 81-83

Plate VII (bar scale: 5µm)

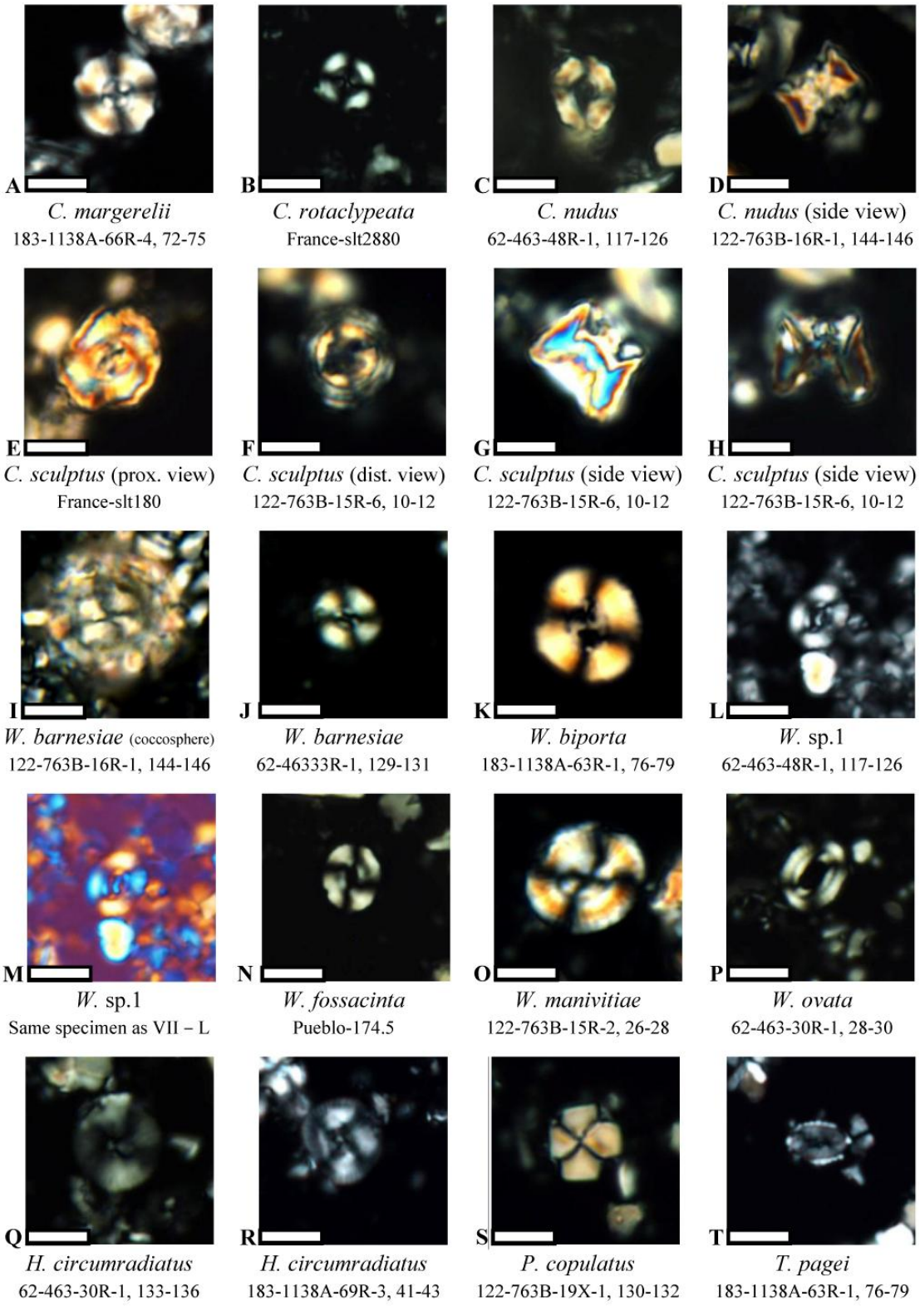

A *C. margerelii*
183-1138A-66R-4, 72-75

B *C. rotaclypeata*
France-slt2880

C *C. nudus*
62-463-48R-1, 117-126

D *C. nudus* (side view)
122-763B-16R-1, 144-146

E *C. sculptus* (prox. view)
France-slt180

F *C. sculptus* (dist. view)
122-763B-15R-6, 10-12

G *C. sculptus* (side view)
122-763B-15R-6, 10-12

H *C. sculptus* (side view)
122-763B-15R-6, 10-12

I *W. barnesiae* (coccosphere)
122-763B-16R-1, 144-146

J *W. barnesiae*
62-46333R-1, 129-131

K *W. biporta*
183-1138A-63R-1, 76-79

L *W.* sp.1
62-463-48R-1, 117-126

M *W.* sp.1
Same specimen as VII – L

N *W. fossacinta*
Pueblo-174.5

O *W. manivitiae*
122-763B-15R-2, 26-28

P *W. ovata*
62-463-30R-1, 28-30

Q *H. circumradiatus*
62-463-30R-1, 133-136

R *H. circumradiatus*
183-1138A-69R-3, 41-43

S *P. copulatus*
122-763B-19X-1, 130-132

T *T. pagei*
183-1138A-63R-1, 76-79

Plate VIII (bar scale: 5µm)

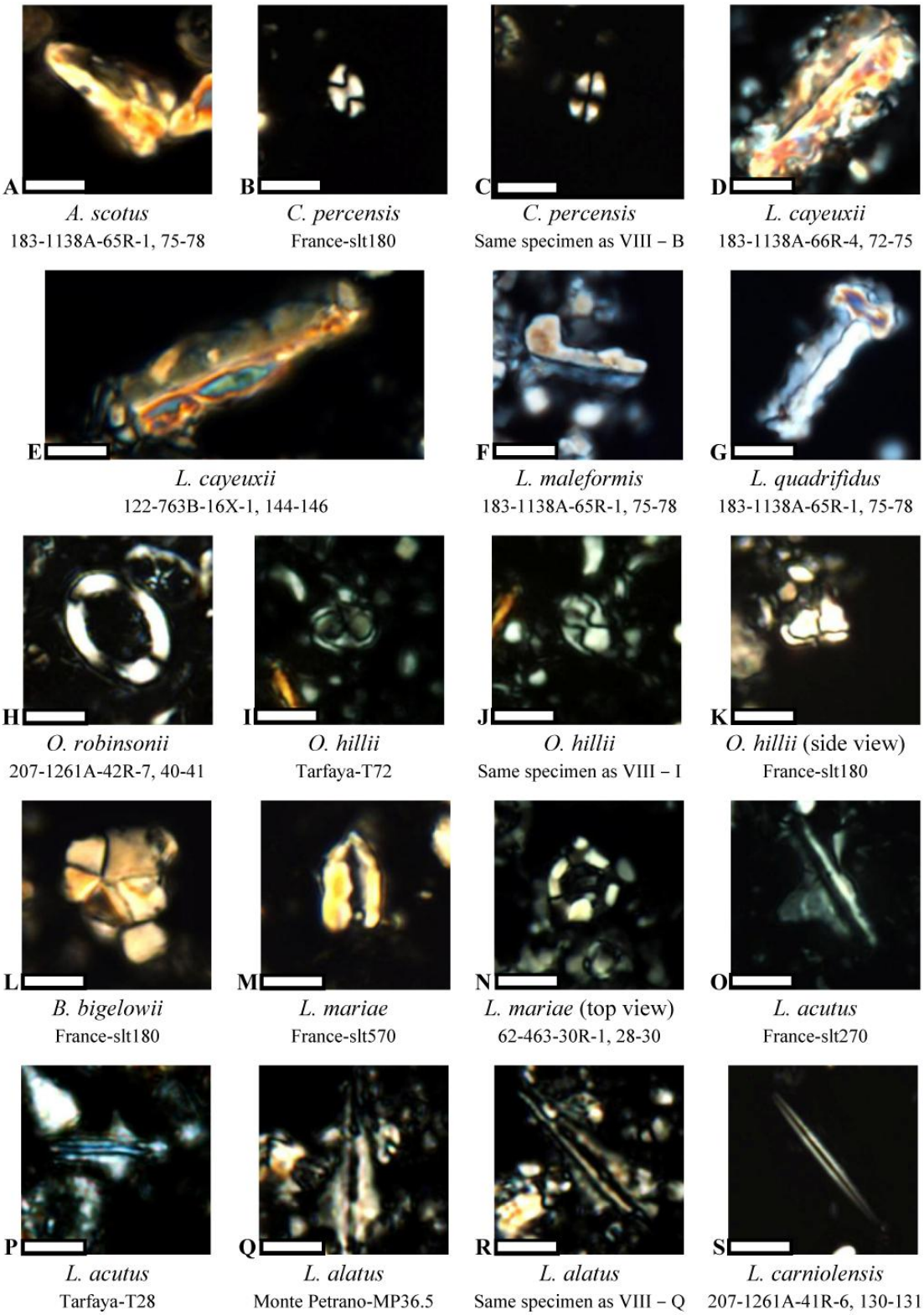

Plate IX (bar scale: 5µm)

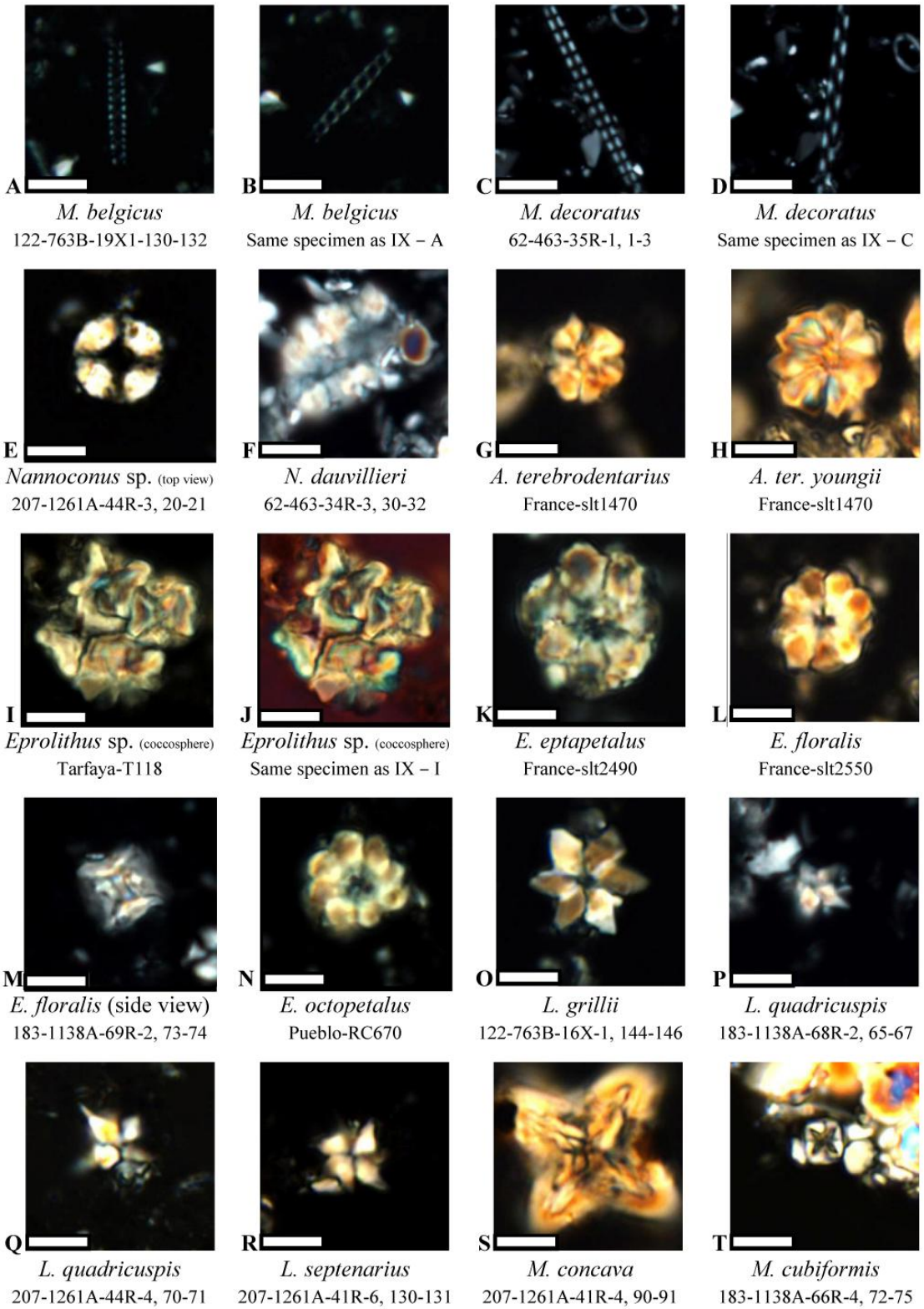

A *M. belgicus* 122-763B-19X1-130-132

B *M. belgicus* Same specimen as IX – A

C *M. decoratus* 62-463-35R-1, 1-3

D *M. decoratus* Same specimen as IX – C

E *Nannoconus* sp. (top view) 207-1261A-44R-3, 20-21

F *N. dauvillieri* 62-463-34R-3, 30-32

G *A. terebrodentarius* France-slt1470

H *A. ter. youngii* France-slt1470

I *Eprolithus* sp. (coccosphere) Tarfaya-T118

J *Eprolithus* sp. (coccosphere) Same specimen as IX – I

K *E. eptapetalus* France-slt2490

L *E. floralis* France-slt2550

M *E. floralis* (side view) 183-1138A-69R-2, 73-74

N *E. octopetalus* Pueblo-RC670

O *L. grillii* 122-763B-16X-1, 144-146

P *L. quadricuspis* 183-1138A-68R-2, 65-67

Q *L. quadricuspis* 207-1261A-44R-4, 70-71

R *L. septenarius* 207-1261A-41R-6, 130-131

S *M. concava* 207-1261A-41R-4, 90-91

T *M. cubiformis* 183-1138A-66R-4, 72-75

Plate X (bar scale: 5µm)

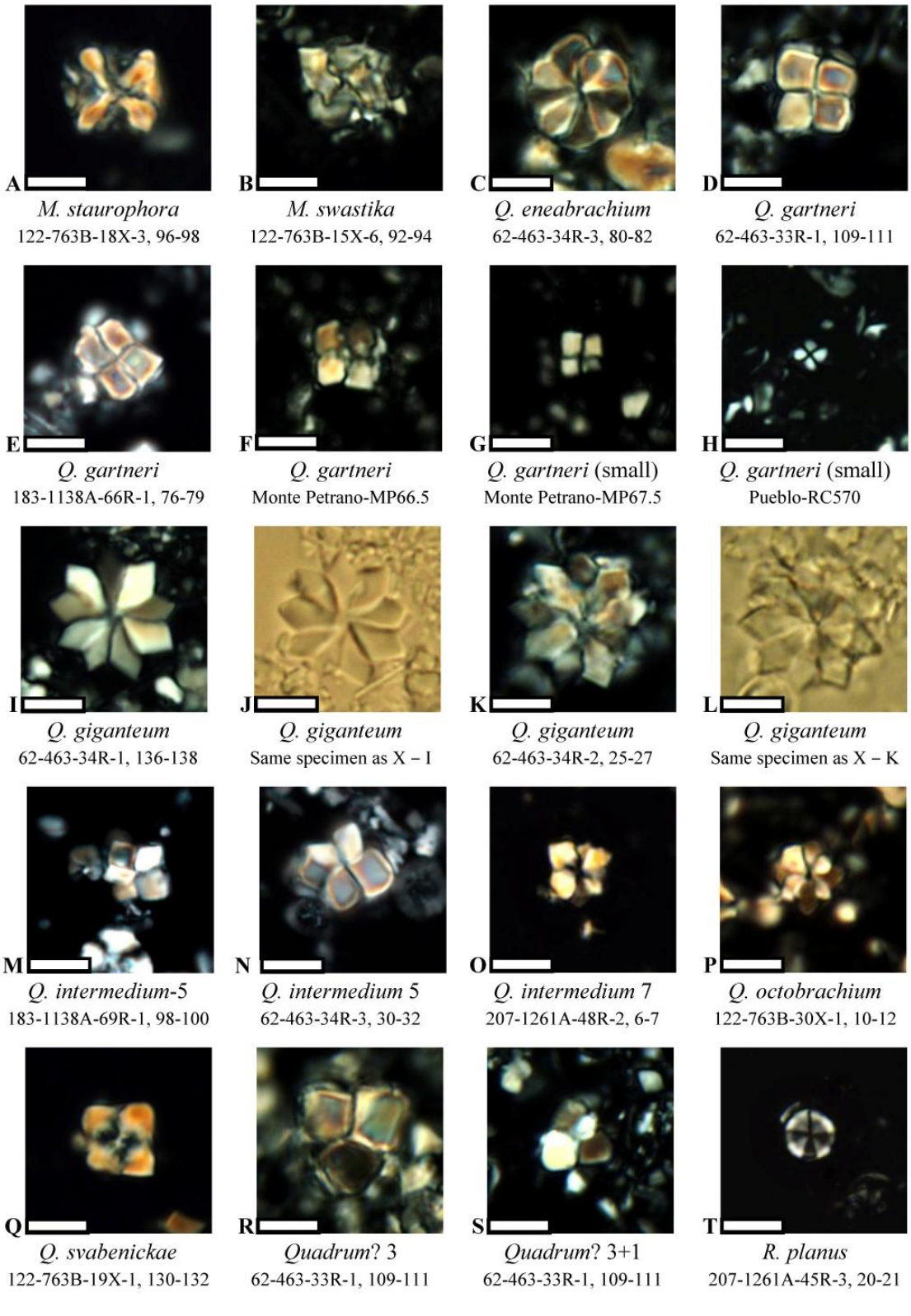

A *M. staurophora* 122-763B-18X-3, 96-98

B *M. swastika* 122-763B-15X-6, 92-94

C *Q. eneabrachium* 62-463-34R-3, 80-82

D *Q. gartneri* 62-463-33R-1, 109-111

E *Q. gartneri* 183-1138A-66R-1, 76-79

F *Q. gartneri* Monte Petrano-MP66.5

G *Q. gartneri* (small) Monte Petrano-MP67.5

H *Q. gartneri* (small) Pueblo-RC570

I *Q. giganteum* 62-463-34R-1, 136-138

J *Q. giganteum* Same specimen as X – I

K *Q. giganteum* 62-463-34R-2, 25-27

L *Q. giganteum* Same specimen as X – K

M *Q. intermedium*-5 183-1138A-69R-1, 98-100

N *Q. intermedium* 5 62-463-34R-3, 30-32

O *Q. intermedium* 7 207-1261A-48R-2, 6-7

P *Q. octobrachium* 122-763B-30X-1, 10-12

Q *Q. svabenickae* 122-763B-19X-1, 130-132

R *Quadrum*? 3 62-463-33R-1, 109-111

S *Quadrum*? 3+1 62-463-33R-1, 109-111

T *R. planus* 207-1261A-45R-3, 20-21

Plate XI (bar scale: 5µm)

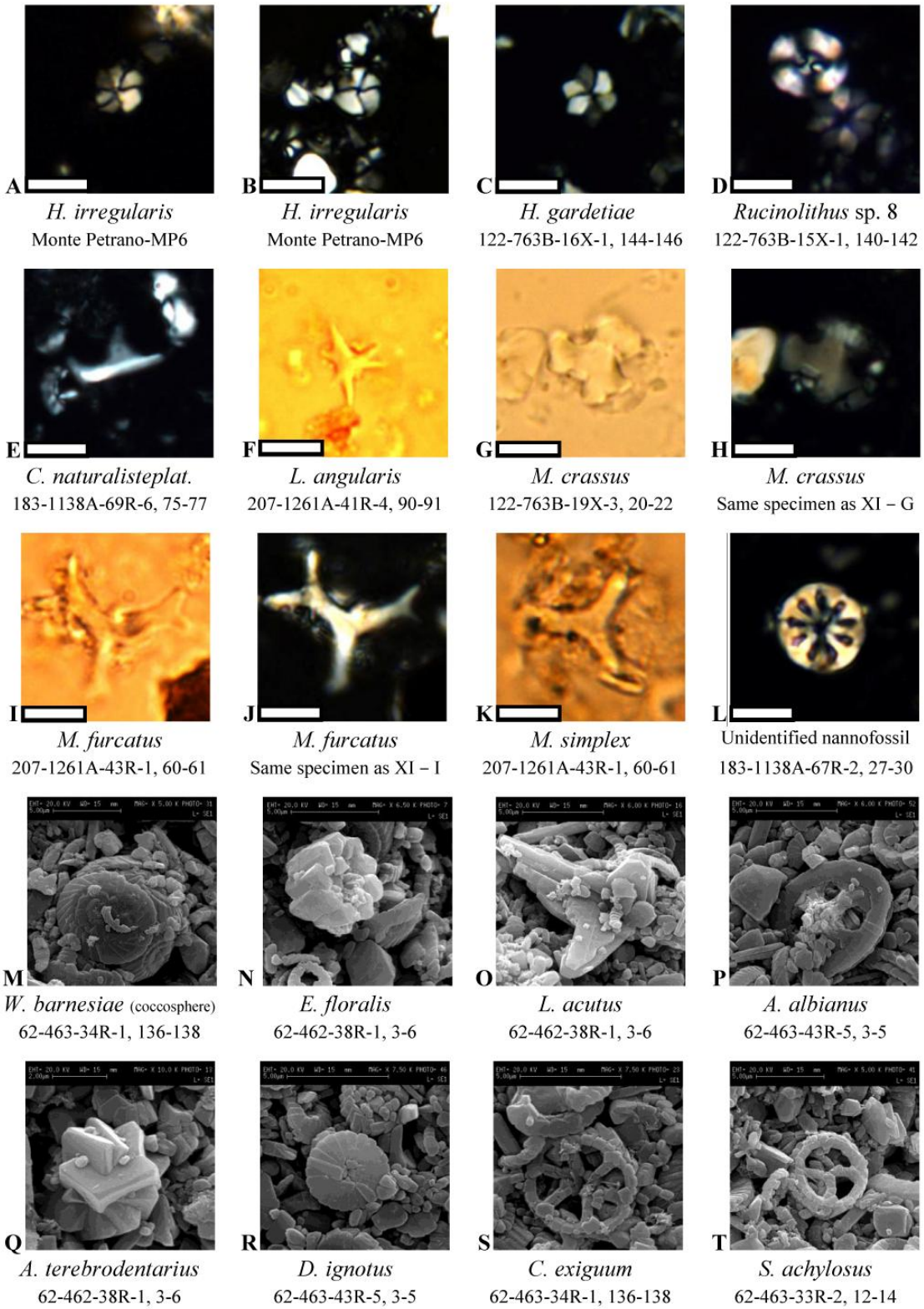

Appendix 4

Tab.2.1. Compilation of the analyzed literature regarding Late Cretaceous calcareous nannofossils

A total of 147 papers were considered. They deal with various localities and are focused on various time intervals during the Late Cretaceous. Analyzed papers focus on taxonomy and biostratigraphy. Very little attention was paid to the evolution and paleoecology.

All the informations are summarized in the table as follows: 1) author; 2) sections; 3) geographic area; 4) stratigraphic interval; 5) range chart: presence ("x") or absence; 6) ammonite biostratigraphy: presence ("x") or absence; 7) planktonic foraminiferal biostratigraphy: presence ("x") or absence; 8) macrofossil biostratigraphy: presence ("x") or absence; 9) correlation with magnetostratigraphy: presence ("x") or absence; 10) correlation with isotopic curves: presence ("x") or absence; 11) illustrations: "SEM" indicates that scanning electron microscope photographs are reported, "TEM" indicates the presence of transmission electron microscope pictures, "LM" indicates that light polarizing microscope photographs are shown, "DR" indicates that the illustrations consist of drawings; 12) taxonomic notes: presence ("x") or absence.

Appendix 5

Tab.2.2. Nannofossil events used as zonal/subzonal markers in Late Cretaceous zonations

Appendix 6

Tab.4.1. Range chart of the Monte Petrano section

Range chart of nannofossil taxa recognized at Monte Petrano. Colour patterns refer to intervals identified using nannofossil assemblage composition. Labeled intervals (A-D) described in the text.

Preservation of nannofossils is reported as follows: M = moderate preservation (some evidence of dissolution and/or overgrowth, primary morphological characteristics somewhat altered, most specimens are identifiable to the species level); P = poor preservation (overgrowth and/or dissolution is extensive, making identification of some specimens difficult).

Estimates of the total calcareous nannofossil abundance, compared to that of other biogenic particles and inorganic components, were recorded as follows: H = high (more than 51% of all particles); M = moderate (11%-50% of all particles); L = low (1%-10% of all particles); VL = very low (less than 1% of all particles).

Abundances of individual nannofossil taxa are reported as follows: C = common (1-10 specimens per field of view); F = few to frequent (1 specimen per 2-20 fields of view); R = rare (1 specimen per more than 20 fields of view).

Appendix 7

Tab.4.2. Range chart of DSDP Site 463

Range chart of nannofossil taxa recognized at DSDP Site 463. Colour patterns refer to intervals identified using nannofossil assemblage composition. Labeled intervals (A-B) described in the text.

Preservation of nannofossils is reported as follows: G = good preservation (little or no evidence of dissolution and/or overgrowth, primary morphological characteristics only slightly altered, most specimens are identifiable to the species level); M = moderate preservation (some evidence of dissolution and/or overgrowth, primary morphological characteristics somewhat altered, most specimens are identifiable to the species level).

Estimates of the total calcareous nannofossil abundance, compared to that of other biogenic particles and inorganic components, were recorded as follows: H = high (more than 51% of all particles); M = moderate (11%-50% of all particles).

Abundances of individual nannofossil taxa are reported as follows: A = abundant (more than 11 specimens per field of view); C = common (1-10 specimens per field of view); F = few to frequent (1 specimen per 2-20 fields of view); R = rare (1 specimen per more than 20 fields of view).

Appendix 8

Tab.4.3. Range chart of the Rock Canyon section

Range chart of nannofossil taxa recognized at Rock Canyon. Colour patterns refer to intervals identified using nannofossil assemblage composition. Labeled intervals (A-C) described in the text.

Preservation of nannofossils is reported as follows: M = moderate preservation (some evidence of dissolution and/or overgrowth, primary morphological characteristics somewhat altered, most specimens are identifiable to the species level); P = poor preservation (overgrowth and/or dissolution is extensive, making identification of some specimens difficult).

Estimates of the total calcareous nannofossil abundance, compared to that of other biogenic particles and inorganic components, were recorded as follows: H = high (more than 51% of all particles); M = moderate (11%-50% of all particles); L = low (1%-10% of all particles); VL = very low (less than 1% of all particles).

Abundances of individual nannofossil taxa are reported as follows: C = common (1-10 specimens per field of view); F = few to frequent (1 specimen per 2-20 fields of view); R = rare (1 specimen per more than 20 fields of view).

.

Appendix 9

Tab.4.4. Range chart of the Clote de Chevalier section

Range chart of nannofossil taxa recognized at Clote de Chevalier. Colour patterns refer to intervals identified using nannofossil assemblage composition. Labeled intervals (A-C) described in the text.

Preservation of nannofossils is reported as follows: G = good preservation (little or no evidence of dissolution and/or overgrowth, primary morphological characteristics only slightly altered, most specimens are identifiable to the species level); M = moderate preservation (some evidence of dissolution and/or overgrowth, primary morphological characteristics somewhat altered, most specimens are identifiable to the species level); P = poor preservation (overgrowth and/or dissolution is extensive, making identification of some specimens difficult).

Estimates of the total calcareous nannofossil abundance, compared to that of other biogenic particles and inorganic components, were recorded as follows: H = high (more than 51% of all particles); M = moderate (11%-50% of all particles); L = low (1%-10% of all particles); VL = very low (less than 1% of all particles).

Abundances of individual nannofossil taxa are reported as follows: A = abundant (more than 11 specimens per field of view); C = common (1-10 specimens per field of view); F = few to frequent (1 specimen per 2-20 fields of view); R = rare (1 specimen per more than 20 fields of view).

Appendix 10

Tab.4.5. Range chart of the Tarfaya Core section

Range chart of nannofossil taxa recognized at Tarfaya Core. Colour patterns refer to intervals identified using nannofossil assemblage composition. Labeled intervals (A-C) described in the text.

Preservation of nannofossils is reported as follows: M = moderate preservation (some evidence of dissolution and/or overgrowth, primary morphological characteristics somewhat altered, most specimens are identifiable to the species level); P = poor preservation (overgrowth and/or dissolution is extensive, making identification of some specimens difficult).

Estimates of the total calcareous nannofossil abundance, compared to that of other biogenic particles and inorganic components, were recorded as follows: H = high (more than 51% of all particles); M = moderate (11%-50% of all particles); L = low (1%-10% of all particles); VL = very low (less than 1% of all particles).

Abundances of individual nannofossil taxa are reported as follows: C = common (1-10 specimens per field of view); F = few to frequent (1 specimen per 2-20 fields of view); R = rare (1 specimen per more than 20 fields of view).

Appendix 11

Tab.4.6. Range chart of ODP Site 1138

Range chart of nannofossil taxa recognized at ODP Site 1138. Colour patterns refer to intervals identified using nannofossil assemblage composition. Labeled intervals (A-D) described in the text.

Preservation of nannofossils is reported as follows: G = good preservation (little or no evidence of dissolution and/or overgrowth, primary morphological characteristics only slightly altered, most specimens are identifiable to the species level); M = moderate preservation (some evidence of dissolution and/or overgrowth, primary morphological characteristics somewhat altered, most specimens are identifiable to the species level); P = poor preservation (overgrowth and/or dissolution is extensive, making identification of some specimens difficult).

Estimates of the total calcareous nannofossil abundance, compared to that of other biogenic particles and inorganic components, were recorded as follows: M = moderate (11%-50% of all particles); L = low (1%-10% of all particles).

Abundances of individual nannofossil taxa are reported as follows: A = abundant (more than 11 specimens per field of view); C = common (1-10 specimens per field of view); F = few to frequent (1 specimen per 2-20 fields of view); R = rare (1 specimen per more than 20 fields of view).

Appendix 12

Tab.4.7. Range chart of ODP Site 1261

Range chart of nannofossil taxa recognized at ODP Site 1261. Colour patterns refer to intervals identified using nannofossil assemblage composition. Labeled intervals (A-D) described in the text.

Preservation of nannofossils is reported as follows: G = good preservation (little or no evidence of dissolution and/or overgrowth, primary morphological characteristics only slightly altered, most specimens are identifiable to the species level); M = moderate preservation (some evidence of dissolution and/or overgrowth, primary morphological characteristics somewhat altered, most specimens are identifiable to the species level); P = poor preservation (overgrowth and/or dissolution is extensive, making identification of some specimens difficult).

Estimates of the total calcareous nannofossil abundance, compared to that of other biogenic particles and inorganic components, were recorded as follows: H = high (more than 51% of all particles); M = moderate (11%-50% of all particles); L = low (1%-10% of all particles); VL = very low (less than 1% of all particles).

Abundances of individual nannofossil taxa are reported as follows: A = abundant (more than 11 specimens per field of view); C = common (1-10 specimens per field of view); F = few to frequent (1 specimen per 2-20 fields of view); R = rare (1 specimen per more than 20 fields of view).

Appendix 13

Tab.4.8. Range chart of ODP Site 763

Range chart of nannofossil taxa recognized at ODP Site 763. Colour patterns refer to intervals identified using nannofossil assemblage composition. Labeled intervals (A-E) described in the text.

Preservation of nannofossils is reported as follows: G = good preservation (little or no evidence of dissolution and/or overgrowth, primary morphological characteristics only slightly altered, most specimens are identifiable to the species level); M = moderate preservation (some evidence of dissolution and/or overgrowth, primary morphological characteristics somewhat altered, most specimens are identifiable to the species level); P = poor preservation (overgrowth and/or dissolution is extensive, making identification of some specimens difficult).

Estimates of the total calcareous nannofossil abundance, compared to that of other biogenic particles and inorganic components, were recorded as follows: H = high (more than 51% of all particles); M = moderate (11%-50% of all particles); L = low (1%-10% of all particles); VL = very low (less than 1% of all particles).

Abundances of individual nannofossil taxa are reported as follows: A = abundant (more than 11 specimens per field of view); C = common (1-10 specimens per field of view); F = few to frequent (1 specimen per 2-20 fields of view); R = rare (1 specimen per more than 20 fields of view).

Acknowledgements

I would like to thanks Prof. Elisabetta Erba for the opportunity she gave me with this Ph.D. project, for her patience, her support and for every scientific discussion.

Thanks to Isabella Premoli Silva and Maria Rose for their help and every good suggestion.

Thanks to Jackie Lees for the opportunity she gave me to work with her in London and to everyone who made that stay an extraordinary experience: Christian, Leisa, Paul, Barbara, Stuart, Jeremy and all my flatmates.

Thanks to everyone I met in these three years at the University: Cristina, Sara, Gabriele, Silvia, Francesca, Cinzia, Dario, Alessia, Irene, Giulia, Gaia, Claudio, Andrea, Irene, Enrico, Federica.

Thanks to all my friends near and far, you are too many to mention you all but you have been fundamental!

Then, many thanks to my parents, without you none of this would have been possible.